Ecole Centrale de Nantes

ÉCOLE DOCTORALE

SCIENCES POUR L'INGENIEUR, GEOSCIENCES, ARCHITECTURE

Année 2013 - 2014 N° B.U. :

Thèse de DOCTORAT

Spécialité : GENIE CIVIL

Présentée et soutenue publiquement par :

JIAN - HAN

le ……11-07-2014……..…
à l'Ecole Centrale Nantes

TITRE

ÉTUDE EXPÉRIMENTALE DU COMPORTEMENT MÉCANIQUE D'UNE ARGILE FORTEMENT SURCONSOLIDÉE SOUS CHARGEMENTS MONOTONES ET CYCLIQUES

JURY

Président :	**Irini DJERAN-MAIGRE**	Professeur- INSA Lyon
Rapporteurs :	**Mahdia HATTAB**	Professeur- LEM3 Université de Lorraine
	Shuilong SHEN	Professeur- Shanghai Jiao Tong University
Examinateurs :	**Jean CANOU**	Chercheur – Ecole Nationale des Ponts et Chaussées
	Zhenyu YIN	Maître de conférences HDR- Ecole Centrale de Nantes
	Pierre-Yves HICHER	Professeur- Ecole Centrale de Nantes
	Christophe DANO	Maître de conférences - Ecole Centrale de Nantes
Invité :	**Alain PUECH**	Directeur scientifique- Fugro GeoConsulting SA

Directeur de thèse : Pierre-Yves HICHER
Laboratoire : Institut de Recherche en Génie Civil et Mécanique
Co-encadrant : Christophe DANO
Laboratoire : Institut de Recherche en Génie Civil et Mécanique N° ED …

Ecole Centrale de Nantes

ÉCOLE DOCTORALE

SCIENCES POUR L'INGENIEUR, GEOSCIENCES, ARCHITECTURE

Année 2013 - 2014 N° B.U. :

DOCTORAL THESIS

Subject : CIVIL ENGINEERING

Written by :

JIAN - HAN

Defenced on July 11 2014
at Ecole Centrale Nantes

TITLE

EXPERIMENTAL STUDY ON THE MECHANICAL BEHAVIOR OF A STIFF CLAY SUBJECTED TO MONOTONIC AND CYCLIC LOADING

JURY

President :	**Irini DJERAN-MAIGRE**	Professeur- INSA Lyon
Reviewers:	**Mahdia HATTAB**	Professeur- LEM3 Université de Lorraine
	Shuilong SHEN	Professeur- Shanghai Jiao Tong University
Examinators :	**Jean CANOU**	Chercheur – Ecole Nationale des Ponts et Chaussées
	Zhenyu YIN	Maître de conférences HDR- Ecole Centrale de Nantes
	Pierre-Yves HICHER	Professeur- Ecole Centrale de Nantes
	Christophe DANO	Maître de conférences - Ecole Centrale de Nantes
Invitee :	**Alain PUECH**	Directeur scientifique- Fugro GeoConsulting SA

Thesis supervisor : Pierre-Yves HICHER
Laboratory : Institut de Recherche en Génie Civil et Mécanique
Co-supervisor : Christophe DANO
Laboratory : Institut de Recherche en Génie Civil et Mécanique N° ED …

Remerciements

Cette étude; initiée et financée par le gouvernement chinois (CSC), a été réalisée à l'Institut de Recherche en Génie Civil et Mécanique de l'Ecole Centrale de Nantes et plus particulièrement au sein de l'Equipe « Matériaux hétérogènes et Géomécanique».

Ma profonde gratitude va au Directeur de cette équipe et qui plus est Directeur de ma thèse, Monsieur Pierre-Yves HICHER, non seulement pour l'accueil chaleureux, qu'il m'a réservé mais également pour sa disponibilité, sa confiance et ses encouragements de nature professionnelle et privée.

Je tiens à remercier Monsieur Christophe DANO. Je lui exprime ici toute ma reconnaissance de m'avoir suivi au cours de ces années, avec beaucoup de disponibilité et de patience pour mon étude expérimentale. Ses conseils avisés m'ont été des plus profitables tant au niveau professionnel que personnel.

Je remercie Madame Irini DJERAN-MAIGRE, d'avoir accepté de présider mon jury, et à Madame Mahdia HATTAB et Monsieur Shuilong SHEN, pour avoir bien voulu rapporter mon mémoire et porter un regard constructif sur le travail présenté. Mes remerciements également à Monsieur Jean CANOU et Monsieur Alain PUECH, pour avoir accepté d'être examinateur dans mon jury.

Je remercie Monsieur Zhenyu YIN, Habilitation à diriger des recherches dans notre équipe, pour ses conseils et son aide précieuse lors de la correction de ma thèse. Je n'oublierai jamais son encouragement.

Mes remerciements vont à Monsieur Jean-Pierre REGOIN, Ingénieur d'études à l'Ecole Centrale de Nantes et Patrick DENAIN, Technicien, pour leur aide dans la mise en service des différents dispositifs.

Chaleureux remerciements à mes collègues : Katia COUSSIN, Yvon RIOU, Zhen LI, Yinfu JIN, Yao MA, Qian ZHAO, Menghuan GUO, Guangtao XU, Qi ZHU, Xiaoli Guo, Gang LI, Qiyin ZHU, Yingjing LIU pour leurs compétences, leur gentillesse, pour leur collaboration et pour l'excellente ambiance qu'ils contribuent à créer. Qu'ils soient assurés de ma sympathie.

Avant de terminer, je voudrais dédier cette thèse à mes parents, à mon petit frère et à tous les membres de ma famille, qui m'ont apporté soutien et encouragement au cours de ces quatre années.

Que ceux que j'ai pu oublier soient aussi remerciés.

Table of Contents

Table of Figures

List of Tables

Abstract

Merville clay of the Flanders Region was deposited in a marine gulf which corresponds now to the area covering northern France, Belgium, and southeastern England. This clay is an example of a stiff-overconsolidated clay, which displays a similar behavior to that of London clay. It is therefore important to study Merville clay for improving our understanding of the mechanical behavior of stiff, non-uniform clays. A model common to these clays would be helpful and this experimental research based on core samples is certainly likely to contribute to developing a general framework for the engineering properties of such soils.

The physical properties of Merville clay were first analyzed in order to provide the mineralogical content as well as the main characteristics of the clayey structure. Then, the mechanical properties were obtained by running oedometer and triaxial tests on samples from different depths in their natural and reconstituted states. The OCR value for the natural samples is about 20. The effects of the structure, fissures, and anisotropy on the mechanical behavior of Merville clay were investigated. The strain rate dependency of the reconstituted and natural samples of Merville clay at high OCRs was analyzed. The test results indicate that the strain rate effect on the undrained shear strength is greater for natural samples than for reconstituted samples.

Cyclic tests with a large number of cycles (i.e., more than one million) were performed on the Merville clay. A threshold value of the stress level was found. If the stress level was smaller than this threshold value, a state of equilibrium could be reached during cyclic loading. The number of cycles in relation with the permanent and cyclic shear strains is reported in stability diagrams. Based on these diagrams, if the permanent and cyclic stresses are combined, the shear strains can be predicted at a given number of cycles. The monotonic shear strength of the samples subjected to previous cyclic loading is higher than the shear strength of the sample without previous cyclic loading.

Keywords: Merville clay, high overconsolidation ratio, triaxial test, critical state lines, strain rate dependency, cyclic test with large number of cycles.

Résumé

L’argile de Merville a été déposée dans un golfe marin qui correspond maintenant au nord de la France, la Belgique et le sud-est de l'Angleterre. Cette argile est un exemple d'argile raide et fortement surconsolidée, qui a un comportement similaire à celui de l'argile de Londres. Cette recherche s’appuie sur une étude expérimentale pour trouver un cadre théorique pour le comportement d’un sol de cette nature.

Les échantillons d’argile, prélevés in situ à différentes profondeurs, entre 3 et 11 m, ont été caractérisés minéralogiquement (illite, quartz, kaolinite majoritairement) et physiquement. La couche est relativement homogène. Des échantillons sont ensuite testés dans leur état naturel puis dans leur état reconstitué (remanié) à l'aide d’essais œdométrique et d’essais triaxiaux. En particulier, on identifie une valeur probable du degré de surconsolidation (OCR), voisin de 20. Les effets de la structure, des fissures existantes dues à l’histoire du matériau et l'anisotropie du comportement mécanique de l'argile de Merville ont été analysés. Dans cette thèse, la dépendance de la réponse mécanique à la vitesse de déformation sur les échantillons naturels et remaniés d’argile de Merville à différents OCRs a également été étudiée.

Les paramètres mécaniques de résistance au cisaillement ont été identifiés au cours d’essais monotones triaxiaux consolidés non drainés, en compression et en extension. Ces paramètres présentent une certaine variabilité lorsqu’on les caractérise sur les échantillons intacts. C’est pour cela que nous avons opté également pour une caractérisation mécanique sur des échantillons reconstitués. Enfin, des essais cycliques à très grand nombre de cycles (plus d'un million) ont été réalisés sur l'argile de Merville. Seuls les forts rapports $R_c = q_{cy}/q_{max}$ de l’amplitude cyclique sur la résistance au cisaillement monotone amènent à la rupture, au cours d’essais alternés. On propose enfin une ébauche de diagramme contour et de diagramme de stabilité. La résistance au cisaillement monotone des échantillons soumis à un chargement cyclique précédent est supérieure à la résistance au cisaillement de l'échantillon sans chargement cyclique.

Mots-clés: Argile de Merville, fort degré de surconsolidation, essai triaxial; ligne d’état critique, dépendance de la vitesse de déformation, essai cyclique à grand nombre de cycles.

Introduction

Background of the research

Various design methods are proposed to engineers to calculate shaft capacity and base resistance of piles under axial and/or lateral loadings. In most cases, they provide precise specifications, often calibrated from field tests (CPT, pressuremeter), that allow to estimate the static capacity of piles. However, because of the development of offshore platforms in the last sixty years and the progress of wind turbines in onshore or near-shore zones nowadays, there is a need to better take into account the effects of time-dependent loads, for instance wind. Indeed, cyclic loading are usually introduced in the geotechnical design of structures through relatively large safety factors. Nevertheless, the base for a more rational approach exists because the behavior of soils under cyclic conditions has been largely investigated for many years. The transition from the elementary behavior of a soil specimen to the design of piles was initiated particularly by K. Andersen who first introduced stability diagrams. However, they are not yet currently used in geotechnical engineering.

As a consequence, the SOLCYP research project was launched, whose main objective was to consider the cyclic loading effects in a more rational way and to introduce them within current design rules. This project comprises different tasks, including:

- Investigation of the elementary behavior of soils (Fontainebleau sand, clays) and soil-structure interfaces;
- Physical modelling of piles through centrifuge testing ;
- Development of numerical strategies to take into account large numbers of cycles into modelling;
- Adaptation of design rules;
- Confrontation with field tests at Merville (in a highly overconsolidated and stiff clay) and at Dunkirk (in a relatively dense sand).

The present work is included in the SOLCYP national project during which field tests have been performed. We were in charge of the physical and mechanical characterization of the soil encountered at Merville, north of France.

Merville clay lying in the Flanders Region was deposited in a marine gulf which corresponds now to the northern France, Belgium and the southeast of England. This clay is an example of a stiff clay, which is similar to other such clays in terms of strength response, stiffness and destructuration processes. The most famous one of such similar clays is the London clay.

Previous experimental studies on the behavior of the clay lying in the Flanders Region (Borel, 2000; Reiffsteck, 2003) highlighted the importance of investigating the relationship between geology and experimental behavior for stratified materials. Studying Merville clay has therefore a general interest for a better understanding of stiff, overconsolidated clays, for which a common model of behavior could be desired. Moreover, the knowledge of the cyclic response of such clay is scarce, that is the reason why a specific campaign of cyclic tests has been carried out during the present research.

Objectives

This research aimed at finding a framework for the behavior of the Merville clay related to its engineering properties based on experimental test results.

Josseaume (1998) indicated that the clay lying at the Flanders Region is a structured, fissured clay and Hieng (1991) presented a series of experimental results, discussing some important parameters of the clay, such as the preconsolidation pressure. Burland (1990) presented a method to prepare the reconstituted samples and defined an intrinsic state to analyze the results of one-dimensional compression tests. Biarez & Hicher (1994) presented another method to normalize the compression curve of clays. The structural anisotropy arises from the structure of the soils, as a consequence of geological processes. In his paper, Burland (1990) presented the test results of London clay in two different directions (horizontal and vertical). Although the shear strengths were different at the same confining pressure, the failure envelopes of the specimens prepared in the two directions were similar.

In this work, an investigation of the physical properties of the Merville clay has been conducted with the support of laboratory experiments. The mechanical properties of the clay have been investigated in terms of stress-strain behavior and strength, considering the influence that structure, fissures and anisotropy have on the soil response. The samples stored in thin-wall PVC tubes were used from different depths within the Merville clay stratum. The clay has been tested in its intact and reconstituted states to highlight the influence of the clay structure for the natural material. The process that induces destructuration of the natural material, such as compression / swelling to high or low stresses, has also been analyzed, although the compression stresses were limited by the apparatus used. An investigation of the effect of anisotropy on the shear strength of the natural samples has been conducted.

Several authors (Zhu & Yin., 2000; Sheaham et al., 1996) have performed an analysis on the strain rate dependency of the shear strength of intact and reconstituted samples at low OCRs. An investigation of the strain rate dependency on the reconstituted and the natural samples of Merville clay at higher OCRs has been conducted.

Besides the research of Brown et al. (1975), few researchers have applied very large numbers of cycles on natural soils. Therefore, cyclic tests with a very large number of cycles (more than one million cycles) on clay samples have been performed in order to obtain the evolution of strains, pore pressure, and resilient modulus.

Based on data of the static and cyclic loadings, an overall behavior has been proposed, which could be expected to apply to similar stiff, fissured clays and to respond to the needs of the geotechnical engineering.

Structure of the thesis

This manuscript contains four parts.

Firstly, the geology of Merville clay is described, the soil profile was obtained based on the appearance and the physical properties of the clay. The microstructure of the clay has been analyzed by the CT imagining and SEM analysis. The mineral content was also obtained.

Secondly, the one-dimensional compression behavior of the clay was studied. One-dimensional compression tests at low and high pressures were conducted on reconstituted and natural samples. The preconsolidation pressure and the yield stress of the natural clay were obtained. The effect of the soil structure has been analyzed. The methods for normalizing the compression curves are introduced and the results of Merville clay are normalized by using these methods.

Thirdly, triaxial tests (UU, CIUC and CIUE) were conducted. The investigation of the shear strength from UU tests based on the Mohr circles at failure was performed. The strain rate dependency of the natural samples with four different OCRs (7, 14, 28 and 56) and of reconstituted samples with three different OCRs (1, 7 and 14) has been analyzed.

The tests for analyzing the anisotropy of the clay were conducted on natural samples prepared in two different directions (horizontal and vertical).

The critical state lines in compression and extension have also been obtained.

Finally, because of the existence of micro-fissures in Merville clay, the natural samples were considered not suitable for a comprehensive study of their behavior under cyclic tests with a large number of cycles. Reconstituted samples at OCR=4 were prepared and subjected to symmetrical two-way cyclic loading. The evolution of strain, pore pressure and resilient modulus has been analyzed and interpreted. A threshold value was obtained from the results of these cyclic tests, above which failure in cyclic regime would occur for a given number of cycles. The post-cyclic shear strengths were obtained by performing compression triaxial tests on specimens which did not failed during the cyclic loading.

Introduction générale

Contexte de la recherche

Diverses méthodes de conception ont été proposées aux ingénieurs pour calculer la capacité portante, addition du frottement latéral et de l'effort de pointe, de pieux sous charges axiales et/ou latérales. Dans la plupart des cas, ils fournissent des spécifications précises, souvent calibrées à partir d'essais sur le terrain (CPT, pressiomètre), qui permettent d'estimer la capacité statique des pieux. Cependant, en raison du développement des plates-formes pétrolières offshores dans les soixante dernières années et des éoliennes onshores et offshores de nos jours, il est nécessaire de mieux prendre en compte les effets des charges en fonction du temps, par exemple l'action du vent et/ou de la houle. En effet, les chargements cycliques sont généralement introduits dans la conception géotechnique des structures relativement importantes par des facteurs de sécurité. Néanmoins, la base d'une approche plus rationnelle existe parce que le comportement des sols dans des conditions cycliques a été largement étudié depuis de nombreuses années. De plus, la transition du comportement élémentaire d'un échantillon de sol à la conception des pieux a été initiée en particulier par K. Andersen qui a introduit les diagrammes de stabilité. Mais ils ne sont pas encore utilisés actuellement dans la géotechnique courante.

Ce constat a donné lieu en France au projet de recherche SOLCYP, dont l'objectif est d'examiner plus systématiquement les effets cycliques dans une approche plus rationnelle et de les combiner avec les règles de conception actuelles. Ce projet comprend différentes tâches, y compris:

- L'étude du comportement élémentaire des sols (sable de Fontainebleau, argiles) et des interfaces sol-structure;
- La modélisation physique des pieux par des tests en centrifugeuse;
- Le développement de stratégies numériques pour prendre en compte un grand nombre de cycles dans la modélisation;
- L'adaptation des règles de conception;

- La confrontation avec des tests sur le terrain à Merville (dans une argile raide très surconsolidée) et à Dunkerque (dans un sable relativement dense).

Travail réalisé

Le présent travail est inclus dans le projet national SOLCYP au cours duquel les essais sur le terrain ont été effectués. Nous étions en charge de la caractérisation physique et mécanique du sol rencontré à Merville, dans le nord de la France.

L'argile de Merville se trouvant dans les Flandres a été déposée dans un golfe marin qui correspond maintenant au nord de la France, la Belgique et le sud-est de l'Angleterre. Cette argile est un exemple d'une argile raide, qui est similaire à d'autres ces argiles en termes de processus de formation géologique, et en conséquence de comportement mécanique. La plus célèbre de ces argiles similaires est l'argile de Londres.

Les études expérimentales antérieures sur le comportement de l'argile se trouvant dans la même région (Borel, 2000; Reiffsteck, 2003) ont souligné l'importance de l'étude des relations entre la géologie et le comportement expérimental des matériaux stratifiés. Étudier l'argile de Merville a donc un intérêt général pour une meilleure compréhension des argiles raides, non uniformes, pour lesquelles un modèle commun de comportement pourrait être souhaitable. De plus, la connaissance de la réponse cyclique d'une telle argile surconsolidée est rare, c'est la raison pour laquelle une campagne spécifique de tests cycliques a été effectuée au cours de la présente recherche.

Objectifs

Cette étude a cherché à trouver un cadre pour le comportement de l'argile de Merville basé sur l'étude expérimentale de ce matériau.

Josseaume (1998) a indiqué que l'argile se trouvant dans les Flandres est une argile structurée fissurée et Hieng (1991) a présenté une série de résultats expérimentaux, en discutant certains paramètres importants de cette argile, telle que la pression de préconsolidation. Burland (1990) a présenté une méthode pour préparer les échantillons reconstitués et défini un état intrinsèque pour une meilleure analyse des résultats des essais oedomériques. Biarez & Hicher (1994) ont présenté

une autre méthode pour normaliser la courbe de compressibilité à l'oedomètre d'argiles de différentes minéralogies.

L'anisotropie mécanique provient de la structure des sols, comme une conséquence du processus de formation géologique. Dans son article, Burland (1990) a présenté les résultats d'essais sur l''argile de Londres dans deux directions différentes (horizontale et verticale). Bien que les réponses contrainte-déformation à la même pression de confinement soit différentes, les enveloppes de rupture de ces deux directions sont similaires.

Suite à ces travaux, une analyse des propriétés physiques de l'argile de Merville a tout d'abord été menée au laboratoire. Les propriétés mécaniques de l'argile ont ensuite été étudiées en termes de comportement contrainte-déformation et de résistance au cisaillement, prenant en compte l'influence de la structure, de la fissuration initiale et de l'anisotropie sur la réponse du sol. Les échantillons provenant de différentes profondeurs dans la couche d'argile de Merville stockés dans des tubes en PVC à paroi mince ont été utilisés. L'argile a été testée à l'état intact, et dans son état reconstitué pour mettre en évidence l'influence de la structure du matériau naturel. Les mécanismes qui induisent la déstructuration du matériau naturel, tel que la compression / gonflement à des contraintes élevées ou faibles, ont également été analysés, bien que les contraintes de compression ont été limitées par les appareils utilisés. Une étude de l'effet de l'anisotropie de la résistance au cisaillement des échantillons naturels a été effectuée. Plusieurs auteurs (Zhu et Yin, 2000 ; Sheaham et al, 1996) ont analysé l'influence de la vitesse de déformation sur la résistance au cisaillement d'échantillons intacts ou reconstitués à faible degré de surconsolidation. Une étude de la dépendance de la vitesse de déformation sur les échantillons remaniés et naturels de Merville à OCR plus élevés a été menée.

A l'exception de Brown et al. (1975), peu de chercheurs ont étudié l'effet d'un très grand nombre de cycles sur le comportement d'argiles naturelles ou remaniées. Par conséquent, nous avons réalisé des essais cycliques à très grand nombre de cycles (plus d'un million de cycles) sur des échantillons de l'argile de Merville pour obtenir l'évolution des déformations, de la pression interstitielle et du module cyclique.

Sur la base des données obtenues par les analyses en chargement monotones et cycliques, le cadre élaboré devrait pouvoir être étendu et s'appliquer à d'autres argiles raides fissurées similaires de façon à être utilisé pour les besoins de l'ingénierie.

Structure de la thèse

Le mémoire de thèse comprend quatre parties.

Tout d'abord, la géologie de l'argile de Merville est décrite, on obtient le profil du sol basé sur l'apparence et les propriétés physiques de l'argile. La microstructure de l'argile a été analysée par l'imagination CT et l'analyse SEM. Les teneurs en minéraux ont également été obtenus.

En second lieu, le comportement en compression oedométrique de l'argile a été étudié. Des essais oedométriques à basses et hautes contraintes ont été effectués sur des échantillons reconstitués et naturels. La pression de préconsolidation et le seuil de plasticité de l'argile naturelle ont été obtenus. L'effet de la structure du sol a été analysé. Les méthodes de normalisation des courbes de compression sont introduites et les résultats de l'argile de Merville sont normalisés à l'aide de ces méthodes.

Troisièmement, les essais triaxiaux (UU, CIUC et CIUE) ont été menés au laboratoire. L'analyse de la résistance au cisaillement des essais UU basées sur les cercles de Mohr à la rupture a tout d'abord été menée. La dépendance de la vitesse de déformation sur des échantillons naturels avec quatre OCRs différents (7, 14, 28 et 56) et sur des échantillons reconstitués avec trois OCRs différents (1, 7 et 14) a été analysée. Les essais pour l'analyse de l'anisotropie de l'argile ont été effectués sur des échantillons naturels préparés dans deux directions différentes (horizontale et verticale). Les enveloppes de résistance maximale en compression et en extension ont été obtenues.

Enfin, en raison de l'existence de micro-fissures dans l'argile de Merville perturbant les résultats, les échantillons naturels n'ont pas pu être utilisés pour effectuer des essais cycliques avec un grand nombre de cycles. Des échantillons reconstitués à OCR = 4 ont été préparés et soumis à des chargements cycliques alternés. L'évolution de la déformation, de la pression interstitielle et du module a été analysée et interprétée. Une valeur du seuil de rupture en chargement cyclique a été obtenue à partir des résultats de ces essais cycliques. La résistance au

cisaillement post-cyclique a été mesurée en effectuant des essais de compression triaxiale sur des échantillons n'ayant pas rompu pendant le chargement cyclique.

1 Literature review

1.1 Clay structure

In soil mechanics, the terms ‘structure’ and ‘bonding’ have generally been used to attempt to identify elements that may or may not be physical components of the soil (Cotecchia & Chandler, 1997). The basic elements of structure exist in all clays, and these elements should be seen as source of similarities in the behavior of different clays. It follows that, in comparing the mechanical behavior of natural and reconstituted clays in order to contribute to a better understanding of an overall clay behavior, one should first look at the similarities in behavior. Of course, there will be some differences which could be of major importance (Skempton & Northey, 1952). The properties of reconstituted clays are termed ‘intrinsic’ properties since they are inherent to the nature of the soil and independent of the natural state. Then the properties of a natural clay differ from its intrinsic properties due to the influence of soil structure (Burland, 1990).

The term ‘structure’ will be used here to define the combination of ‘fabric’, the arrangement of the component particles, and ‘bonding’, the interparticle forces, which are not of a purely frictional nature (Lambe & Whitman, 1969). Fabric includes inhomogeneities, layering, distribution of the soil particles and fissures (Coop & Cotecchia, 1995). Bonding is the combination of forces acting to connect the particles as well as to chemical reactions at contacts.

Although soils are composed of discrete particles and particle groups, a soil mass is almost always treated as a continuum for engineering analysis and design purpose. Nevertheless, the specific values of properties such as strength, permeability, and compressibility depend on the size and shape of the particles, their arrangements, and the forces between them, especially for fine-grained soils (Mitchell & Soga, 2005).

A clay particle is formed of a sequence of structural units constituted of minerals of hydrated layered silicates of aluminium and magnesium, which have a more or a less stable spacing depending on the strength of the links between the units. The constituent layers and the links between them define different minerals, such as kaolinite, illite and chlorite, which have stable

structures due to strong links between the units, and montmorillonite which has an unstable structure, as the basal links are provided by hydrated cations as shown in Fig.1.1 (Veniale, 1985; Blyth & De Freitas, 1984). The orientation and distribution of these particles in a soil mass define the fabric of the clay (Lambe & Whitman, 1969).

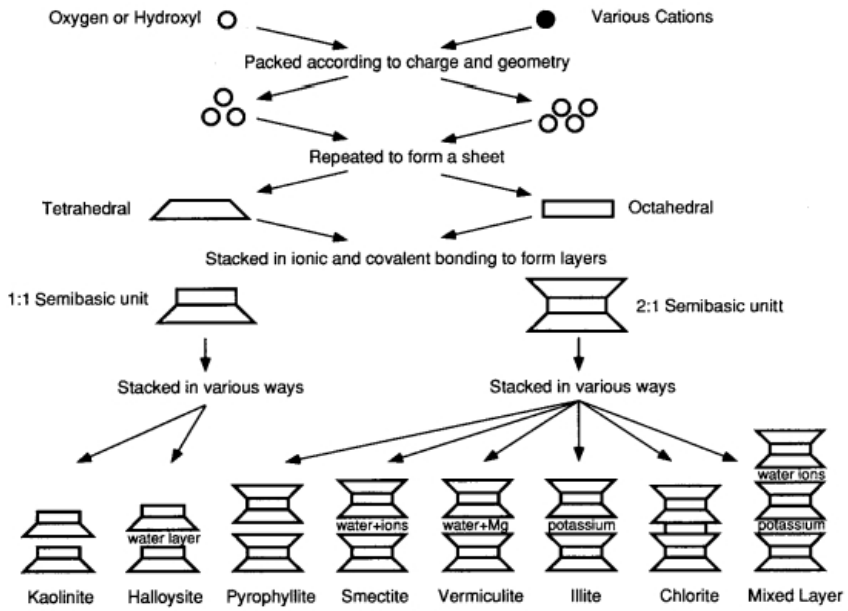

From Mitchell & Soga, (2005)

Fig. 1.1 Structure of the main clay units.

1.1.1 Clay fabric

Soil fabric is a main factor determining soil properties and behavior. It is necessary to consider the size, the form and the function of different fabric units and to keep in mind the scale at which the fabric is of interest. The strength of intact, homogeneous soft clay will be influenced greatly by the particle arrangements at a microscale, whereas that of stiff fissured clay will be mainly controlled by the properties of the fissures.

Many soil deposits are formed by deposition from flowing or still water. Accordingly, knowledge of particle associations in suspensions is a good starting point for understanding how soil fabrics are formed and changed throughout the history of a soil. Clean sands and gravels are usually comprised of single grain arrangements. Particle associations in clay suspensions may be more complex (Mitchell & Soga, 2005). Sides & Barden (1970) provided a classification of fundamental fabrics, which are summarized in Fig.1.2. If the net effects of the attractive and

repulsive forces between the clay particles are attractive, the particles will tend to move toward each other and become attached. They identify these particles as a flocculated fabric; if the net influence is repulsive they tend to move away, and they identify that as a dispersed fabric; a turbostatic fabric, where edge to face contacts are present between domains and stacks with highly oriented particles. For the flocculated fabric, they distinguish between a 'cardhouse' fabric with a single particle arrangement, the 'bookhouse' with particles arranged in groups, called domains, which are parallel, and the 'honeycomb' fabric characterized by non-uniform strains occurring during compression compared to the 'stack' fabric.

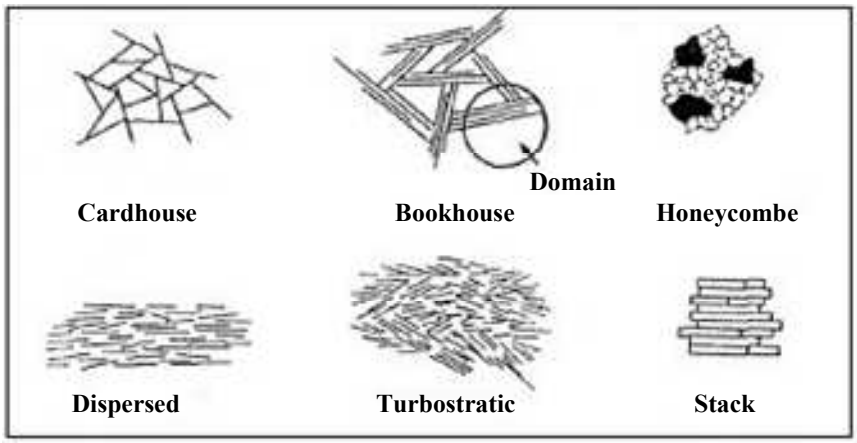

From Sides & Barden., (1970)

Fig. 1.2 Classification of fabric.

The condition of deposition significantly affects the fabric of the sediment and the two most significant factors are likely to be the rate of deposition and the stillness of the water. Slow deposition in still water leads to an open fabric. Rapid deposition, possibly with significant current, gives rise to a more orientated fabric, which is consequently more compact (Burland, 1990). The presence of pyrite framboids is usually an indicator of anaerobic sulphide diagenesis developing in the early stages of consolidation, implying the existence of a confined, reducing environment. The fabric formed during deposition is termed 'primary fabric' and it can be modified by post-depositional phenomena.

1.1.2 Bonding

The inter-particle bonding is defined as the combination of all the inter-particle forces, which are not of purely frictional nature. They can be of electrostatic or electromagnetic nature, such as Van der Waal forces and viscous stresses within the adsorbed water layer, or, in general, all the

factors acting to keep the soil particles together. Bonding is not necessarily (although it may be) a solid link, particularly with clays.

Because interatomic bonds within clay particles are strong primary valence bonds, whereas usual interparticle bonds are of the secondary valence or hydrogen bond type, individual particles are strong compared to groups of particles. Thus, most soil masses behave as assemblages of particles in which deformation processes are dominated by displacements between particles and not by deformations of particles themselves. The type of bonding between the unit layers of the clay minerals, coupled with the adsorption properties of the particle surfaces, controls soil swelling.

The structure of clay, as defined above, is thus a physico-chemical equilibrium between the soil particles. This equilibrium develops during the geological life of the soil as a result of mineralogy, electrostatic and magnetic interactions between crystals, ion concentration and water chemistry during deposition, osmotic pressure, temperature and organic content. Either externally induced variations of these factors or the development of chemical reactions within the sediments can cause substantial changes of both the fabric and the bonding of the clay with time. Depositional and post-depositional processes contribute, therefore, to the formation and the evolution of the soil structure, which can be considered as the result of all the processes that a soil has undergone during its geological history.

Because soils behave as particulate materials and not as continua, knowledge of these internal forces and of the factors influencing them is a necessary pre-requisite to the understanding and quantification of compressibility, deformation, and strength in constitutive relationships.

1.1.3 Anisotropy

If the distribution and shapes of particles are statistically independent of the orientation of the chosen axes, the clay can be considered isotropic. That is to say, its mechanical properties are isotropic and thus the mechanical law which governs its behavior will be isotropic, and can therefore be written independently of the orientation of the axes chosen to define the stress and strain tensors. But in general, the natural clays are commonly anisotropic because of their mode of deposition (Hicher, 1985; Graham & Houlsby, 1983).

Depositional and post-depositional processes define the conditions of equilibrium of the particles and contacts and therefore govern the soil response to subsequent changes in stresses and strains. The particle deposition and compression occur under gravity and hence are directionally dependent. Particle arrangement and contacts are therefore anisotropic. This determines differences in the soil response depending on the direction of the application of the stress changes. For example, nonspherical particles tend to deposit with their long axial in the direction perpendicular to gravity, and, therefore, the assembly will be inherently stiffer in the depositional (vertical) direction than in the horizontal direction. This is inherent or structural anisotropy.

The inherent or structural anisotropy arises from the structure of the soils, as a consequence of geological processes, which is created by the application of an anisotropic stress tensor during deposition. It refers strictly to natural soils, if it were possible to reconstruct the complete history of a sample it would not be necessary to distinguish between the inherent anisotropy and induced anisotropy which might be expected to exist in reconstituted soils that have undergone an anisotropic plastic strain history. This strain-induced anisotropy can be distinguished from the "stress induced" anisotropy, (Ballester & Sagaseta, 1979) which results solely from the anisotropy of the current stress condition and is independent of the strain and stress history of the material. Biarez & Hicher (1994) described this 'stress induced' anisotropy as mechanical anisotropy.

1.1.4 States of structure

In their paper, Leroueil et al. (1984) described that the clayey soils can be encountered or produced in four different states of structure, based on their experience: intact, destructured, remoulded and resedimented clays. The intact state occurring during natural deposition is created by the complex geological processes, such as deposition environment, weathering etc. The destructured state is obtained from intact clays submitted to strains large enough for the original clay structure to be broken. The remoulded state is defined by the fact that the clay strength is reduced to a minimum by imparting sufficient mechanical energy. The resedimented state is obtained by deposition of clay particles originally remoulded and mixed to slurry and by consolidation under the self-weight of the soil column of increasing thickness. Experimental studies done by Locat (1982) put clearly in evidence the different behaviors of a clay in the various structural states defined previously, shown in Fig.1.3.

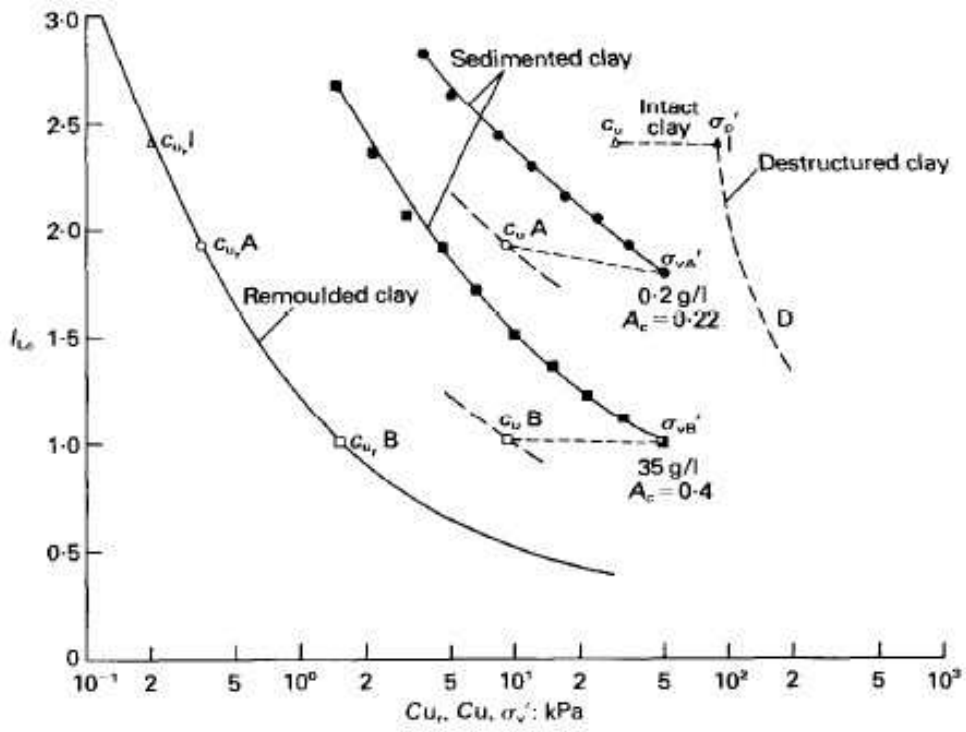

From Locat & Lefebvre, (1982)

Fig. 1.3 Undrained shear strength-liquidity index and effective stress-liquidity index relations for Grande Baleine clay.

In this work, the term ‘structure’ mentioned above is used for clays in their intact state. To understand the properties of clays better, besides the intact clays, the clays which we call ‘remoulded’ or ‘reconstituted’ clays are of interest. The reconstituted clays correspond to the destructured state (Gasparre, 2005). They have been thoroughly mixed at a water content equal to or greater than the liquid limit (preferably $1.25w_L$) without air drying or oven drying, and then consolidated preferably under one-dimensional condition. Ideally the chemistry of the water should be similar to that of the pore water in the clay in its intact state. Burland (1990) therefore defined the properties of a reconstituted soil as ‘intrinsic’. The term intrinsic has been chosen since it refers to the basic, or inherent, properties of a given soil prepared in a specified manner and which are independent of its natural state. Because the water content of the slurry and the pressure for consolidation of the reconstituted state are different with those of the resedimented state. The ‘reconstituted state’ is the state of a fully ‘destructured material’ which is the fifth important state of structure in addition to the four states defined by Leroueil et al. (1984).

1.1.5 Degree of sturcturation

Most clays lose a proportion of their strength when remoulded (Skempton & Northey, 1952). The loss of strength that accompanied the disturbance of many natural clays is quantified by the sensitivity S_t of the undisturbed structure as the ratio of the undisturbed to fully remolded strength at the same water content (Fig.1.4).

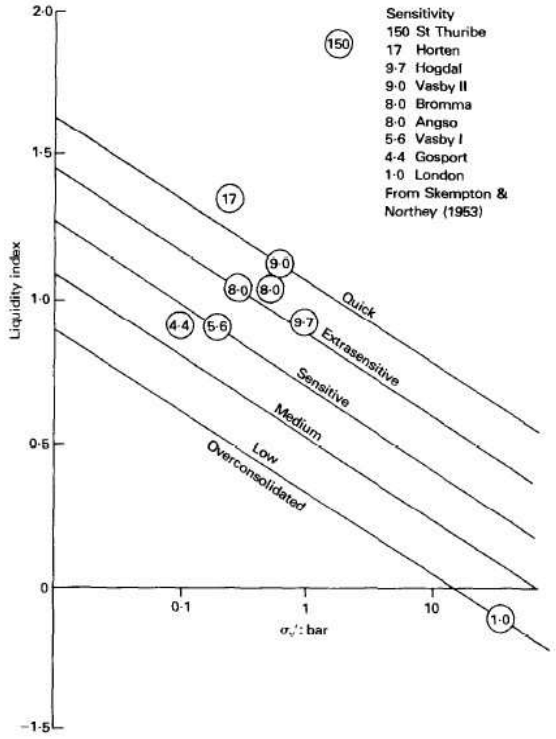

From Leroueil et al., (1984)

Fig. 1.4 Sensitivity chart.

The sensitivity is generally regarded as the parameter embodying the differences of the microstructures of the natural and the remoulded clay (Cotecchia, 1996). Schmertmann (1969) defined "swelling sensitivity" S_s as the ratio of the intrinsic to the intact swelling indices C^*_s/C_s, which may be a sensitive indicator of fabric and interparticle bonding in the natural soil.

The enhanced resistance of natural clays (especially highly overconsolidated) to compression is also reflected in shear strengths that are located above the intrinsic State Boundary Surface (*SBS*) defined by the Critical State Framework (Smith et al., 1992; Burland, 1990).

Burland et al. (1996) observed that the ratio of the normalized strength at the critical state (DE/DF in Fig.1.5) could be useful in measuring the influence of the material structure. They highlighted also that the cohesion is a significant parameter of bonding and the ratio between the

cohesion of the natural and reconstituted materials might also be used to evaluate the structure effect. In measuring the cohesion, the curvature of the failure surface of the natural material at very small stresses should be taken into consideration.

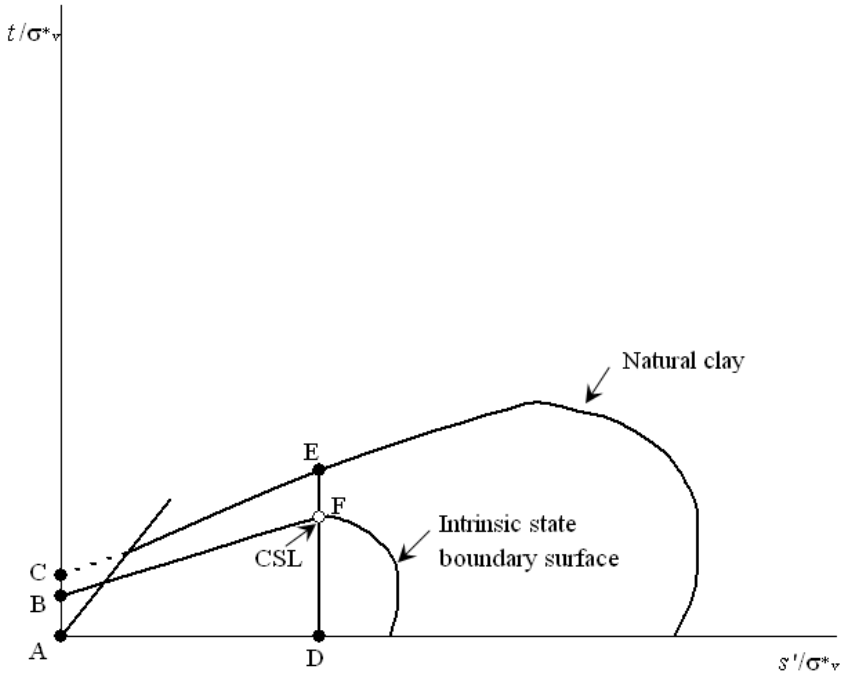

From Burland, (1996)

Fig. 1.5 Comparison of natural and intrinsic state boundary surface showing increased resistance to compression and shearing.

1.2 One-dimensional compression behavior of soils

The compression of soil comprises the volume reduction due to the compression of all the constituents (soil particles, pore water, pore air, etc.) and the consolidation corresponding to the decrease of the pore volume (emigration of the pore water). In this thesis, we consider only the volume change due to consolidation. The underlying assumption is that the soil in consideration is well saturated so that it has very low undrained compressibility. In this section, we limit our focus on K_0 compression-oedometer tests, as they are conventionally considered in laboratory as 'consolidation tests'. An oedometer consists of a confining ring housing a tested soil sample and a top cap with a porous stone through which pore water can escape. The vertical load may be applied by dead weights, pneumatic pressure, motor, etc. Usually, only the vertical stress is known in an oedometer test. For the horizontal directions, we only know the imposed condition of zero

normal strain; the horizontal stresses are expressed as $K_0\sigma'_v$. There are two ways of applying vertical loads: (1) (Conventional) step loading: this is the simpler, classical, standard method. Vertical loads are increased in steps by, for example, adding dead weights. (2) *CRS* (Constant rate of strain) loading: the vertical strain is increased at a constant rate by means of a loading machine. Therefore, the e - $\log(\sigma_v)$ relationship is obtained continuously. The strain rate has to be small enough to prevent any pore water rise during the compression (perfectly drained condition).

A detailed analysis should be made of the compression behavior of soils from oedometer tests, investigating the effects of the soil structure through comparison between the behavior of the intact soil and that of the same soil in a reconstituted state. The normalizing parameters commonly used in the literature to analyze the effects of structure on the compression behavior of clays are presented in the following section. When the state in the effective stress space excesses the initial elastic domain, the soil stiffness decreases significantly and the destructuration begins to occur.

1.2.1 Normalizing factors

Based on the results of the one-dimensional compression tests of normally consolidated reconstituted clays, Biarez & Hicher (1994) have presented a diagram to normalize the sediment curve of clays. Based on this diagram, we can predict the compression index C_c at the given Atterberg limits (w_L and w_P). This method will be discussed in Chapter 3.

Burland (1990) proposed to use instead the *ICL* line (Intrinsic Compression Line), the term 'intrinsic' being applied to the properties of reconstituted clays. In what follows, the symbol '*' will refer to the intrinsic properties of the materials. The intrinsic compression curves for various reconstituted clays in the e - σ'_v plane is shown in Fig.1.6. These curves can be normalized by a normalizing parameter which is defined as the void index I_v which will be described in Chapter 3.

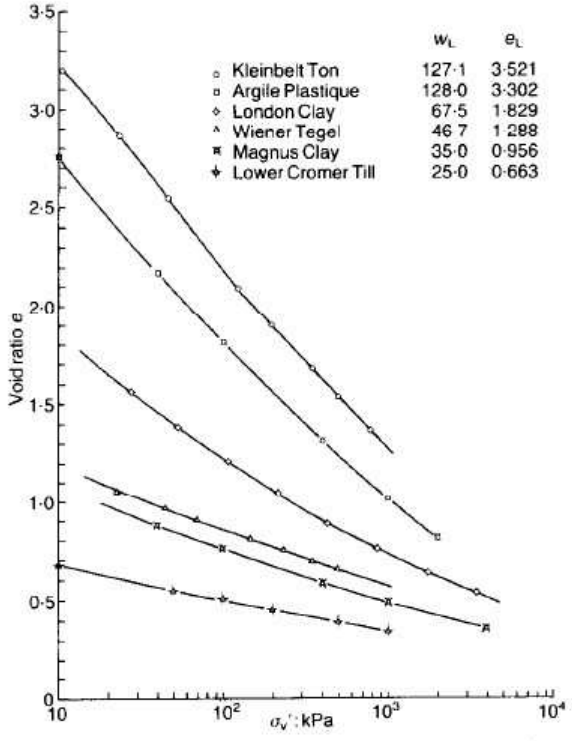

From Burland, (1990)

Fig. 1.6 One-dimensional compression curves for various reconstituted clays.

The void index may be thought of as a measure of the intrinsic compactness of a sediment. When I_v is less than zero the sediment is compact, whereas, when I_v is greater than zero the sediment is loose.

Clearly, there is a close analogy between the void index (= $(e - e^*_{100})/ C^*_c$) and the liquidity index (= $(w - w_p)/(w_L - w_p)$). It is of the utmost importance to be clear about the difference between these two indices. The void index is defined in terms of two directly measured mechanical properties (e^*_{100} and C^*_c) derived from a one-dimensional compression test. In contrast liquidity index is defined in terms of two essentially empirical tests (the liquid limit and plastic limit tests) both of which subject the soil to extremely complex physical processes.

In terms of void index I_v versus $\log(\sigma'_v)$, it can be seen that a reasonably unique line is achieved (Fig.1.7) which is termed the intrinsic compression line (*ICL*). The equation of the *ICL* is represented in Chapter 3. The available experimental evidences suggest that the ICL is insensitive to the test conditions.

Burland (1990) fitted a regression line through the natural sedimentation compression curves given by Skempton (1970), and identified a unique Sedimentation Compression Line (*SCL*). The *SCL* of the natural soils lies above the *ICL* as result of the structure developed by the natural soils during the sedimentation process and the distance between the *ICL* and the *SCL*, called the "sedimentation sensitivity" (S_t), is a measure of the acquired strength of the natural sediments with respect to the strength of the reconstituted clay.

The differences between intact strength and intrinsic strength are due to two main factors: the void ratio at failure and the soil structure (fabric and bonding) (see Fig.1.8). The influence of the void ratio can be eliminated by a normalizing parameter termed the 'equivalent intrinsic pressure' σ^*_{ve}. It is defined as the vertical effective pressure on the *ICL* corresponding to the void ratio of the soil. Dividing the strength by the normal effective pressure eliminates the influence of the differences in void ratio as shown in Fig.1.9.

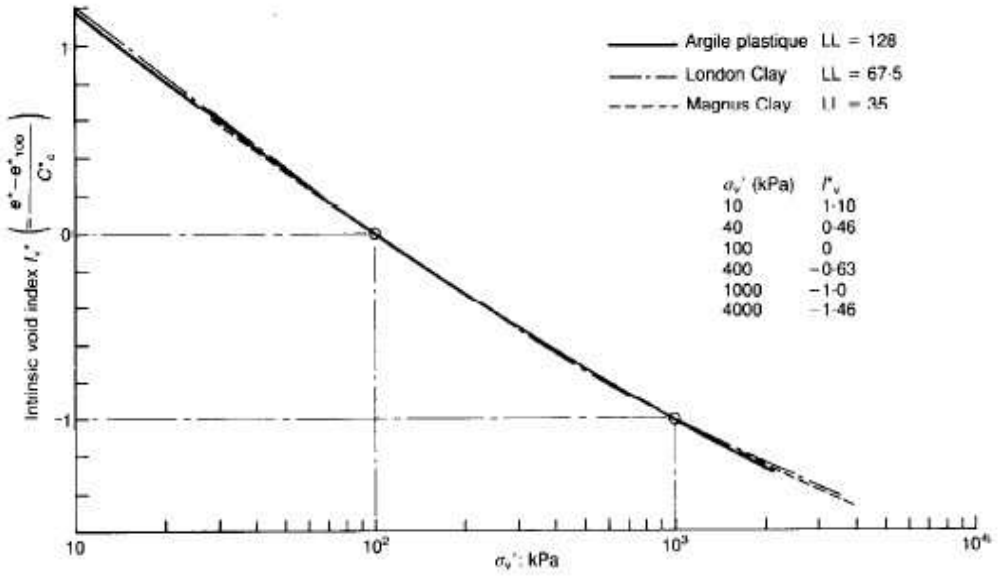

From Burland, (1990)

Fig. 1.7 Normalized intrinsic compression curves giving intrinsic compression line.

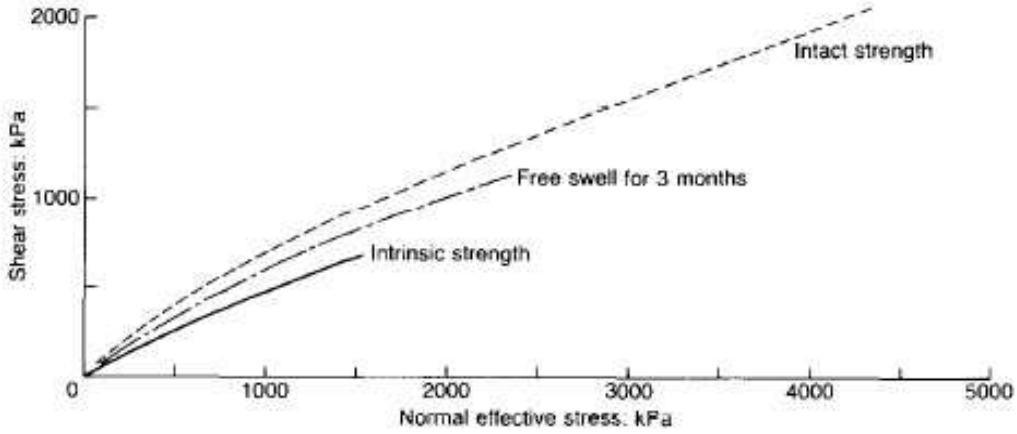

From Burland, (1990)

Fig. 1.8 Todi clay: Mohr-Coulomb failure envelops.

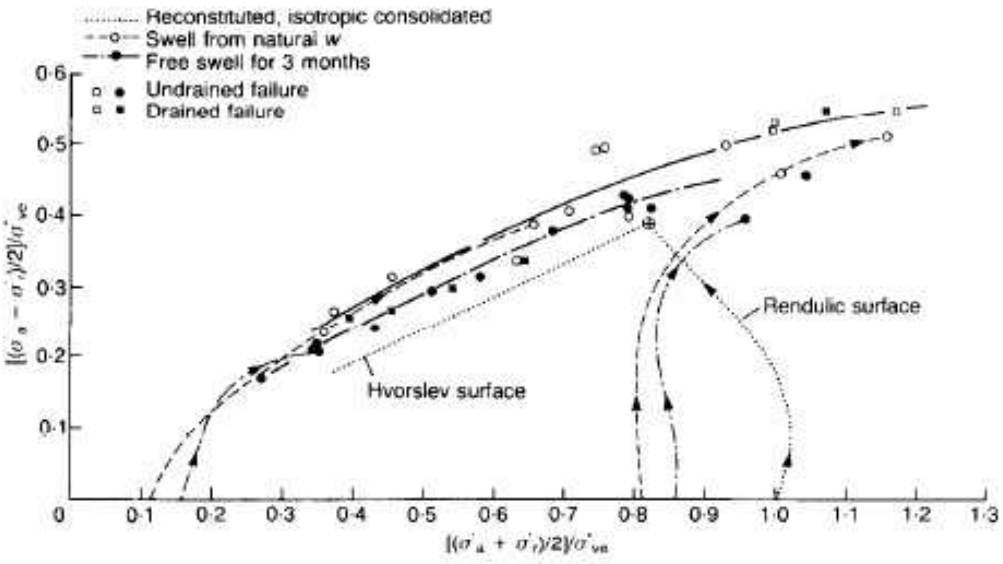

From Burland, (1990)

Fig. 1.9 Todi clay: results normalized by the equivalent pressure σ^*_{ve} at failure.

1.2.2 Post-yield behavior

Hight et al. (1992) used the term ‘gross yield’ to refer to the state, mentioned above, at which the soil stiffness decreases significantly. Beyond gross yield, the plastic strain increments become substantially larger as a result of the degradation of the soil structure. This structural degradation is defined as ‘destructuring’ by Leroueil & Vaughan (1990). Generally, a substantial change in the hardening relationship occurs at gross yield, which is reflected in changes in the relationship of both strength and stiffness with the consolidation *v*-*p*' state. The locus of the gross yield states, in both compression and shear, is thus likely to be important in modeling soil behavior.

Cotecchia & Chandler (2000) showed that an overconsolidated natural clay, if reloaded one-dimensionally, exhibits gross yield as it reaches the *SC* curves (Y in Fig.1.10), at a stress σ'_{vy} which is close to the geological preconsolidation stress σ'_{vc}. This behavior may be exhibited by either reconstituted or natural clays (paths R-Y^* and O-Y, Fig.1.10). Both types of clay return to a sedimentation structure as they reach the *SC* curve. However, oedometer reloading of natural undisturbed samples, or in situ reloading at an engineering time scale, occurs at relatively high loading rates compared with geological time-scale rates, resulting in the oedometer compression curve falling below the *SC* curve (path Y-Z_2). The oedometer compression curve will follow the SC curve (path Y-Z_1) if the sensitivity of the clay is low ($S_t \approx 1.0$ to 1.5), or if loading rates are comparable to those of geological time. However, many natural clays will possess a post-sedimentation structure that reflects some diagenesis, so that with oedometer reloading they retain post-sedimentation structural elements and cross the *SC* curve, moving some distance to the right before gross yielding (path O-Y shown in Fig.1.11). In this case, the post-sedimentation structure still dominates the clay's behavior at stress levels greater than the previous geological loading. Hence, clays with a sedimentation structure at gross yield will have a 'yield stress ratio', ($YSR=\sigma'_{vy}/\sigma'_{v0}$; Burland, 1990) equal to the overconsolidation ratio ($OCR=\sigma'_{vc}/\sigma'_{v0}$). Clays which retain a post-sedimentation structure at gross yield have a yield stress ratio which exceeds the overconsolidation ratio. In general, the yield stress may be unrelated to the stress history of the soil, and so for a natural clay it is the yield stress ratio, rather than the geological overconsolidation ratio, which controls compression and strength behavior.

After gross yield (path Y-Z_3), the sample follows a path steeper than the *SC* curve, its gradient depending on the subsequent structural changes. It has been observed that the compression curve after yield can converge towards the *ICL*, demonstrating a "meta-stable" structure that degrades with strains, or move along a line parallel to the *ICL*, demonstrating the presence of "stable" elements of structure that do not degrade with strains. In Fig.1.12, the compression curves of Boom Clay, with a meta-stable structure, and Sibari Clay, with a more stable structure are presented (Coop & Cotecchia, 1995). In Fig.1.13, the swelling sensitivity indices, i.e. C^*_s/C_s, as compression proceeds are shown (Burland, 1995). As a result of structural breakdown of Boom clay, the swelling curves of the intact material tend to become parallel to the

intrinsic swelling curve of the reconstituted soil. A soil can have both stable and meta-stable elements, so that after yielding the compression curve of the natural material can bend downwards towards the *ICL*, due to the breakdown of the metastable elements, but can then stabilize on a line which is parallel to the *ICL* and above it due to the presence of stable elements. Coop & Cotecchia (1995) suggested that the meta-stable elements in structure are likely to be associated with bonding, while the stable elements are likely to result from fabric. Baudet & Stallebrass (2004) allowed stable and meta-stable elements of structure to be modeled considering the intrinsic proprieties of the soils, which do not require high pressure tests on natural samples to be performed.

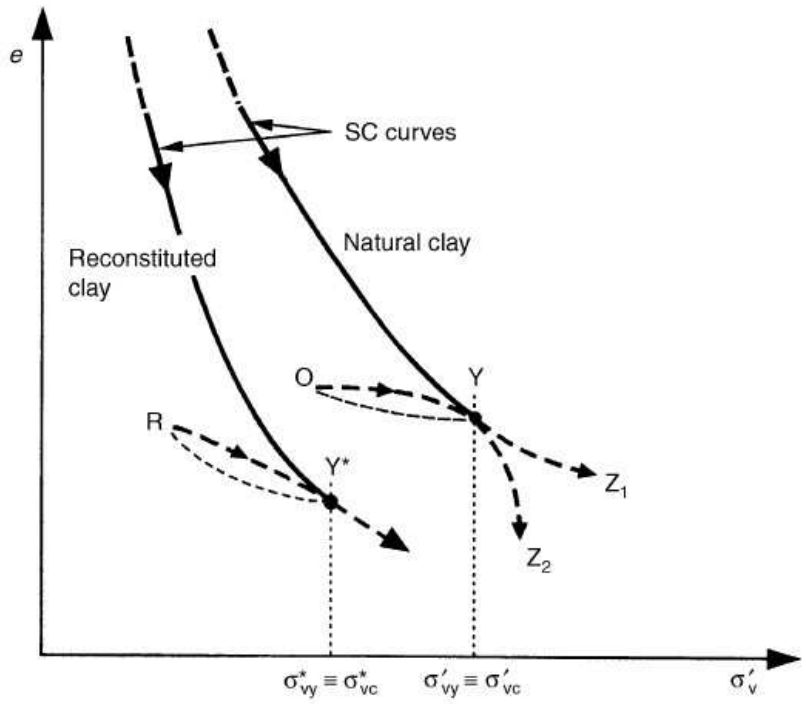

From Cotecchia & Chandler, (2000)

Fig. 1.10 The natural clay is simply overconsolidated.

The yielding state is demonstrated by a discontinuity in the stress-strain behavior under monotonic stress changes. Yield of structure is demonstrated by an irreversible post-yield change in the stiffness and strength of the material. The yield stress is strain-rate dependent and increases with the strain rate. This has been observed in structured clays (Lo & Morin, 1972; Sangrey, 1972; Tavenas et al., 1978; Graham et al., 1983; Leroueil et al., 1985).

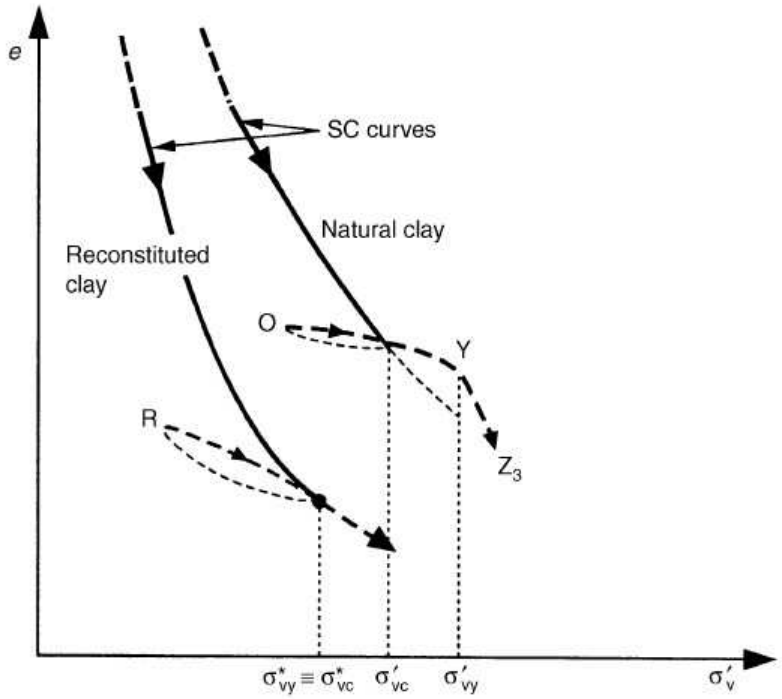

From Cotecchia & Chandler, (2000)

Fig. 1.11 The natural clay is overconsolidated with a post-sedimentation structure at gross yield.

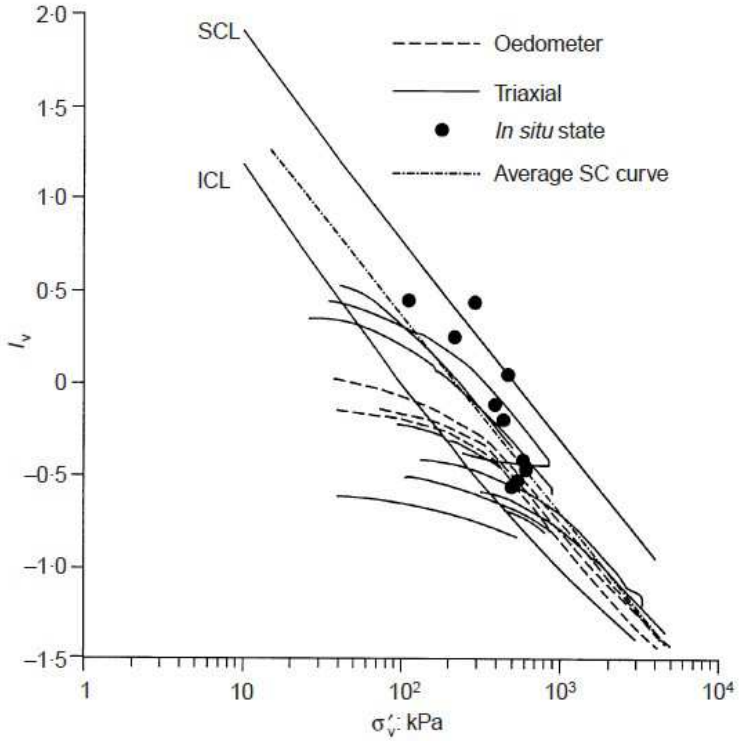

From Coop & Cotecchia, (1995)

Fig. 1.12 One-deimensional compression behavior of the Sibari Clays.

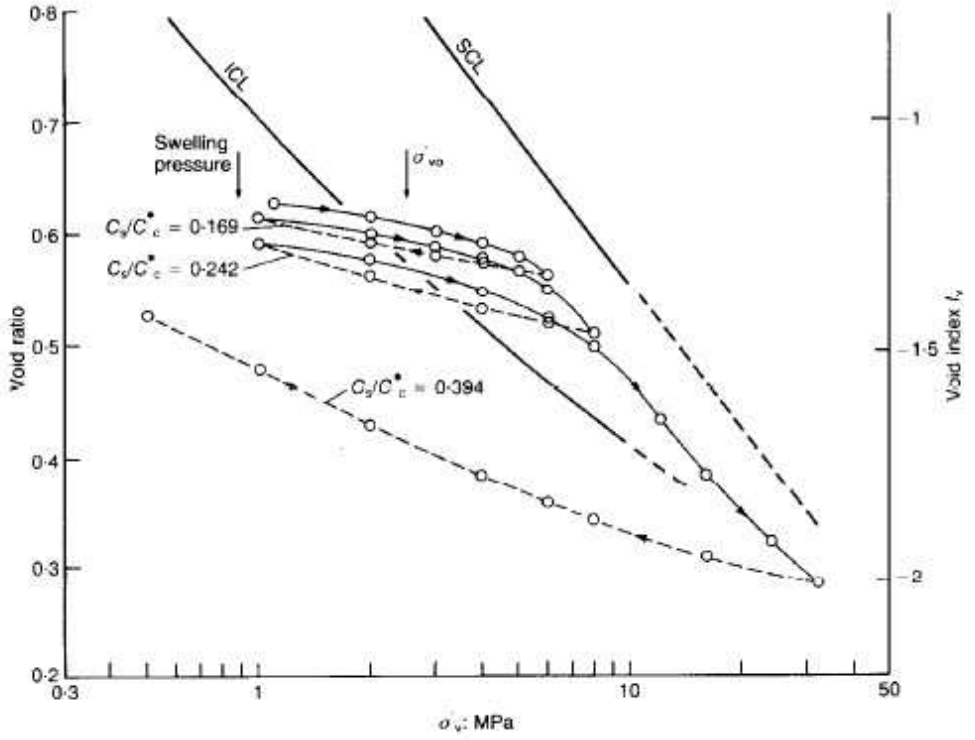

From Burland, (1990)

Fig. 1.13 Boom Clays.

1.2.3 Destructuration

Destructuration is related to the cumulative volumetric and deviatoric plastic strains, the "destructuration strains", which can occur during both consolidation and shear stages. The mechanism of destructuration depends on the direction of the stress path (Kavvadas & Amorosi, 2000; Baudet & Stallebrass, 2004) and on the fabric of the soil. The arrangement of the particles influences the capability of the soil to sustain better one or the other component of the "destructuration strains". The influence of the two components of the destructuration strains is still the subject of debate in the literature.

Leroueil & Vaughan (1990) pointed out that swelling might cause changes to the structure of some soils through disruption of interparticle bonding and yield, similar to that induced by compression to very high pressures. Some swelling tests were carried out on Gault Clay (Samuels, 1975). In Fig.1.14, after loading up to 7000 kPa, the first sample had become approximately twice as expansive as the one only subjected to unloading (C_s/C^*_c =0.166 and 0.098, respectively). And the cyclic swelling and compression oedometer test is a well adapted procedure to investigate the

susceptibility of the clay to structural breakdown. Thus, this loading process must lead to the destruction of part of the bonding. Since the slope of the swelling curve of the intact material typically starts changing as soon as the destructuration begins and is expected to be parallel to the intrinsic swelling curve when the destructuration is complete, we can use the swelling sensitivity (C^*_s/C_s) which could be argued to be more representative in showing the evolution of the effects of structure with stresses.

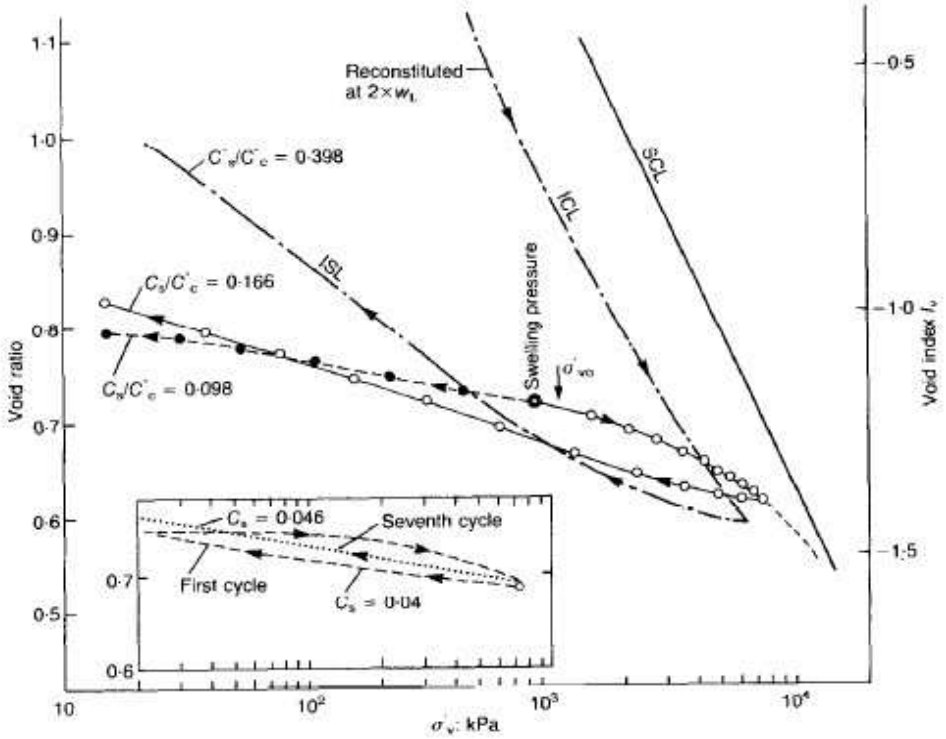

From Samuels, (1975)

Fig. 1.14 Gault Clay.

1.3 Factors affecting the tri-dimensional behavior of soils

When we perform static triaxial tests in the laboratory, the soil behavior is affected by many factors, such as the sample dimensions, the fissures in the sample, the anisotropic consolidation, the strain rate, the membrane effect etc. In this section, we limit our focus on the anisotropic consolidation, the strain rate effect and the role of fissures. At the end of this section, we discuss some factors affecting the strength at large strains.

1.3.1 Strain rate effects

Tavenas & Leroueil (1977) and Tavenas et al. (1978) presented results showing the strain rate effects on several parts of the limit state curve. Graham et al. (1983) obtained similar results from triaxial (in compression and extension) and oedometer tests. Boudali (1995) studied the strain rate effects along different loading paths, showing that the entire limit state was dependent on the strain rate. More specifically, he showed that the limit state curve varies homothetically with the strain rate, its shape remaining the same.

To characterize the influence of the strain rate on the shear strength, Bjerrum (1973) proposed that the undrained shear strength varies almost linearly with the logarithm of the strain rate. This relationship will be discussed in Chapter 4. To avoid the problem related to the spatial variability of the natural clay characteristics, Graham et al. (1983) advocated performing tests with relaxation phases and by-step changes of the strain rate (Fig.1.15) to quantify the influence of the strain rate.

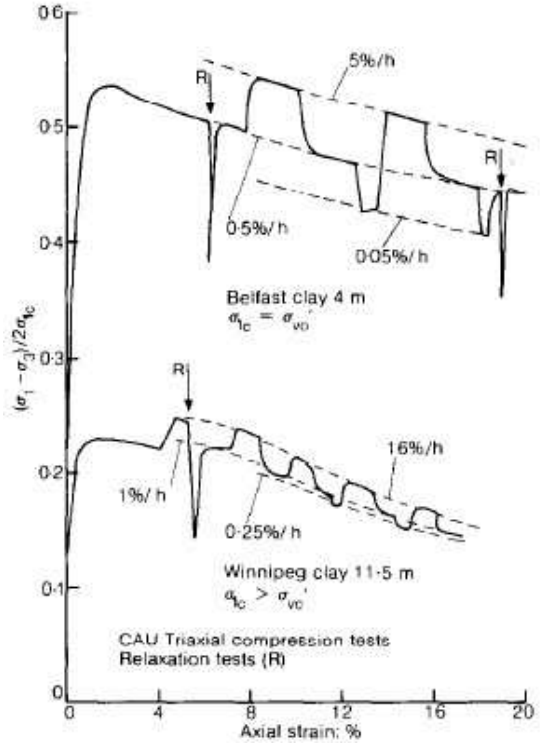

From Graham et al., (1983)

Fig. 1.15 Stress-strain curves for triaxial compression tests at different rates.

The strain rates used to investigate the strain rate dependency appear often to be quite high, especially for clays, and therefore undissipated or non-uniformly distributed pore pressures could affect the data. Overshooting and undershooting effects are more evident in sand or dense gravel, where drainage and pore pressure distributions are less problematic. In his thesis, Gasparre (2005) showed that the measurements of the actual pore pressure became problematic at high rates of shearing and even the mid-height probe was not free from these effects. From slow and medium rate (less than 0.2%/min) shear tests on London Clay, up to the maximum pore pressure, the behavior of London Clay was insensitive to the rate of shearing, but at faster shearing rates the undrained strength of the soil increased. He observed that the failure strains tended to decrease with increasing the rate of shearing, but the strains at the maximum pore pressure were unaffected by the rate of shearing. The author observed that the behavior of the clay was influenced by the negative pore pressures generated on the shear plane, and at faster shearing rates the time for equalization of pore pressure was smaller.

The undrained shear strength and apparent preconsolidation pressure of soils decrease with decreasing strain rate or increasing duration of testing. Preconsolidation pressures obtained from one-dimensional consolidation tests and undrained shear strengths obtained from triaxial tests are just two points on a soil's yield envelope in the stress space. For a given metastable soil structure, the degree of strain rate dependency of the preconsolidation pressure is similar to that of the undrained shear strength (Soga & Mitchell, 1996). If the apparent preconsolidation pressure depends on the strain rate at which the soil is deformed, then the same analogy can be expanded to the assumption that the size of the entire yield envelope is also strain rate dependent (Tavenas & Leroueil, 1977). The effective stress failure line of soil is uniquely defined regardless of the magnitude of the strain rate applied in undrained compression (Nakase & Kamei, 1986). The rate dependency of the undrained shear strength decreases with increasing overconsolidation, since there is no contraction or collapse tendency observed during creep of heavily overconsolidated clays. Sheahan et al. (1996) prepared reconstituted specimens of Boston blue clay at different overconsolidation ratios and sheared them at different strain rates in undrained conditions. The results show that the undrained stress path and the strength were much more strain rate dependent for lightly overconsolidated clay (*OCR* =1 and 2) than for the overconsolidated clay (*OCR* =4 and

8). The results also show that the shape of strength failure envelope is independent of the strain rate.

1.3.2 Effect of fissures

Some materials have natural discontinuities, which are often the result of stress release arising from some geological processes (Skempton et al., 1969).

Biarez & Hicher (1994) showed that during one-dimensional unloading, the ratio $K = \sigma'_h/\sigma'_v$ increases and at a given point the horizontal stresses become greater that the vertical one.and it is possible to reach the plastic limit (point P in Figure 1.16). This plastic unloading is often accompanied by the beginning of cracking. As a consequence, highly overconsolidated clay can present in situ intensive fissuration sometimes over more than 10m in the upper part of the clay layer.

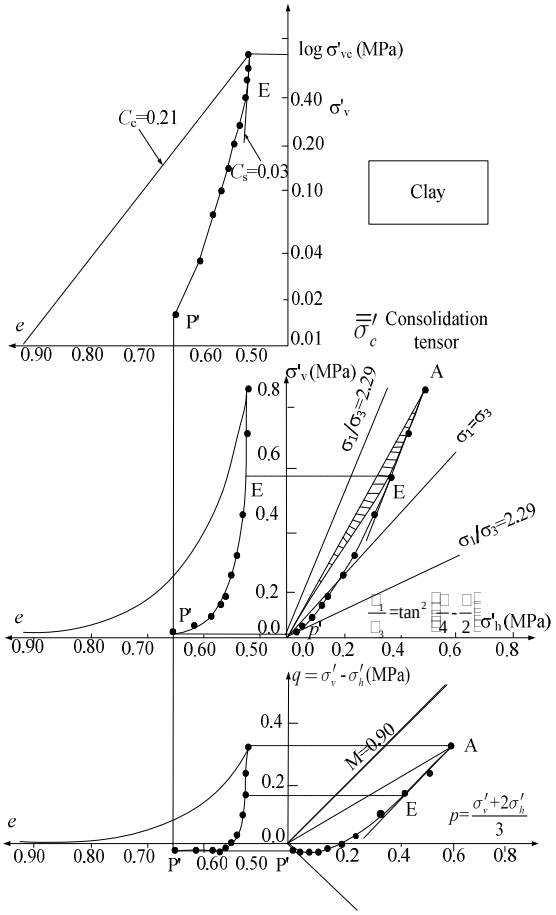

From Biarez & Hicher, (1994)

Fig. 1.16 Clay behavior during 1D unloading.

In this thesis, the Flanders clay in Merville has a similar geological history as the London clay. Hence, we present here the description of the fissures in London clay. London clay is categorized as an overconsolidated, fissured stiff clay of high plasticity. The fissures in the clay have relatively small sizes, with a typical length of less than 15 cm. The fissures generally become smaller, their number per unit clay volume increases and their spacing becomes smaller towards the ground surface. The fissures typically have matt surfaces, implying no trace of shearing along them. This is also supported by the fact that no change in orientation of the clay particles was recognized when observed with a polarizing microscope. The surface shape can be either planar or conchoidal (Nishimura, 2005; Molenkamp, 1998; Bishop, 1966).

Fissures seem to increase the permeability of the material, even if they are apparently closed and are thought to be responsible for the so-called ‘sample size’ effect on strength measurements.

Fissure influence is a problem difficult to quantify because it involves both the form of the fissures and their spacing, their length and orientation. Fissures affect the overall behavior of the clay, particularly its failure characteristics. In the case where the rupture occurs along a fissure, one obtains a lower limit of the shear strength; if rupture occurs within the intact soil mass, an upper limit of the shear strength is then obtained, as showed in Fig.1.17 (Ward et al., 1965). Skempton (1964) suggested that, in addition to reducing the London clay strength and allowing the clay to soften, the fissures cause concentrations of shear stresses which locally exceed the peak strength of the clay and lead to progressive failure. Various studies have been conducted on the influence of fissures on the geotechnical characteristics of clay, in particular by Skempton & La Rochelle (1965), and Skempton et al. (1969), who showed that, unlike the shear strength which can decrease by 20% to 30%, the internal friction angle is not very much affected by the presence of fissures.

Hieng (1991) indicated that the remolding of the samples during the sampling operations and preparation of test specimens occurs in two ways: firstly, a mechanical distortion and, secondly, a stress relaxation at the peripheral part of the sample. And this stress relaxation can lead to a modification of the initial stress system. This phenomenon is even more harmful for a fissured clay, because the stress relaxation can induce the opening of the existent fissures, and also leads to the creation of new fissures. The geological formation of Flanders Clay has been subjected to

significant unloading. So there is a good reason to think that Flanders Clay has an extensive network of fissures. But it should be noted that pre-existing fissures in a clay sample can influence its shear strength; in most cases there is the formation of new fissures or widening of old ones, whereas certain are closed during shearing. This makes it difficult to complete analysis of laboratory tests, especially for undrained tests. The lowest values of the shear strength are obtained on specimens with a fissure whose orientation coincides roughly with the fracture plane, whereas the maximum values of the shear strength are obtained from specimens without fissures. Intermediate values of resistance are obtained with samples having a variety of micro-cracking. This classification of the shear strength according to the fissure network can also be seen in Fig.1.17 (Ward et al., 1965). Josseaume (1998) showed that the shear strength of the fissured samples is much lower than the remoulded samples in laboratory and in-situ tests on Flanders Clay. And based on the results of triaxial tests, Hieng (1991) noted that the behavior of the Flanders clay can be based on the sketch in Fig.1.17.

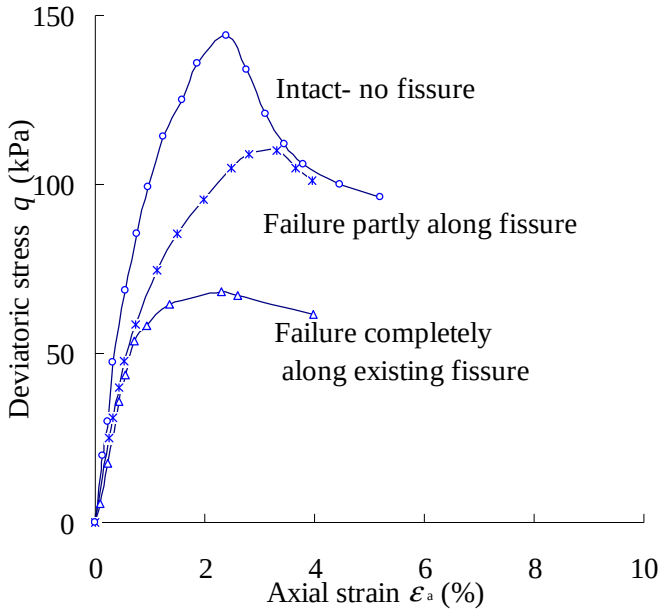

From Ward et al., (1965)

Fig. 1.17 Effect of fissures on laboratory stress-strain characteristics.

In Hicher & Shao (2002), Biarez & Hicher collected and compared test results obtained by Bishop et al. (1965) on London Clay and Josseaume (1998) on Flanders Clay shown in Fig.1.18. They stated that these two clays, close in their mineralogy and geological histories, can be

distinguished by the depth at which the tested samples were taken: 20 to 40 m for the London Clay, less than 10 m for the Flanders Clay.

This aspect affects the triaxial test results obtained for each material. The Flanders Clay has lower as well as more scattered values of maximum strength, due to the fissuration induced by the decompression which helps the strain localization during the loading.

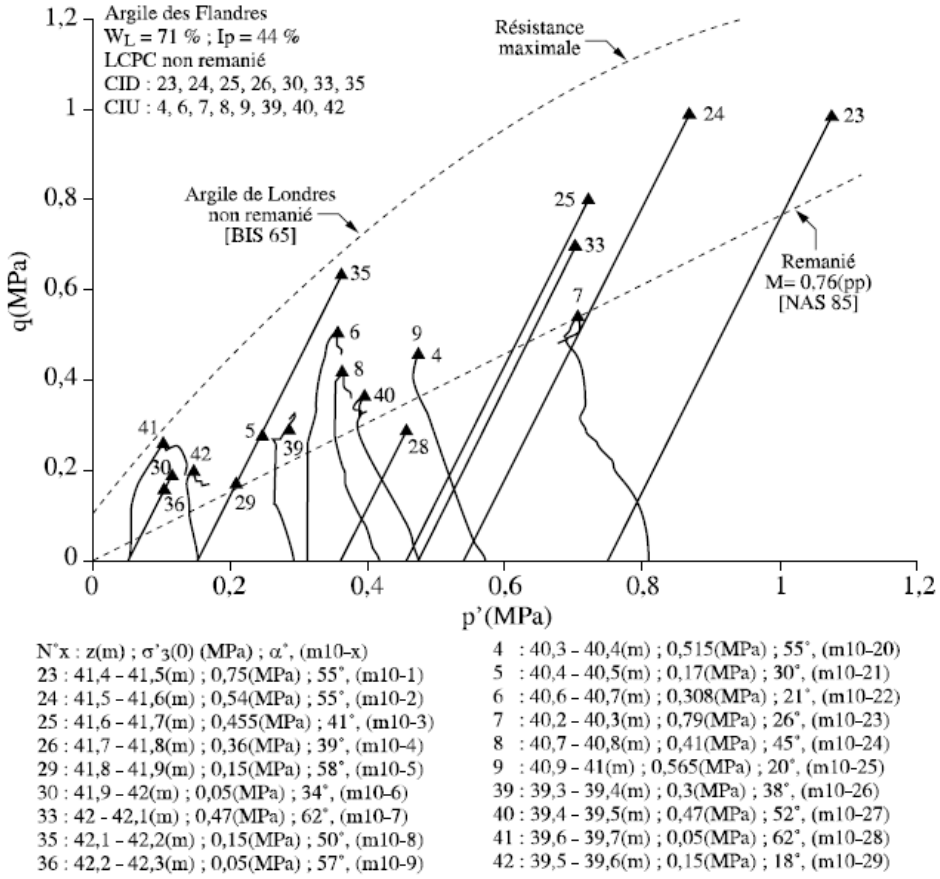

From Hichre & Shao, (2002)

Fig. 1.18 Drained and undrained triaxial tests on the Flanders clay.

1.3.3 Large strain strength

Skempton (1964) examined the shear strength of an overconsolidated clay by carrying out slow drained tests, in which the clay was subjected to displacement amounting to several inches (Fig.1.19). Under a given effective pressure, there is a definite limit to the resistance the clay can offer, and this is the 'peak strength' τ_f. In ordinary practice the test is stopped shortly after the peak strength has been clearly defined, and τ_f is referred to simply as the 'shear strength' of the clay under the given effective pressure. If, however, the test is continued, then we find that as the

displacement increases so the resistance or strength of the clay decreases. But this process, which may be called 'strain-softening', is not without limit, for ultimately a certain 'residual strength' q_r is reached which the clay maintains even when subjected to large displacements.

Based on the above work on residual strength by Skempton, Lupini et al. (1981) introduced three modes of residual strength. (1) The turbulent mode occurs when behavior is dominated by rotund particles, or, possibly, in soils dominated by platy particles, when the coefficient of interparticle friction between these particles is high. Residual strength is high, no preferred particle orientation occurs and brittleness is due to dilatant behavior only. (2) The sliding mode occurs when behavior is dominated by platy, low-friction particles. A low-strength shear surface of strongly orientated platy particles then develops. The residual friction angle depends primarily on mineralogy, pore water chemistry and on the coefficient of interparticle friction. A shear surface, once formed, is not significantly affected by subsequent stress history. Brittleness during first shearing is due primarily to preferred particle orientation. (3) The transitional mode occurs when there is no dominant particle shape, and involves turbulent and sliding behavior in different parts of a shear zone. The properties of the soil in residual shear change progressively across the transitional range from those typical of turbulent shear to those typical of sliding shear. Based on an analysis of a range of British clays, Vaughan et al. (1978), proposed the plasticity index I_p as a useful parameter to divide soils having turbulent or sliding behavior. They observed that for soils with I_p<25% the shearing behavior was prevalently turbulent; for soils with I_p >30% the shearing behavior was sliding.

Gasparre (2005) pointed out that, although there are many examples of soils that fail to respect this relationship, as other parameters are also involved, in general terms the undrained strength of low plasticity clays is controlled by the water content, as these soils undergo turbulent shearing and their behavior in an overconsolidated state is basically ductile. Plastic clays, instead, undergo sliding shearing, so their peak undrained stress is controlled by the initial stress before shearing and their shearing behavior in a overconsolidated state is generally brittle (Fig.1.20, Gasparre, 2005). The brittleness is thought to be due to the presence of bonding, as this increases the peak strength of the material, but has no influence on the large strain strength.

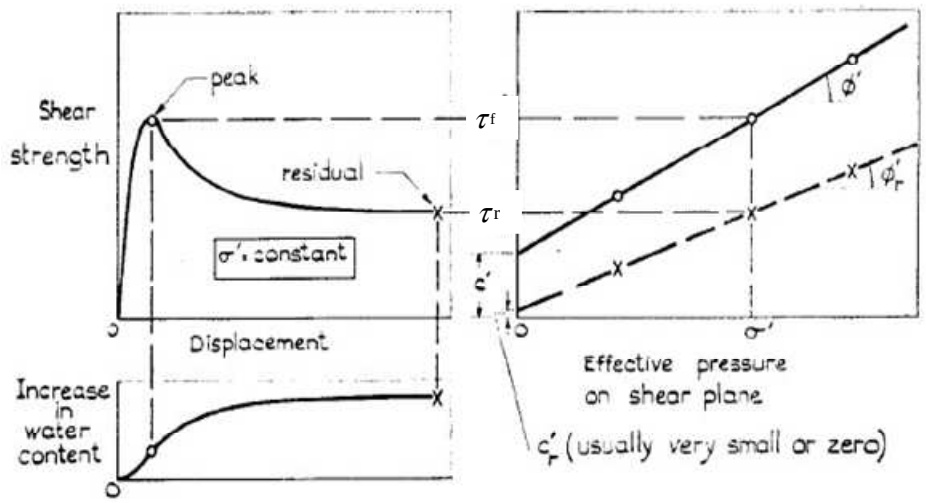

From Skempton, (1964)

Fig. 1.19 Cyclic stress ratio (CSR) versus number of cycles to liquefaction (N) for simulated samples

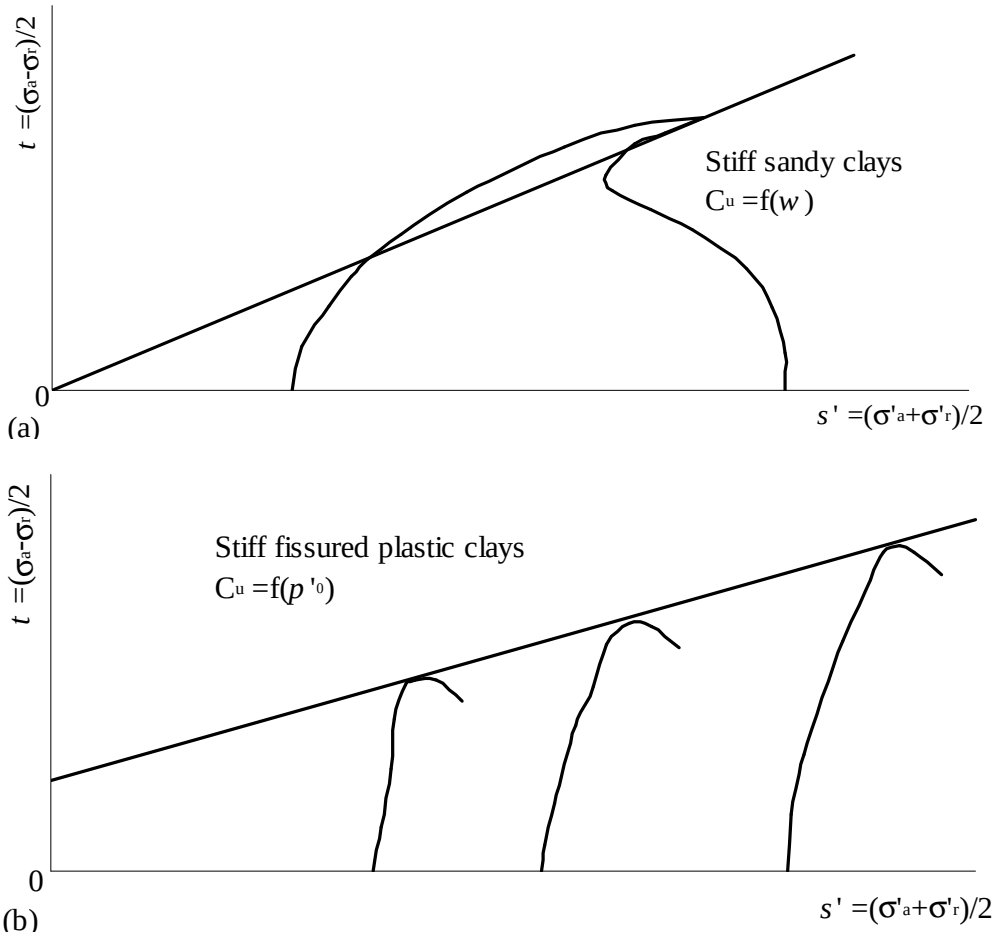

From Gasparre, (2005)

Fig. 1.20 Idealized undrained shearing behavior of overconsolidated clays with (a) low plasticity and (b) high plasticity.

Burland (1990) defined the strength corresponding to the post-peak plateau as “post-rupture strength” of stiff clays, which is believed to be that remaining after breakage of interparticle bonds (Fig.1.21). Burland et al. (1996) observed that the post-rupture strength envelope tends to lie close to the intrinsic critical state line of the reconstituted material. In stiff clays, the localization of strains is thought to be the consequence of the strain softening.

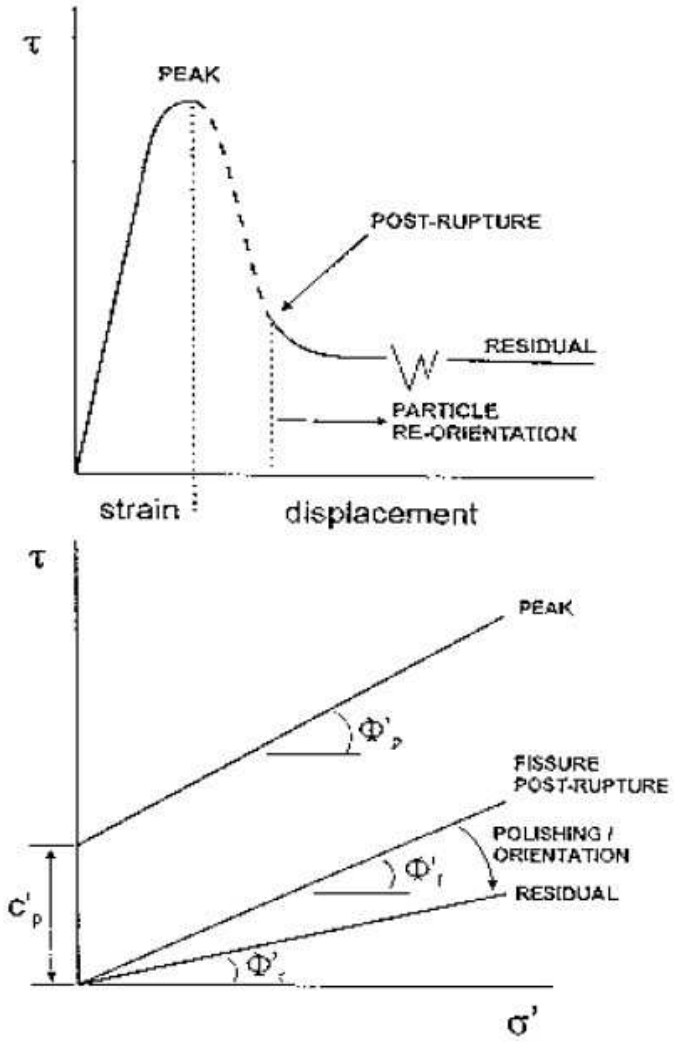

From Burland, (1990)

Fig. 1.21 Strength of stiff plastic clays.

1.4 Behavior of clay subjected to cyclic loadings

Strength decrease may occur in a saturated soil subjected to cyclic loading of waves, wind etc. The amplitude of the cyclic load on the foundation soil can be only dozens or hundreds of kilopascals, which does not lead to the destabilization or a large displacement of the foundation.

But it has been recognized that the behavior of soils subjected to repeated cycles of loading and unloading may differ considerably from its behavior during a single loading cycle. There are many situations in which the duration of the series of loading cycles is such that little or no drainage of the pore water can take place during the period of the repeated loading, which will make the pore pressure increase and as a result, the bearing capacity of the foundation can become significantly lower. It is therefore useful to study the effects of repeated loading under undrained conditions in the laboratory.

Many studies on the behavior of clays under cyclic loading in the laboratory have been done during the last four decades. Clay behavior has been studied under constant stress and constant strain amplitude cyclic loading, both one-way and two-way loading, under isotropic and anisotropic consolidation stress, using triaxial and simple shear apparatus (Sangrey et al., 1969; Sangrey & France, 1980).

Seedd & Chan (1966) have performed earthquake oriented studies of clay strength under cyclic loading conditions, which is the very early literature about the behavior of clay under repeated loading. After gathering a large quantity of tests results, Boulanger & Idriss (2006) have proposed some new criteria for the liquefaction of fine-grained saturated soils. Monotonic and cyclic undrained loading behavior for saturated soils were reviewed, from which they showed that there is a transition in fine-grained soil behavior from behavior that is more fundamentally like sands (sand-like behavior) to behavior that is more fundamentally like clays (clay-like behavior) over a fairly narrow range of plasticity indices (I_p). For practical purposes, clay-like behavior can be expected for fine-grained soils that have $I_p \geq 7$. For evaluating the seismic behavior, it is recommended that the term liquefaction be reserved for describing the development of significant strains or the loss of strength in fine-grained soils exhibiting sand-like behavior, whereas the term cyclic softening failure be used to describe similar phenomena in fine-grained soils exhibiting clay-like behavior. Boulanger & Idriss (2004) advocated that the sensitivity of clay is a very important factor affecting the cyclic softening of clay; thus the clay with a high overconsolidation ratio and low sensitivity will not produce significant engineering problems even under strong earthquake condition. They have done a very comprehensive work on clay strength under

earthquake loading, which has important referential value for launching a study on the clay cyclic strength under wave, wind and traffic loading.

To obtain the knowledge about strength and deformation properties of soils subjected to cyclic loading for the foundation design of gravity platforms installed on offshore oil and gas fields, Andersen et al. (1980,1988) and Andersen (2004) have done a comprehensive research on the behavior of Drammen clay under repeated loading in the laboratory. The tests results show that there are various factors affecting the cyclic clay properties, such as the type of test (e.g., triaxial or direct simple shear), the average and the cyclic shear stresses, the overconsolidation ratio (*OCR*) etc. They used an effective stress analysis to demonstrate the differences between the static shear strength with and without previous undrained cyclic loading.

1.4.1 Shape of the cyclic loading

In this thesis, we focus on stress-controlled tests which include symmetrical and non-symmetrical loading tests (Fig.1.22). Cyclic tests also can be divided into one-way cyclic tests and two-way cyclic tests. Defined in Biarez & Hicher (1994), one-way test in which q is cycled between zero and q_c (Fig.1.22 (b)) shows a significant plastic strain during the first cycle. When q_c >0, the tests are in compression, and when q_c <0, those are in extension. In two-way cyclic test each cycle, consisting of alternating axisymmetric compression and extension, involves a sudden 90^0 change in the directions of the major and minor principal stresses as they interchange.

Early studies on the cyclic strength of clay began in connection with pavement design problems. Traffic loads that produced shear stress pulsations in the ground were generally simulated by repeated compressive loading on triaxial test specimens in the laboratory. These repeated loads were applied as repeated axial compression loading to an isotropically confined sample. The sample responded by straining a certain amount in the compressive direction and then recovering a lesser amount with each cycle when the axial stress was reduced to zero. Continued load repetitions generally led to a continued compressive strain accumulation and, in some cases, to an actual shear failure of the specimen. It is reasoned that for the earthquake problem, the cyclic stresses should reverse rather than always loading in one direction. And cyclic loading tests on clays for earthquake stability analyses began to be performed using symmetrical reversing

stresses. The practice has continued to the present and has been extended to the problem of stability of offshore structures subjected to wave loading.

Hicher (1979, 1985) indicated that during two-way loading the cyclic strain is predominant and the average shear strain is small, whereas during one-way loading the average shear strain prevails in spite of cyclic shear strain being small. And the effect of two-way cyclic loading was found to be considerably more severe than that of the one-way cyclic loading. The permanent shear strain and excess pore pressure in clay develop more rapidly under two-way cyclic loading than under one-way cyclic loading. These tendencies suggest that clay samples under two-way loading tend to proceed towards the critical state faster than in the case of one-way loading.

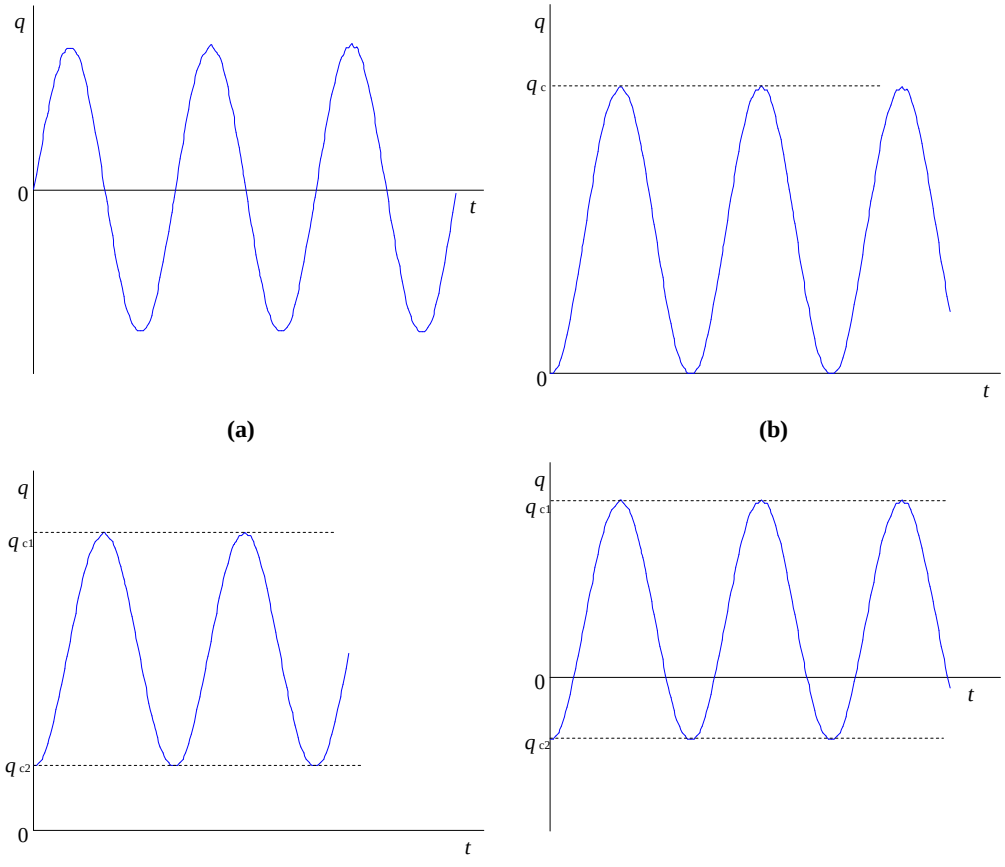

From Hicher, (1979)

Fig. 1.22 Test conditions: (a) symmetrical loading test, (b) non-symmetrical loading test (one-way cyclic test), (c) non-symmetrical loading test (q_{c1} and q_{c2} have the same sign) and (d) non-symmetrical loading test (q_{c1} and q_{c2} have the same sign).

1.4.2 Stress level

The laboratory cyclic tests are conducted to simulate the in-situ stresses as closely as possible. Then the general behavior of soils subjected to the combination of an average static stress and a cyclic stress. In this thesis, based on Fig.1.22, the average static stress is defined by $q_m=(q_{c1}+q_{c2})/2$, and the cyclic stress $q_{cy}=(q_{c1}-q_{c2})/2$. Hyodo et al. (1994) have performed a series of undrained cyclic triaxial compression tests on a high plasticity marine clay. The testing was performed using various combinations of initial static and subsequent cyclic shear stresses on isotropically and anisotropically consolidated specimens. For adding the initial static shear stress, they did not use the K_0 consolidation but use another method: a period of 24 hours consolidated anisotropically by applying a static deviatoric stress at a constant effective mean principal stress in the triaxial cell. They indicated that the clay cyclic shear strength decreases with increasing the initial static deviatoric stress. And a unique hyperbolic relationship of the peak axial strain ε_p (Fig.1.23) and the effective stress ratio η_p (= $(q_m+q_{cy})/p'$) is given by the following equation:

$$\varepsilon_p = \frac{a_1 \eta_p}{1-\eta_p / \eta_{ult}} \tag{1.1}$$

where $1/a_1$ is the slope of the initial tangential line of the ε_p-η_p curve and η_{ult} is the value of η at the asymptote of the hyperbola in Fig.1.24. When at a given stress cycle, the effective stress ratio η_p can be obtained, then the peak axial strain is evaluated by substituting η_p into Eq. (1.1).

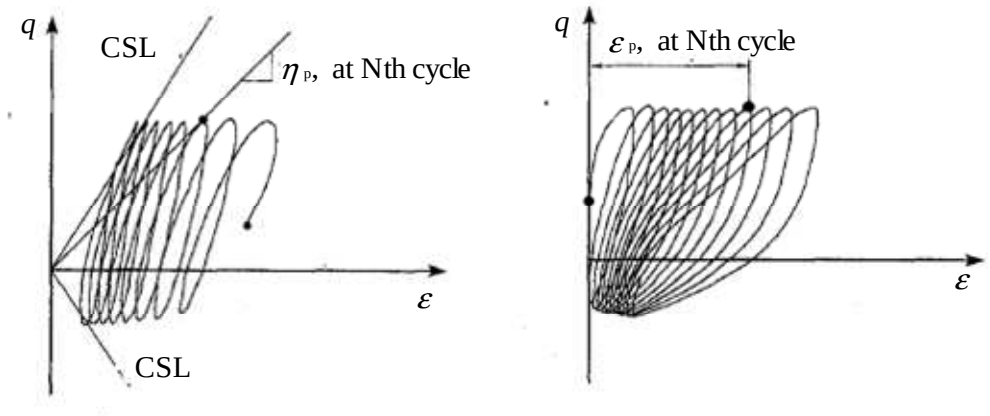

From Hyodo et al., (1994)

Fig. 1.23 Schematic diagram for peak axial strain ε_p and corresponding effective stress ratio η_p at an arbitrary cycle during cyclic loading.

Sangrey et al. (1969) has shown that at cyclic stress levels below a certain magnitude called the critical level of repeated loading (*CLRL*) the clay would develop strain until a state of equilibrium is reached. Hicher (1979) indicated that this state is a stabilization of the material in the cyclic domain. At this stage, a closed hysteresis loop occurs with subsequent cycles. That means after a great number of cycles, we note that strains and pore pressures will be almost constant (Fig.1.25). And Yudhbir & Rehman (1977) have drawn the equilibrium lines for one-way cyclic tests on normally consolidated clay, in which each point corresponds to a one-way test at a given cyclic stress value at the state of equilibrium (Fig.1.26). The critical cyclic stress ratio q_c/q_{max} is defined herein as the maximum cyclic stresses on this line divided by the maximum shear stress in a static compression test. They found that the critical cyclic stress ratio increased when the consolidation pressure increases, whereas Sangrey et al. (1969) and Hicher (1979) indicated that this ratio is constant, independent of the consolidation pressure. For cyclic stress ratios above the critical cyclic stress ratio, strains and pore water pressure increase continuously as the number of cycles increases.

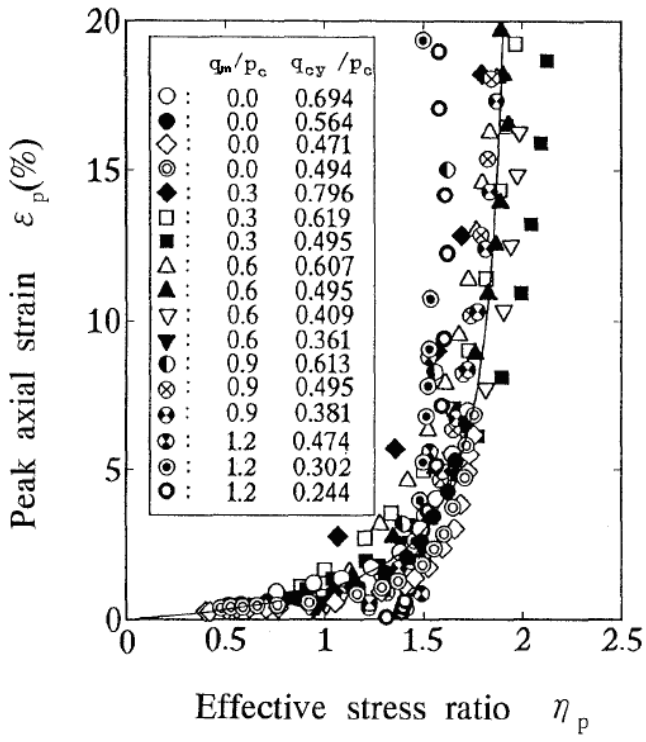

From Hyodo et al., (1994)

Fig. 1.24 Relationship between peak axial strain and effective stress ratio during cyclic loading.

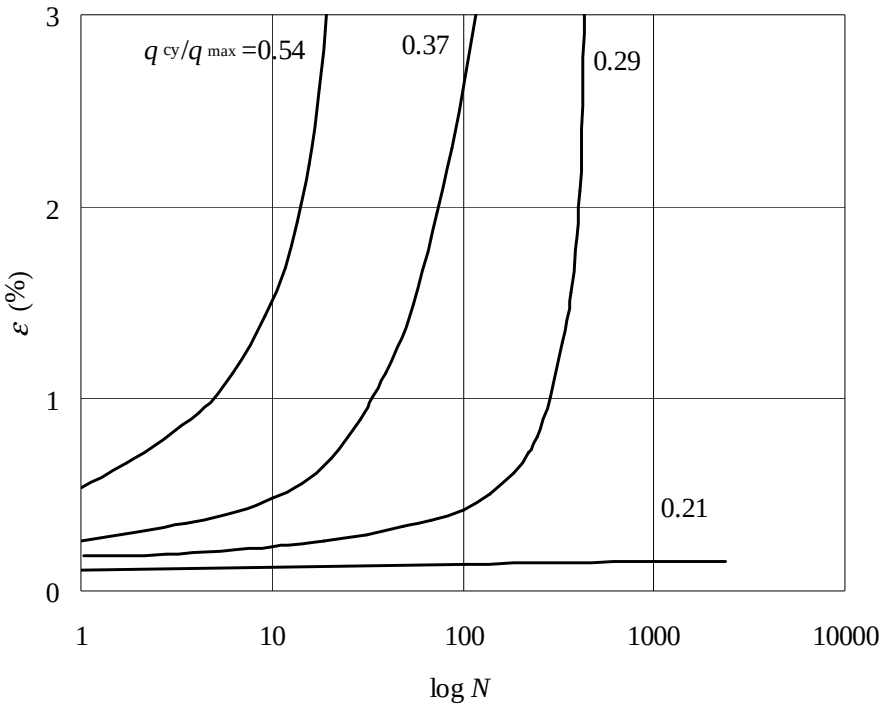

From Hicher, (1979)

Fig. 1.25 The relationship between the number of cycles and the cyclic strain with different values of cyclic deviatoric stresses. Triaxial symmetrical loading test at normally consolidated Black clay.

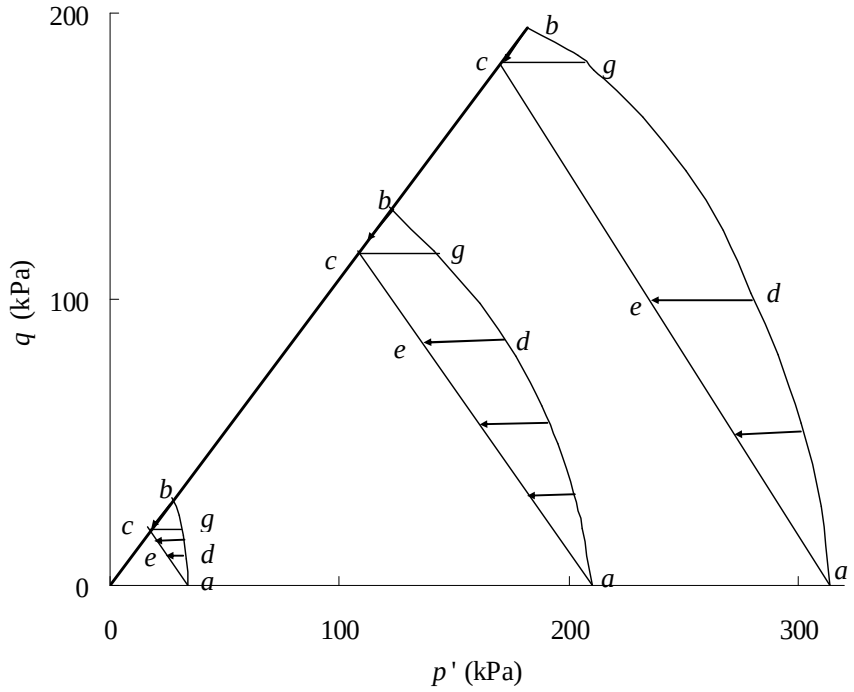

From Yudhbir & Rehman, (1977)

Fig. 1.26 The equilibrium lines for a normally consolidated clay.

1.4.3 Failure criteria

The semantic problem of defining failure in a cyclic loading test has not been specifically solved, and the proposed definitions have not been universally accepted. Some early publications are vague about the failure criteria used, while others use several different criteria. On some occasions, when pore pressures have been measured, the critical factor appears to be whether or not the repeated loads lead to a pore pressure buildup which brings the soil to the effective stress failure envelope. If the stress level is below the critical level of repeated loading (*CLRL*), nonfailure equilibrium is reached, closed stress-strain hysteresis loops are measured, and the final soil behavior is essentially elastic. On the contrary, if above the critical level of repeated loading the effective stress failure envelope is reached (Sangrey et al., 1969). For sand soils, pore pressures are usually measured, and this enables an effective stress failure criterion to be defined, for example, the condition of zero transient effective stress (Seed & Lee, 1966). However, clay behavior under undrained cyclic loading is more complex than sand behavior, because of its dependency on such factors as time-dependent creep and preconsolidation periods which can be overlooked for the cyclic behavior of sand. Therefore, to avoid difficulties involved with defining failure in terms of effective stress, failure criteria for cyclic tests have been defined in terms of a cyclic strain amplitude for both sands and clays. Various criteria have been used in different studies ranging from about ±2.5% single amplitude cyclic strain to 20% double amplitude cyclic strain in the cyclic stress controlled laboratory test.

Hyodo et al. (1994) proposed that when the double amplitude cyclic strain ε_{DA} or the peak accumulated axial strain ε_p reaches 10%, failure occurs. This failure criterion is based on the results in Fig.1.24, where the asymptote of the hyperbolic relation is obtained for ε_p=10%, which does not mean that the effective stress reaches the failure envelops in the p'-q plane. Yasuhara et al. (1992) pointed out that when the double amplitude cyclic strain ε_{DA} reaches 5%, failure happens.

Andersen et al. (1980, 1988) and Andersen (2004) proposed that failure under cyclic loading may occur either at large cyclic strains, large cyclically induced average strains, or at a combination of the two. If the combination is such that the stress path during one cycle is close to the failure lines both in compression (active) and extension (passive) sides, cyclic shear strains

will be predominant. If the stress path is much closer to one of the failure lines, average shear strains will be predominant. Whether the average shear strain will be compression or extension depends on which of the failure lines is approached during cyclic loading. Thus the failure is defined as either an average shear strain, γ_m, of 15% or a cyclic shear strain, γ_{cy}, of 15%. And $\gamma_m = 0.5(\gamma_{max} + \gamma_{min})$, $\gamma_{cy} = 0.5(\gamma_{max} - \gamma_{min})$, where γ_{max} and γ_{min} are the maximum and minimum shear strains within the cycle.

As mentioned above, there are different failure criteria. Nowadays, the failure criterion adopted for interpreting the laboratory test data must be considered to be somewhat empirical, especially for cases where failure does not involve a sudden collapse or sudden change from very low to very large strains within a few cycles. Nevertheless a specified cyclic strain is required to be the failure strain criteria during cyclic loading in the laboratory tests.

Based on the analysis of test results on Drammen clay, Andersen (1988, 2004) proposed to construct synthetic diagrams to interpret the overall behavior of clays subjected to cyclic loads. These diagrams include the relationship between the cyclic and permanent shear stresses at failure, the relationship between cyclic and permanent shear stresses, number of cycles, and shear strains as shown in Fig.1.27 (a), Fig.1.27 (b) and Fig.1.27 (c) (q_{cy} and q_m represent the cyclic and permanent deviatoric stresses, respectively, q_{max} represents the maximum stress in compression tests and σ'_0 is the effective confining pressure).

Based on Fig.1.27 (a), if the combination of the cyclic and permanent deviatoric stresses is given, one can predict the number of the cycles to failure, N_f, and the cyclic and permanent shear strains. (In Fig.1.27 (a), the points with the same symbol have the same cyclic and permanent shear strains.) The cyclic and permanent shear strains at this given number of cycles can also be predicted in Fig.1.27 (b). For symmetrical cyclic loading tests, the variation of the cyclic shear strain with the number of cycles is the main aspect to study. Each curve with a certain value of the cyclic shear strain as functions of the number of cycles is shown in Fig.1.27 (c). The failure envelope indicates that, at a given number of cycles, the sample would fail if the value of the stress level q_{cy}/q_{max} is above the failure envelope. Otherwise, the sample will not fail. Thus, this diagram can be used also to estimate the equilibrium state.

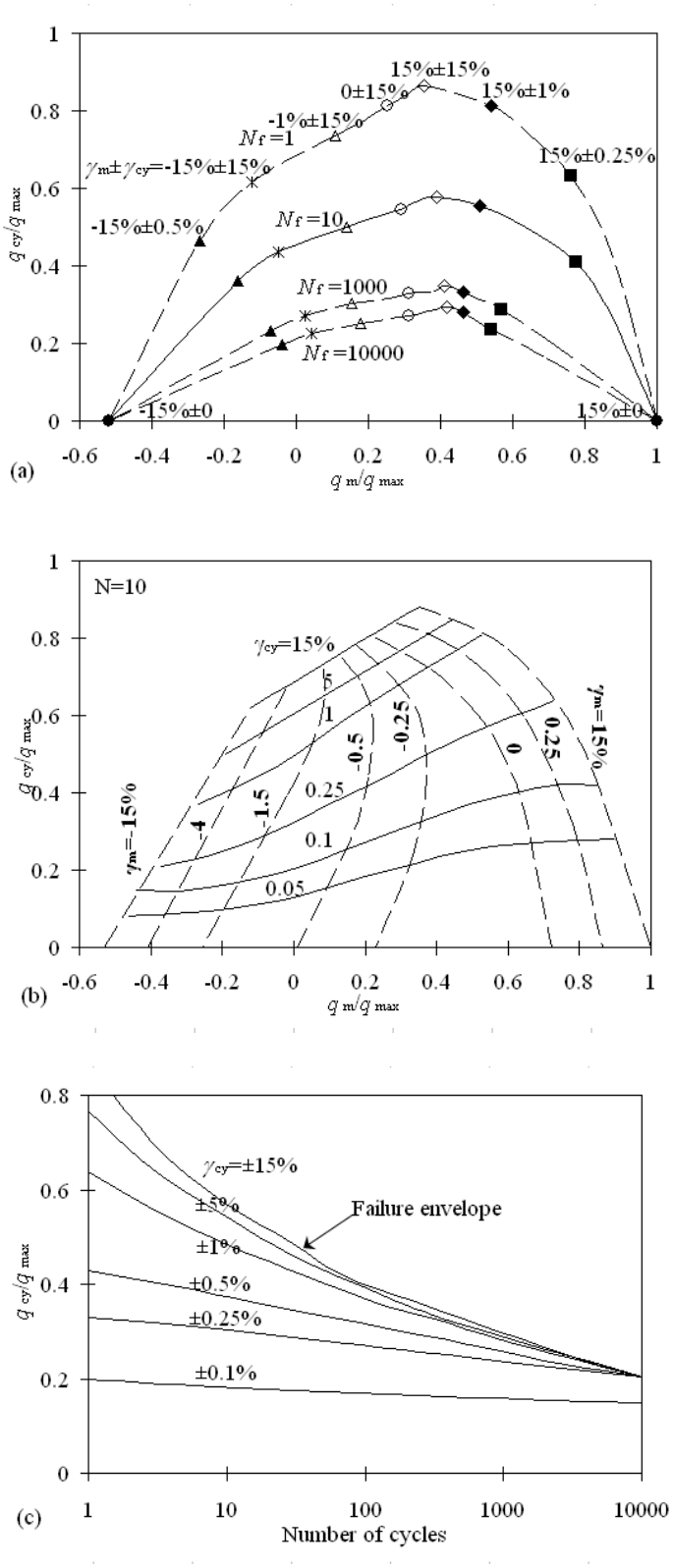

From Andersen, (2004)

Fig. 1.27 (a) Number of cycles to failure, N_f, and shear strain at failure, $\gamma_m \pm \gamma_{cy}$, (b) cyclic and permanent shear strains after a given number of cycles, N=10 and (c) cyclic shear strain as function of number of cycles with q_m =0 in triaxial tests on Drammen clay with OCR=4 .

1.4.4 Post-cyclic static shear strength

An important group of geotechnical engineering problems requires the knowledge of the peak strength of soil after a limited number of repeated loading cycles. These problems include: loading of structural foundations after earthquakes, stability of slopes and foundations experiencing environmental loading by wind and waves, loading of soils by traffic and changes in the ultimate capacity of driven piles. Since the time interval between a repeated loading history and a subsequent loading may vary, the strength immediately after repeated loading and the strength after a period of drainage are of interest.

The post-cyclic static shear strength can be determined in the laboratory by subjecting the specimens to cyclic loading followed by static loading up to failure. The ratio of post-cyclic over pre-cyclic undrained strength is generally considered to be related to the ratio between the maximum axial strain developed during cyclic loading (ε_p) and the axial strain at rupture during pre-cyclic monotonic loading (ε_{fs}). Lee & Focht (1976) and Thiers & Seed (1969) indicated that if the ratio, $\varepsilon_p/\varepsilon_{fs}$, is less than 0.5, the post-cyclic undrained strength does not have any significant difference with the pre-cyclic undrained strength. Otherwise, if this ratio is more than 0.5, the post-cyclic strength will decrease, and much greater the strain ε_p is, more the post-cyclic strength decreases (Fig.1.28). Díaz-Rodríguez et al. (2000) suggested that the undrained strength ratio is related not only to the maximum axial strain during cyclic loading, but it also depends on other cyclic loading parameters, such as the cyclic stress level, the number of cycles, the residual strain and pore pressure induced by cyclic loading. The influence of the cyclic stress level is shown in Fig.1.29. The failure ratio $R_f=(q_{cf}/q_{max})$ defined as the deviatoric stress at failure after cyclic repeated loading divided by the static maximum deviatoric stress.

Andersen et al. (1988) and Andersen (2004) stated that the undrained bearing capacity of the soil may be significantly lower for cyclic than for static loads. The undrained static bearing capacity of the soil may also be reduced by cyclic loading. To analyze the foundation design problems, it is necessary to determine the strength and the deformation properties from laboratory tests where the loading conditions of the various soil elements are simulated as closely as possible. With the existing types of laboratory equipment, it is not possible to simulate all these different loading situations. However, triaxial and direct simple shear (*DSS*) tests represent some important

conditions, and when performed at various combinations of average and cyclic shear stresses, the results from these tests provide valuable information about the cyclic soil behavior. If the preceding cyclic loading caused large cyclic shear strain in triaxial or *DSS* testing, the specimens suffer a significant reduction in the static shear strength. This is in agreement with previous test results. Tests with small cyclic, but large average shear strains during cycling loading may also experience a reduction in the subsequent static shear strength.

In his study, Andersen (1988) showed that, although the post-cyclic undrained strength may be effected by the cyclic loading, the effective stress strength parameters, c' and ϕ', do not seem to be influenced by an undrained cyclic loading in the case of overconsolidated clays. For normally consolidated specimens, however, the post-cyclic static stress path passes the failure line for normally consolidated clays and approaches the failure line for overconsolidated clay, indicating an increase in the post-cyclic cohesion intercept, c' (Fig.1.30).

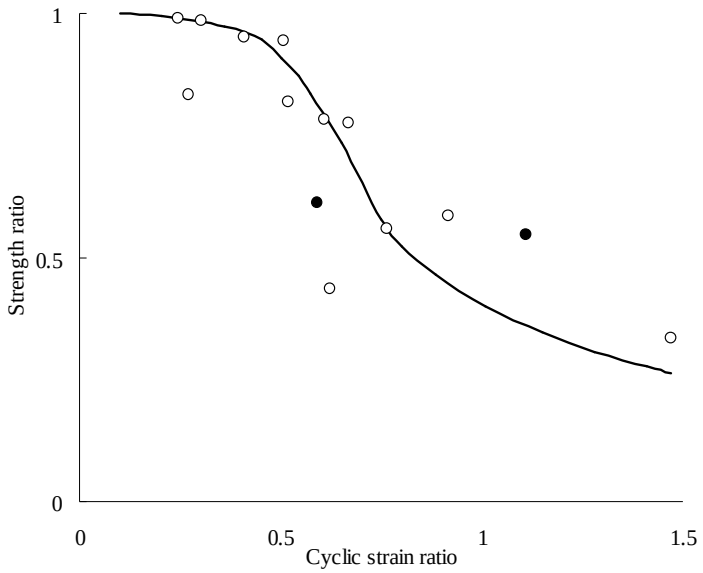

From Lee et al., (1976)

Fig. 1.28 The stress ratio of post-cyclic and pre-cyclic undrained strength versus the cyclic strain ratio.

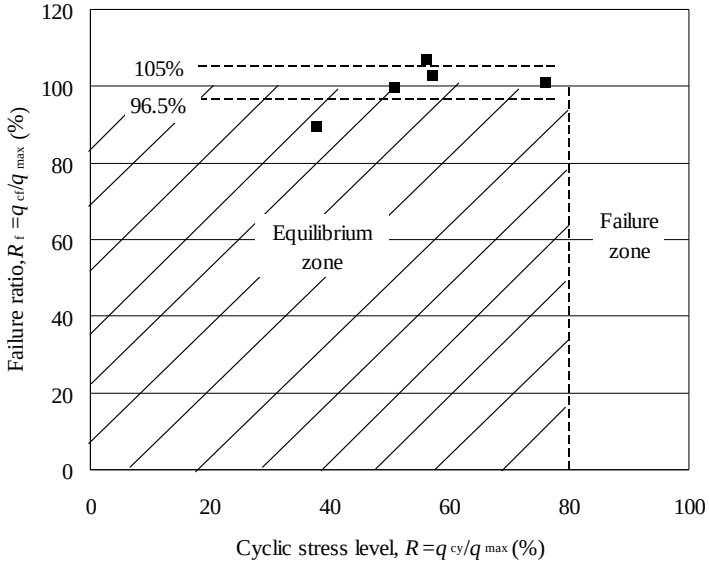

From Díaz-Rodríguez et al., (2000)

Fig. 1.29 Failure ratio versus cyclic stress ratio, if R <0.8, post-cyclic strength has not significant difference with pre-cyclic strength.

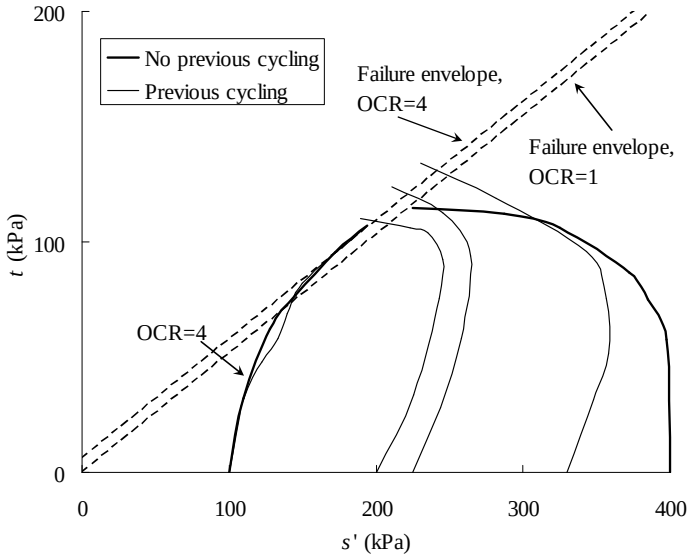

From Andersen, (1988)

Fig. 1.30 Effective stress paths for undrained static triaxial tests with and without previous undrained cyclic loading at Drammen clay.

It is generally accepted that the failure of soils under repeated loading is a consequence of the accumulating excess pore pressure during cyclic loading. In one early effective stress study of clays, Sangrey et al. (1969) showed that the critical level of repeated loading separates the higher cyclic stress levels, which develop sufficient excess pore pressure to reach the effective stress

failure condition, from the cyclic stress levels which reach a non failure equilibrium. They proposed that the excess pore pressures accumulated to equilibrium is related to the cyclic stress level and that, when presented in an effective stress space, these equilibrium effective stress conditions define a locus called the equilibrium line (Fig.1.26). Brown et al. (1975) reported that repeated loading on very dilative (heavily overconsolidated) clay specimens resulted in small accumulations of excess negative pore pressure. Consequently, the critical level of repeated loading is not very different from the conventional undrained shearing resistance. France & Sangrey (1977) presented the results of cyclic loading including drainage intervals and showed that when normally consolidated and lightly overconsolidated clays are loaded in this way they do not fail under repeated loading but, instead, the water content decreases and the critical level of repeated loading increases. For heavily overconsolidated clays, however, the repeated loading with drainage results in significant strength decrease.

We can summarize that the most dramatic effect of repeated loading on most saturated soils is a loss of strength or failure after some number of loading cycles. The potential for strength loss and failure increases as the level of cyclic stress increases and lower levels of undrained repeated loading do not produce failure even under a large number of stress cycles. But we should note that the test results presented by Brown et al. (1975) on a silty clay showed that even after 10^6 cycles, permanent strain was continuing to build up at a significant rate in nearly all the tests, but failure had not occurred in most of the samples. Hence, failure in repeated load tests could occur after large number of cycles, in excess of 10^6, the maximum applied in these experiments. This is in contrast to earlier findings concerning small number of stress levels for which failure condition were more easily defined.

1.4.5 Influence of OCRs and load frequencies

Most of the results found in the literature are on normally consolidated clays. Nevertheless, there exist several previous researches on the influence of *OCR*, especially for heavily overconsolidated clays, concerning the mechanical properties under cyclic loading.

In the article of Wang & Cai (2008), the effects of accumulative plastic strain on degradation characteristics of Hangzhou saturated soft clay subjected to undrained cyclic loading are

investigated at different overconsolidation ratios (*OCR* =1, 2, 4, 8). The result is that as the *OCR* is increased, the number of cycles at failure increases. That means that the overconsolidation improves the cyclic soil strength. This conclusion is also observed in the article of Vucetic & Dobry (1988), and they indicated that the clay's modulus degradation with the number of cycles is affected by the *OCR*, even a moderate change of the overconsolidation ratio has a significant effect on the rate of modulus degradation.

The overconsolidated samples have a different cyclic behavior than the normally consolidated samples. In general, at the same effective consolidation stress, the samples with higher overconsolidation ratios are stronger under cyclic loading. These results were obtained at low to moderate overconsolidation ratios (*OCR*=1, 2, 4, 8), but there are few studies on heavily overconsolidated clay (*OCR*≥10).

Thammathiwat & Chim-oye (2004) indicated that the cyclic strength increased with increasing of loading frequencies for a given confining pressure but excess pore pressure decreased with increasing of loading frequencies. Li et al. (2011) stated that, for a give number of cycles, larger shear strains are generated at lower frequency.

Due to the invariable confining pressures and invariable loading frequencies for the nautral and reconstituted samples of Merville clay, respectively, the effects of *OCR*s and loading frequency are not the emphasis of this study.

1.5 Structure of the thesis

As mentioned above, most researchers have performed cyclic tests with hundreds, thousands or nearly ten thousands cycles, few have applied larger number of cycles (hundred thousand or even a million cycles). Therefore, we will center this study on the effect of a very large number of cycles on clay samples.

This thesis consists of six chapters. Following this chapter of analyzing previous studies on the subject, the aims of this research are presented.

An introduction of Merville clay is presented in Chapter 2. The physical properties of this clay are obtained in the laboratory and complemented by results on Flandrien Clay obtained in other studies.

In Chapter 3, the test procedures, from sampling to static triaxial testing, are described. The one-dimensional compression behavior of Merville clay is analyzed. Discussion about the effect of overconsolidation and bonding in natural clay is done based on our test results.

Chapter 4 describes the static triaxial test procedures from sampling to testing. The analysis of test results is presented. Again, the effect of high overconsolidation ratio and bonding are analyzed by comparing natural and remolded samples. The effect of initial fissuration is also discussed.

In Chapter 5, both the natural and reconstituted samples of Merville clay are used to perform cyclic triaxial tests. The analysis and discussion for the results of cyclic tests with a great number of cycles of Merville clay are presented.

Finally, Chapter 6 gives the conclusions obtained in this research and presents the perspectives.

2 Physical properties of Merville clay

2.1 Introduction

The samples of Merville clay used in the present research were collected at Merville, in the local airport area where previous geotechnical investigations have already been conducted (Ali et al., 2010; Canépa et al., 2002; Ferber & Abraham, 2002).

In this chapter, an overview of the geological aspects of the Merville clay will be presented for a better understanding of how the geological history can influence the mechanical behavior of this soil. The material lies within the Flanders clay deposit located in the northern Europe. Silts of low to medium plasticity are found at the test site to a depth of about 2.4 m underlain by a highly plastic and overconsolidated clay layer (Fig.2.1). The Merville clay used in this study is located beneath the depth of 3 m in agreement with previous studies (Ali et al., 2010; Canépa et al., 2002; Ferber & Abraham, 2002). The water table is also about 3 m below the ground level.

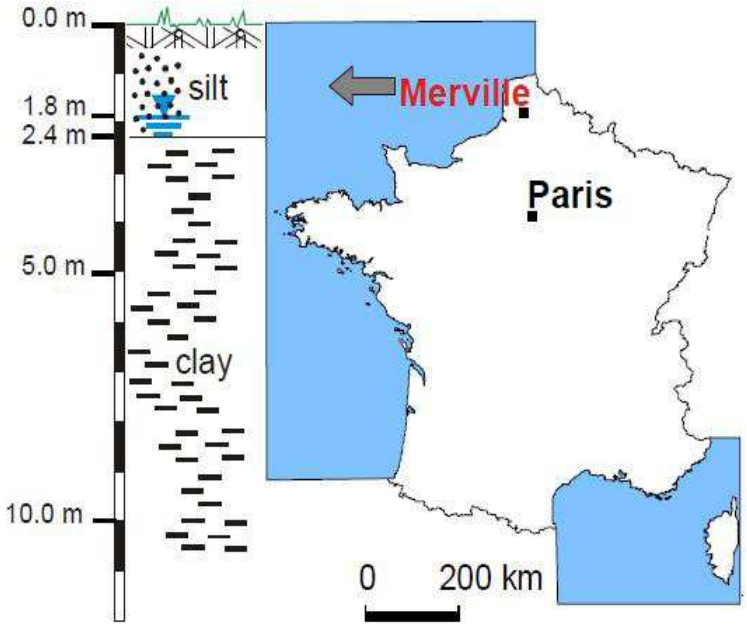

From Ali et al., (2010)

Fig. 2.1 Location of Merville site.

The Merville clay is of marine origin. It is recognized as an overconsolidated stiff clay of high plasticity. It presents fissures in its top part according to the process of sedimentation. The clay lying at the Flanders Region was deposited in the Ypresian (early Eocene of the tertiary era)

in a marine gulf stretching across the whole areas which are now located at the northern France, Belgium and the southeast of England. So the Merville clay has some similar behavior with the London clay. It was then covered by tertiary sedimentation which continued until the Pliocene. The soil surface then stood probably about 200m above the present surface of the clay. The formations overlying the clay and the top of it were later eroded. This erosion process was sustained to Quaternary, by the depositing of the Flandrian alluvial deposits on the clay remaining in place which has an effective vertical stress much lower than that was applied during the Pliocene. So the clay is known as a stiff, heavily overconsolidated clay (Josseaume, 1998). The over-consolidation ratio (*OCR*) is estimated about 30 (see Chapter 3).

Its dominant clay minerals are illite and montmorillonite, with subsidiary kaolinite. Although the clay fraction and Atterberg limits vary slowly with the depth, the clay fraction is typically around 20% ~ 40% in clayey facials and the plasticity index I_p varies around 40 ~70. This chapter will review its geological and physical aspects.

The geology of the Merville clay is important to the present study in some regards. Firstly, knowledge of its geological history is useful when estimating the stress-history of the clay. The influence of the stress-history on the yielding behavior of soils is relatively well known, and the possible role of recent stress history on stiffness characteristics has attracted attention in recent years (e.g., Josseaume, 1998; Borel, 2000). In attempting to reproduce the in-situ behavior of the Merville clay, its stress-history cannot be ignored. Secondly, the lithology of the Merville clay exhibits certain variations in the two directions (vertical and horizontal). Since one of the primary objectives in the present study is to investigate anisotropy across the vertical and horizontal sections, this understanding is also essential.

The present chapter is concerned with the general features of the Merville clay. The specific description of the materials tested in this study will also be provided in this chapter. The mechanical properties of the Merville clay will be discussed in later chapters.

2.2 Physical parameters of soil at Merville and soil profile

In 1986, some identification tests on Merville clay were performed by Borel (2000). He summarized the test results and presented the range values for each parameter in Table 2.1. Later, Reiffsteck (2003) carried out also water content and Atterberg limits tests. The obtained parameters are presented in Table 2.1. The values of water contents agree with those measured in 1986, whereas the liquid limit and plasticity index show a large decrease.

Table 2.1 Identification parameters of Merville clay (Borel, 2000).

	w (%)	w_L (%)	I_P (%)	Clay size content (%)	$CaCO_3$ Content (%)	G_s
Merville (1986)	27~33	86~98	58~69	30~40	6.8~8.8	2.74~2.75
Merville (2003)	32.3	69.2	40.5			

2.2.1 Grain size distribution

The previous studies have shown that the value of clay content was about 30% to 40%. In our study, the sample is taken from the borehole SC2 at a depth of 7.5 m. Mortar and pestle are used in two times to break the clay sample into very little particles, even into powder. Each step takes more than two hours. Then, the very little pestled particles are placed in a wide-mouthed flask with distilled water. Appropriate quantities are about 30 g for this clay. The amount of water used is about 200 ml. The mixture is shaken thoroughly until all the soil particles are in suspension. This mixture is then placed in a constant temperature room for seven days. During these seven days, the mixture will be shaken for about 5 to 10 minutes each day.

After this sample preparation, the method of sedimentometry (with 5% of hexameta-sodium-phosphate to avoid flocculation) has been used for obtaining the clay size content. The apparatus is presented in Fig.2.2.

The particle size curve of Merville clay taken at 7.5 m is presented in Fig.2.3. The previous results for other samples at different depths (4.5 m and 9 m) are also shown in this figure. Based on Fig.2.3, the clay size content ($\leq$0.002 mm) of the Merville clay is about 26% which is less than that presented in Table 2.1. But those results obviously depend on the preparation method.

Fig. 2.2 Apparatus for sedimentometry.

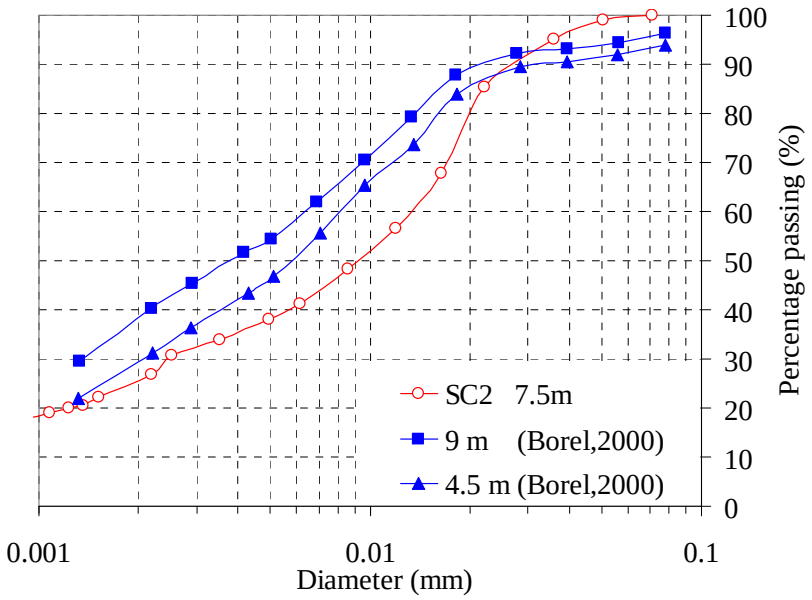

Fig. 2.3 Calculation scheme in distinct element method

2.2.2 Specific gravity G_s

The specific gravity of the tested material is measured by the pycnometer method (Fig.2.4).The measured specific gravities of some soil samples at different depths are shown in Table 2.2.

Table 2.2 Specific gravity of the samples from different depths.

Depth below ground level (m)	Specific gravity G_s		
	Borehore of SC1	Borehore of SC2	Borehore of SC3
0~1			
1~2	2.65	2.68	2.75
2~3			2.77
3~4			
4~5			
5~6	2.67		
6~7	2.71		2.65
7~8	2.77	2.51	2.62
8~9		2.69	2.69
9~10		2.62	
10~11	2.74		2.72

Fig. 2.4 Apparatus for specific gravity measurement.

2.2.3 Water content

The distribution of the water content with depth is presented in Fig.2.5, Fig.2.6 and Fig.2.7 for each borehole. These figures show that the soil between 3m and 11m, in its intact state, has nearly constant water content. The water content range is about 29.0% ~ 35.6%, except for the

samples at the depth between 4 m and 5 m in the borehole of SC3, which is higher than the values shown in Table 2.1. The saturation degrees for all the samples below 3 m are equal to 100%, whereas the saturation degrees for the samples above 3 m are less than 100%.

2.2.4 Atterberg limits

Fig.2.5, Fig.2.6 and Fig.2.7 show the profiles of the liquid limits w_L and plasticity limits w_P with depth. At depths between 3m and 11m, the values of the liquid limit and plasticity limit of Merville clay are relatively constant.

The values of the plasticity index of Merville clay from these three boreholes are between 46.1% and 61.4% which is between the two ranges presented in Table 2.1. The liquid limit range is 89.4% ~ 100.6%, agreeing with the range presented by Borel (2000).

It is difficult to define an exact value for the over-consolidation ratio (*OCR*) of Merville clay, especially within the zone affected by weathering. The clay was deposited in a marine environment some million years ago, since when it has undergone several cycles of unloading and reloading. Periglacial processes, chemical bonding, and ageing have all served to change the soil's 'apparent' *OCR* from its 'mechanical' *OCR*.

The geological evidence suggests that the current vertical effective stress above the Merville clay in the ground is about 100 kPa. Results of high-pressure oedometer tests (Josseaume, 1998) indicate that the preconsolidation pressure is probably around 3400 kPa. The corresponding value for the apparent *OCR* of the Merville clay is therefore about 30.

As shown in Fig.2.5, Fig.2.6 and Fig.2.7, the water contents are smaller than the corresponding plastic limits for this highly overconsolidated clay (depths between 3 m and 11 m).

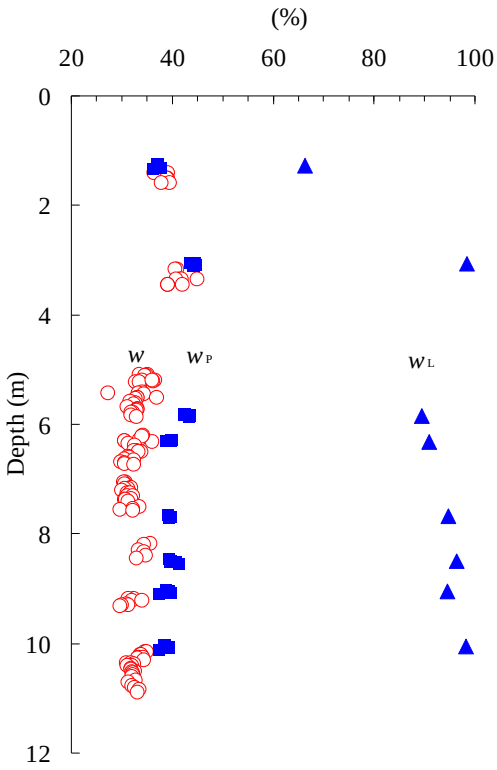

Fig. 2.5 Identification parameters with depth of SC1.

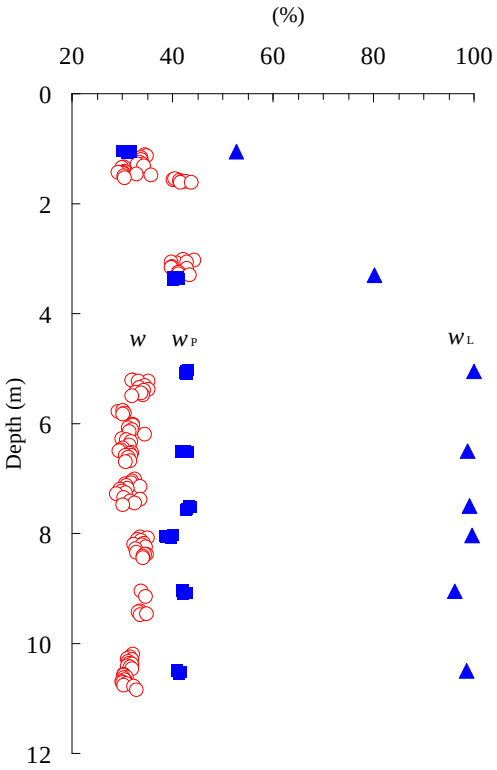

Fig. 2.6 Identification parameters with depth of SC2.

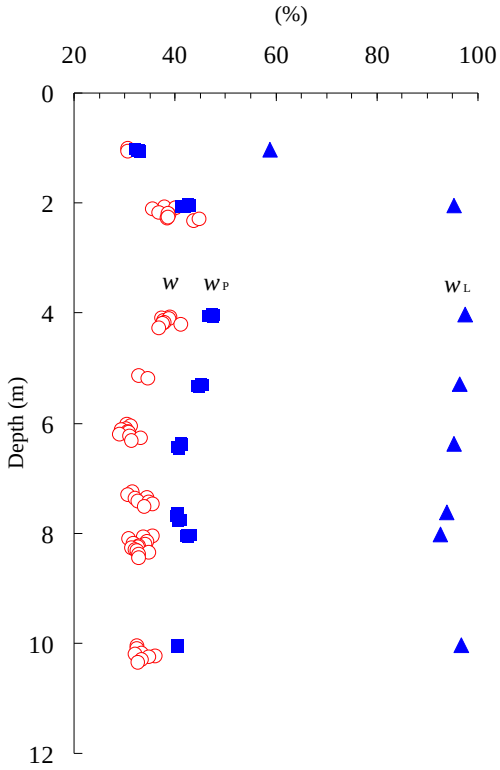

Fig. 2.7 Identification parameters with depth of SC3.

2.2.5 Soil profile

As mentioned above, the Merville clay was deposited in the same marine gulf as the London clay. There are many references about the overall features and mechanical properties of London clay. The geologic information concerning Merville clay can refer to London clay.

According to the difference of the deposition situation, the London clay lying in different sites may have different ground conditions. The London clay at Canons Park (London, UK; Bond & Jardine 1991; Bond & Jardine 1995) has a similar ground condition as the Merville clay used in this study. The ground conditions at Canons Park comprise superficial deposits of topsoil, gravel, and silty clay, overlying heavily overconsolidated clay layers. Fig.2.8 shows a simplified soil profile for the site. The London clay extends from about 2.5 m to approximately 25 m below the ground level, and forms three distinct units, disturbed London clay, intact brown London clay and blue London clay.

In this study three boreholes (SC1, SC2 and SC3) were drilled in Merville at depth from 0 m to 11 m, from where the samples were extracted. The samples were stored in 1-meter long

thin-wall PVC tubes. The inner diameter of the tubes is 11.0 cm. The soil profile for each borehole is very similar.

According to Fig.2.1, the depth of the Merville clay is from 3 m to 11 m. The soil from 0 m to 3 m is composed of gravel and silty clay (Fig.2.9 (a)) and will not be studied later on. The Merville clay consists also of two distinct units. The soil from 3 m to 7 m is the stiff, brown, silty fissured clay (Fig.2.9 (b) and Fig.2.9 (c)). The fissures which originate from the erosion process are easily activated by the disturbance during drilling and handling (e.g. sample preparation). The Merville clay below 7 m is a stiff, grey-brown, silty fissured clay (Fig.2.9 (d)), which appears undisturbed.

As mentioned above, the layer between 3 m to 4 m has different water content, probably related to the variation of the water table, assumed to be close to 3 m deep. However, following the in situ observations, it is difficult to clearly position the head to the water table.

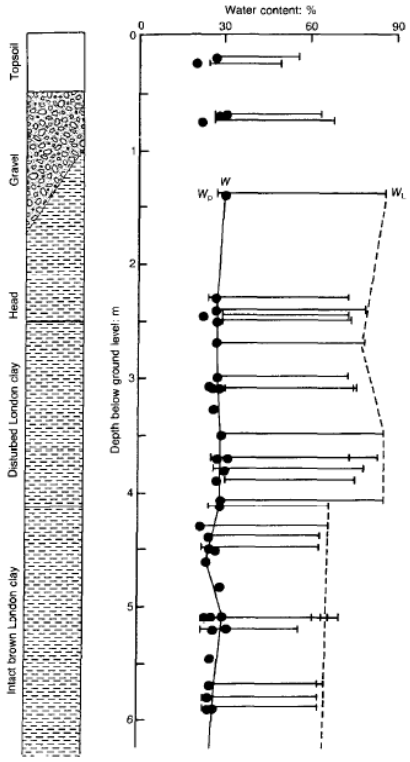

From Bonds & Jardine, (1991, 1995)

Fig. 2.8 Index properties profile for London clay at the Canons Park site.

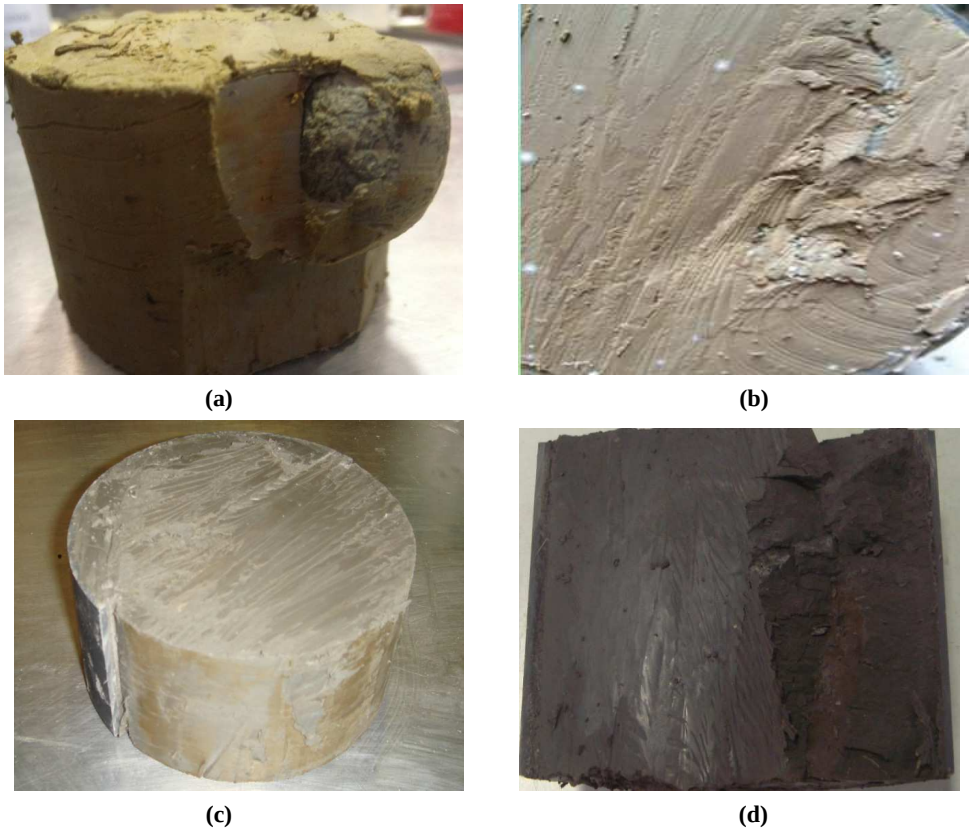

(a) **(b)**

(c) **(d)**

Fig. 2.9 Appearance of the soil at Merville: (a) yellow silt at 1.3 m with a gravel, (b) brown sample at 3.3 m, (c) brown sample at 6.2 m and (d) grey-brown sample at 7.2 m.

2.3 Microstructure of Merville clay

Firstly, microstructural identification was carried out in order to establish a potential link with subsequent mechanical experiments. Computer tomography imaging and scanning electron microscope (SEM) were used to examine the microstructural features, identifying possible differences at the micro-level and different chemical components of clay.

2.3.1 Computer tomography (CT) imagining

Computer tomography imaging is a valuable non destructive method to observe the inner structure of a sample, in particular fissure patterns before testing or shear deformation and fracture features of soil samples after shearing (e.g., Desrues et al., 1996; Wong, 1999). The principles and equipment details of the CT scanner can be found in the above-mentioned references. Only a brief description will be presented herein. The scanner used in the present study is a X-Radia XCT400 X-ray tomography machine present at Ecole Centrale de Nantes. The clay specimen encased in a

Plexiglas tube to prevent any drying during observations was positioned and fixed on a metal pedestal (Fig.2.10). During the CT scanning process, an X-ray beam (140 keV, 10 W, 71 µA) crosses the sample which rotates along the vertical axis (2500 cross section for a rotation of 180 degrees) and finally reaches a 1024*1024 detector. More precisely, the X-ray attenuation obtained from different angular positions is combined to generate the pixels (picture elements) of the matrix.

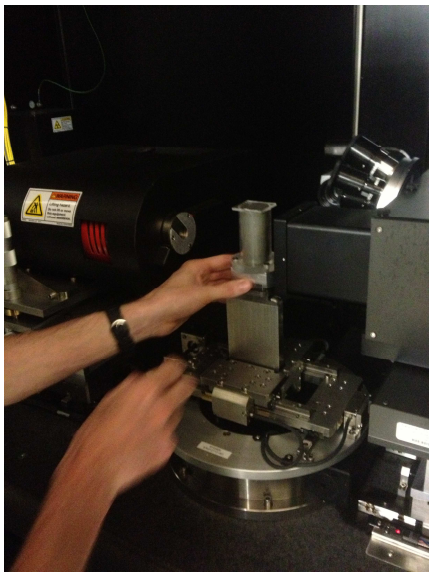

Fig. 2.10 Fixing the specimen taken at the depth of 5.2 m for CT imagining.

Fig.2.11 to Fig.2.13 show the CT imagining of an natural specimen with a visible crack on the top part. This specimen was taken at 5.2 m depth. The light areas represent a denser part in the specimen, whose mineralogical nature was not found. Visual inspection does not allow distinguishing the differences between the light and the black clay parts.

The fissure is observed at the top of the specimen in Fig.2.11 and Fig.2.12 which is the dark area in the specimen. The length and the width of the fissure were measured by a post-analysis after images reconstruction. The largest value of the width is about 0.34 mm, and the length is about 18.00 mm. Few light areas are observed on the surface (including the top face) of the specimen. However, it is interesting to note that a lot of light areas are also present inside the specimen (Fig.2.13). The lighter the area is, the denser the material is. The lightest area is observed from the surface extending to the interior. The value of the widest part of this area is about 1.52 mm.

These light areas make the specimen inhomogeneous. There are no other fissures observed in the interior of the specimen.

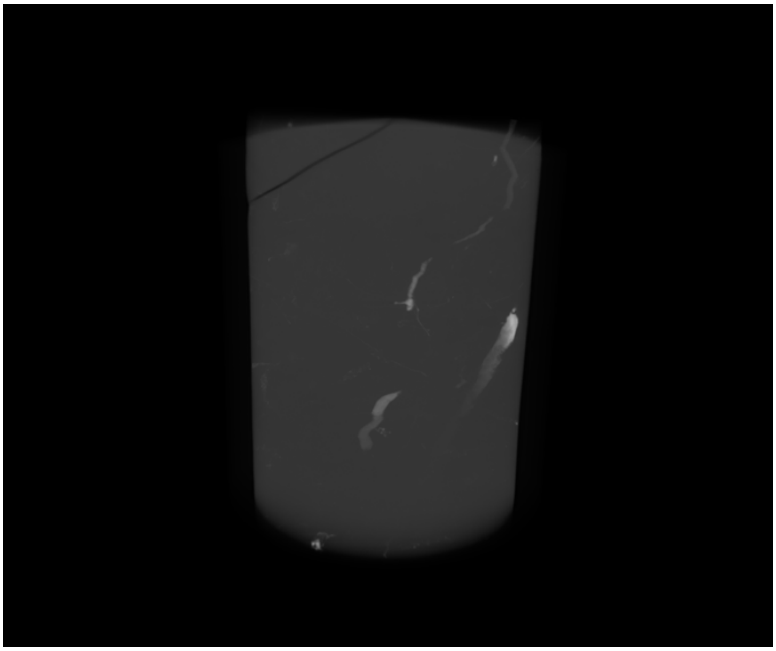

Fig. 2.11 CT imagining for a fissured specimen in 3-Dimensions.

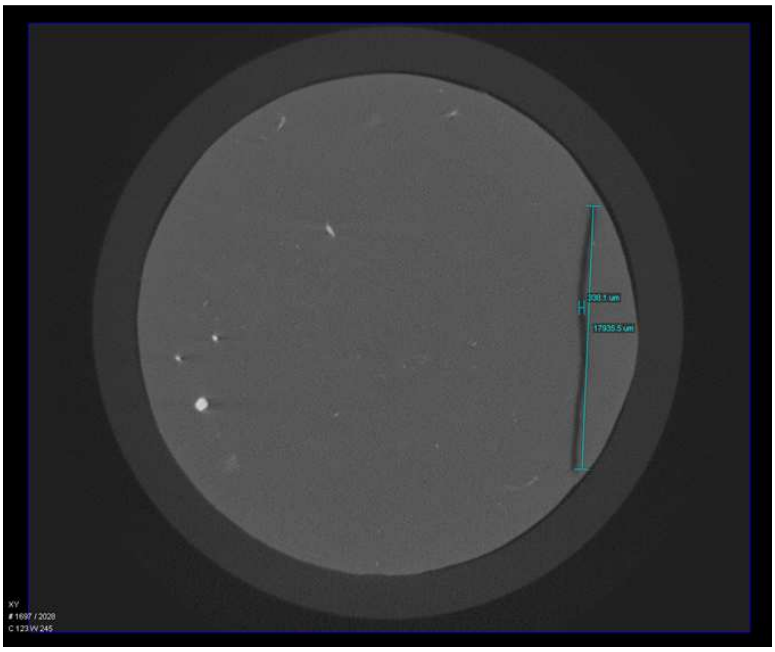

Fig. 2.12 CT imagining of a fissured specimen in planform.

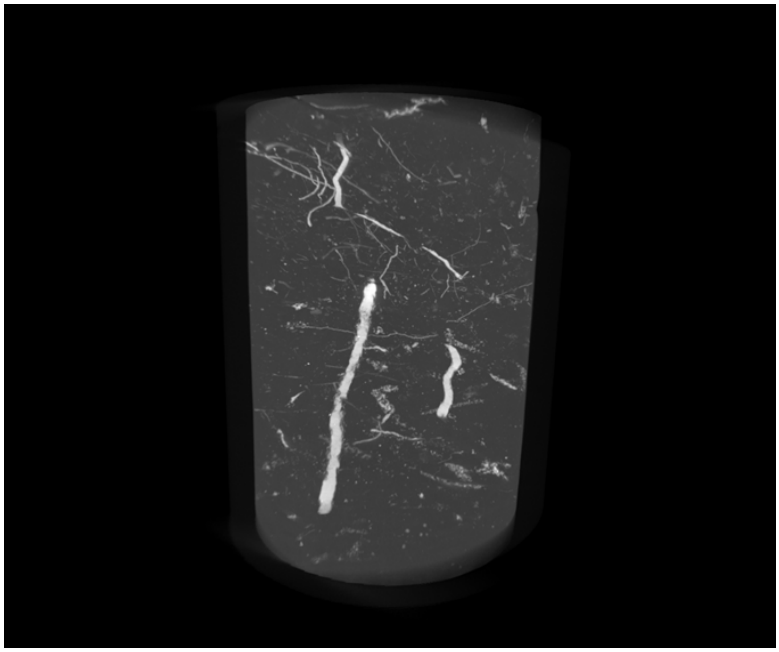

Fig. 2.13 CT imagining of a specimen in perspective.

2.3.2 SEM analysis

The main goal of this investigation was to examine the fabric of the clay before and after the compression test, and identify the chemical components of the clay particles. The SEM analyses were conducted at Ecole Centrale de Nantes (Fig.2.14), using a scanning electron microscope (SEM). The basic principle of the apparatus and the techniques used are similar to those documented in the literature (e.g. Smart & Tovey, 1982). An electron gun shoots a narrow electron beam against the sample's surface, while it is under low vacuum. Three magnetic lenses compress the size of the beam so that the size of the area being scanned reduces. On impact with the sample, the electrons are reflected in a way that depends on the topography of the constituents of the sample and a receiver-decoder of the reflected electrons produces a signal, which is converted into magnified images of the area being scanned (Fig.2.15).

Fig. 2.14 Scanning electron microscope in Ecole Centrale Nantes.

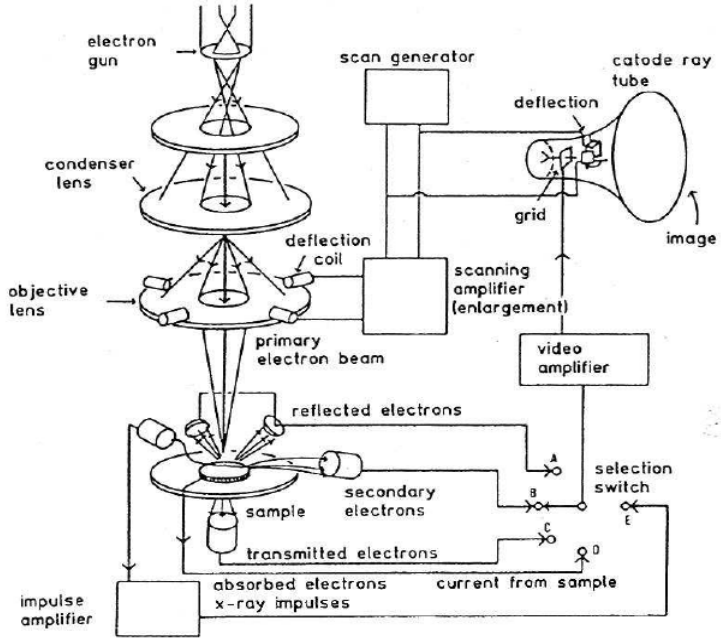

Fig. 2.15 Schematic diagram of electron microscope (manual of Cambridge 500 SEM).

The samples were air-dried for testing. In stiff clays, though, the shrinkage due to air-drying does not affect dramatically the soil structure and air-drying was therefore adopted.

In the following sections, the main features of the samples at the same depth (10 ~11 m) will be described. The photos of the natural sample were obtained in a plane oriented in the vertical direction (Fig.2.16).

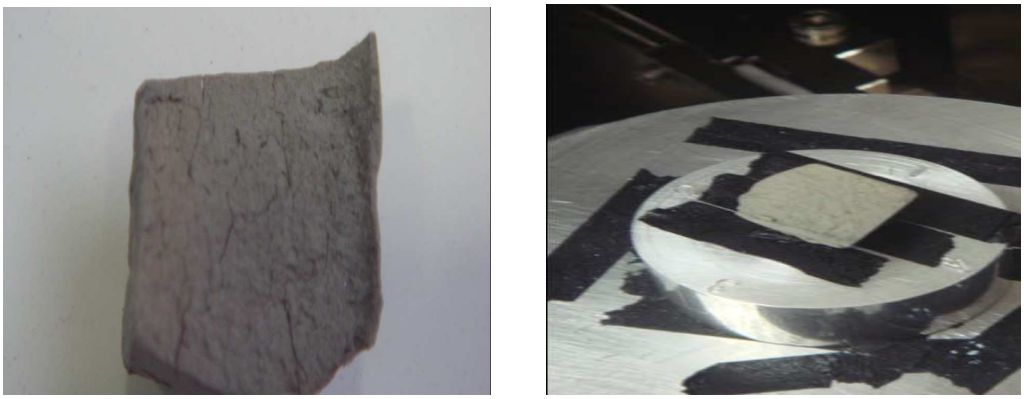

(a) **(b)**

Fig. 2.16 Sample for the SEM: (a) vertical plane and (b) fixing the sample.

In this study, the chemical composition of small zones within the clay was investigated, using a system composed of a scanning electron microscope with an X-ray receiver and diffractometer. The samples from SC3 2 ~3 m, SC3 4 ~5 m and SC3 8 ~9 m were analyzed.

Table 2.3 X-ray analysis on the sample at SC3 4 ~5 m.

Position (° 2θ)	Height (cts)	Rel. Int. (%)	Mineral
6.1	191.1	34.1	M?C?
8.7	101.7	18.1	Illite
11.4	55.2	9.9	M?C?
12.5	58.1	10.4	Kaolin
17.7	64.4	11.5	Illite
19.8	45.2	8.1	Quartz
20.9	123.2	22.0	
25.1	42.4	7.6	Kaolin
26.6	560.4	100.0	Quartz

Note: cts represents ‘contents’; Rel. Int. represents ‘relative intensity’; M?C? represents ‘Montmorillonite? Chlorite?’.

The clay platen were scanned at a rate of 5 seconds per 0.02° step width, using 0.3 mm slits from 2° to 62°. The minerals were quantified using the areas of reflections (peaks) for which there is no, or minimal, interference from other clay minerals. These areas were weighted using the relative intensity (Rel. Int. (%)). The value of relative intensity is determined by the height of the

detected area to the maximum height of the clay mineral in the diffractogram. In this study, the mineral with the maximum height is the quartz (see Fig.2.17 and Fig.2.18).

The scans obtained form the Merville clay sample at 4 ~5 m are shown in Fig.2.17 and the results are summarized in Table 2.3. The scans obtained form the Merville clay sample from different depths are shown in Fig.2.18.

In Fig.2.17 and Fig.2.18, the terms 'I', 'K', 'Q' represent the illite, the kaolinite and the quartz, respectively. Based on the results in Fig.2.18, it is obvious that the samples at different depths have similar mineral contents. The results presented in Table 2.3 can be used to analyze the mineral contents obtained on other samples.

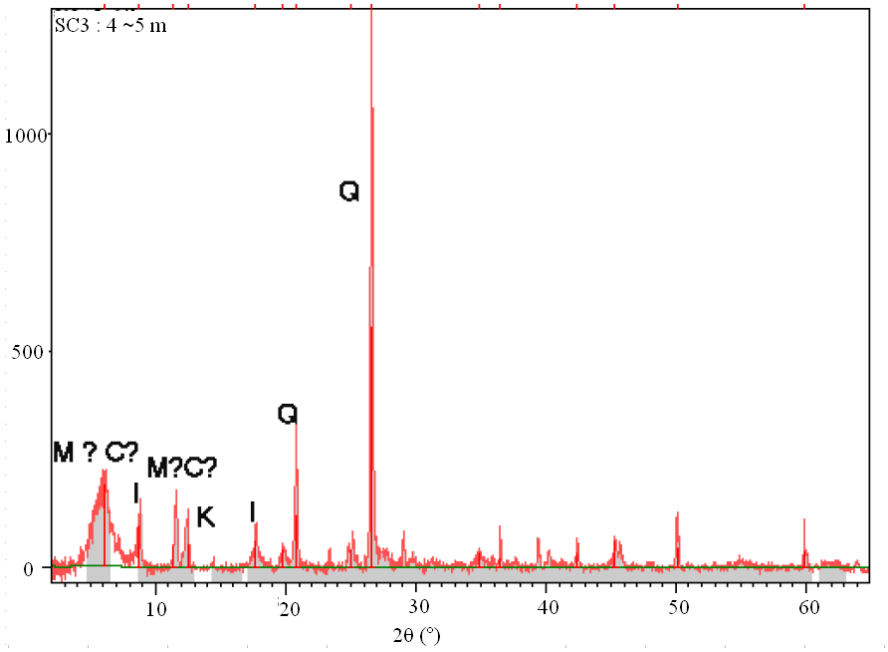

Fig. 2.17 X-ray analysis for the sample taken at 4 ~5 m of SC3.

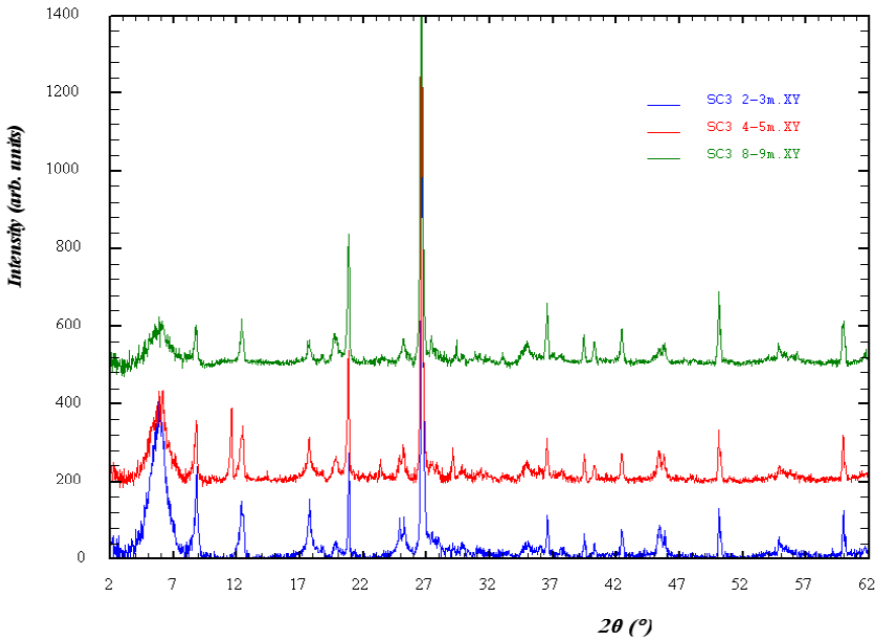

Fig. 2.18 X-ray analysis for the samples at different depths.

An analysis of Merville clay minerals was performed by Borel & Reiffsteck (2006) in LCPC (Laboratoire Central des Ponts et Chaussées), using X-ray diffractometry on a sample of Merville clay taken at 4.2 m. The main mineral component of the sample is crystalline quartz. Other non-clayey mineral components are plagioclase, feldspar and hematite. The clay fraction is a secondary phase. It consists of swelling minerals: montmorillonite. Other clayey minerals detected in less proportion are kaolinite, muscovite-illite and chlorite (Table 2.4). The mineral calcite is not detected in the sample taken at 4.2 m (Borel & Reiffsteck, 2006).

Table 2.4 Composition of clay fraction (sample taken at 4.2 m).

Clay fraction			
Montmorillonite	Muscovite-illite	Kaolinite	Chlorite
50%	20%	15%	15%

We performed a similar analysis on three clay samples of the SC3 borehole (depths of 2 ~3 m, 4 ~5 m and 8 ~9 m, respectively) reduced in a powder state. X-ray observation results show the main presence of quartz and illite. Smaller fraction of kaolinite and montmorillonite were also detected.

Fig.2.19 to Fig.2.23 show the photos of a sample taken at about 10.4 m deep with different magnifications. Based on the description of London clay in Gasparre (2005), at low magnification (Fig.2.19), the clay seems quite densely packed and well-orientated. At high magnifications (Fig.2.20, Fig.2.21 and Fig.2.22), a typical detrital clay fabric with particles aggregated in domains is recognizable. The rough shape of the clay particles indicates that the Merville clay deposited in a high-energy marine environment, due to wave and current action. However, the winnowing effects of waves did not remove the clay fraction completely.

In this study, the scanning electron microscope-energy dispersive spectroscopy (SEM-EDS) was used to examine the chemical composition of selected areas of natural clay samples. Areas, as small as 1*1 μm^2, were investigated and the results were presented as diffractograms indicating the chemical elements present (not minerals) (Fig.2.23).

The diffractograms of Fig.2.23 (a) and Fig.2.23 (b) relate to the individual white framboid crystal and a typical clay particle, respectively. In these two cases, silica and oxygen peaks with some metal ions, typically Al^{3+} and K^+ are presented. These components are expected to be the most important components of illite, quartz and kaolinite. The ion Na^+ is not found in Fig.2.23 (a) and Fig.2.23 (b).

These results show that calcium is widespread throughout the clay particles. The ion carbon is not detected in Fig.2.23 (a) and Fig.2.23 (b). Borel (2000) indicated that the content of $CaCO_3$ in the Merville clay is 6.8% ~ 8.8% as shown in Table 2.1.

To prove the existence of carbonate in the Merville clay used in this study, the standard chemical method using hydrochloric acid was used on a powder (grain size lower than 400 µm) obtained from the grinding of the dry initial clay. Then the powder was subjected to an attack of excess concentrated hydrochloric acid: the chemical reaction produces carbon dioxide, the volume measured is released into a graduated burette. The carbonate content is:

$$[T_{carb}(\%)] = \frac{1.2 \times V_b \times p}{m \times (\theta_b + 273)} \tag{2.1}$$

where T_{carb} is the carbonate content, V_b is the volume of CO2 (cm^3 or ml) , p is the air pressure (kPa), m is the mass of the sample (g) and θ_b is the temperature in the test room (Celsius degree).

The test results are presented in Table 2.5 which indicates the existence of carbonate. The carbonate content in the silty samples at 1 ~2 m and 3 ~4 m are less than 1%, whereas the carbonate content of the clayey samples below 5m are between 4% and 6%. That is a little less than the result presented by Borel (2000).

Table 2.5 Carbonate content distribution with depth.

Borehole	Depth	Temperature	Pressure	Mass	Volume of CO_2	Calcium Carbonate content
		θ_b	p	m	V_b	T_{carb}
	(m)	(°C)	(kPa)	(g)	(cm^3)	%
SC2	1~2	19	100.7	9.84	18.5	0.78
		19	100.7	10.03	19.0	0.78
SC2	3~4	20	100.8	10.16	23	0.93
		20	100.9	10.04	22.5	0.93
SC1	5~6	20.5	100.9	5.02	66	5.42
		20	100.9	5.06	70	5.72
SC1	7~8	20	100.9	5.16	51	4.08
		20.5	100.9	5.73	56	4.03
SC2	9~10	20	100.9	4.83	66	5.65
		20	101.0	5.12	67	5.41
SC1	10~11	20	100.9	5.05	46	3.76
		20	100.9	5.29	49	3.83

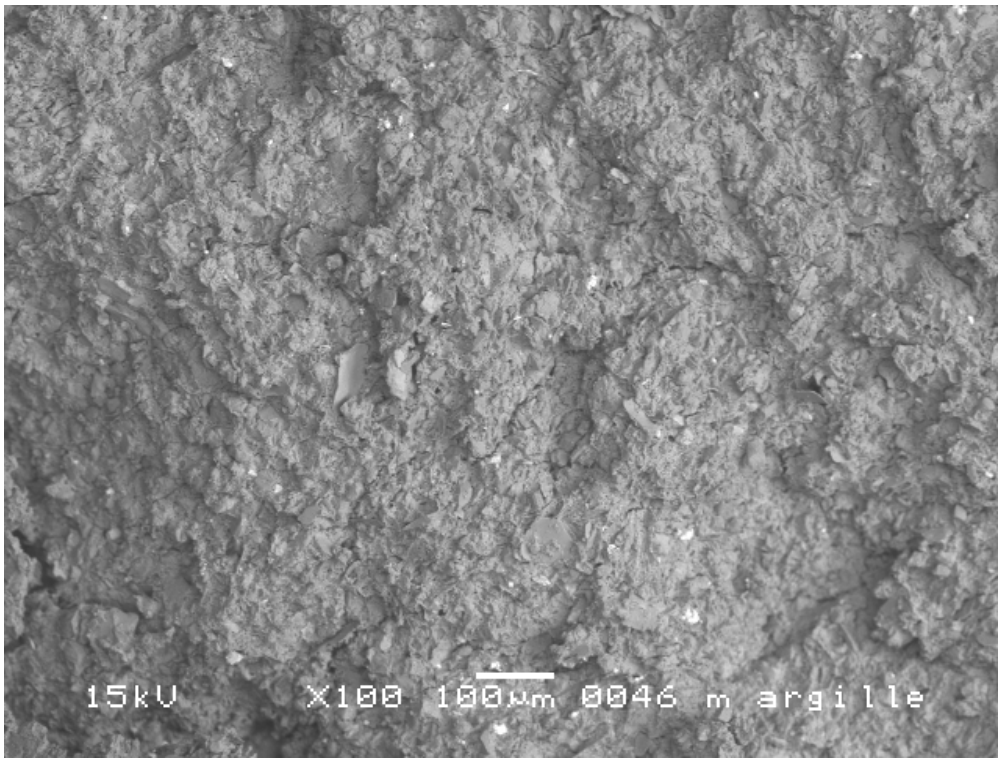

Fig. 2.19 Natural sample taken at 10.4 m with some fissures.

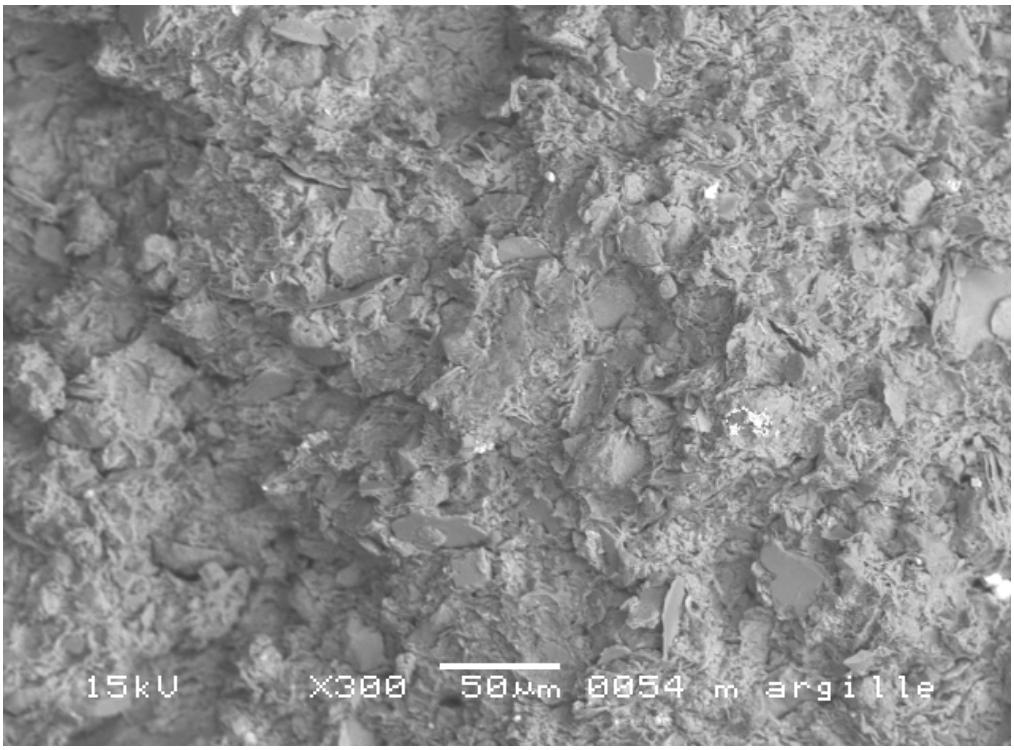

Fig. 2.20 Natural sample.

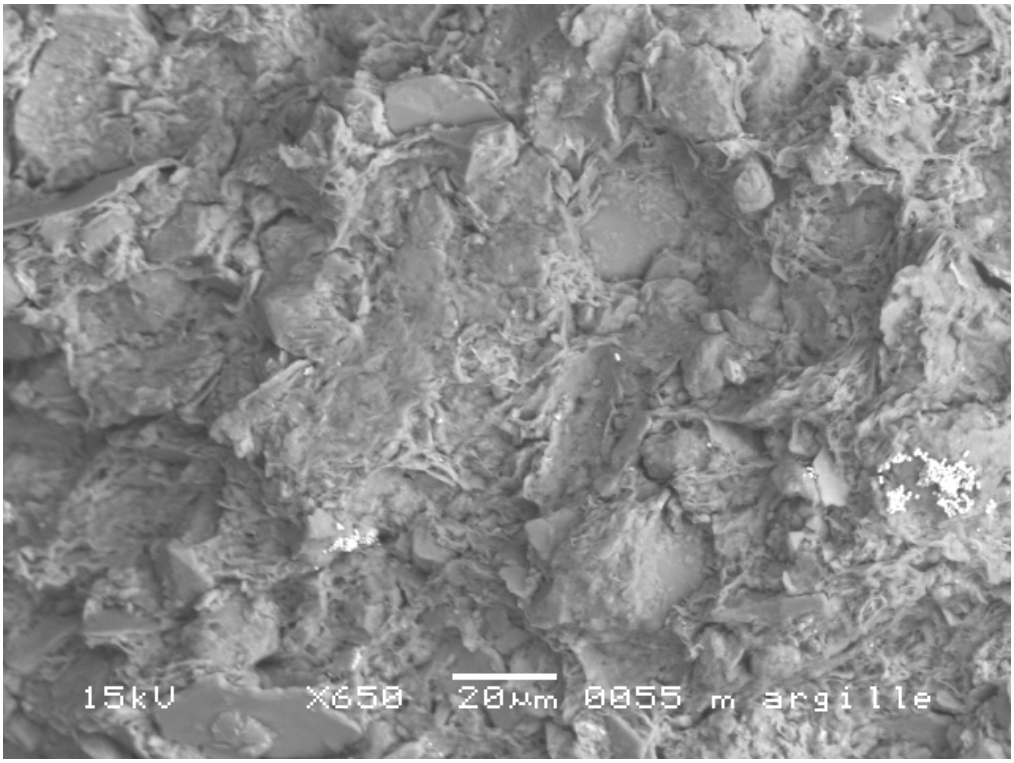

Fig. 2.21 Natural sample: orientated domains and white framboid crystals.

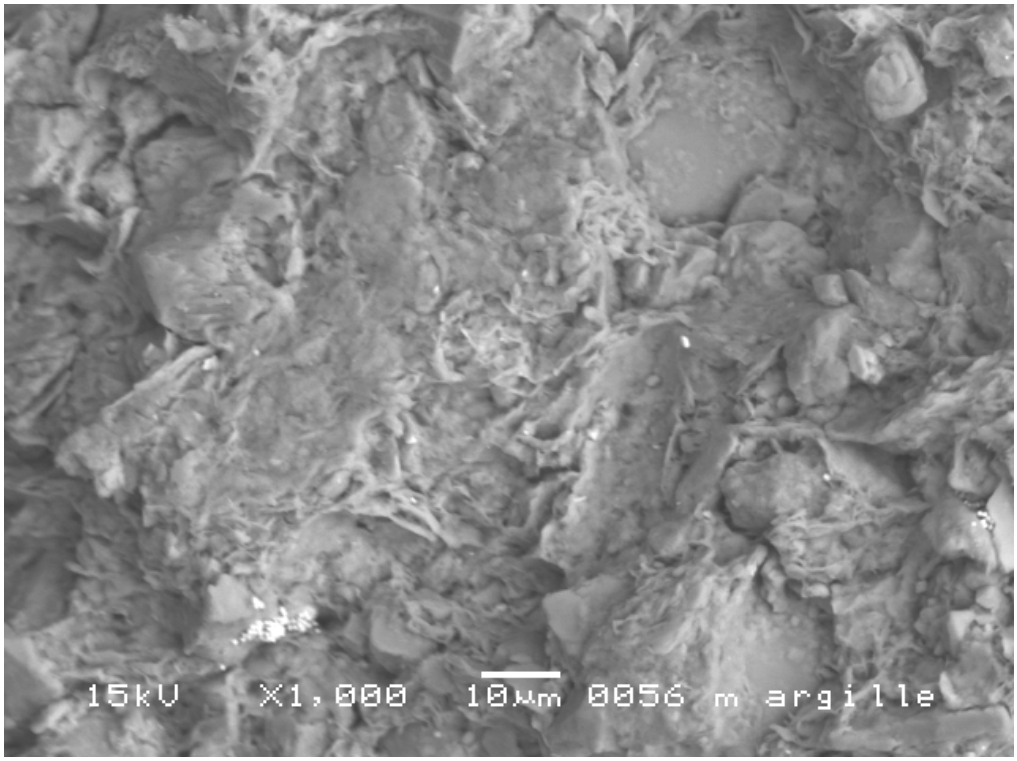

Fig. 2.22 Natural sample: rough and sharp edges of the particels around a grain.

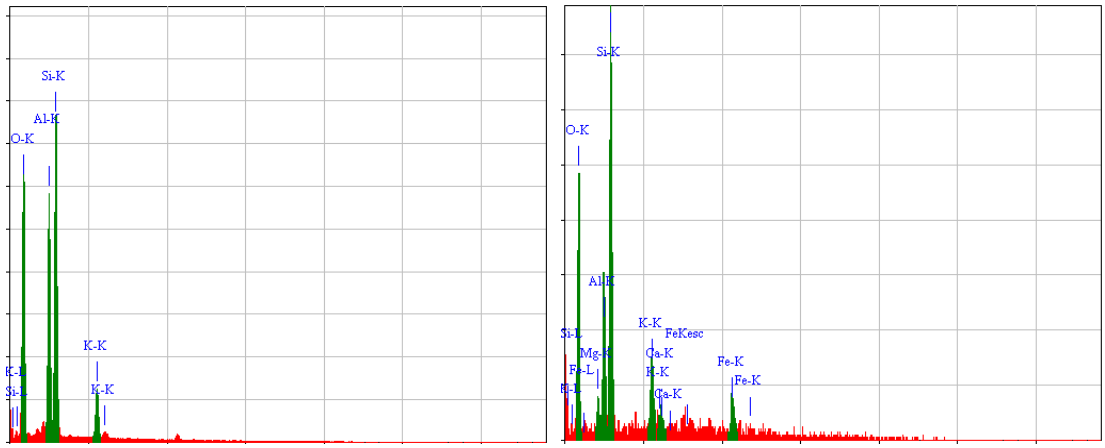

(a) **(b)**

Fig. 2.23 Diffractograms resulting from the micro-chemical analysis: (a) white framboid crystal and (b) clay particle.

2.4 Conclusions

The Merville clay is an overconsolidated, fissured, stiff clay which is located beneath the depth of 3 m. From the test results conducted in the laboratory, the following conclusions concerning its physical properties can be drawn.

(1) The Atterberg limits of Merville clay are relatively constant for the depths between 3 m and 11 m. The liquid limit range is 89.4% ~100.6% and the plasticity index range is 46.1% ~ 61.4%. These values correspond to a highly plastic clay.

(2) The water content is smaller than the plastic limit, indicating a high overconsolidation ratio. The water content is higher at the top of the layer, between 3m and 4m. This can be explained by the development of fissures due to the unloading of the clay during its geological history (see chapter 1).

(3) The clay size content of the Merville clay is about 26%. The value of the specific gravity G_s of Merville clay is at the range of 2.51 ~2.77.

(4) The CT images show much heterogeneity in the microstructure, particularly the existence of denser parts randomly distributed inside the clayey material.

(5) Based on X-ray analyses, the samples of Merville clay at different depths have similar mineral contents.

3 One-dimensional compression behavior of Merville clay

3.1 Introduction

The study on Merville clay along 1D compression stress path (oedometer) has two objectives:

1) Investigating the effects of the clay structure through comparisons between the behavior of the intact soil and that of the same clay in a reconstituted state. Analyzing the effects of structure on the compression behavior of clays with the normalizing parameters commonly found in the literature.

2) Defining the characteristics of compressibility of the clay, especially the preconsolidation pressure. The mechanical behavior of clay depends significantly on its overconsolidation ratio which relates to its preconsolidation pressure.

This study of oedometer tests on Merville clay includes two parts:

1) The first part consists of the tests at low pressure levels, that is to say, the traditional oedometer tests where the maximum applied vertical stress is about 1 MPa. Six oedometer tests were conducted. However, the results obtained in this study were not clearly representative of the actual properties of this clay, especially in regards of the preconsolidation pressure of this clay. This situation led us to consider a complementary study which would be better suited for the characteristics of Merville clay.

2) Consequently, the second part of the oedometer study on Merville clay focused on applying high pressure loading. During this study, the tests were performed in a strain-controlled mode, wherein the clay samples were loaded at the maximum stress of about 12 MPa.

3.2 Preconsolidation pressure

The preconsolidation pressure of a soil is the maximum pressure at which the soil has been consolidated during its geological history.

During the formation of the clay, its state follows the virgin consolidation curve in the diagram 'void ratio, *e* - logarithmic effective vertical stress, σ'_v' shown in Fig.3.1.

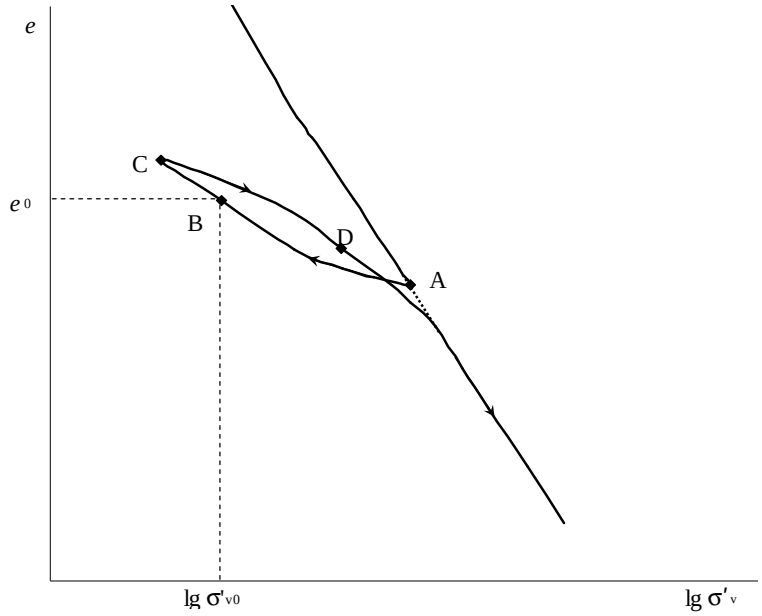

From Biarez & Hicher, (1994)

Fig. 3.1 Deformation path of a soil.

The value of the void ratio, e_0, and the value of the effective vertical stress, σ'_{v0}, are the in-situ values of the soil. The following path relative to the unloading (due to erosion for instance) is represented in Fig.3.1 by the segment AB: the point A represents the soil state at the end of the period of its initial loading, and the point B represents the soil state after its geological unloading, which is also the soil state before sampling. After the sample preparation, the soil state will vary and will be defined by the point C which represents the state in the laboratory.

This may be a simplified mapping for the geological history of the soil before the laboratory testing. From these theoretical considerations, some authors have identified methods for determining the preconsolidation pressure, that is to say, the value of the point A in Fig.3.1.

The determination of the preconsolidation pressure is conventionally performed using the results of oedometer tests, following several methods (Casagrande, Schmertmann, etc.). In this study, Casagrande method was used to obtain the preconsolidation pressure.

The procedure of Casagrande method can be explained as follows: firstly, obtain the point O of maximum curvature on the consolidation curve, then draw a horizontal line from this point, draw a line tangent to the curve at the point, then bisect the angle made from the horizontal line in part 1 and the tangent line in part 2 by a straight line in part 3, extend the 'straight portion' in part 4 of the recompression curve (high effective stress, low void ratio: almost vertical on the right of the graph) up to the bisector straight line. Finally, the point E where the lines in part 3 and part 4 intersect is the preconsolidation pressure. This procedure is shown in Fig.3.2.

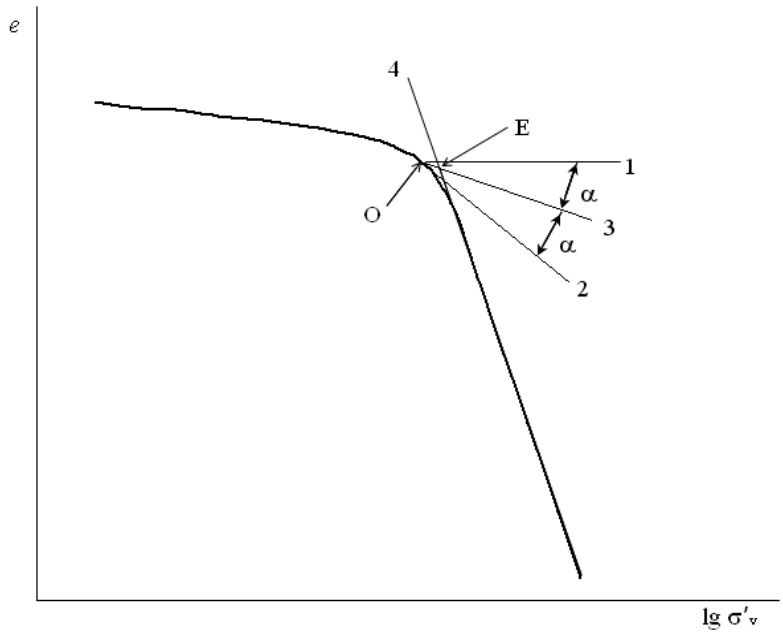

Fig. 3.2 Sketch of the procedure of the method of Casagrande.

3.3 Oedometer test

3.3.1 Preparation of specimen

3.3.1.1 Preparation of natural specimen

The specimens of 70 mm in diameter and 19 mm in height are cut from a sample of 110 mm in diameter and 50 mm in height, separated from the tube. This sample is first roughly trimmed so

that the sample dimensions are slightly greater than that of the confining ring. One end of the confining ring is equipped with a sharp edge. The confining ring is then drived into the sample by a progressive and vertical pressure. A few centimeters (1 to 3 cm) in diameter of the soil are allowed to exceed the confining ring. The excess soil is carefully carved away and is used for water content measurements.

Both sides of the confining ring are leveled off. The whole is then weighed. Both sides of the specimen remaining in the confining ring are then covered with filter papers. The two porous stones are placed on the top and bottom of the specimen for drainage during the consolidation process. This assembly is then placed into a loading frame.

In this chapter, the presence of fissures in Merville clay is not observed during the preparation of the intact specimen. The oedometer tests are all conducted in a room which has a constant temperature (about 20 $^{\circ}$C).

3.3.1.2 Preparation of reconstituted specimen

Reconstituted clay is used as a remoulded state and is prepared at a water content equal to or greater than the liquid limit (w_L). Burland (1990) recommended that the clays should be reconstituted at a water content between w_L and 1.5 w_L (preferably 1.25w_L) without air drying or oven drying, and then consolidated, preferably under one-dimensional condition.

In the laboratory, the natural clay samples at a depth between 4 ~11 m, where the mineralogy is assumed homogeneous, were used. The samples were dried in an oven, then grinded into a powder state (particle size lower than 80 μm), then weighed. The water was mixed with the powder so that the water content of the slurry was between w_L and 1.5 w_L.

The slurry was poured into a consolidometer. The inner diameter of the tube made of Plexiglass with a smooth surface was 90 mm and the height was about 450 mm. In general, the outer part of a reconstituted clay in a consolidometer suffers shear deformation because of the friction between the clay and the tube.

The consolidometer is presented in Fig.3.3. The tube, corresponding to a confining ring of an oedometer test, has a thickness of about 6 mm. Drainage was allowed from both the top and

bottom of the specimen. The interface between the sample and the tube was lubricated with silicone grease to avoid friction.

Fig. 3.3 The consolidometer for preparing the reconstituted samples.

The vertical load was applied through dead weights. In this study, the reconstituted samples were prepared under two different vertical stresses σ'_v, 100 kPa and 300 kPa, respectively. The samples were allowed to consolidate under this load until the axial displacement changes were less than 0.1 mm per day. The consolidation took at least three weeks.

The preparation of the reconstituted specimen in the oedometer apparatus followed the same procedure than the preparation of the intact specimen mentioned above.

3.3.2 Saturation of the specimen

In general, achieving the saturation of the specimen is an important phase for doing the oedometer test, according to the assumptions of the Terzaghi consolidation theory. Any default in the saturation is reflected first by a settlement due to the compressibility of air. This can change the evolution of settlement, especially at the beginning of the oedometer test.

The sample reserved in the tube can remain intact (or almost intact) due to the appearance of capillary tensions. The capillary tensions offset, at least, the effects of unloading. The saturation results in canceling these capillary tensions, which causes the swelling of the sample. On the other

hand, the saturation by simple immersion is not sufficient in some cases. To remedy this shortcoming, it is necessary to apply a pressure against the specimen. This pressure will result in the complete saturation.

In this study, the initial vertical pressure is about 4.6 kPa. As a result of the effect of swelling, the first point of the compression curve is the point C shown in Fig.3.1. This point is not the initial point B representative of the in-situ conditions (initial void ratio, e_0, and in-situ effective vertical stress, σ'_{v0},). In this study, no back pressure can be applied and the pore pressures were not measured for all the oedometer tests.

3.3.3 Procedure of the oedometer tests

3.3.3.1 Procedure of the oedometer test at low pressure levels

The incremental loading compression test was used to obtain the behavior of Merville clay in oedometer tests at low pressure levels. The main characteristics of this test are the following sequences:

1) The first applied load is the pressure required to prevent the swelling during the saturation. This load is used to ensure a good contact between the upper piston and the specimen. In this study, this load is about 4.6 kPa for the intact specimen. The reconstituted specimen was set up in the apparatus with the first applied load equal to the vertical stress, σ'_v, used in the consolidometer.

2) From the second load, which is generally equal to half of the in-situ effective vertical stress, $0.5\sigma'_{v0}$, the successive incremental load is fixed at $0.25\sigma'_{v0}$ until the probable range of in-situ effective vertical stress, σ'_{v0} is reached.

3) After the completion of the first loading-unloading cycle, the loading rate ($i=\sigma'_{n+1}/\sigma'_n$) is fixed equal to 2 until the last loading step.

4) The duration of each step is 24 hours.

3.3.3.2 Procedure of the oedometer test at high pressure levels

In the laboratory, the apparatus presented in Fig.3.3 cannot be used to perform the oedometer test at high pressure levels (more than 10 MPa).

The constant strain-rate (*CRS*) consolidation test is used to apply high vertical stresses. *CRS* consolidation tests were performed by using a 50 kN Wykeham Farrance testing machine which is a strain controlled machine. The specimens for these tests were 70 mm in diameter and 19 mm in height. The axial strain rate used in these tests was 0.63 %/h (0.002 mm/min). During loading, the drainage was permitted from both the top and the bottom of the specimen. The strain rate was chosen small enough so that no excess pore pressure was expected during loading.

As mentioned above, the first applied load is the pressure required to prevent the swelling during the saturation. This load is used to ensure a good contact between the upper piston and the specimen. In these tests, this load is about 8.9 kPa for the intact specimen. The reconstituted specimen was set up in the apparatus with the first applied load equal to the vertical stress, σ'_v, used in the consolidometer, which corresponds to the preconsolidation pressure for the reconstituted samples.

3.4 Results of oedometer tests

3.4.1 Results of oedometer tests at low pressure levels

The specimens for these tests were taken at the depth of 4 m ~11 m. The basic parameters about these specimens are presented in Table 3.1.

In Sections 2.1 and 2.2 of Chapter 2, the depth of water table in Merville is assumed to be 3 m. The soil from 0 m to 3 m is the gravel and silty clay head. The average value of the specific weight γ_h of this soil is 18.3 kN/m^3. The soil from 3 m to 11 m is Merville clay. The average value of the saturated specific weight γ_{sat} of Merville clay is 19.6 kN/m^3. From the information mentioned above, the in-situ effective vertical pressure, σ'_{v0}, can be estimated for all the intact specimens. All the intact samples were taken below the water table. Based on the test results shown at Chapter 2, the degrees of saturation of these intact samples were 100%.

The clay at the depth of 7 m ~11 m was taken for preparing the reconstituted specimen of the test OL6 in Table 3.1. For the reconstituted specimen, the effective vertical pressure, σ'_{v0} represents the preconsolidation pressure, σ'_p. The degree of saturation of this reconstituted sample was 100%.

Table 3.1 Basic parameters of specimens – Oedometer tests at low pressure levels.

Test name	Type of specimen	Depth (m)	γ_h (kN/m^3)	γ_d (kN/m^3)	w_0 (%)	σ'_{v0} (kPa)	e_0
OL1	Intact	6.12	20.6	15.8	34.1	84.9	0.713
OL2	Intact	6.27	19.4	15.1	33.3	86.3	0.762
OL3	Intact	7.24	19.7	15.6	30.4	95.6	0.614
OL4	Intact	8.41	19.5	15.0	32.9	106.8	0.719
OL5	Intact	9.14	19.0	15.4	34.5	113.8	0.820
OL6	Reconstituted	7 ~11	16.8		50.8	100	1.347

From Fig.3.4 to Fig.3.9, the compression curves from the oedometer tests at low pressure levels for intact and reconstituted samples are presented. The swelling indexes are also shown for each intact sample in these figures. Based on the test results, the values of swelling indexes for each intact sample are presented in Table 3.2.

For all the intact samples, the vertical stress was increased up to 100 kPa and then decreased down to 4.6 kPa. After unloading, the void ratio does not change much compared to the initial void ratio. That may be due to an internal bonding which is sufficiently strong to resist structural breakdown. Note that, after loading up to about 800 kPa, the intact sample has become approximately twice (or more) as expansive as the one subjected to the first unloading. Thus the process of loading must have destroyed some of the bonding.

Josseaume et al. (1991) indicated that the preconsolidation pressure for the Flanders clay is 3400 kPa, as shown in Fig.3.10. The maximum vertical pressure for the oedometer test at low pressure level is less than 1000 kPa. It is clear that the normal consolidation line has not been reached for the intact samples.

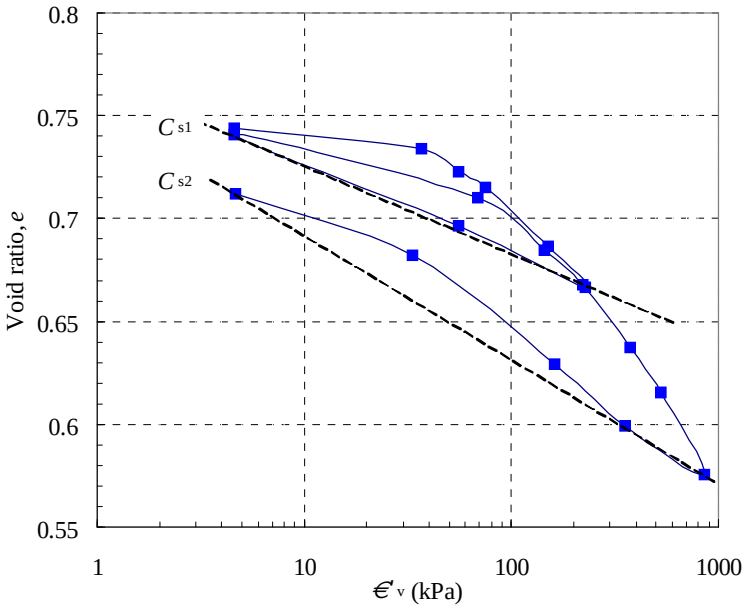

Fig. 3.4 Compression curve for natural sample (OL1).

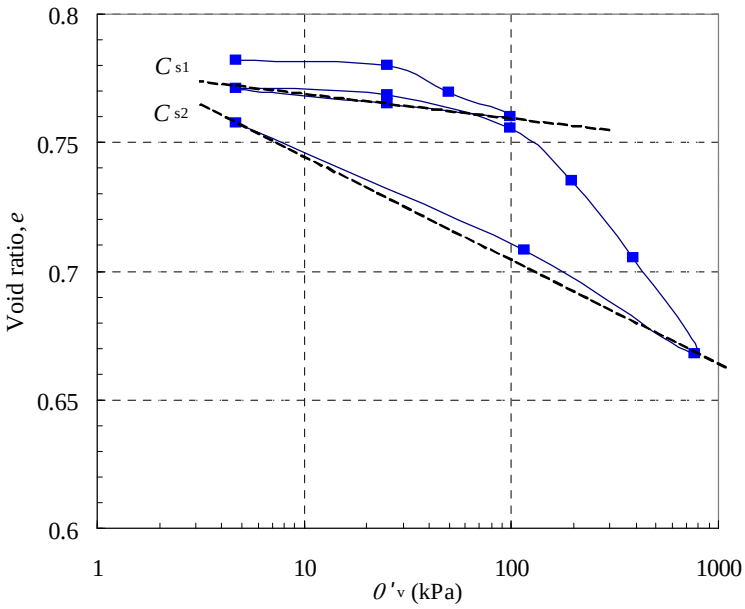

Fig. 3.5 Compression curve for natural sample (OL2).

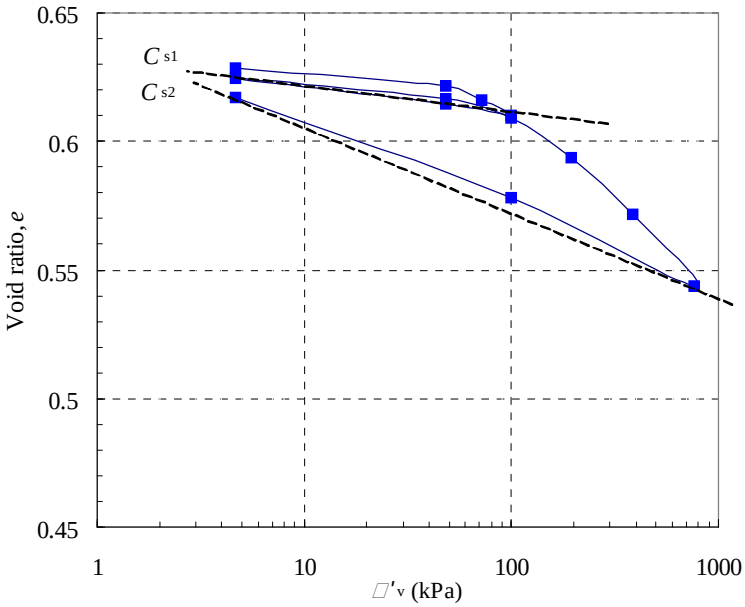

Fig. 3.6 Compression curve for natural sample (OL3).

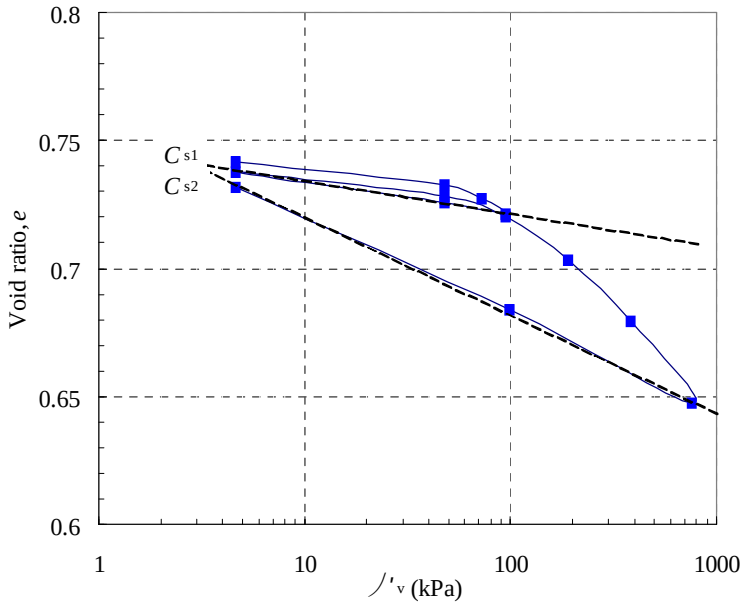

Fig. 3.7 Compression curve for natural sample (OL4).

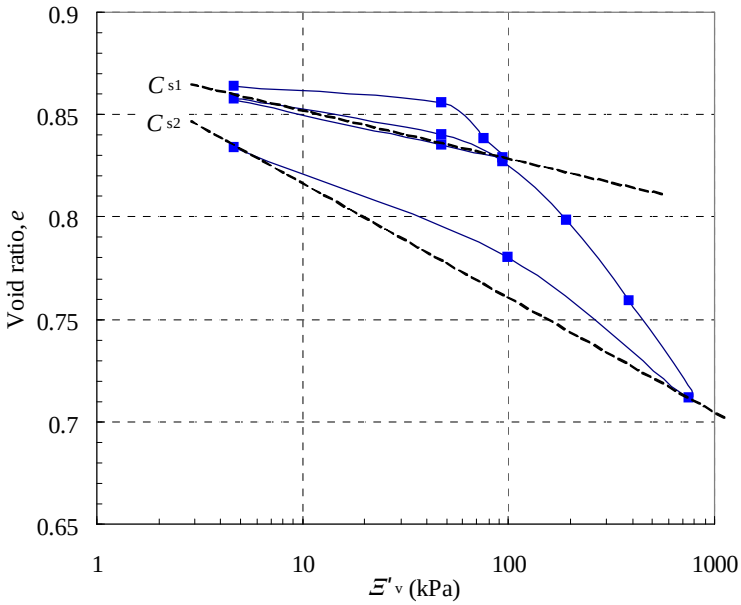

Fig. 3.8 Compression curve for natural sample (OL5).

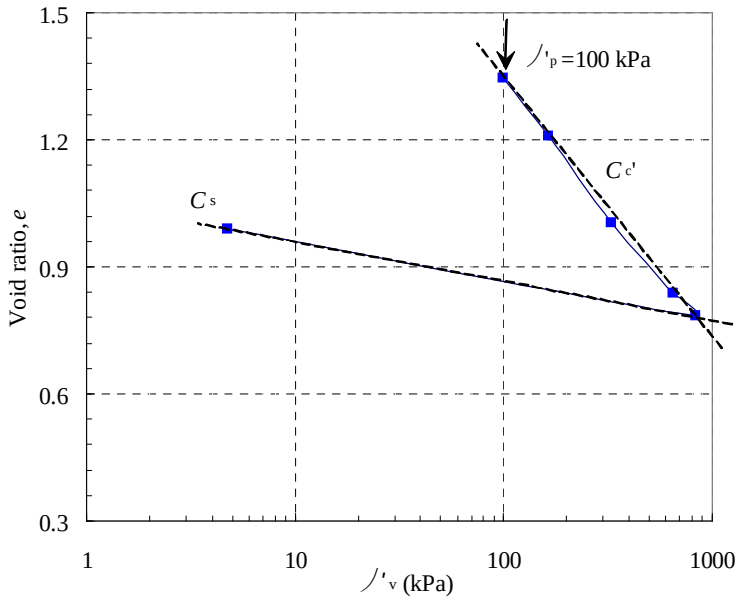

Fig. 3.9 Compression curve for reconstituted sample (OL6).

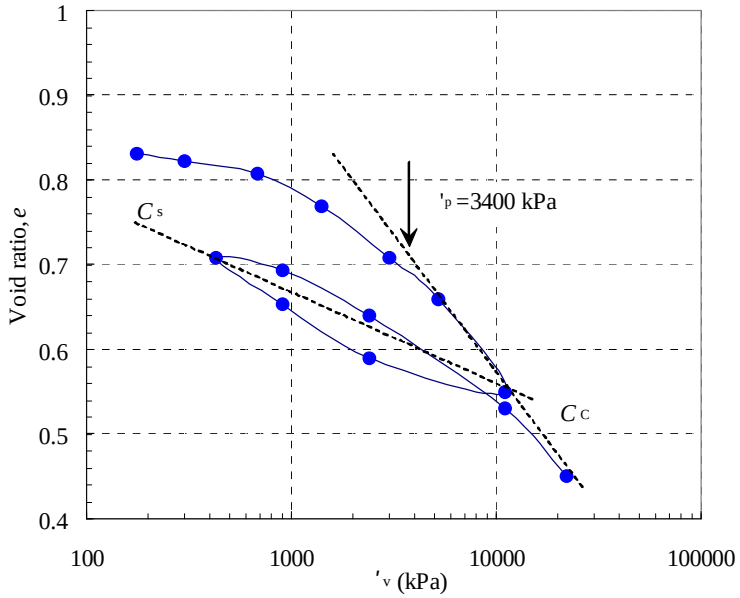

From Josseaume et al., (1991)

Fig. 3.10 Preconsolidation pressure of Flanders clay at the depth of 42.9 m.

Table 3.2 Results of oedometer tests at low pressure levels.

Test name	Type of specimen	C_{s1}	C_{s2}	C_s	C_c'
OL1	Intact	0.044	0.062		
OL2	Intact	0.009	0.041		
OL3	Intact	0.011	0.033		
OL4	Intact	0.013	0.038		
OL5	Intact	0.022	0.055		
OL6	Reconstituted			0.123	0.610

The Merville clay (7 ~11 m) was used to prepare the reconstituted sample. The preconsolidation pressure applied to the reconstituted sample is 100 kPa which is shown in Fig.3.10.

The compression index denoted C_c' at the maximum pressure less than 1 MPa and the swelling index C_s of the reconstituted sample are presented in Table 3.2. The compression curve plotted in Fig.3.9 represents the intrinsic compression curve of the clay since it was reconstituted at a water content between w_L and 1.5 w_L.

3.4.2 Results of oedometer tests at high pressure levels

As mentioned above, there are two reasons for performing oedometer tests at high pressure levels. The first aim is to assess the preconsolidation pressure of intact Merville clay. The second aim is to complete the intrinsic compression curve of Merville clay.

In this section, in addition to the result of the oedometer test OL6, a reconstituted specimen at the same depth (7 ~11 m) was prepared for obtaining the void ratio corresponding to σ'_v=1000 kPa. The other reconstituted specimen from the intact Merville clay (3 ~7 m) was also used to perform the oedometer test at high pressure level.

To examine the effect of the strain rate on the behavior of the Merville clay in oedometer tests, two intact specimens at the same depth were prepared. One test (Fig.3.11) used the reference strain rate (0.63 %/h). The procedure for the second test (Fig.3.12) involved changes in the strain rate: reference strain rate for loading up to 220 kPa, then one tenth of the reference strain rate (0.063 %/h) for loading up to 330 kPa, then ten times the reference strain rate (6.3 %/h) from 330 kPa to 1050 kPa, and again the reference strain rate for loading from 1050 kPa to the end of this test. For analyzing the effect of strain rates on the preconsolidation pressure and yield stress, the different strain rates were applied before the preconsolidation pressure in the compression curve.

The basic parameters about these specimens are presented in Table 3.3. The degrees of saturation of all the specimens at high pressure levels were 100%.

Table 3.3 Basic parameters of specimens – Oedometer tests at high pressure levels.

Test name	Type of specimen	Depth (m)	γ_h (kN/m^3)	γ_d (kN/m^3)	σ'_{v0} (kPa)	w_0 (%)	w_L (%)	e_0
OH1	Intact	7.43	19.3	14.3	97.4	34.8	93.8	0.793
OH2	Intact	7.53	19.3	14.4	98.4	34.8	93.8	0.791
OH3	Intact	9.48	19.2	14.3	117.1	34.8	96.1	0.805
OH4	Reconstituted	4 ~7	17.3	11.7	100	47.1	90.8	1.266
OH5	Reconstituted	7 ~11	18.2	13.2	300	38.1	93.8	0.953

Note: Different strain rates for test OH2.

The compression curves of oedometer tests at high pressure levels for intact and reconstituted samples are presented in Fig.3.11 to Fig.3.15. The swelling indexes are shown for each intact sample in these figures. The preconsolidation pressure is marked in the compression curve of each intact sample, following the Casagrande method for over-consolidated clays. The values of swelling indexes and compression index of each intact sample are presented in Table 3.4. In his paper, Hieng (1991) used also the Flanders clay located at Dunkirk to carry out the 1D compression tests at high pressure levels. The samples of Dunkirk clay were all taken at the depth of more than 30 meters. The test results are shown in Table 3.4. The preconsolidation pressures of Dunkirk clay are determined by the simplified method.

Note that, as the load increases, the swelling index also increases. Evidently, the loading process leads to the destruction of part of the bonding. The slope of the swelling curve of the intact material typically starts changing as soon as the destructuration begins and is expected to be parallel to the swelling curve of reconstituted sample when the destructuration is complete. After loading up to more than 10000 kPa, the swelling indexes of the three intact samples are similar, approximately equal to the swelling indexes of the reconstituted samples presented in Table 3.5. That means that the structure of each intact sample is completely destroyed at the end of the loading process.

Table 3.4 Results of natural samples at high pressure levels .

Test name	C_{s1}	C_{s2}	C_{s3}	C_s	C_c	σ'_p (kPa)
OH1	0.098			0.150	0.755	2800
OH2	0.073	0.115		0.139	0.591	2600
OH3	0.084	0.096	0.130	0.144	0.686	2750
Hieng 1				0.120	0.340	5000
Hieng 2				0.100	0.290	3600
Hieng 3				0.100	0.310	2800

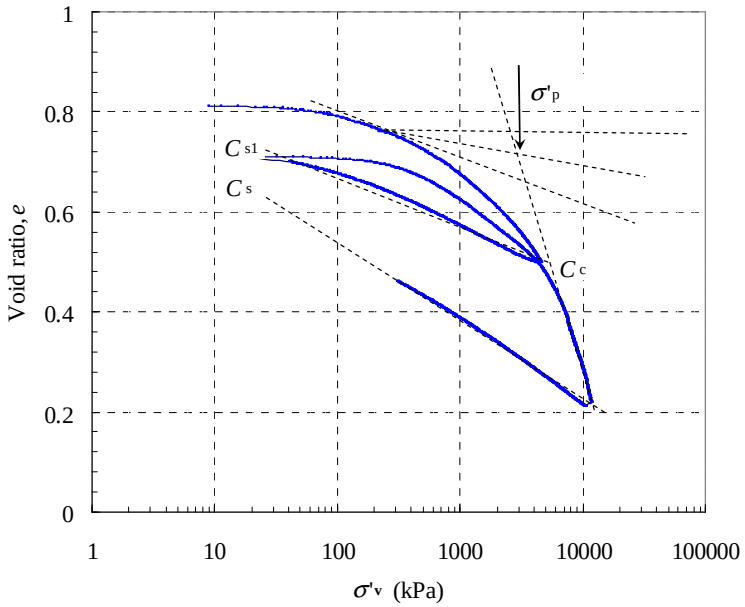

Fig. 3.11 Compression curve for natural sample (OH1).

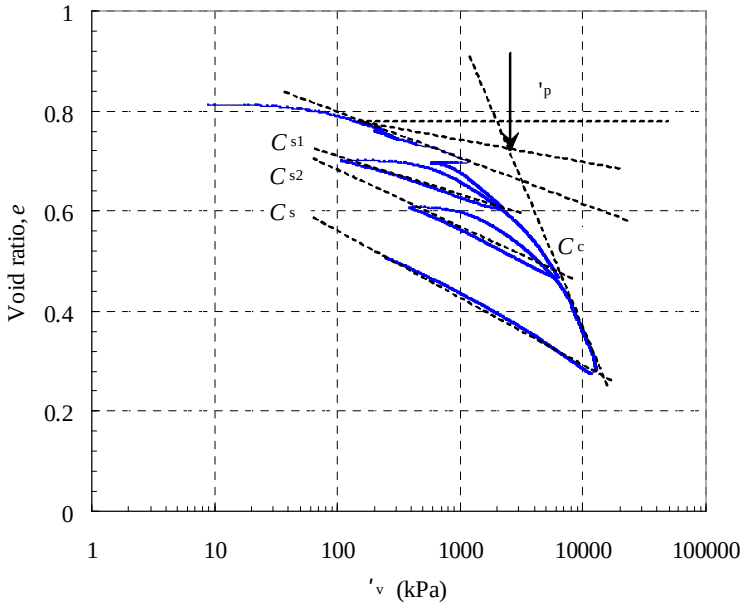

Fig. 3.12 Compression curve for natural sample (OH2).

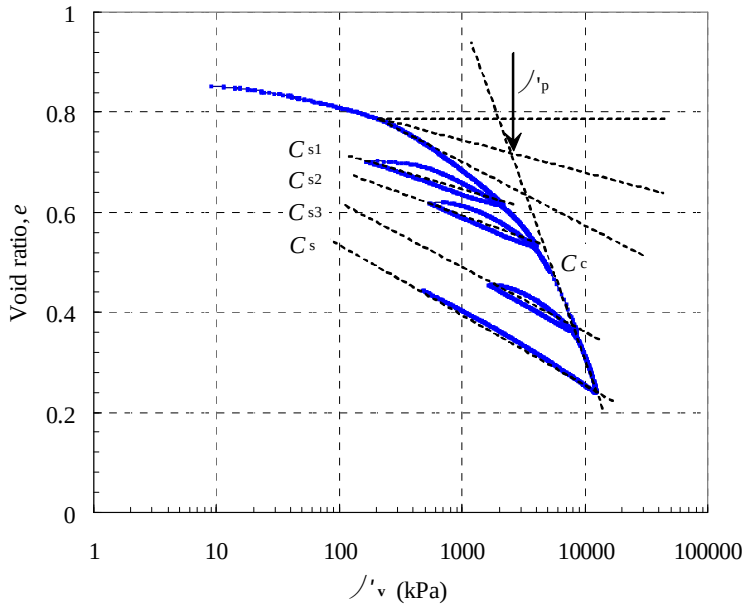

Fig. 3.13 Compression curve for natural sample (OH3).

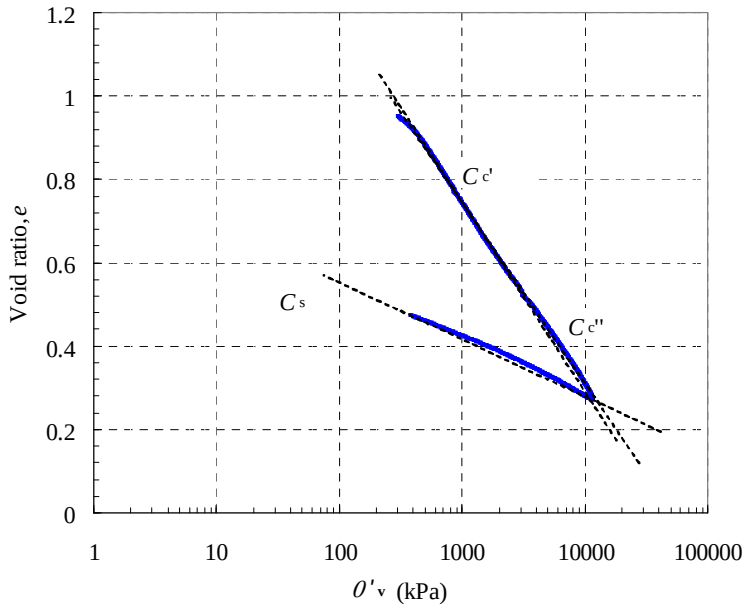

Fig. 3.14 Compression curve for reconstituted sample (OH4).

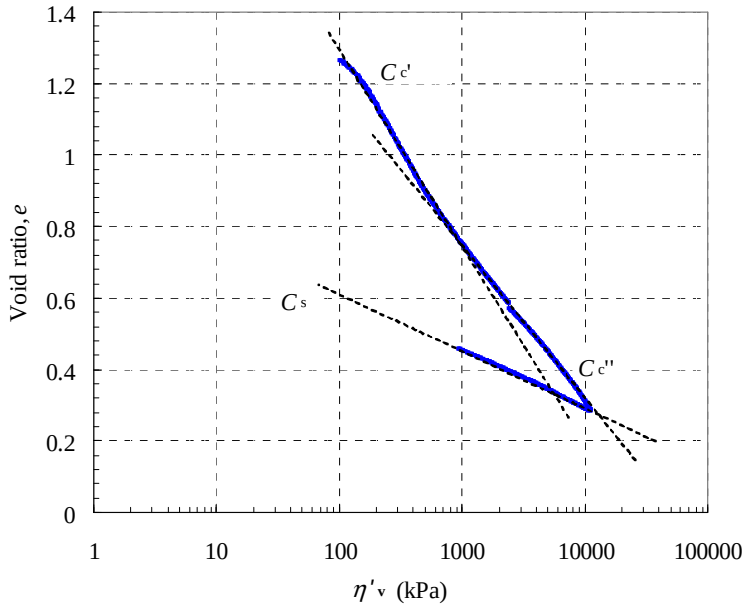

Fig. 3.15 Compression curve for reconstituted sample (OH5).

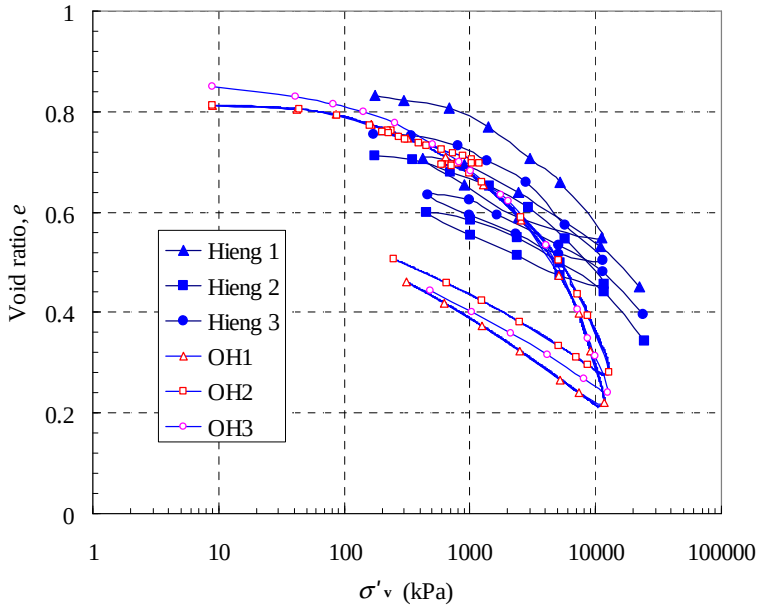

Fig. 3.16 Test results on natural Flanders clay at high pressure levels.

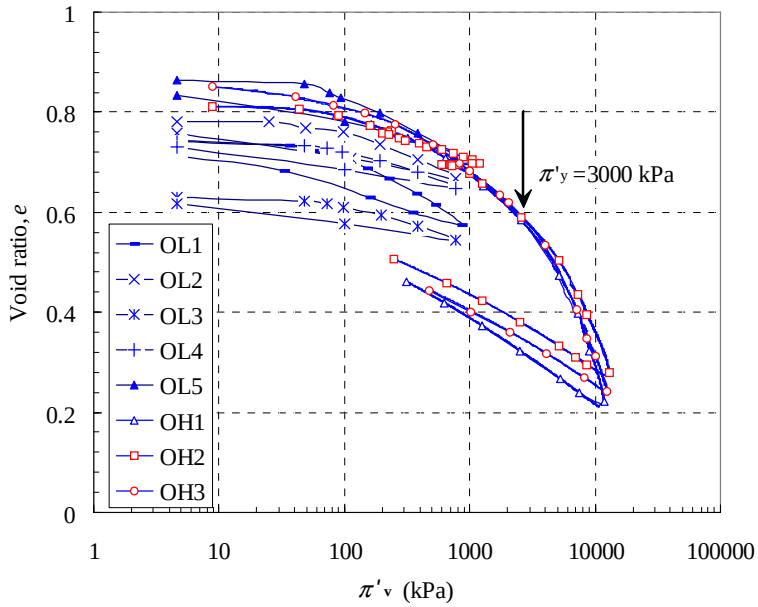

Fig. 3.17 Compression curves for natural samples at low and high pressure levels.

As mentioned in Chapter 1, Hight et al. (1992) and Cotecchia & Chandler (2000) indicated that there is a stress state which they called 'gross yield', at which the soil stiffness decreases significantly. Beyond gross yield, the plastic strain increments become substantially larger as a result of the degradation of the soil structure. This yield stress σ'_y is a little higher than the preconsolidation stress σ'_p. As a result of the existence of the yield stress of Merville clay shown in Fig.3.17, the measured preconsolidation pressure of Merville clay is better to be called 'apparent preconsolidation pressure' which includes two parts: the real preconsolidation pressure and bonding stress.

Based on the test results shown in Fig.3.16 and Table 3.4, the compression indexes of Dunkirk clay are smaller than Merville clay. This indicates that the structure resistance of Dunkirk clay used by Hieng (1991) is stronger than that of Merville clay. The preconsolidation pressure of Dunkirk clay is greater than that of Merville clay.

Clays which retain a post-sedimentation structure at gross yield have yield stress σ'_y greater than the preconsolidation pressure σ'_p. In Fig.3.17, the compression curves without the unloading-reloading cycles of intact samples are presented. There are two intact samples taken at the same depth to conduct oedometer tests at high pressure levels (tests OH1 and OH1). However, the test OH2 was conducted with different strain rates during loading before the apparent

preconsolidation pressure. The aim is to obtain the strain-rate effect on the yield stress and destructuration. The yield stresses of the three tests are similar, not affected by the strain rates. The yield stress (σ'_y) of the natural Merville clay from the oedometer tests is about 3000 kPa, a little more than the apparent preconsolidation pressure (σ'_p). The compression index of test OH2 is smaller than that of test OH1. It means that the resistance of Specimen OH2 to destructuration is greater.

Based on the test results presented in Fig.3.14 and Fig.3.15, the compression curve of each test is not a straight line in the semi-log plot, thus, the compression index has not a unique value. As mentioned above, the symbol C_c' is used to represent the compression index at the maximum pressure less than 1 MPa. For the oedometer tests at high pressure level, the compression index C_c'' is the mean slope from 1 MPa to the maximum pressure. Including test OL6, there are different compression indexes and swelling indexes presented in Table 3.5. A regression curve has been plotted to obtain the mean values of intrinsic parameters, which is shown in Fig.3.18. The mean values for the intrinsic swelling index C_s^* and compression index C_c^* of Merville clay are 0.152 and 0.600, respectively.

Table 3.5 Results of oedometer tests for all the reconstituted samples.

Test name	Depth (m)	σ'_p (kPa)	C_s	C_c'	C_c''
OL6	7 ~11	100	0.123	0.610	
OH4	4 ~7	100	0.158	0.553	0.441
OH5	7 ~11	300	0.145	0.468	0.435

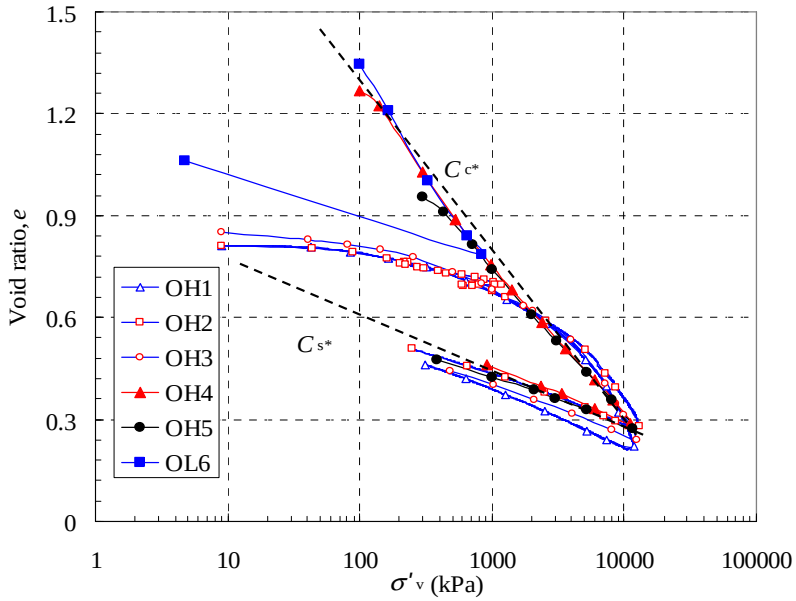

Fig. 3.18 Compression curves of reconstituted and natural samples.

3.4.3 Discussion about the test results

Two classes of parameters may be used to characterize the clayey sediment properties. The first one concerns the geotechnical index properties linked to the mineralogical nature of the material and can be represented, for example, by the Atterberg limits, or by their equivalent void ratios, void ratio at liquid limit $e_L=(\gamma_s/\gamma_w)w_L$ and void ratio at plastic limit $e_p=(\gamma_s/\gamma_w)w_p$, where γ_s and γ_w are the unit weight of the solids and of the water, respectively. The second relates to the mechanical parameters that express the geometric arrangement of particles and their evolution. Particles may be bonded due to cementation during the sedimentation and consolidation processes.

Biarez & Hicher (1994) presented a method (Biarez & Hicher model) to normalize the clay sediment curve. Based on a large number of results of clays, Biarez & Hicher observed that the 6.5 kPa and 1000 kPa stresses on the oedometric path correspond, on average, to w_L and w_p, respectively (or e_L and e_p). This leads to Eq. (3.2) for the compression index, using Eq. (3.1).

$$\begin{cases} w_{sat} = w_L \text{ for } \sigma_v^{'} = 6.5\,\text{kPa} \\ w_{sat} = w_p \text{ for } \sigma_v^{'} = 1\,\text{MPa} \end{cases} \tag{3.1}$$

$$C_c = 0.009(w_L - 13) \tag{3.2}$$

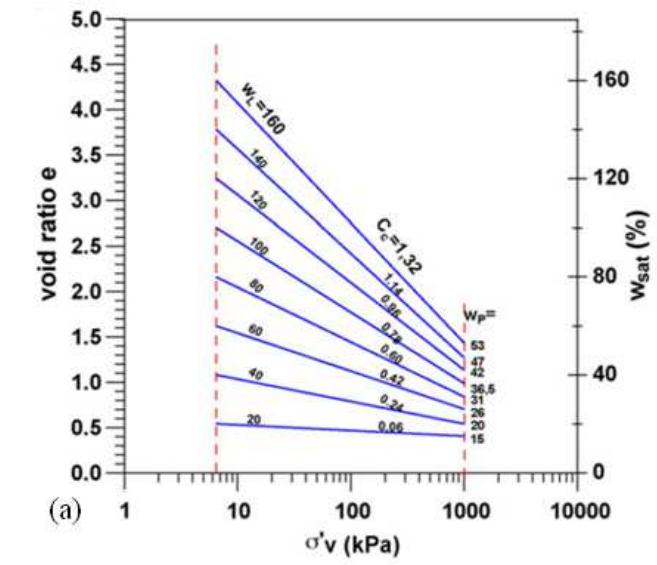

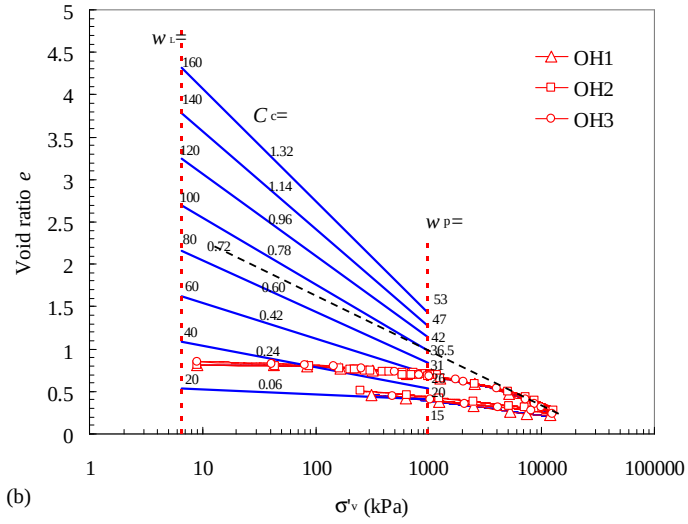

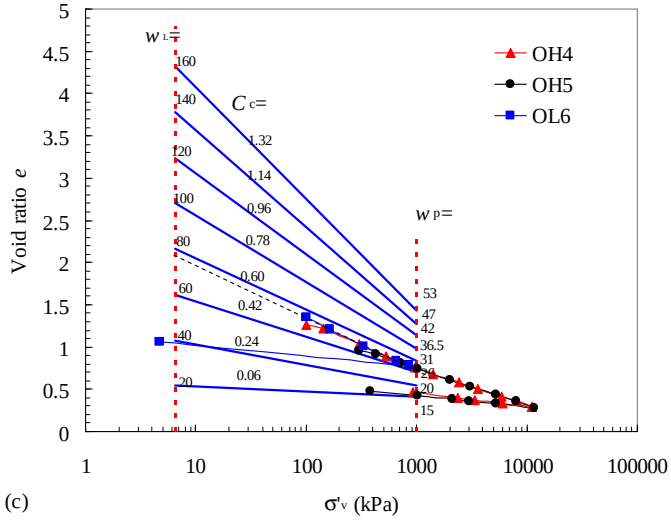

Fig. 3.19 (a) Biarez & Hicher model (1994) for the normally consolidated clays, (b) oedometer test results on natural samples of Merville clay and (c) oedometer test results on reconstituted samples of Merville clay.

The liquid limits of intact samples of Merville clay are between 93.8% and 96.1% at different depths. The values of compression indexes of intact samples are about 0.72. These results on intact samples fit well with the observation of Biarez & Hicher in Fig.3.19 (b). When the liquid limit is between 80% and 100%, the corresponding compression index is between 0.60 and 0.78. Therefore, the abacus in Fig.3.19 (a) can be a reference to check up on the value obtained for the compression index C_c of a soil, with a given liquid limit w_L. As mentioned above, the values of compression indexes of reconstituted samples are in the range of 0.44 ~0.61. The compression curves at low pressure levels (less than 1 MPa) fit well with the observation of Biarez & Hicher (1994), whereas the compression curves at high pressure levels do not fit well as shown in Fig.3.19 (c). Eq.(3.1) and Eq.(3.2) can reproduce the clay behavior only for maximum vertical pressures less than 1000 kPa. For oedometer tests at high pressure levels, another model for normalizing the compression curves should be discussed.

It is very important to distinguish clearly between the properties of a natural soil and its intrinsic properties. The term intrinsic has been chosen since it refers to the basic, or inherent, properties of a given soil prepared in a specified manner and which are independent of its natural state. Burland (1990) suggested that an asterisk could be used to denote an intrinsic property (e.g. C_c^* is the intrinsic compression index, and C_s^* is the intrinsic swelling index).

One important normalized factor is defined as the void index I_v by the following equation (Burland, 1990):

$$I_v = \frac{e - e_{100}^*}{e_{100}^* - e_{1000}^*} \tag{3.3}$$

The quantities e_{100}^* and e_{1000}^* are the intrinsic void ratios corresponding to σ'_v=100 kPa and 1000 kPa respectively. The intrinsic compression index C_c^* is defined as $e_{100}^* - e_{1000}^*$. When $e = e_{100}^*$, I_v = 0 and when $e = e_{1000}^*$, I_v = -1. It can be seen that a reasonably unique line is achieved which is termed the intrinsic compression line (ICL). In his paper, Burland (1990) presented an equation for reproduce the data of test results. The equation of the ICL was represented with sufficient accuracy by the following cubic relation:

$$I_v = 2.45 - 1.285x + 0.015x^3 \quad (3.4)$$

where x = log σ'_v in kPa.

According to Eq. (3.4), we obtained the following relation from the results on reconstituted samples of Merville clay:

$$I_v = 2.66 - 1.418x + 0.022x^3 \quad (3.5)$$

where x = log σ'_v in kPa.

Based on the test results on Merville clay, the values of e^*_{100} and C^*_c are 1.314 and 0.600, respectively. These values are chosen in order for Eq. (3.5) to fit the intrinsic compression line. The normalized compression curves for Merville clay are presented in Fig.3.20.

The sedimentation compression line (SCL) is obtained from Burland (1990). The compression curves of reconstituted samples compare very well with the intrinsic compression line. It can be seen that the compression curves of intact samples (without unload-reload stages) cross the ICL. The post-yield oedometer compression curves of tests OH1 and OH3 are a little steeper than the SCL. The post-yield compression curve of test OH2 is more or less parallel to SCL.

The compression curves of these three intact samples converge slowly on the ICL, which will be discussed below.

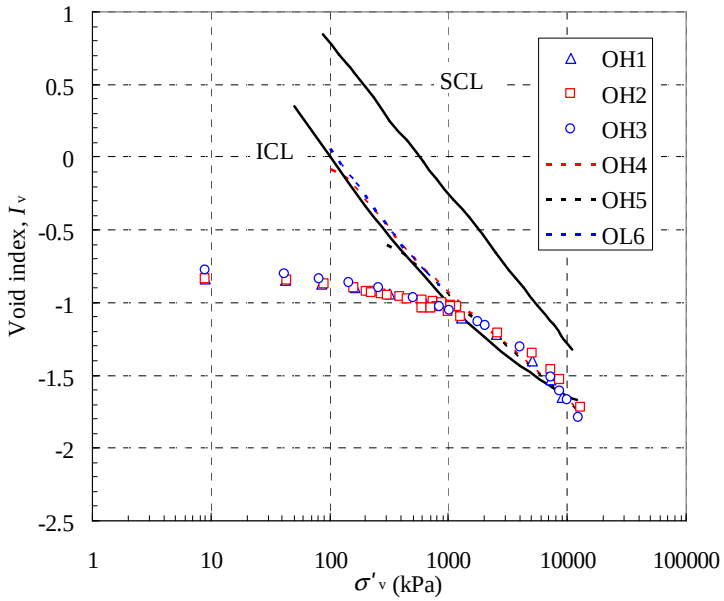

Fig. 3.20 Normalized compression of reconstituted and natural samples of Merville clay.

The ratio of the yield stress of the natural material to the vertical stress on the ICL at the same void ratio ($\sigma_y^{'} / \sigma_e^*$) is defined as "stress sensitivity" (S_σ) and may be regarded as a parameter embodying the differences of the microstructures of the natural and reconstituted clays (Burland et al., 1996; Cotecchia & Chandler, 1997, 2000). A current value of S_σ may be defined as the ratio of the current vertical stress on the compression curve of the natural sample to the vertical stress on the ICL at the current void ratio. This current value of S_σ quantifies the spacing between the compression curve of the natural clay and the ICL and can therefore changes with an increase in stress depending on the shape and location of the compression curve of the natural soil after the gross yield.

It has been observed that the compression curve after gross yield can converge towards the ICL, demonstrating a "meta-stable" structure that degrades with strains, or move along a line parallel to the ICL, demonstrating the presence of "stable" elements of structure that do not degrade with strains, in which case would remain constant.

As destructuration occurs, the swelling line of the intact sample steepens, tending to become parallel to the swelling line of the reconstituted material, so the ratio of the intrinsic to the intact swelling indices C_s^* / C_s, which Schmertmann (1966) defined as "swell sensitivity" (S_s), can also be used as an indicator of differences between intact and degraded structures.

Current values of stress sensitivity are plotted in Fig.3.21 and have been calculated using the current point on the post-yield compression curve of the natural samples. When S_σ is used in this way, it is essentially quantifying the distance between the post-yield compression curve of the intact soil and its ICL and therefore is a quantification of the degradation of the structure in compression. It has the advantage over S_s in that it does not require unload-reload stages, but this method can only give an indication of the changes in the structure after yield. As seen in Fig.3.21, the value of S_σ increases immediately after the gross yield, then decreases for all the samples, indicating that the post-yield compression paths of the intact samples are not parallel to the ICL, but on the contrary, converge slowly to the ICL.

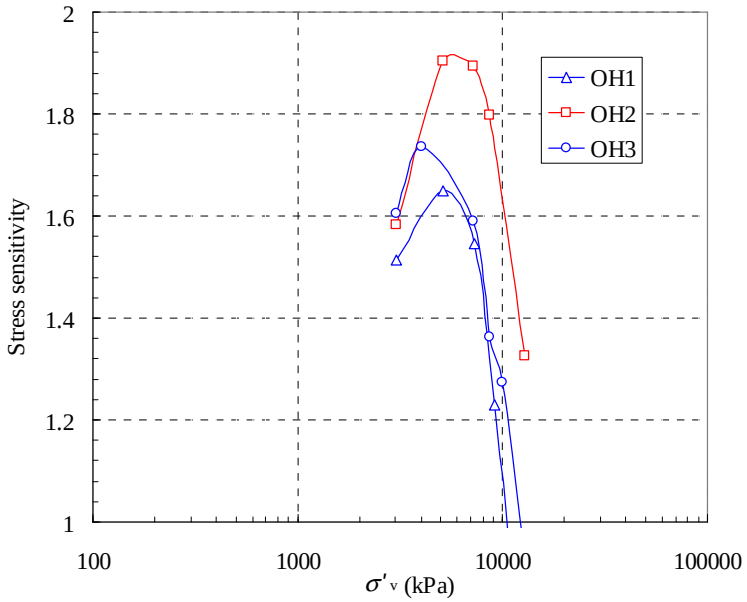

Fig. 3.21 Change of current stress sensitivity with increasing stresses after gross yield.

It is obvious that the decreasing curves of tests OH1 and OH3 are steeper than that of test OH2. When the compression curves of tests OH1 and OH3 have already converged on the ICL, the compression curve of the test OH2 has not. These observations make clear that the destructuration is less pronounced for Specimen OH2.

The curvature of the ICL (Burland, 1990) can complicate the evaluation of the distance between the natural and intrinsic compression curves and therefore the values of the current stress sensitivity and the assessment of the effect of structure on the compression of soils. That is shown in Fig.3.21 that the stress sensitivity is less than 1.0 at very high stresses.

The swelling sensitivity could be argued to be more representative in showing the evolution of the effects of structure with stresses because the slope of the swelling curve of the intact material typically starts changing as soon as the destructuration begins and is expected to be parallel to the intrinsic swelling curve when the destructuration is complete.

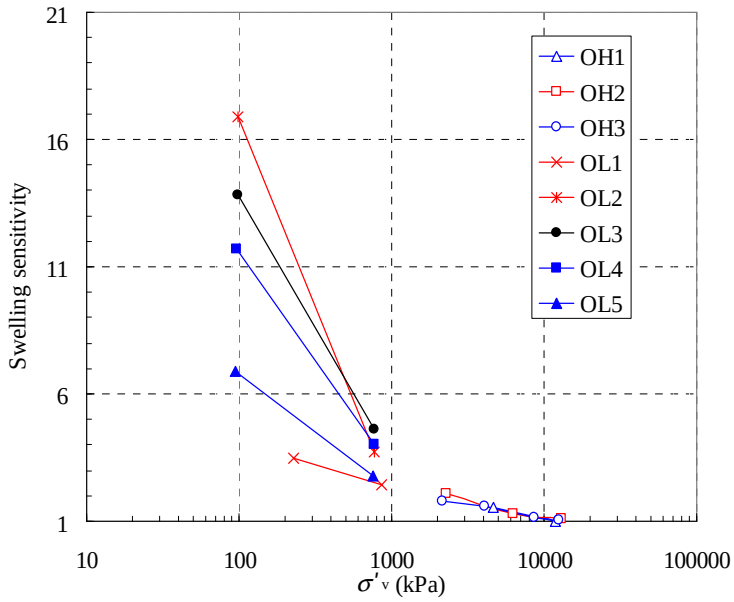

Fig. 3.22 Change of swelling sensitivity with increasing stresses for all the natural samples.

The change of swelling sensitivity with increasing stresses for all the intact samples as shown in Fig.3.22 is a good representation of the process of destructuration of the intact samples. In each case, the value of the plotted vertical stress is the maximum value before the start of the unload-reload stage used to define the value of swelling sensitivity. For tests at high pressure levels, the swelling curves of the intact samples became parallel to the SCL at large stresses, so the values of S_s are approximately equal to 1.0, confirming that the destructuration process was complete.

The swelling sensitivities for all the tests have the tendency to reach 1.0 as the stresses increase. It accords with the gradation of destructuration. It is interesting to observe that, with the depth increasing (without tests OL1 and OL2), the gradient of the changing swelling sensitivity decreases. The gradients of tests OL1 and OL2 may be affected by the micro-fissures in the samples at the depth of 6 ~7 m. This observation may be used as a reference for Merville clay at

different depths to obtain the swelling sensitivity without performing oedometer tests. This observation requires more test results to be confirmed.

3.5 Conclusions

In this chapter, a series of oedometer tests were carried out at both low and high pressure levels. Preparation of the specimens and the procedure of the oedometer tests were introduced. All the specimens were saturated before loading and the pore pressure was not measured during the tests. The imposed loading rate was kept small enough to prevent any change in pore pressure during loading.

For all the intact samples at low pressure levels (<1 MPa), the vertical stress was increased up to 100 kPa and then decreased down to 4.6 kPa. After unloading, the void ratio does not change much compared to the initial void ratio. It may be due to the existence of an internal bonding which is sufficiently strong to resist structural breakdown. After loading up to about 800 kPa, the intact sample has become approximately twice (or more) as expansive as the one subjected to first unloading. Thus this loading history must have destroyed some of the bonding.

Based on results of oedometer tests at high pressure levels, the apparent preconsolidation pressure of Merville clay is obtained by using Casagrande method. The value is about 2750 kPa which is less than the apparent preconsolidation pressure of Dunkirk clay (gross yield of about 3000 kPa). After loading up to more than 10 MPa, the swelling indexes of three intact samples are similar, approximately equal to the swelling indexes of reconstituted samples. That means that the structure of each intact sample is almost completely destroyed at the end of this loading process.

Two methods can be used to estimate the compression curves of the oedometer tests. The Biarez & Hicher's model is based on the relationship between C_c and w_L defined by Eq. (3.1) and (3.2). Although this model can estimate the clay behavior only for maximum vertical pressures less than 1000 kPa, the abacus in Fig.3.19 (a) can be a reference to check up the obtained compression index C_c of a soil, with a given liquid limit w_L.

For oedometer tests at high pressure levels, Burland method (1990) was used for normalizing the compression curves. This method is based on the definition of the void ratio index in order to

obtain the intrinsic compression line (ICL).The compression curves of reconstituted samples compare very well with the intrinsic compression line in the plane (I_v , $\log\sigma'_v$). It can be seen that the compression curves of intact samples cross the ICL. The post-yield compression curves of intact samples converge slowly to the ICL. This result was confirmed by the relationship between the current stress sensitivity S_σ and the vertical stress $\log\sigma'_v$. For tests at high pressure levels, the swelling curves of the intact samples became parallel to the SCL at high stresses, so the values of S_s became approximately equal to 1.0, confirming that the destructuration process was complete.

4 Behavior of Merville clay in triaxial tests

4.1 Introduction

In this thesis, the experimental study was done in the context of the design problem occurring beneath structures subjected to complex loading, such as wind turbine systems. A soil beneath such a structure is affected by static, cyclic and dynamic forces. Here, the dynamic effects (such as seismic loading, vibrations…) are out of the scope of this study. Therefore, a complete investigation of the behavior under both static and cyclic loading was conducted in the laboratory, using triaxial tests.

In this chapter, monotonic triaxial tests on Merville clay aim to study the behavioral parameters and the factors affecting the soil behavior, including the effects of existing fissures and strain rate.

In practice, monotonic consolidated triaxial tests with pore pressure measurement aim at determining the different geotechnical parameters related to the undrained behavior of a given clayey material, especially the friction angle, the variation of the undrained cohesion and the critical state lines (compression line and extension line). To do this, the triaxial study is divided into two subsets: the compression tests (UU, CIUC), on one hand, and the extension tests (CIUE), on the other hand.

Firstly, we present the testing procedures developed, all the tests performed and the results obtained. Then, we develop the interpretation of the tests and successively address the influence of the fissures, the influence of the strain rate and the analysis of various geotechnical parameters of Merville clay.

4.2 Test program and procedures

Different types of triaxial tests were carried out and various test procedures were tested during this triaxial study of Merville clay.

4.2.1 Test program

In this study, aiming to obtain the undrained behavior of Merville clay, three types (UU, CIUC and CIUE) of tests were conducted.

UU test: Carried out in the laboratory on unconsolidated specimens, sheared by compression in undrained condition.

CIUC test: The specimens were first reconsolidated in the laboratory under a given isotropic consolidation pressure, and then sheared by compression in undrained condition.

CIUE test: The CIUE test procedure was identical to that of the CIUC test. However, the shear mode was different, and at the inverse of the CIUC test, wherein the deviatoric stress is positive and increases as the axial stress increases during the shearing, the shearing of the CIUE test was performed by reducing the axial stress.

About 100 triaxial tests were carried out to analyze the behavior of Merville clay on both intact and remolded samples.

The experimental program began by conducting 40 UU tests. The main objective of these tests was to determine the undrained cohesion of the natural specimens.

53 CIUC triaxial tests were then carried out on intact and reconstituted specimens. Among these tests, 20 natural and 5 reconstituted specimens taken from different depths and consolidated under different effective pressures were sheared after isotropic consolidation, 13 natural specimens at the same depth and 9 reconstituted specimens were prepared for analyzing the strain rate effect, and 6 natural specimens were prepared for analyzing the strength anisotropy of Merville clay.

4 CIUE triaxial tests were also performed in the laboratory, 2 tests on natural specimens, and 2 test on reconstituted specimens.

4.2.2 General procedures

According to the ASTM standards (D 2850-95 and D4767-95), the different types of tests were carried out with the procedures (comprising a number of test phases presented later in the section 4.3) as follows:

a) UU test: performed following the procedures:

—Prepare the specimen;

—Place the specimen in the triaxial cell;

—Shear the specimen. The pressure in the triaxial cell is better chosen nearby the in-situ pressure. Josseaume (1998) indicated that the value of the coefficient of earth pressure at rest (K_0) is variable between 0.9 and 1.1. The value of the in-situ vertical pressure of Merville clay (the depth between 3 m and 11 m) is in the range of 50 ~140 kPa. In this section, four different cell pressures are chosen to do the UU tests: 0 kPa, 100 kPa, 200 kPa and 400 kPa.

b) CIUC test and CIUE test: the successional operations are performed as follows:

—Prepare the specimen;

—Place the specimen in the triaxial cell;

—Apply the back pressure and accomplish the saturation of the specimen;

—Isotropic consolidation of the specimen under the certain pressure set for each test, the drainage circuit being open;

—Shear the specimen.

In this study, the back pressure applied before the consolidation of specimen, in addition to perfect saturation, has the advantage of improving the drainage of the specimen.

4.2.3 Specimen preparation

The method for preparing the reconstituted sample was presented in the section 3.3.1.2.

The natural and reconstituted specimens were prepared by cutting cylinders having the dimensions equal to 35 mm in diameter and 70 mm in height, having both flat and parallel faces on both sides of the specimen. They were taken from the center of the core using a knife and a wire. Once the cutting was finished, we used the caliper rule to measure the specimen's height and diameter at three different levels (at both ends and at the centre of the specimen); the value of the diameter taken into account was the average of these three measurements. The time of this operation had to be minimized in order to reduce any possible drying of the specimens, which might change the initial suction and water content and even cause the opening of eventual fissures within natural samples. In this study, the time of preparation for each specimen was less than 10 min.

After being weighted, the specimen was then covered with a lateral filter paper (excepting UU tests) and two filter paper disks on both ends. The assembly was mounted between two porous stones in the triaxial cell (Fig.4.1 (a) and Fig.4.1 (b)) and, then, coated with a latex membrane which is fixed by means of two O-rings. Before fixed by the O-rings, we added air-free water between the specimen and the membrane to minimize the content of the air for a perfect saturation. Then, the operation continued by filling the triaxial cell with the water.

(a)

(b)

Fig. 4.1 (a) Convention triaxial apparatus and (b) Triaxial apparatus used for performing extension and cyclic triaxial tests.

4.2.4 Saturation

Although the soil samples are generally saturated in situ, it is necessary to saturate the filter papers and the porous stones in the triaxial cell. The saturation of the system was checked by

increasing the cell pressure by about 50 kPa and measuring B = $\Delta u_b / \Delta \sigma_3$. When the B value is higher than 95%, the specimen is considered to be saturated.

In their study on the stiff London clay, Bishop et al (1965) and Atkinson (1975) applied back pressures u_b of 211 kPa and 281 kPa respectively for the complete saturation of the specimen. During this study, the back pressure of Merville clay was usually between 200 and 400 kPa.

4.2.5 Consolidation

In this study, the specimens were consolidated under a given effective pressure between 50 kPa and 700 kPa. During the consolidation stage, the drainage system remained open. The consolidation was completed when the volume change of the specimen was stabilized which can be measured by the GDS system. The duration of this consolidation phase reached sometimes 20 days, but in general, it lasted from 7 to 10 days.

4.2.6 Shearing stage

One of the important factors which affect the shear strength of soils is certainly the strain rate. In this study, according to ASTM standards (D 2850-95 and D4767-95), the axial strains rates were 43.5 %/h and 2.57 %/h for UU test and CIUC test, respectively.

Moreover, the influence of the strain rate is dependent on the test condition (drained or undrained). Thus, after studying the strain rate effect on the behavior of the clay in undrained triaxial tests, Graham et al. (1983), Prepaharan et al. (1989) and Sheahan et al. (1996) made some conclusions. They reported that, if the strain rate was too high, it produced a non-uniform distribution of excess pore pressures across the specimen during shearing, which could affect the test results. Because of the clamping due to the porous stones, the ends of the specimen cannot deform freely during shearing. Therefore, the deformation of the specimen is not strictly cylindrical, and the stress state is not perfectly uniform. If the strain rate is very high, as mentioned above, the pore pressure at two ends of the specimen is greater than that at the center of the specimen. It is important to point out that this phenomenon is more prominent in the case of overconsolidated soils than normally consolidated soils (Hieng, 1991).

In the other hand, if the strain rate is low enough, the circulation of water in the specimen allows the total dissipation of the pore pressure gradients which developed from the ends to the center of the specimen. Thus a uniform pore pressure in the specimen is obtained.

Early works by Richardson & Whitman (1963), Alberro & Santoyo (1973), and Vaid & Campanella (1977) demonstrated that a higher strain rate results in a higher undrained shear strength. Vaid & Campanella (1977) found that the undrained strength increased by 5 ~10% for a 10-fold increase in rate of testing for Saint-Jean-Vianney clay. Graham et al. (1983), Lefebvre and LeBoeuf (1987), and Sheahan et al. (1996), among others, conducted studies on the strain rate dependent stress-strain behavior of a wide range of cohesive soils. Graham et al. (1983) found that undrained shear strength increases by about 9% ~20% for a 10-fold change in strain rate for highly plastic natural soft clays. The study of the strain rate effect on a stiff clay was also performed by Sorensen et al. (2007). They indicated that the undrained shear strength increases by about 2% ~4% for a 4-fold change in strain rate for London clay.

Another important factor which affects the shear strength of the clay is the fissures in the specimen. The fissures are “small fractures existing in clay and siltstone beds, but not crossing the bed or horizons within the bed” (Fookes & Parrish, 1969). Faults and sheeting, which are low-angle joints, were added by Skempton et al. (1969) to the above types of fissures.

The distribution and the orientation of the discontinuities are thought to reflect the structure bedding and the erosion history of the clay. Based on the study of London clay at Wraysbury and Edgware, Skempton et al. (1969) observed that the fissures are randomly orientated and have an irregular area. The mean size of the fissures decreases and the number per unit volume correspondingly increases as the upper surface of the clay is approached, suggesting that stress releases and weathering play an important role in fissure genesis.

Terzaghi (1936) pointed out that such minor structural features are characteristic of overconsolidated clays, and showed that the overall strength of these ‘stiff, fissured clays' could be as low as one fifth to one tenth of the strength as measured on small samples of intact clay. In the case where the rupture occurs along a fissure, one obtains a lower limit of the shear strength; if rupture occurs within the intact soil mass, an upper limit of the shear strength is then obtained, as

shown in Fig1.17 (Ward et al., 1965). Thus, the London clay and Flanders clay clearly belong to this category.

In addition to analyze factors which affect the shear strength of the clay in triaxial tests, we also investigated the shear strength anisotropy of natural Merville clay. CIUC triaxial compression tests were performed on specimens cut from the same depth with their long axes either vertical or horizontal. It should be noted that, if not otherwise specified, all the specimens were cut vertically from the Merville clay stored in the PVC tubes.

4.3 Test results and analysis

All the intact specimens of Merville clay were taken below the water table. Based on the test results shown at Chapter 2, the degrees of saturation of these intact samples were 100%. In all the tables below, the symbol, ε_r, represents the axial strain at the maximum deviatoric stress q_f. The symbols, σ'_a and σ'_r, represent the effective axial stress and effective radial stress, respectively. The deviatoric stress, q, is equal to the value of $(\sigma'_a-\sigma'_r)$.

4.3.1 UU test results on natural samples and analysis

The basic parameters of the specimens and UU test results are presented in Table 4.1. According to the results of UU triaxial tests, the values of all the excess pore pressures Δu were very small, probably due to an imperfect saturation of the specimens. The relations between the deviatoric stress q and the axial strain ε_a are presented in Fig.4.2 to Fig.4.11, for the UU tests.

Many problems encountered in soil mechanics are related to the characteristics of soil strength. However, it should be noted that the term of shear strength, includes both a concept of failure and a concept of excessive deformation. Thus, the failure of the soil occurs, for example, both by the debonding between soil particles and a sliding along the rupture plane, thereby producing the distortion in the soil mass. The shear strength of a soil is defined as the value of the shear stress at the time of failure of the soil, also called deviatoric stress at failure.

In practice, the difference between the maximum and the minimum principal stresses $(\sigma'_a-\sigma'_r)_f$ or $(\sigma_a-\sigma_r)_f$ at failure is used as a measure of the shear strength of the soil.

The shear strength of a soil is usually expressed by the following equation

$$\tau_f = c' + (\sigma_f - u)\,\mathrm{tg}\,\phi' \tag{4.1}$$

where: τ_f is the shear strength on the rupture plane, σ_f is the total normal stress in this plane, u is the pore pressure, c' is cohesion intercept, ϕ' is the effective internal friction angle. This equation corresponds to the Mohr-Coulomb theory which corresponds to as straight line in the Mohr plane.

For UU tests, the interpretation is usually made in total stresses. For perfectly saturated samples, the failure envelope for the total stress Mohr's circles will be a horizontal line and hence is called a ϕ=0 condition In Fig.4.12, the total stress Mohr's circles at failure of the natural samples at the depth of 5 ~6 m from the borehole SC1 are shown. Only at high confining pressures (200 and 400 kPa), the values of the shear strengths are similar, whereas lower values are obtained at lower confining pressures (0 and 100 kPa). The proper reasons for this phenomenon can be found either in the non-homogeneity of the clay microstructure or in the non-saturation of the specimens or in both of them.

As mentioned above in Chapter 2, the Merville clay is a fissured clay. The micro fissures may exist in natural samples of UU tests. The effect of fissure will be discussed in Section 4.3.2. in this Chapter. Unlike the CIUC tests, there is not a stage for checking the saturation of the specimens in UU tests. The samples may be unsaturated during UU tests at low confining pressure, especially the confining pressure (0 kPa) which is smaller than the in-situ stress. According to the results shown in Table 4.1, the shear strength values of the natural specimens at the same depth and from the same borehole were not equal to each other. Thus, the effects of fissuration, non-homogeneity and non-saturation exist in the samples for all the depths in the three boreholes (SC1, SC2 and SC3).

Based on the results presented in Table 4.1, and Fig.4.2 to Fig.4.11, the breaking of the soil specimens can be easily observed in the curves of the deviatoric stress versus axial strain, such as for the specimen UU26. Then the shear strength $(\sigma'_a-\sigma'_r)_f$ and the axial strain at the breaking ε_f, which represent the peak point in the curve, can be obtained. However, for other specimens, the failure of the soil was difficult to determine from the stress-strain curve, such as for the specimen UU2. The value of the deviatoric stress increased continuously until the shearing test was finished,

the axial strain reaching 30% at that time. Thus, the shear strength $(\sigma'_a-\sigma'_r)_f$ and the axial strain at failure ε_f could not be obtained, even though a shear band could be observed within the specimen.

In this study, we chose the value of the largest axial strain at failure equal to 15%. For the specimens with $(\sigma'_a-\sigma'_r)_f$ and ε_f difficult to determine, the maximum deviatoric stress at the axial strain no more than 15% was used to represent the shear strength, and this axial strain represented the axial strain at failure. The results are shown in the Table 4.1 to Table 4.6. From this series of UU tests, we can conclude that, due mainly to the influence of the fissures in the natural specimens, the results show significant scatter in the shear strength, as well as in the strain amplitude at failure.

Table 4.1 Test results on natural specimens (UU).

Unit	Specimen name	Depth (m)	Initial state				Cell pressure (kPa)	Features at the maximum deviatoric stress		
			γ_h (kN/m^3)	γ_d (kN/m^3)	w_0 (%)	σ'_{v0} (kPa)		ε_f (%)	$(\sigma'_a-\sigma'_r)_f/2$ (kPa)	$(\sigma'_a+\sigma'_r)_f/2$ (kPa)
SC1	UU1	5.07	20.4	15.4	34.5	74.8	0	1.58	37.5	45.8
	UU2	5.12	20.4	15.4	34.7	75.3	97.2	14.92	67.3	159.8
	UU3	5.17	20.5	15.5	35.2	75.7	196.8	7.22	97.0	290.4
	UU4	5.22	20.2	15.1	34.2	76.2	396.1	4.06	103.1	496.6
	UU5	7.03	19.7	14.8	30.5	93.6	0	14.86	143.5	167.4
	UU6	7.10	19.6	14.5	30.7	94.3	97.0	8.89	213.7	294.4
	UU7	7.16	19.7	14.6	31.4	94.8	196.8	13.37	116.0	312.3
	UU8	7.20	19.3	15.1	30.5	95.2	394.4	10.04	137.8	526.2
	UU9	9.18	20.3	14.5	31.8	114.2	0	5.64	119.2	131.4
	UU10	9.22	20.0	14.8	32.1	114.6	96.6	14.80	154.4	242.8
	UU11	9.30	19.9	14.9	31.1	115.4	196.6	3.69	310.9	498.4
	UU12	9.33	20.4	14.9	30.0	115.7	395.8	3.58	328.4	724.6
	UU13	10.13	19.5	14.4	34.7	123.3	0	2.32	124.1	133.2
	UU14	10.18	18.9	14.5	33.8	123.8	94.8	7.14	144.8	240.5
	UU15	10.23	19.3	14.8	33.6	124.3	196.6	4.08	252.5	428.1
	UU16	10.28	19.1	14.9	33.8	124.8	396.4	14.92	119.0	502.0
SC2	UU17	5.23	19.8	15.4	32.1	76.3	0	0.95	30.8	34.8
	UU18	5.28	19.2	15.1	33.5	76.8	98.2	3.28	91.5	196.0
	UU19	5.76	19.3	15.0	32.2	81.4	197.7	5.39	186.4	403.7
	UU20	5.82	19.0	14.9	30.8	82.0	397.1	14.64	111.3	527.7
	UU21	7.02	19.0	14.5	32.3	93.5	0	2.17	25.9	43.2
	UU22	7.06	19.8	15.2	31.3	93.9	84.0	0.65	16.0	116.9

	UU23	7.13	19.5	15.0	32.2	94.5	197.5	4.07	209.3	425.6
	UU24	7.18	20.1	15.0	31.2	95.0	397.3	4.54	244.6	660.0
	UU25	8.08	20.0	14.5	33.6	103.7	0	2.46	37.6	54.1
	UU26	8.13	19.2	15.3	33.5	104.1	98.2	3.85	194.1	310.3
	UU27	8.19	20.2	15.2	33.6	104.7	197.6	3.55	128.9	345.1
	UU28	8.24	20.2	15.3	34.1	105.2	399.3	14.64	129.5	474.9
SC3	UU29	4.08	19.5	14.5	38.5	65.3	0	2.45	40.8	45.3
	UU30	4.12	19.3	14.2	38.5	65.7	96.9	4.49	32.5	165.1
	UU31	4.20	18.6	14.3	37.7	66.4	196.5	4.90	77.4	279.5
	UU32	4.22	18.9	14.2	38.3	66.6	396.1	14.9	76.2	477.7
	UU33	6.06	19.3	14.7	31.3	84.3	0	3.24	77.3	79.8
	UU34	6.09	19.3	15.2	30.4	84.6	96.7	12.79	121.2	222.0
	UU35	6.15	19.1	14.6	30.6	85.1	196.2	14.93	134.6	324.7
	UU36	6.20	19.7	15.0	30.5	85.6	395.7	3.80	245.5	635.8
	UU37	8.08	19.5	15.1	33.5	103.7	0	1.96	35.3	38.5
	UU38	8.18	19.7	15.0	33.2	104.6	96.1	2.13	95.6	196.3
	UU39	8.23	19.6	15.0	32.8	105.1	196.3	9.03	220.3	420.6
	UU40	8.32	19.8	15.3	32.3	106.0	395.5	4.09	270.3	668.6

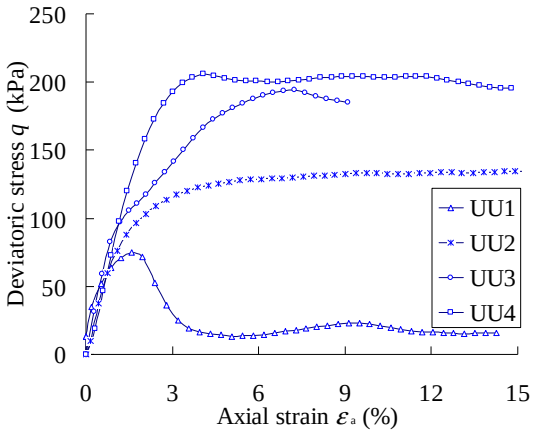

Fig. 4.2 UU test results on natural specimens at the depth of 5 ~6m from the borehole SC1.

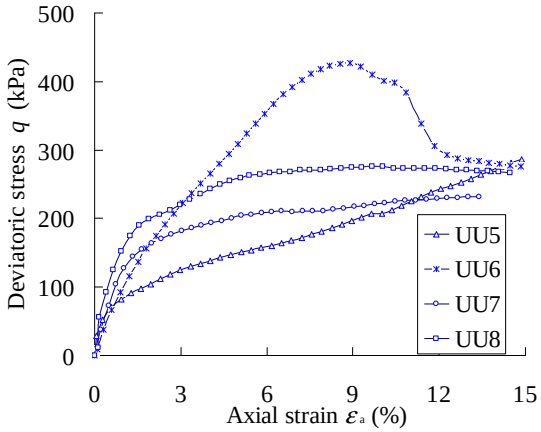

Fig. 4.3 UU test results on natural specimens at the depth of 7 ~8m from the borehole SC1.

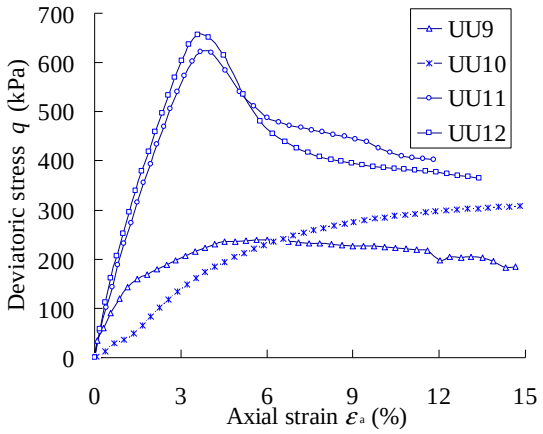

Fig. 4.4 UU test results on natural specimens at the depth of 9 ~10m from the borehole SC1.

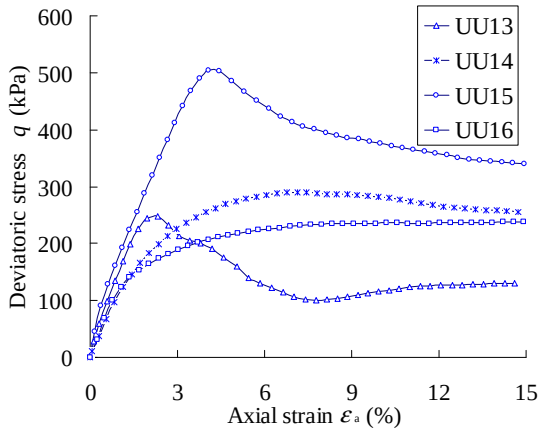

Fig. 4.5 UU test results on natural specimens at the depth of 10 ~11m from the borehole SC1.

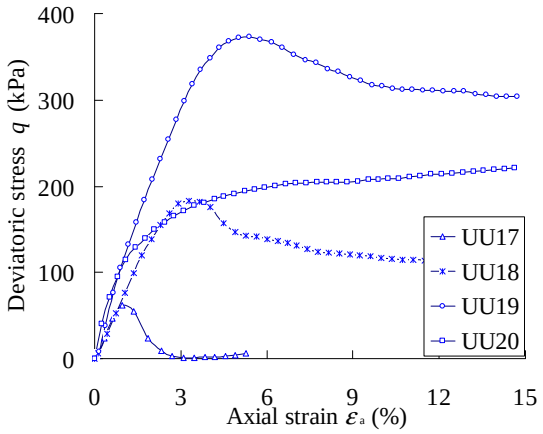

Fig. 4.6 UU test results on natural specimens at the depth of 5 ~6m from the borehole SC2.

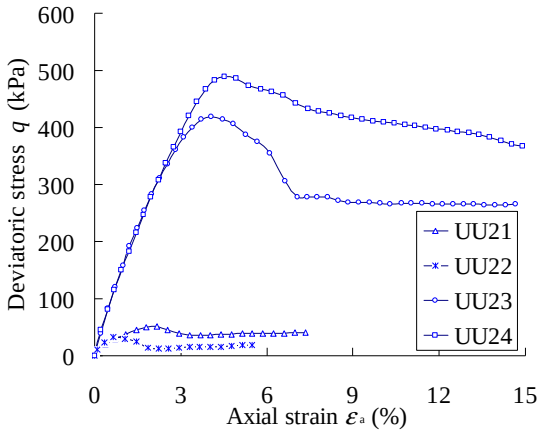

Fig. 4.7 UU test results on natural specimens at the depth of 7 ~8m from the borehole SC2.

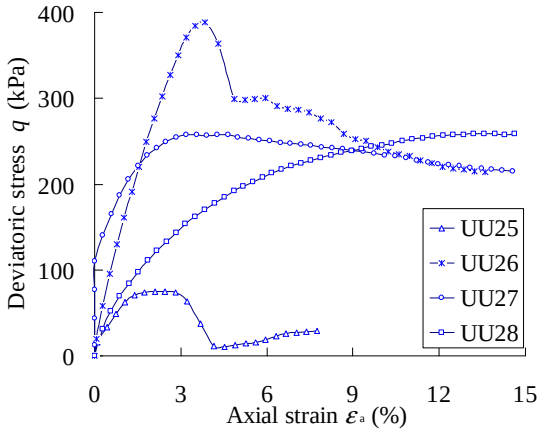

Fig. 4.8 UU test results on natural specimens at the depth of 8 ~9m from the borehole SC2.

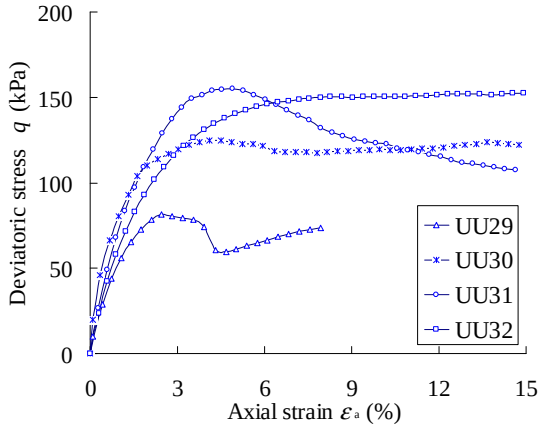

Fig. 4.9 UU test results on natural specimens at the depth of 4 ~5m from the borehole SC3.

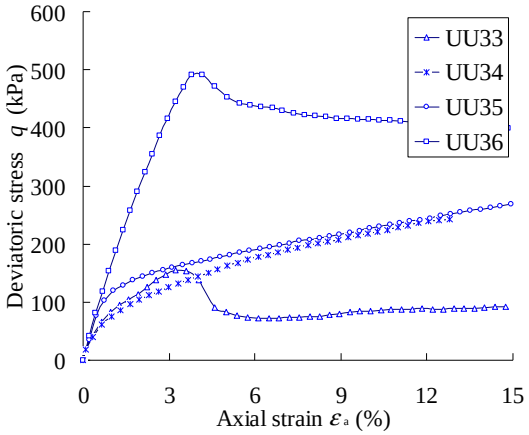

Fig. 4.10 UU test results on natural specimens at the depth of 6 ~7m from the borehole SC3.

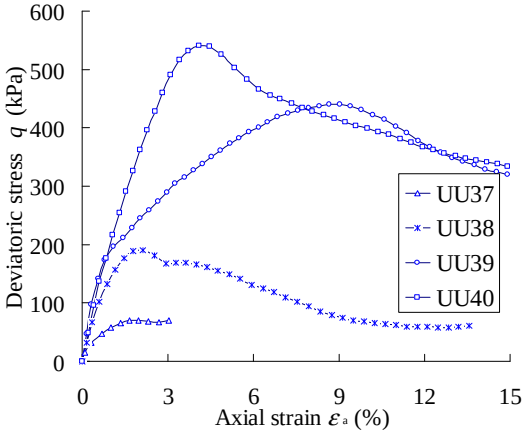

Fig. 4.11 UU test results on natural specimens at the depth of 8 ~9m from the borehole SC3.

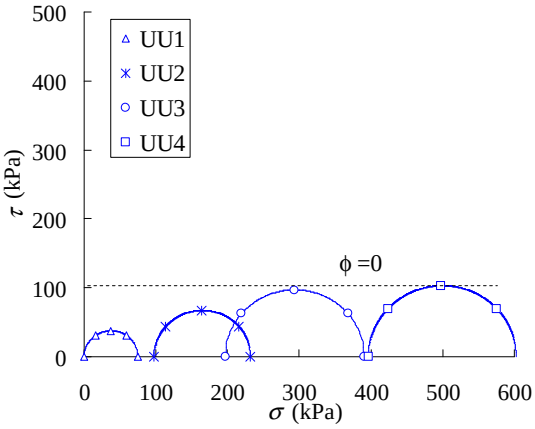

Fig. 4.12 Mohr's circles at failure of natural specimens at the depth of 5 ~6m from the borehole SC1.

4.3.2 CIUC and CIUE test results on natural samples and analysis

The basic parameters of the specimens subjected to CIUC and CIUE tests are presented in Table.4.2. According to the results of CIUC and CIUE tests, the curves of the relationship between the deviatoric stress q and the axial strain ε_a, the relationship between the excess pore

pressure Δu and the axial strain ε_a, and the effective stress paths are presented in Fig.4.13 to Fig.4.22. The failure of a stiff clay manifests itself usually by a sudden and then a gradual plastic flow, hence the term 'brittle and progressive fracture' was given to this type of failure by several authors, such as Hieng (1991), Josseaume (1998), and Gasparre (2005) etc. The value of the axial strain at failure for an intact specimen of a stiff clay is small, mostly less than 4 ~5%.

It is this aspect of the phenomenon that makes it interesting to study the behavior of the stiff clay after the peak stress. The peak stress is reached after a given deformation of the soil mass and, after the peak, there is a sudden drop in the shear stress, which passes from its value q_f at peak to a value q_d. Then the failure of the clay mass will continue, but gradually. As the deformation increases, the shear stress will decrease slowly to stabilize at its residual value q_r as the deformation increases.

Based on the results in Fig.4.13 to Fig.4.22, like for some of the results of UU tests, the peak points in the stress-strain curves could not be observed for many natural specimens although these specimens were already broken. For specimens showing a peak deviatoric stress, the axial strain at the peak was less than 6%, and mostly even less than 4%. Almost all the specimens did not reached the residual states. For some specimens (such as CIUC10 and CIUC18), the deviatoric stress stabilized at the residual strength after the rupture, whereas the excess pore pressure did not stabilized. For most specimens, both deviatoric stress and excess pore pressure did not reach the residual state.

Bjerrum & Kenney (1967) gave an explanation of this type of failure, which would result from a combined action of the structural resistance and frictional resistance of the soil particles. During the formation of the clay, cementing bonds develops between particles due to the precipitation of fine particles from the chemical alteration of the soil. The cementation bond strength added to the action of surface energy forces (Van der waals forces), is the structural resistance of the soil, whereas the contact forces between the solid grains of the soil during shearing is the frictional resistance. The total resistance is the combined effect of these two resistances.

During the shearing of a cohesive soil, the structural resistance is the first to be mobilized. Having reached its maximum (Fig.4.23), the cementing bonds break, thus approaching the solid grains and multiplying their points of contact, this generates the frictional resistance. From this moment, there is a contradictory evolution of two processes: the frictional resistance increases, the structural resistance decreases with the breaking of the bonds. This combination of effects may result in either an increasing or a loss of the total sliding resistance of the soil, depending on whether one of the processes prevails over the other or not. This balance of the forces, which depends on the nature of the soil and the strain rate, etc., would be responsible for the variation of the shear strength according to the test rate and fundamentally determine the shape of the stress-strain curve of different types of soils. Fig.4.23 presents the stress-strain curve of a plastic overconsolidated clay. We can notice the predominance of the structural strength over the frictional strength, which is usually the case in stiff overconsolidated clays.

As shown in Fig.1.17, there are three different curves representing the effect of fissures in the samples. Comparing Fig.1.17 and Fig.4.23, the stress-strain curve of an intact non fissured sample represents the predominance of the structural strength. Whereas, when the frictional strength has the predominance, it means that there are existing fissures or no cementing in the sample. As the existence of bonds in the natural sample of Merville clay has been demonstrated in Chapter 3, there are fissures inside the specimen when the frictional strength is dominant.

The soil structure is affected by the presence of fissures. The structural strength of the sample with fissures will be smaller than that of the non fissured sample taken at the same depth and subjected to the same confining pressure. This was demonstrated by the results obtained on Merville clay, as shown by the results obtained on the specimens CIUC19 and CIUC20: tested at smaller confining pressure, Specimen CIUC19 is stronger than Specimen CIUC20.

Table 4.2 Test results on natural specimens (CIUC and CIUE).

Unit	Specimen name	Depth (m)	Initial state			Effective confining pressure	Features at the maximum (CIUC) or minimum (CIUE) deviatoric stress			
			γ_h (kN/m^3)	w_0 (%)	σ'_{v0} (kPa)	σ'_0 (kPa)	ε_f (%)	Angle α (^{o})	$(\sigma'_a-\sigma'_r)_f/2$ (kPa)	$(\sigma'_a+\sigma'_r)_f/2$ (kPa)
SC1	CIUC1	5.45	19.8	33.6	78.4	100.0	14.24	45	67.3	127.7
	CIUC2	5.47	20.2	34.0	78.6	97.1	14.55	45	54.7	106.9
	CIUC3	5.53	19.8	33.2	79.2	198.3	11.3	45	128.1	258.6
	CIUE1	5.85	20.1	33.0	82.3	94.2	-2.65	29	-38.4	101.2
	CIUE2	5.88	19.7	32.8	82.5	193.6	-2.07	68	-52.0	189.1
	CIUC4	7.36	19.7	31.7	96.8	96.6	13.5	50	132.3	180.9
	CIUC5	7.40	19.5	32.1	97.1	100.3	5.31	52	86.6	158.1
	CIUC6	7.55	19.8	32.8	98.6	200.5	6.36	67	149.3	239.2
	CIUC7	7.58	19.7	32.2	98.9	399.0	14.90	55	198.6	395.8
	CIUC8	10.47	19.6	32.6	126.6	195.5	8.40	58	180.9	264.2
SC2	CIUC9	5.35	19.6	34.0	77.5	100.4	2.84	55	112.6	139.1
	CIUC10	5.46	19.8	34.2	78.5	99.9	3.20	50	100.2	145.5
	CIUC11	7.42	19.9	32.6	97.3	49.8	2.25	45	66.7	82.8
	CIUC12	7.35	19.8	31.8	96.7	99.2	12.96	58	106.4	159.3
	CIUC13	7.48	19.4	31.6	97.9	95.8	9.85	45	137.9	215.6
	CIUC14	8.32	19.3	33.0	106.0	93.1	5.49	45	110.6	149.9
	CIUC15	8.39	19.4	33.8	106.6	194.8	9.42	38	159.6	234.6
SC3	CIUC16	7.04	19.5	34.2	93.7	49.7	4.09	65	138.8	174.4
	CIUC17	7.08	19.6	33.8	94.1	100.0	3.45	45	149.4	199.5
	CIUC18	7.16	19.9	34.6	94.8	199.6	3.94	45	172.5	261.1
	CIUC19	10.20	19.2	32.7	124.0	46.3	3.29	56	196.8	190.2
	CIUC20	10.25	19.0	33.1	124.5	95.4	14.96	45	71.6	114.6

Note: the symbol α represents the angle of the rupture plane.

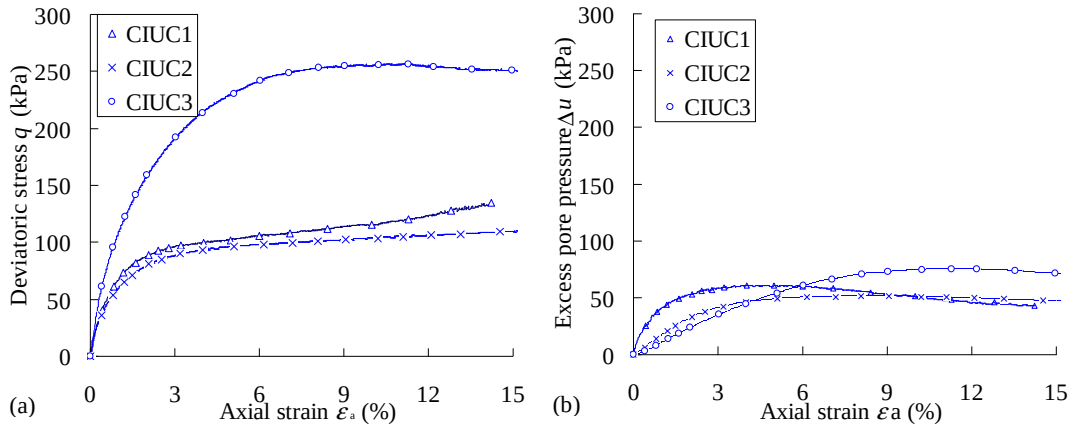

Fig. 4.13 CIUC test results on natural specimens at the depth of 5 ~6 m from the borehole SC1: (a) deviatoric stress versus axial strain and (b) excess pore pressure versus axial strain.

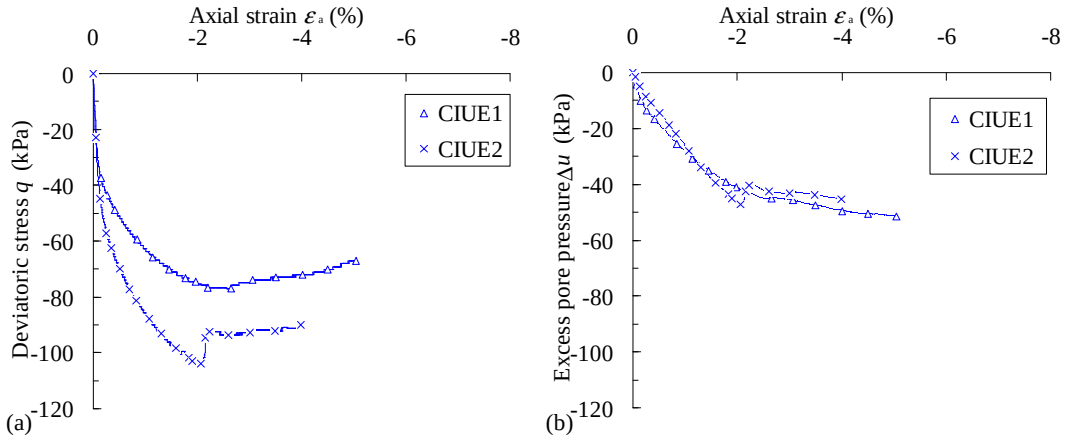

Fig. 4.14 CIUE test results on natural specimens at the depth of 5 ~6 m from the borehole SC1: (a) deviatoric stress versus axial strain and (b) excess pore pressure versus axial strain.

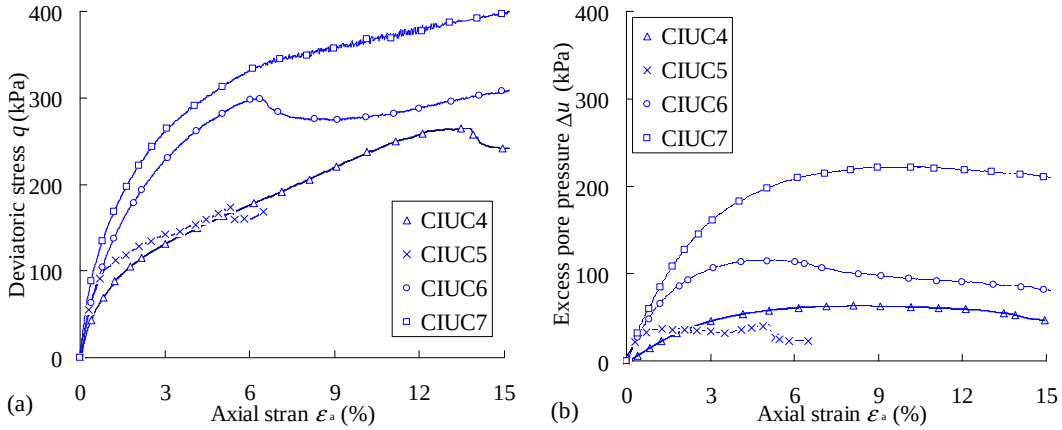

Fig. 4.15 CIUC test results on natural specimens at the depth of 7 ~8 m from the borehole SC1: (a) deviatoric stress versus axial strain and (b) excess pore pressure versus axial strain.

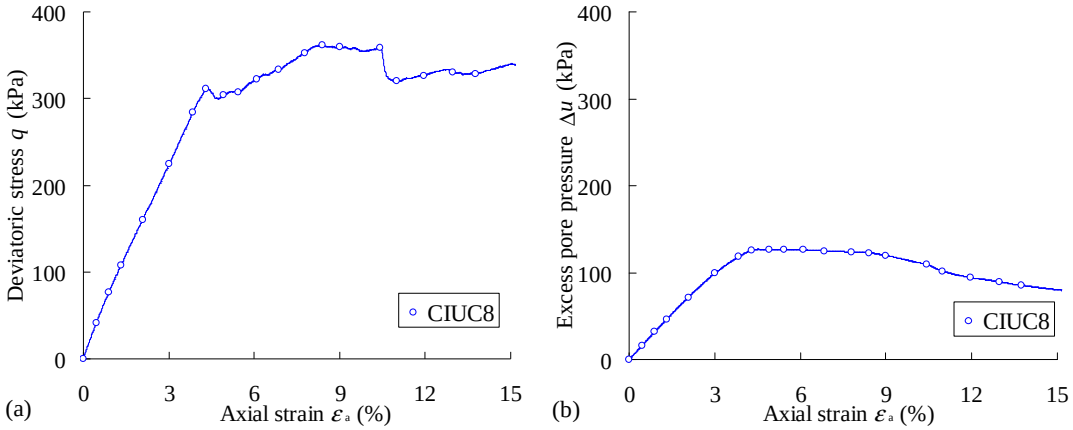

Fig. 4.16 CIUC test results on natural specimens at the depth of 10 ~11 m from the borehole SC1: (a) deviatoric stress versus axial strain and (b) excess pore pressure versus axial strain.

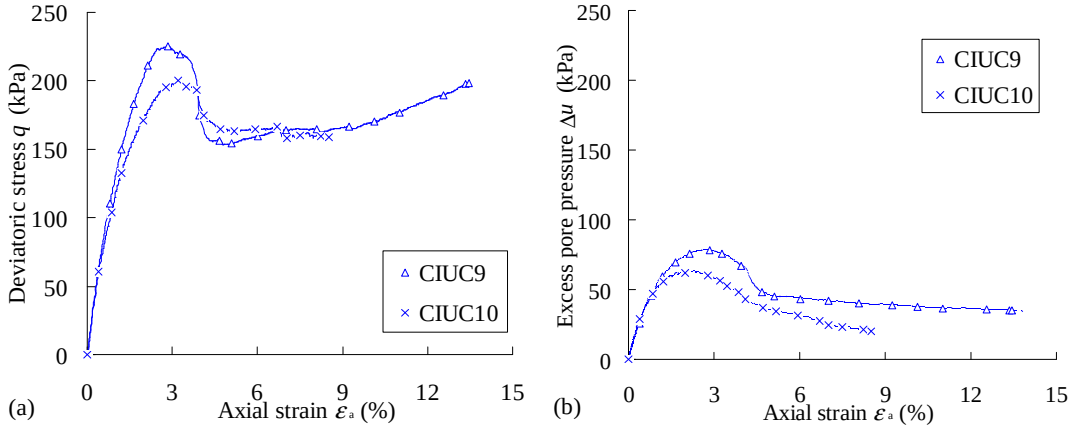

Fig. 4.17 CIUC test results on natural specimens at the depth of 5 ~6 m from the borehole SC2: (a) deviatoric stress versus axial strain and (b) excess pore pressure versus axial strain.

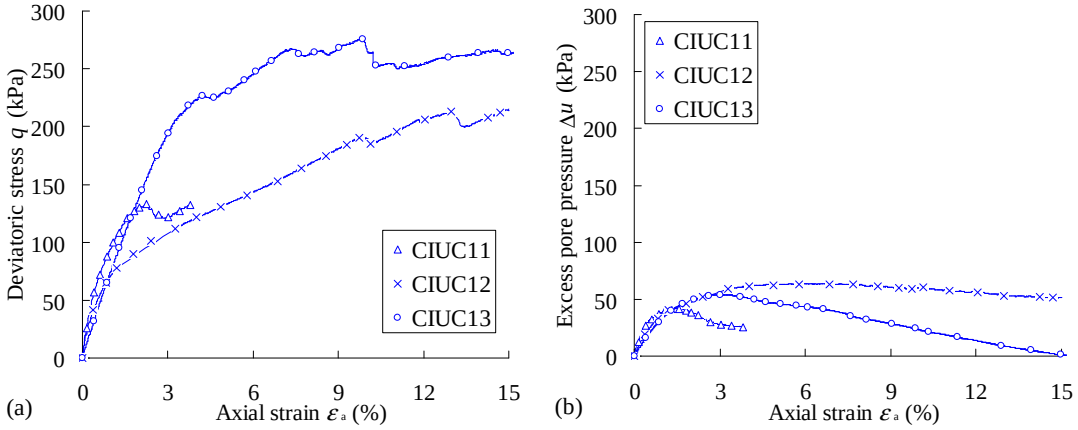

Fig. 4.18 CIUC test results on natural specimens at the depth of 7 ~8 m from the borehole SC2: (a) deviatoric stress versus axial strain and (b) excess pore pressure versus axial strain.

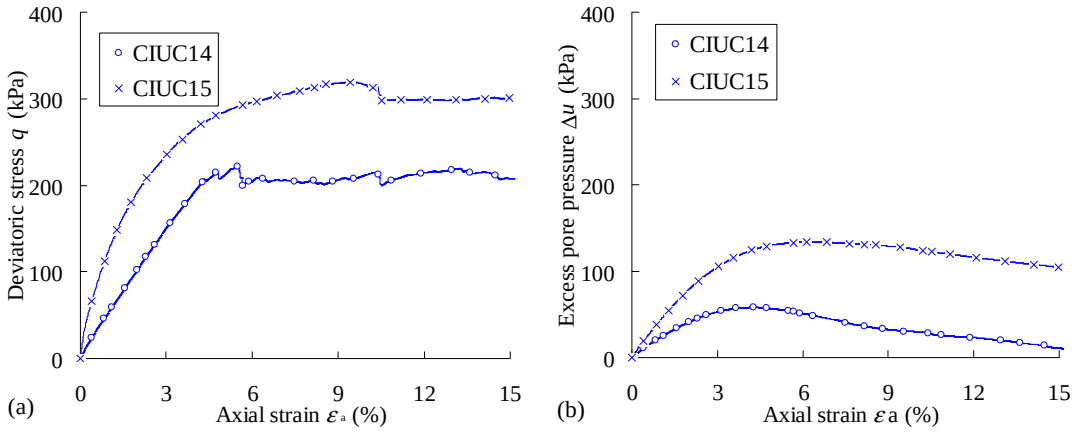

Fig. 4.19 CIUC test results on natural specimens at the depth of 8 ~9 m from the borehole SC2: (a) deviatoric stress versus axial strain and (b) excess pore pressure versus axial strain.

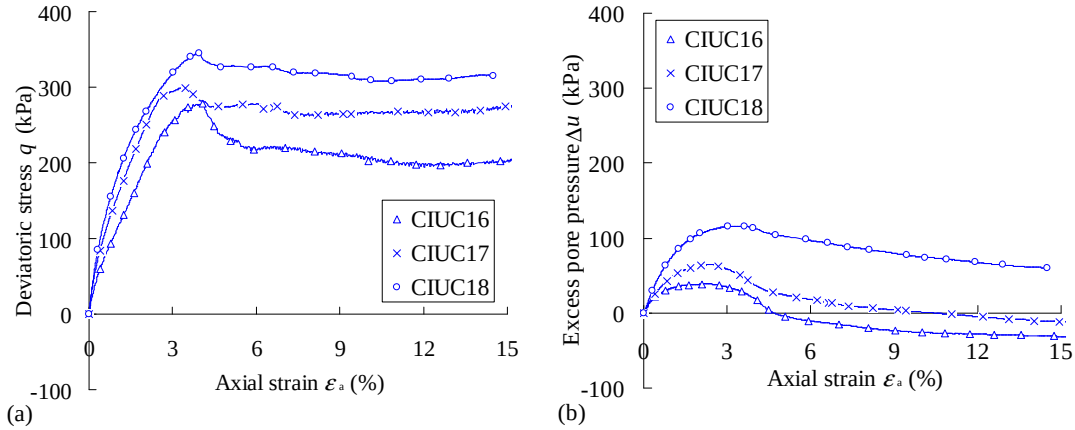

Fig. 4.20 CIUC test results on natural specimens at the depth of 7 ~8 m from the borehole SC3: (a) deviatoric stress versus axial strain and (b) excess pore pressure versus axial strain.

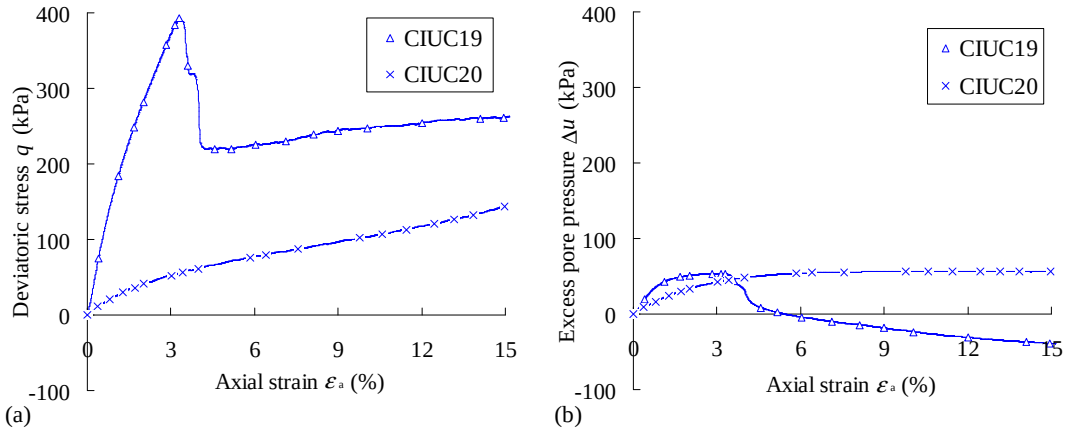

Fig. 4.21 CIUC test results on natural specimens at the depth of 10 ~11 m from the borehole SC3: (a) deviatoric stress versus axial strain and (b) excess pore pressure versus axial strain.

The effective stress paths of natural samples from three different boreholes were presented in Fig.4.22 (a), Fig.4.22 (b) and Fig.4.22 (c), respectively. Then based on the results on Flanders clay and London clay summarized by Biarez & Hicher (Hicher & Shao, 2002) in Fig.1.18, we summarized the results on these three clays shown in Fig.4.22 (d). Each hollow point represented the maximum deviatoric stress of each triaxial test on Merville clay. The maximum deviaotric stresses of Merville clay are similar with the results on Flanders clay, whereas are below the maximum stress line of London clay.

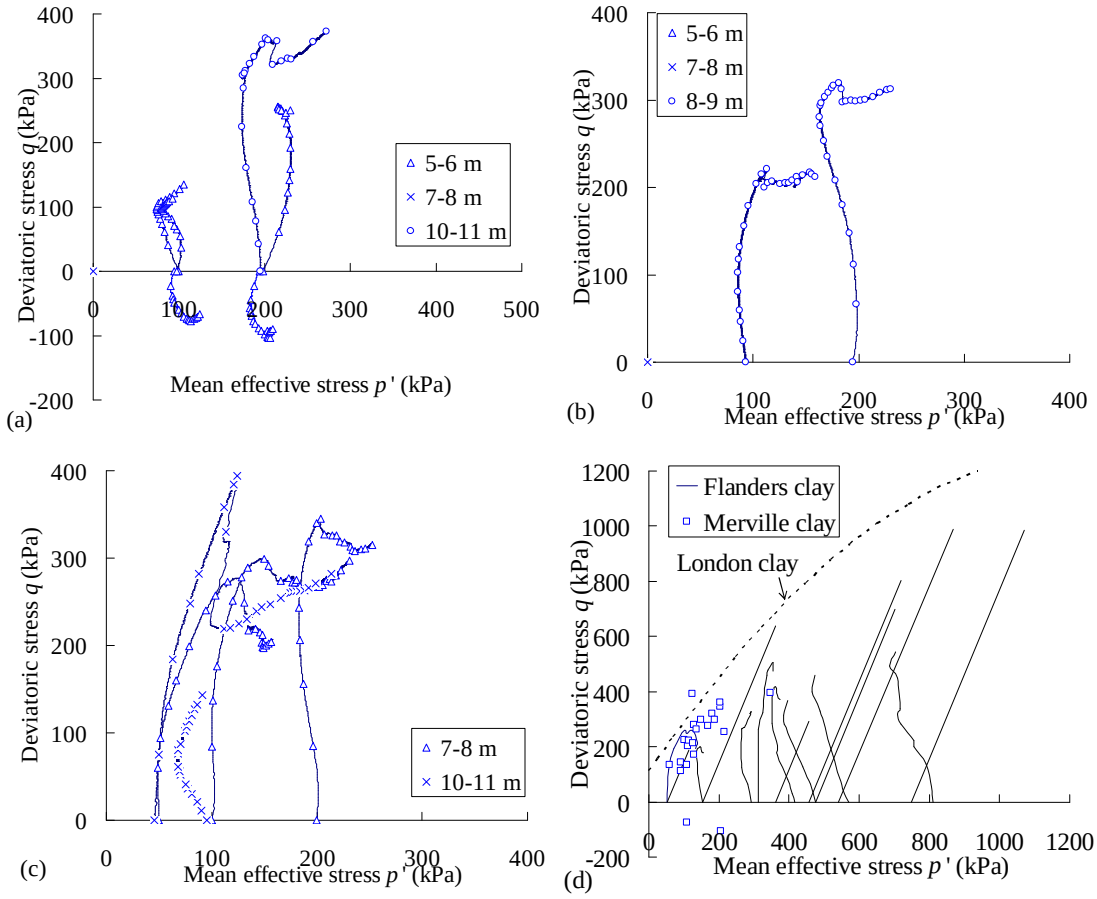

Fig. 4.22 CIUC and CIUE effective stress paths of natural specimens from: (a) the borehole SC1, (b) the borehole SC2, (c) the borehole SC3 and (d) all these three boreholes of Merville clay comparing with the Flanders clay and London clay.

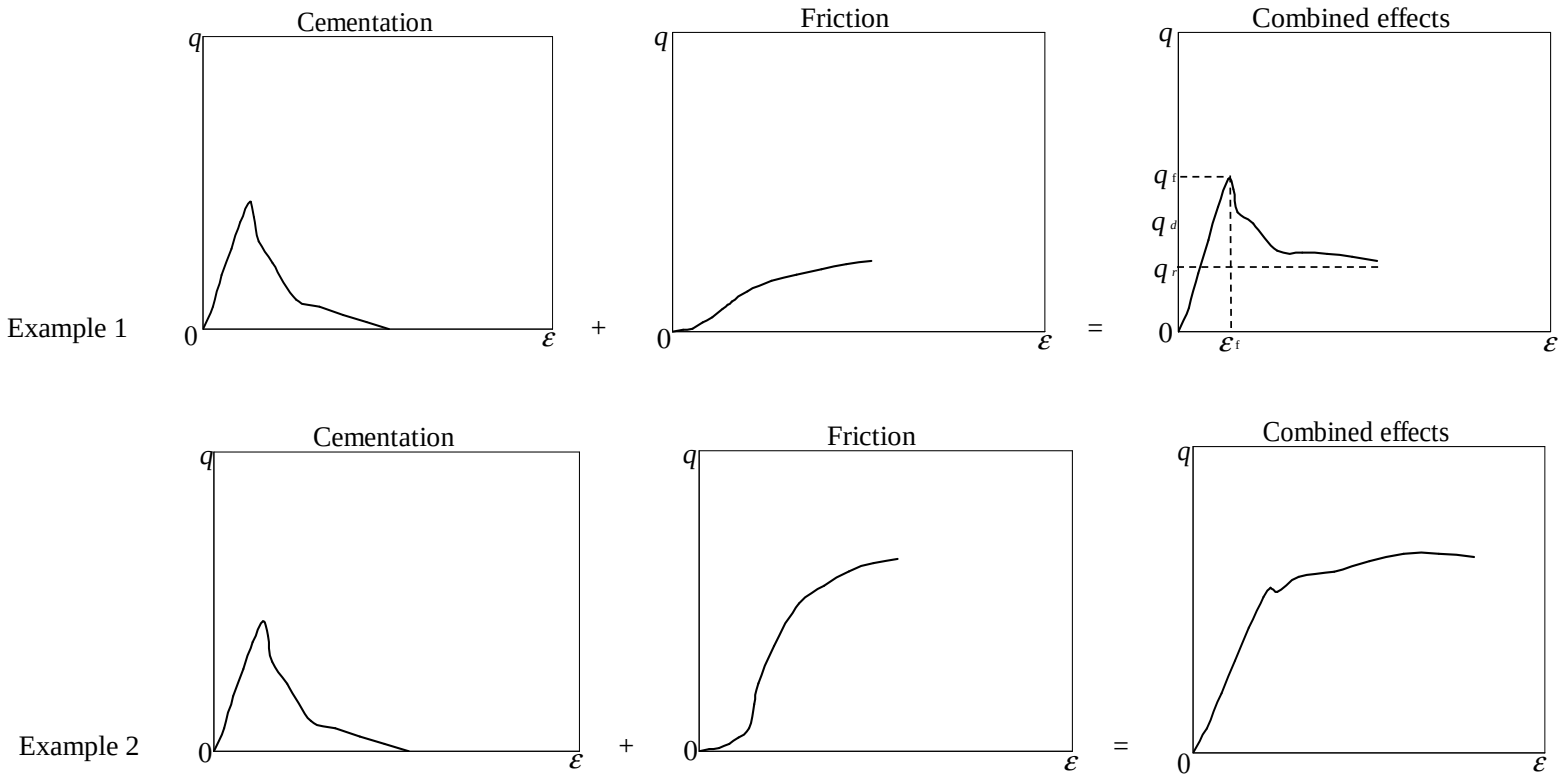

From Bjerrum & Kenney, (1967)

Fig. 4.23 The scheme of the development of shear strength during the deformation of the soil.

4.3.3 CT imagining and SEM analysis for a natural sample after shearing

In Chapter 2, the procedures and machines of the CT imagining and SEM analysis for a natural sample before testing were introduced. In the following sections (Section 4.3.3.1 and Section 4.3.3.2), the micro-analysis for another natural sample after shearing is done.

4.3.3.1 CT imagining

A natural specimen taken at 10.5 m depth was prepared for a compression test. The specimen was broken with a clear failure band after the compression test shown in Fig.4.24. Fig.4.25 to Fig.4.28 present the CT imagining of this specimen.

Fig. 4.24 A specimen with a shear band for CT imagining.

There is a shear band running through the specimen. The plane is not perfectly straight. The angle of this plane with the horizontal plane is about 58°. The values shown in Fig.4.26 are 3032.7 μm, 250.8 μm and 989.2 μm from top to bottom. Thus, the value of the widest part of the shear band on the top face is about 0.99 mm. The shear band has a rough plane in Fig.4.27. The values from top to bottom are 354.7 μm, 3596.3 μm, 1043.7 μm and 494.0 μm respectively. Thus, the value of the most bulgy part is about 1.04 mm. We can also observe the light areas on the surface (including the top face) of the specimen. The specimen at 10.5 m depth is also inhomogeneous with some denser inclusions.

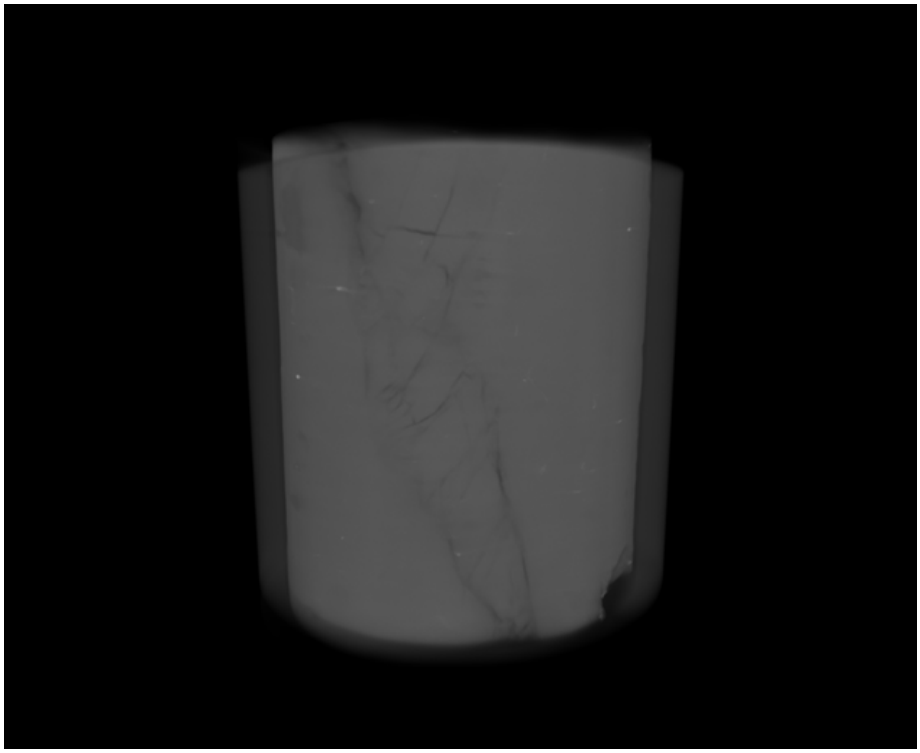

Fig. 4.25 CT imagining of the specimen with a shear band in 3D.

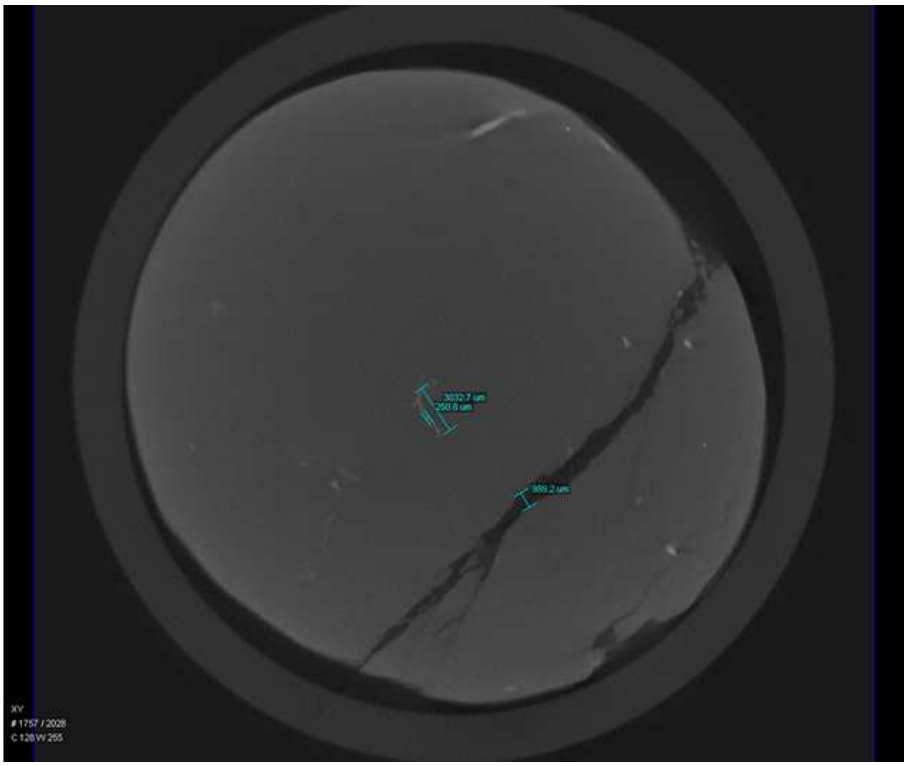

Fig. 4.26 CT imagining of the specimen with a shear band in planform.

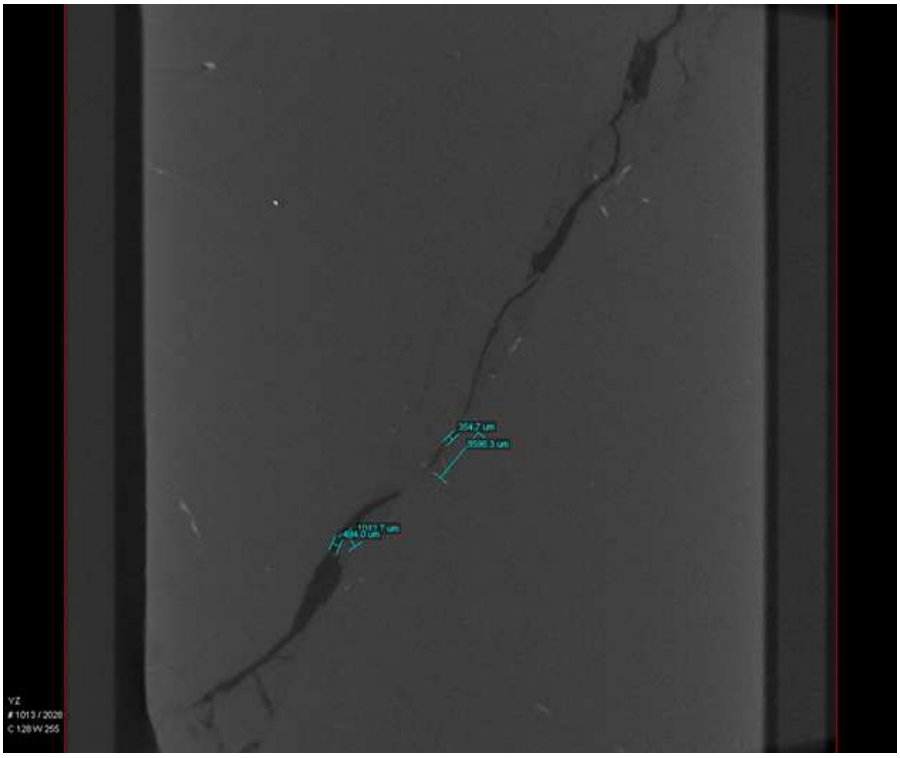

Fig. 4.27 CT imagining of the specimen with a shear band in longitudinal section.

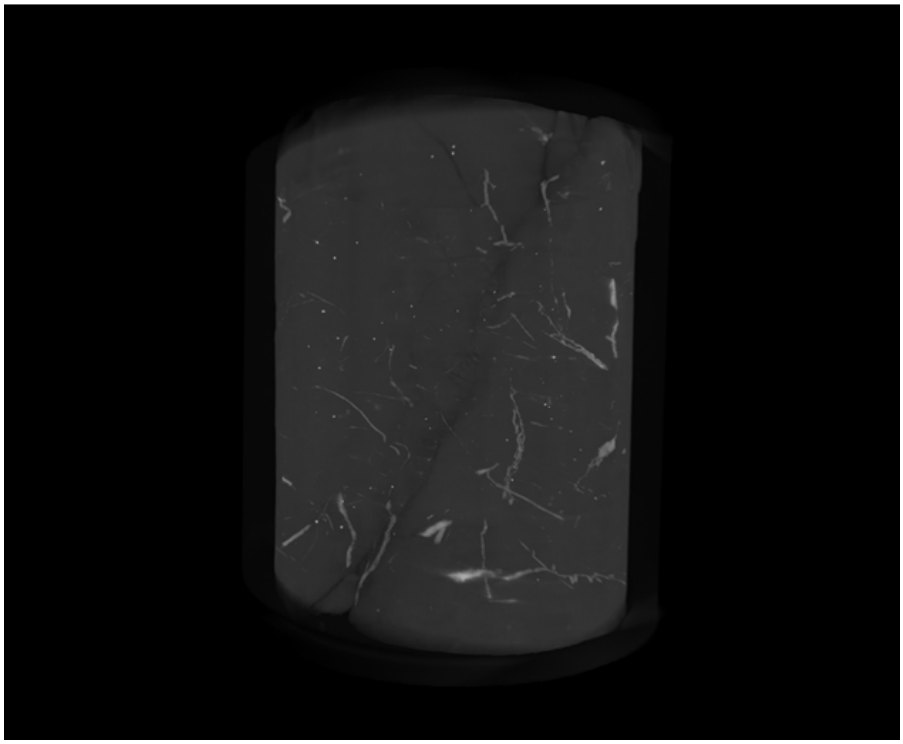

Fig. 4.28 CT imagining of the specimen with a shear band in perspective.

4.3.3.2 SEM analysis

A small part of the same specimen close to the shear band was prepared (Fig.4.29). Fig.4.30 to Fig.4.33 show photos of this sample at different magnifications.

At low magnification, the sample after the compression test reveals the presence of non oriented fabrics, whereas some parts appear very smooth due to significant shearing within the shear band. At high magnification, the structure appears very different from that observed in the natural sample taken at 10.4 m depth in Fig.2.20 to Fig.2.22. Broken clay particles can be seen throughout the whole scanning plane and have no rough shape. The framboid crystals can also be observed.

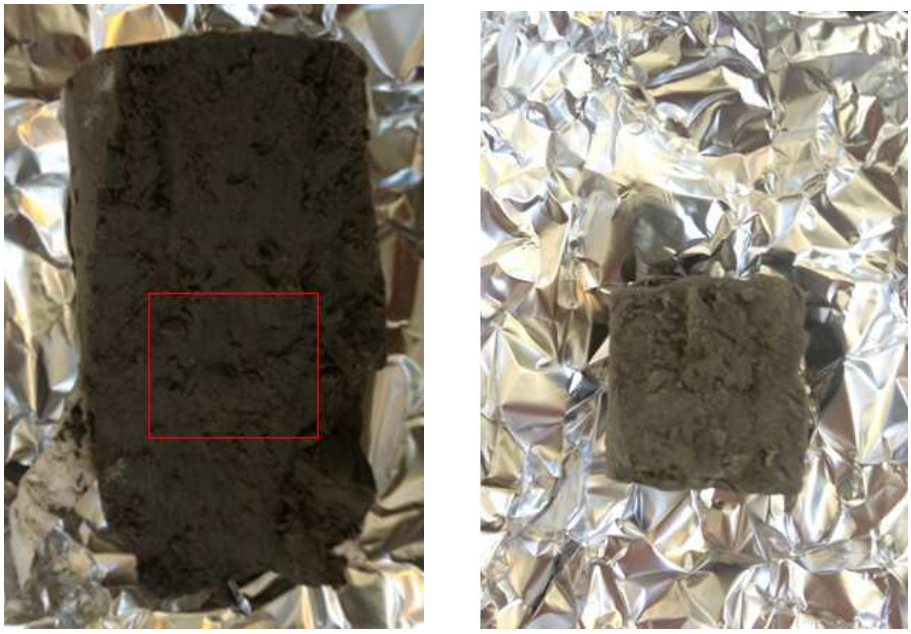

(a) **(b)**

Fig. 4.29 The natural sample taken at 10.5 m: (a) shear band after triaxial test and (b) one part selected for SEM analysis.

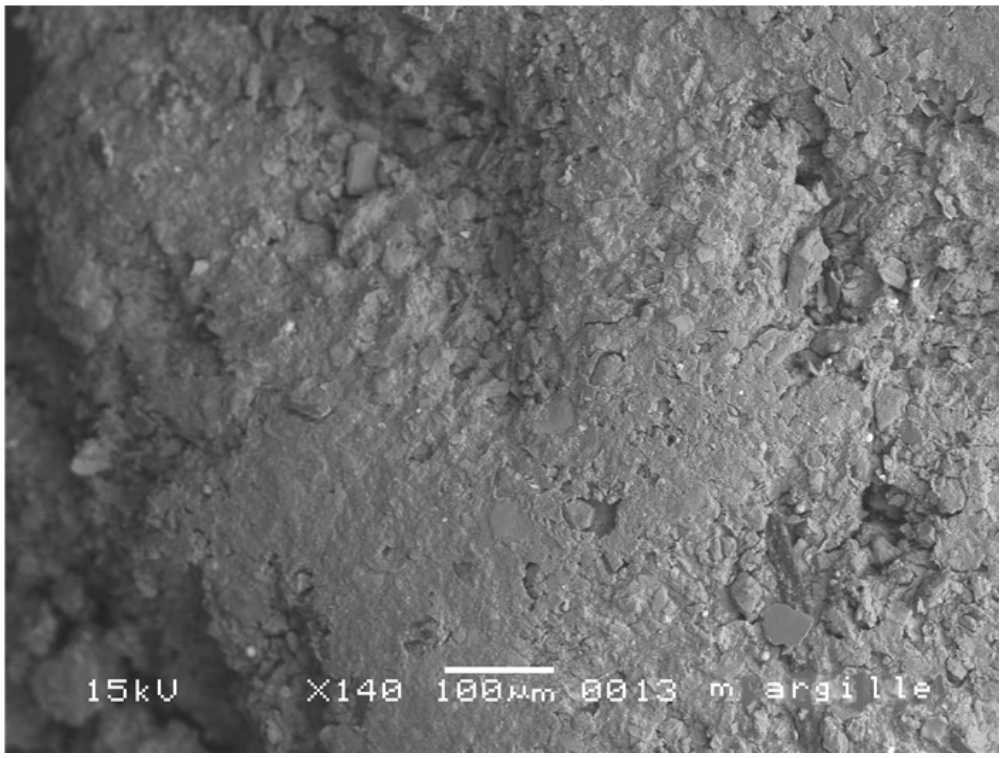

Fig. 4.30 Merville clay sample with a shear band: smooth surface.

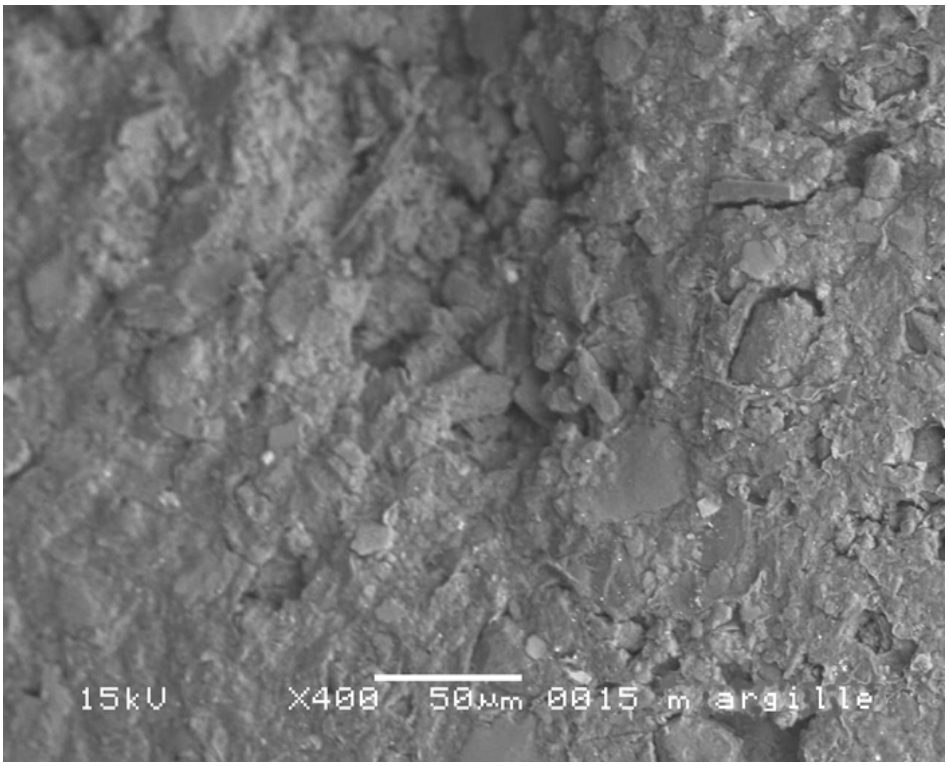

Fig. 4.31 Merville clay sample with a shear band: non-oriented particles in the concave.

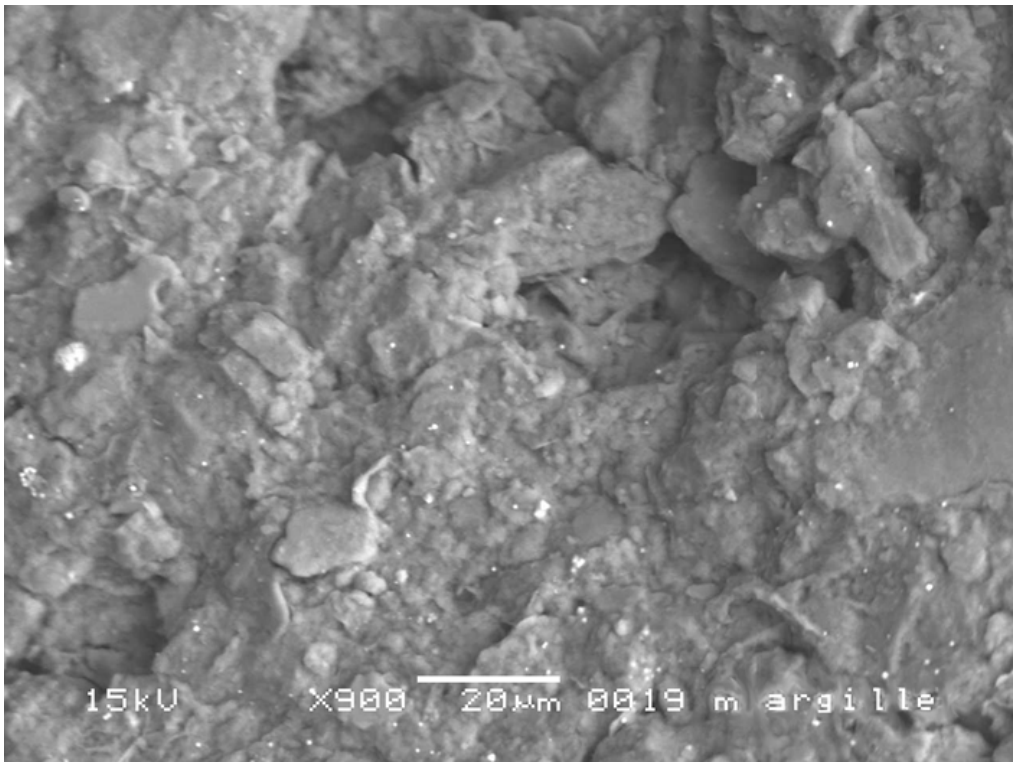

Fig. 4.32 Merville clay sample with a shear band: white framboids crystals.

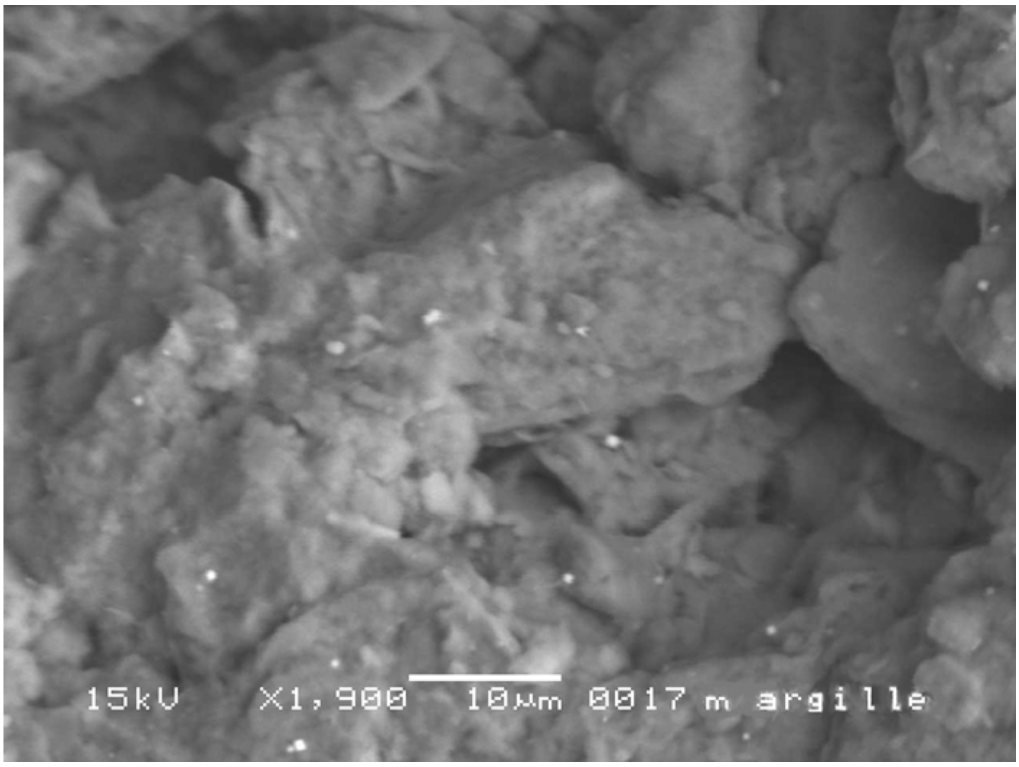

Fig. 4.33 Merville clay sample with a shear band: broken particles.

4.3.4 Strain rate dependency

As mentioned above, one of the important factors affecting the shear strength is the strain rate. Thus, in this section, the strain-rate dependency of the shear strength for the natural and reconstituted samples of Merville clay is discussed.

Various studies reported in the literature show that different soils, for example, sands, weak rocks and soft clays, have different responses to the change in strain rate (Casagrande & Wilson 1951; Lo & Morin 1972; Lefebvre & LeBoeuf 1987). Some comprehensive researches on reconstituted clay have been done by Sheahan et al. (1996) and Zhu & Yin (2000), with *OCR* varying from 1 to 8. Progress in quantifying and understanding the undrained strain rate effects requires additional comprehensive data on a variety of soil types. There are not many reliable data available on the time-dependent behavior of stiff clays with different *OCR*s, particularly natural stiff clays. Some laboratory tests on London clay with different strain rates have been conducted by Sorensen et al. (2007). But the influence of *OCR* on the strength behavior was not analyzed.

Thus, this thesis focuses on investigating the influence of strain rate and *OCR* on the strength behavior of Merville clay.

4.3.4.1 Reconstituted samples

In this study, three series of undrained triaxial compression tests on reconstituted samples with *OCR*=1, 7 and 14 were performed. Table 4.3 presents the results of CIUC tests at different strain rates. It gives the pre-shear consolidation stress condition (effective consolidation pressure σ'_0, and the OCR), and the stress-strain properties at the maximum deviatoric stress.

Fig.4.34 (a) shows the relationship between q/σ'_0 and the axial strain ε_a, where q is normalized with respect to the consolidation pressure σ'_0. The undrained shear strength of normally consolidated reconstituted samples increases with an increase in the strain rate. Fig.4.34 (b) indicates the changes in the normalized pore pressure $\Delta u/\sigma'_0$ with the axial strain during shearing. With similar values of the consolidation pressure σ'_0, the evolutions of the pore pressure at different strain rate are similar, even for the higher strain rate of 25.89 %/h. Thus, we believed that the eventual non-uniformity of the pore pressure may be ignored during shearing. The stress

ratios q/p' versus axial strain are illustrated in Fig.4.34 (c). The curves at the two higher strain rates of 2.57 %/h and 25.89 %/h are similar, whereas, the stress ratio is slightly lower at the strain rate of 0.26 %/h during shearing. Fig.4.34 (d) shows that higher strain rates correspond to higher peak stresses. The best-fitting line for the relationship between the normalized peak stress and the axial strain rate can be represented by a straight line in a semi-logarithmic plane.

Fig.4.35 to Fig.4.36 present the relationship between the normalized deviatoric stress and the axial strain (a), the relationship between the normalized pore pressure and the axial strain (b), the relationship between the stress ratio and the axial strain (c), and the relationship between the normalized peak stress and the axial strain rate (d) for the test series with *OCR*=7 and 14, respectively. The strain-rate effects on the deviatoric stress and pore pressure response appear clearly. Similar to the tests at *OCR*=1, higher strain rate leads to higher shear strength. Unlike the response of pore pressure in the *OCR*=1 test series, the pore pressures in the *OCR*=7 and 14 test series firstly increase and then decrease with an increase in axial strain. The increasing stages of pore pressure and the maximum pore pressure for three different strain rates of each *OCR* test series are similar, thus, we believed that here also the non-uniformity of the pore pressure may be ignored during shearing for the overconsolidated reconstituted samples. Fig.4.35 (c) shows that higher strain rate results in higher stress ratio, however, a similar phenomenon is not observed in Fig.4.36 (c). Fig.4.35 (d) and Fig.4.36 (d) show that higher strain rates correspond to larger peak stresses in the *OCR*=7 and 14 test series, respectively. The best-fitting line for the relationship between the normalized peak stress and the axial strain rate can be represented by a straight line in a semi-logarithmic plane for each *OCR* test series.

Table 4.3 Test results on reconstituted specimens at different strain rates.

Unit	Depth (m)	Initial state of specimens			Consolidation pressure (kPa)		*OCR*	Strain rate (%/h)	Features at the maximum deviatoric stress		
		σ'_v (kPa)	w_0 (%)	m (g)	First stage	Second stage			ε_f (%)	q_f (kPa)	Δu_f (kPa)
SC2	10 ~11	100	50.4	117.8	99.1		1.0	0.26	4.75	85.3	37.3
		100	50.3	119.2	100.1		1.0	2.57	4.52	89.1	42.0
		100	50.2	118.0	99.6		1.0	25.89	4.27	92.3	40.5
		100	50.3	118.7	699.8	99.0	7.1	0.26	6.04	183.5	22.5
		100	49.8	118.8	697.0	100.2	7.0	2.57	5.79	197.5	32.5
		100	50.1	119.0	701.0	99.7	7.0	25.89	5.64	219.6	33.3
		100	49.8	117.1	700.3	50.7	13.8	0.26	4.87	121.3	15.2
		100	49.9	117.3	699.1	49.7	14.1	2.57	4.88	134.9	10.5
		100	49.9	118.0	699.0	49.8	14.0	25.89	7.61	154.1	9.2

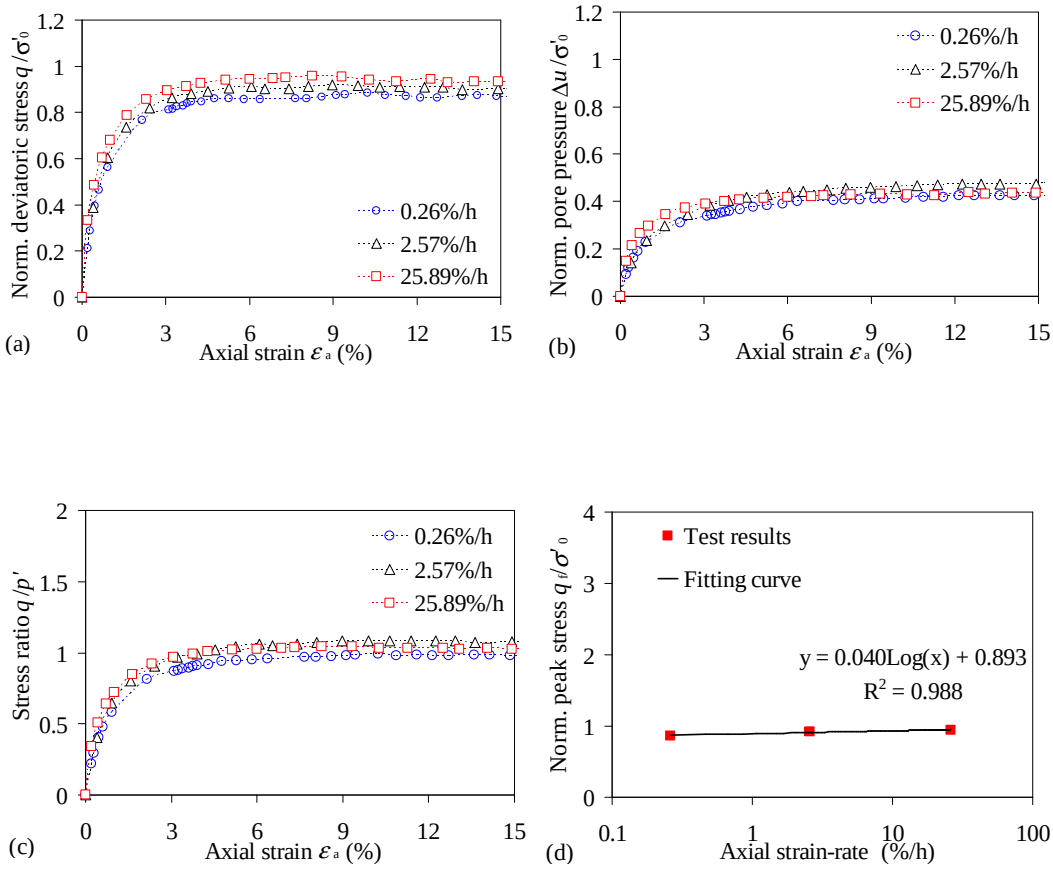

Fig. 4.34 Test results on reconstituted specimens at OCR =1: (a) normalized deviatoric stress versus axial strain, (b) normalized pore pressure level versus axial strain, (c) stress ratio versus axial strain and (d) normalized peak shear stress versus axial strain.

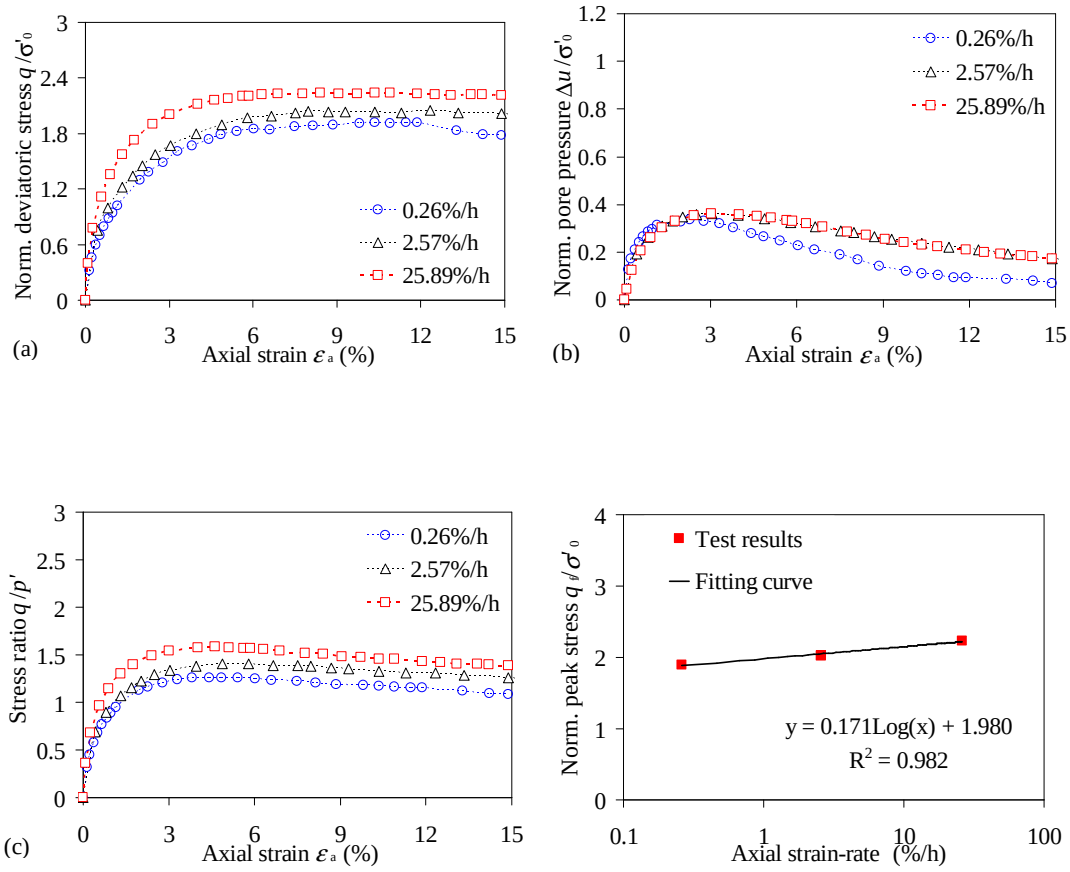

Fig. 4.35 Test results on reconstituted specimens at *OCR* =7: (a) normalized deviatoric stress versus axial strain, (b) normalized pore pressure level versus axial strain, (c) stress ratio versus axial strain and (d) normalized peak shear stress versus axial strain.

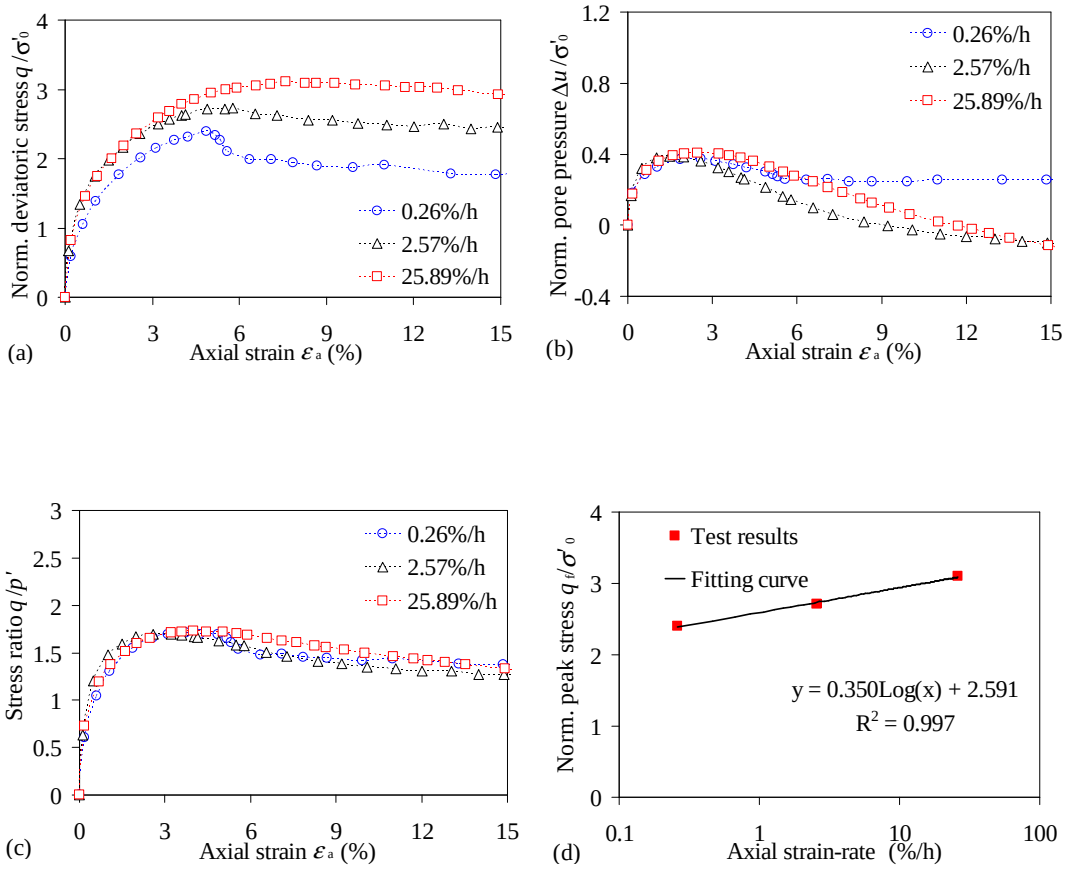

Fig. 4.36 Test results on reconstituted specimens at *OCR* =14: (a) normalized deviatoric stress versus axial strain, (b) normalized pore pressure level versus axial strain, (c) stress ratio versus axial strain and (d) normalized peak shear stress versus axial strain.

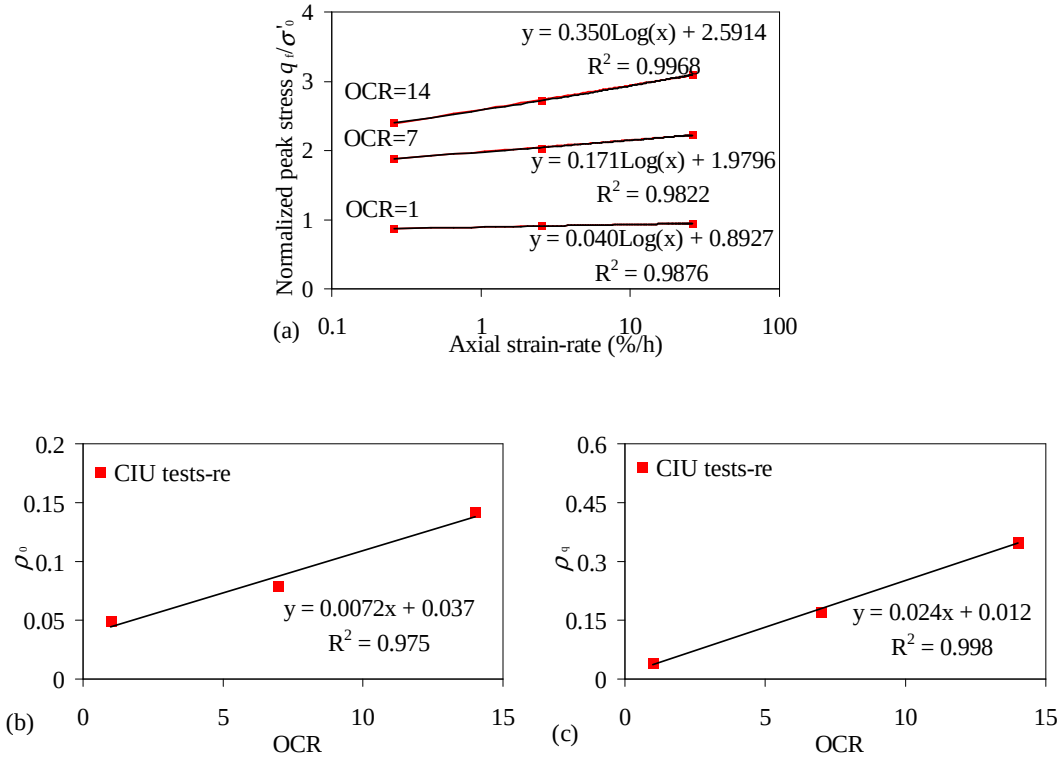

Fig. 4.37 (a) Relationship between normalized peak shear stress and axial strain rate, (b) relationship between ρ_0 and *OCR* and (c) relationship between ρ_q and *OCR*.

To characterize the influence of the strain rate on the shear strength, Bjerrum (1973) suggested that the undrained shear strength varies almost linearly with the logarithm of the strain rate, expressed as follows:

$$\frac{\left(q_f / \sigma'_0\right)_{\dot{\varepsilon}_a}}{\left(q_f / \sigma'_0\right)_{\dot{\varepsilon}_{a0}}} = 1 + \rho_0 \log\left(\frac{\dot{\varepsilon}_a}{\dot{\varepsilon}_{a0}}\right) \tag{4.2}$$

where $\left(q_f / \sigma'_0\right)_{\dot{\varepsilon}_a}$ is the normalized undrained shear strength for a given strain rate $\dot{\varepsilon}_a$; ρ_0 is the coefficient of strain rate influence defined for a reference strain rate $\dot{\varepsilon}_{a0}$.

The strain rate of 0.26 %/h is chosen as the reference strain rate $\dot{\varepsilon}_{a0}$ for each OCR test series of reconstituted samples. For *OCR*=1, 7 and 14, the values of the coefficient, ρ_0, are 0.040, 0.079, and 0.142, respectively, which are obtained from Eq.(4.2). A straight line is used to represent the relationship between ρ_0 and OCR shown in Fig.4.37 (b). The average value of $\bar{\rho}_0$ is 0.090.

Fig.4.37 (a) shows the relationships between the normalized undrained shear strength (q_f/σ'_0) and the axial strain rate ($\dot{\varepsilon}_a$) summarized from Fig.4.34 (d), Fig.4.35 (d), and Fig.4.36 (d). For each OCR, the set of test points is fitted with a straight line in a semi-log diagram, and the equations of these lines are shown in the Figure. The slope of each line reflects the rate of the undrained strength increase with the strain rate. The slope of q_f/σ'_0 versus $\log(\dot{\varepsilon}_a)$ can be denoted as (Zhu &.Yin, 2000):

$$\rho_q = \frac{\Delta\left(q_f / \sigma'_0\right)}{\Delta \log\left(\dot{\varepsilon}_a\right)} \tag{4.3}$$

Fig. 4.37(a) demonstrates that higher OCR values correspond to larger values of the slope. For *OCR* values of 1, 7 and 14, the values of the slope ρ_q are 0.040, 0.171 and 0.350, respectively. In their study, Zhu &.Yin (2000) obtained values of the slope ρ_q equal to 0.0141, 0.0343, 0.0565 and 0.0469 for the reconstituted samples of Hong Kong marine clay with *OCR* values of 1, 2, 4 and 8, respectively. For a given *OCR* value (such as *OCR* =1), the effect of the strain rate is greater on reconstituted samples of Merville clay than on Hong Kong marine clay.

Fig. 4.37(c) shows the relationship between ρ_q and *OCR*, in which ρ_q appears to increase linearly with the OCR. It can be concluded that for reconstituted samples the strain rate influence on the normalized undrained shear strength is greater for higher *OCRs*.

4.3.4.1 Natural samples

In this study, four series of undrained consolidated triaxial compression tests of samples with *OCR*=7, 14, 28, and 56 were performed. Table 4.4 presents the results of tests on the overconsolidated specimens. It gives the pre-shear consolidation stress condition (effective consolidation pressure σ'_0, and actual *OCR*), and the stress-strain properties at the maximum deviatoric stress (failure) and at the maximum excess pore pressure during shearing.

Values of interest for the comparative study are presented in Table 4.4. For each test, the axial strain ε_{uf} at the maximum excess pore pressure is less than the axial strain ε_f at the peak stress, which means that the maximum excess pore pressure Δu_m is reached earlier than the peak shear stress q_f.

Fig.4.38 (a) presents the relationship between the normalized deviatoric stress and the axial strain for the test series with *OCR*=7. Strain localization and shear band formation were observed within these overconsolidated specimens even at the lowest strain rate. The axial strain corresponding to the peak stress increases with an increase in the strain rate.

In the study of the strain rate effect, one possible problem is the redistribution of pore water at high strain rates. However, based on the data in Table 4.4, we can notice that the values of the maximum pore pressures Δu_m and the axial strains ε_{uf} for three different strain rates are very similar. Fig.4.38 (b) presents the relationship between the excess pore pressure and the axial strain. The two curves at the low strain rates (0.26 %/h and 2.57 %/h) are almost identical before reaching the maximum pore pressure. However, for the highest strain rate (25.89 %/h), the value of normalized pore pressure is greater before reaching the maximum pore pressure.

The relationship between the stress ratio and the axial strain is shown in Fig.4.38 (c), where $p' = (\sigma'_1+2\sigma'_3)/3$ is the mean effective stress. These three curves almost coincide during the first stages of the loading and then diverge before the peak of the stress-strain curve. Fig.4.38 (d) shows that higher strain rates correspond to larger peak stresses. The best-fitting line for the relationship between the normalized peak stress and the axial strain rate can be represented by a straight line in a semi-logarithmic plane.

Fig.4.39 to Fig.4.41 present the relationship between the normalized deviatoric stress and the axial strain (a), the relationship between the excess pore pressure and the axial strain (b), the relationship between the stress ratio and the axial strain (c), and the relationship between the normalized peak stress and the axial strain rate (d) for the test series with *OCR*=14, 28 and 56, respectively. Strain localization and shear band formation were observed in these overconsolidated specimens for the tests at the three strain rates. The values of the axial strain corresponding to the peak stress and the maximum pore pressure are almost equal. Fig.4.39 (a) to Fig.4.41 (a) show that higher strain rate leads to higher shear strength. In each figure of Fig.4.39 (b) to Fig.4.41 (b) for the evolution of the pore pressure, the three curves are almost identical before reaching the maximum pore pressure, which means that the evolution of the pore pressure is almost independent of the strain rate before reaching the maximum pore pressure. We can conclude that

in the tests at the strain rate of 25.89 %/h with OCR=14, 28 and 56, the non-uniformity of the pore pressure may be ignored.

Fig.4.39 (d) to Fig.4.41 (d) show that higher strain rate leads to higher peak stress. The best-fitting line for the relationship between the normalized peak stress and the axial strain rate can also be represented by a straight line in a semi-log diagram.

The results of these four series of undrained triaxial compression tests on natural samples with *OCR*=7, 14, 28, and 56 are summarized in Fig.4.42.

Table 4.4 Test results on natural specimens at different strain rates.

Unit	Depth (m)	Initial state of specimens					Effective confining pressure σ'_0 (kPa)	*OCR*	Strain rate (%/h)	Features at the maximum deviatoric stress				Features at maximum excess pore pressure	
		Preconsolidation pressure (kPa)	γ_h (kN/m^3)	γ_d (kN/m^3)	w_0 (%)	σ'_{v0} (kPa)				ε_f (%)	Angle α (°)	q_f (kPa)	Δu_f (kPa)	ε_{uf} (%)	Δu_m (kPa)
SC2	10.38	2750	19.5	14.8	31.5	125.7	401.4	6.9	0.26	2.61	61	631.2	164.0	2.31	168.1
	10.43	2750	19.7	14.9	31.8	126.2	399.8	6.9	2.57	3.14	64	690.2	160.3	2.54	167.9
	10.30	2750	19.5	14.9	31.3	125.0	400.1	6.9	25.89	3.64	64	768.8	185.2	3.06	194.2
	10.20	2750	19.5	14.8	31.6	124.0	199.3	13.8	0.26	3.49	64	426.6	107.2	2.99	117.2
	10.25	2750	19.5	14.8	31.8	124.5	200.3	13.7	2.57	3.33	64	484.0	116.3	3.09	117.3
	10.28	2750	19.5	14.8	31.5	124.8	200.1	13.7	25.89	3.70	61	532.3	113.9	3.30	116.4
	10.53	2750	19.5	14.8	32.1	127.2	100.3	27.4	0.26	3.70	68	371.0	65.2	2.37	81.6
	10.73	2750	19.6	14.8	32.1	129.1	101.2	27.2	0.52	3.20	63	387.4	77.9	2.38	81.8
	10.65	2750	19.7	15.0	31.6	128.3	100.8	27.3	2.57	2.96	63	415.3	80.7	2.47	88.8
	10.58	2750	19.7	14.9	32.1	127.7	99.4	27.7	25.89	3.10	65	455.2	74.0	2.61	78.1
	10.15	2750	19.7	15.0	31.5	123.5	50.8	54.1	0.26	2.92	61	312.4	35.0	1.60	41.0
	10.60	2750	19.6	14.9	31.2	127.9	49.9	55.1	2.57	2.50	54	336.6	34.1	1.55	37.2
	10.48	2750	19.7	15.0	31.3	126.7	49.3	55.8	25.89	2.69	58	383.3	31.2	2.13	36.9

Note: Δu_m is the maximum excess pore pressure, ε_{uf} is the axial strain corresponding to Δu_m.

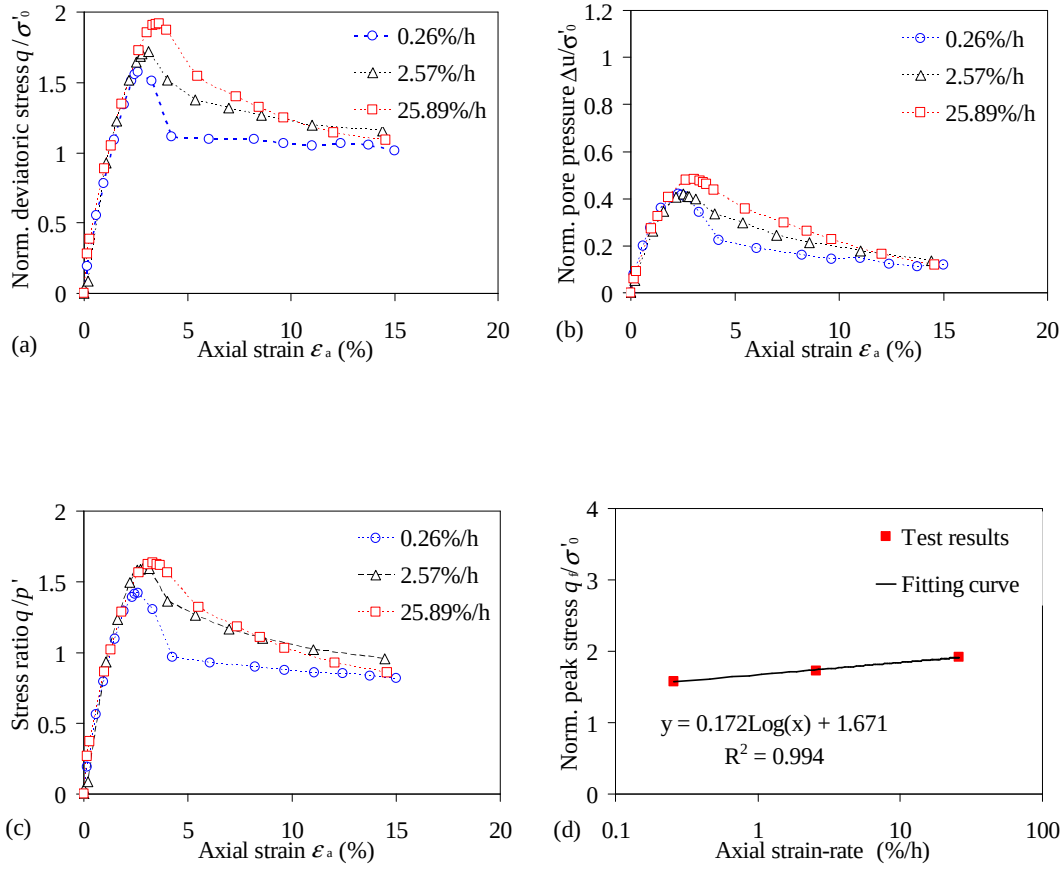

Fig. 4.38 Test results on natural specimens at *OCR* =7: (a) normalized deviatoric stress versus axial strain, (b)normalized excess pore pressure versus axial strain, (c) stress ratio versus axial strain and (d) normalized peak shear stress versus axial strain rate.

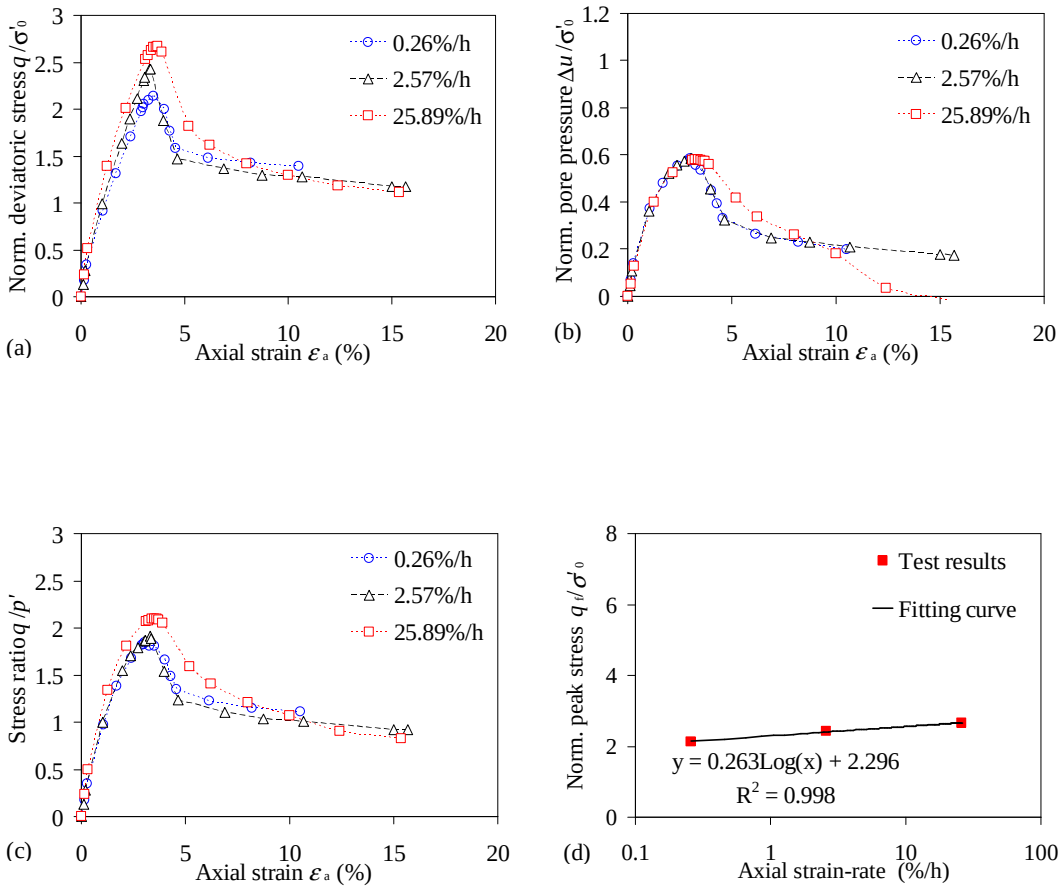

Fig. 4.39 Test results on natural specimens at *OCR* =14: (a) normalized deviatoric stress versus axial strain, (b) normalized excess pore pressure versus axial strain, (c) stress ratio versus axial strain and (d) normalized peak shear stress versus axial strain rate.

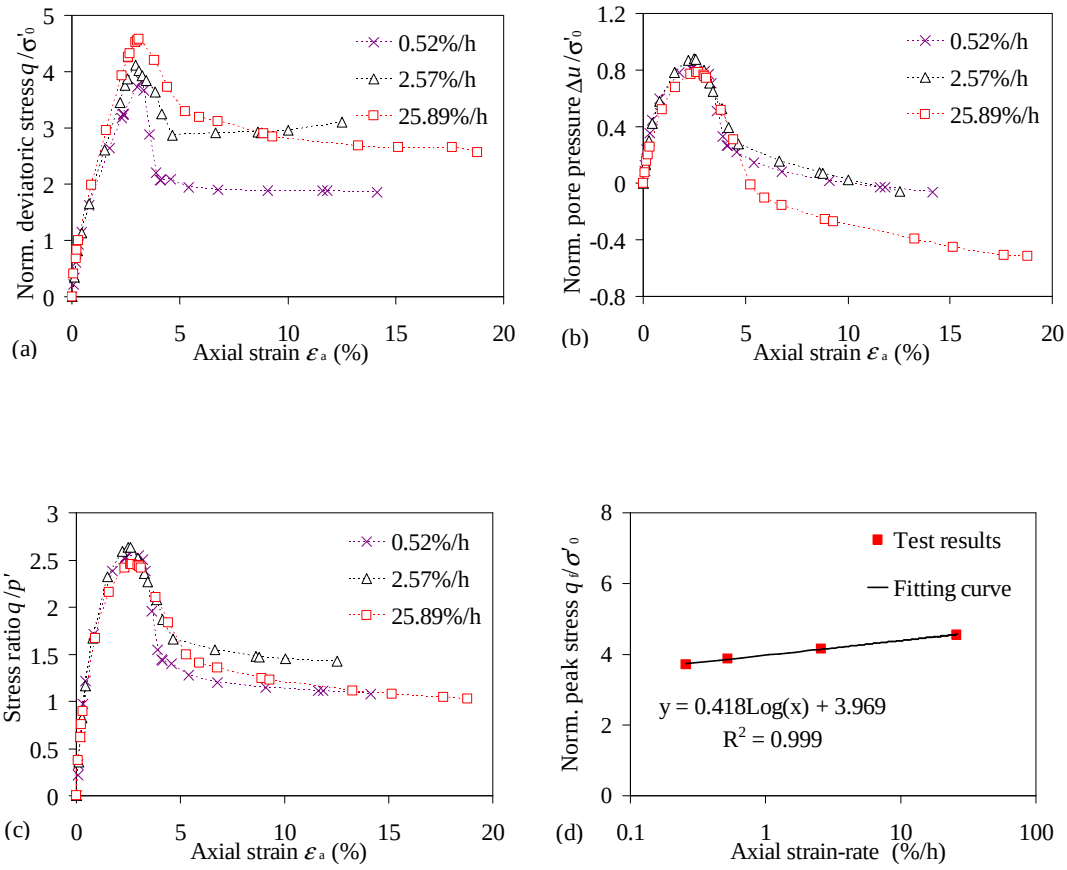

Fig. 4.40 Test results on natural specimens at *OCR* =28: (a) normalized deviatoric stress versus axial strain, (b) normalized excess pore pressure versus axial strain, (c) stress ratio versus axial strain and (d) normalized peak shear stress versus axial strain rate.

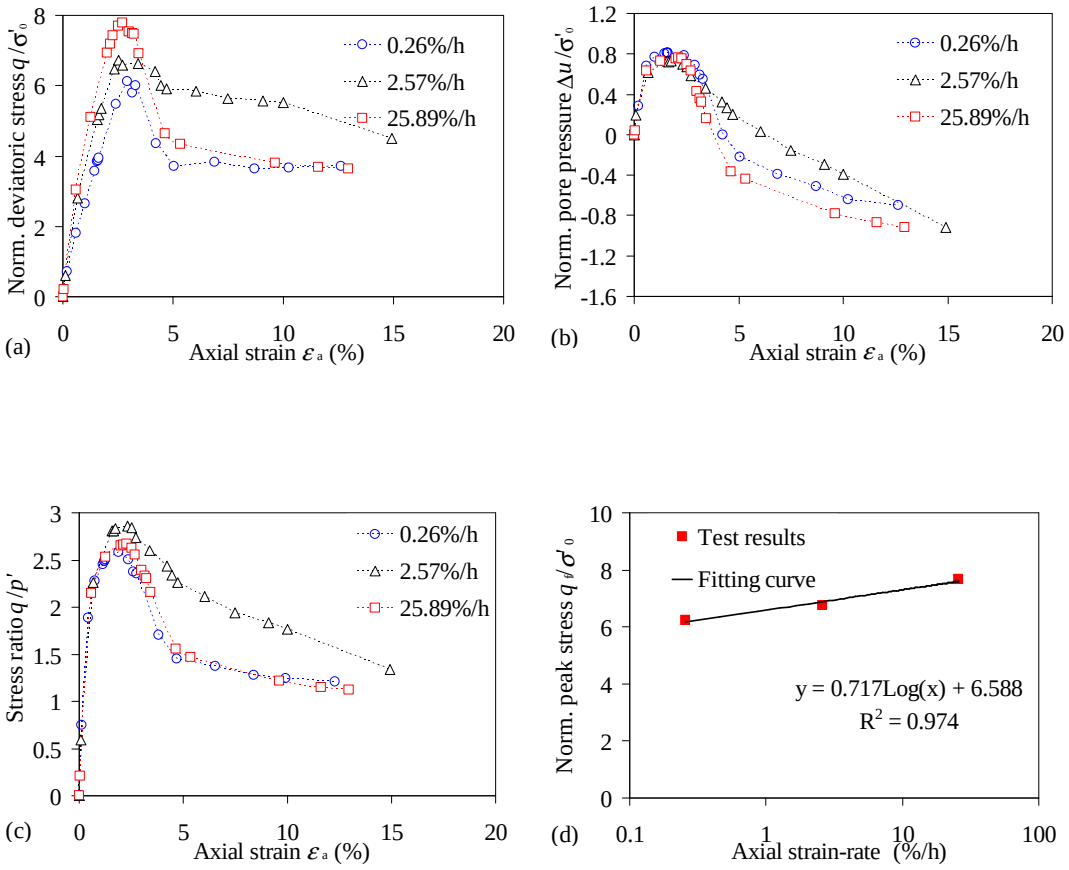

Fig. 4.41 Test results on natural specimens at *OCR* =56: (a) normalized deviatoric stress versus axial strain, (b) normalized excess pore pressure versus axial strain, (c) stress ratio versus axial strain and (d) normalized peak shear stress versus axial strain rate.

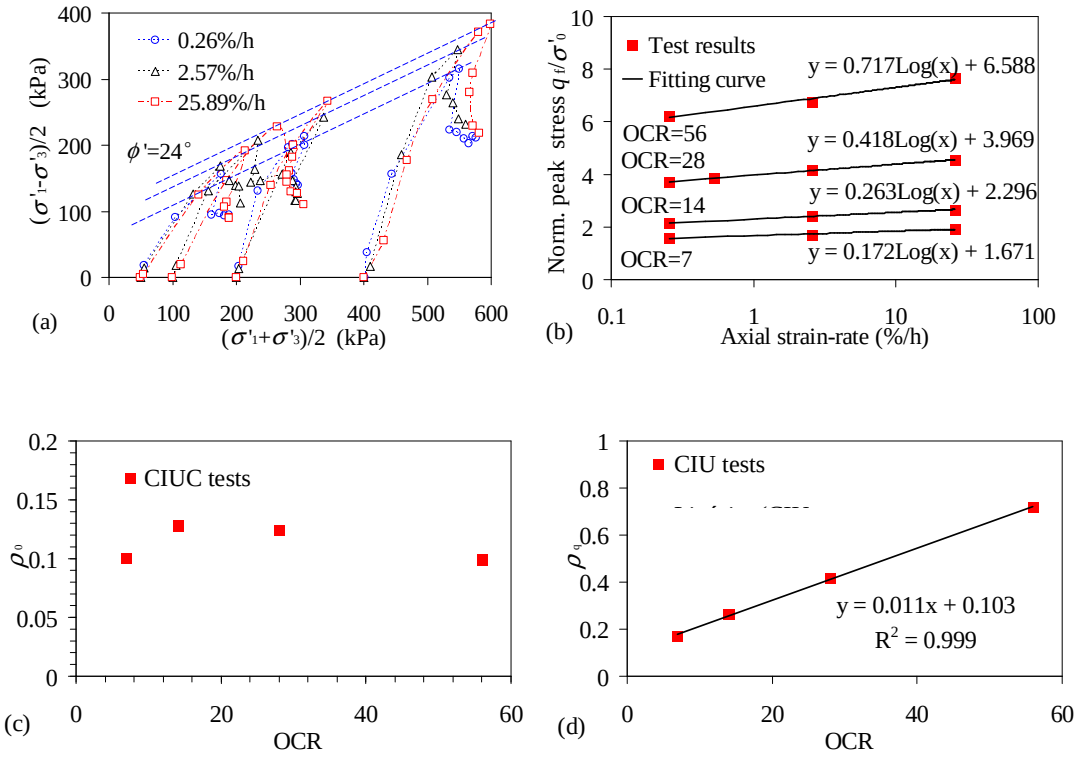

Fig. 4.42 (a) Undrained effective stress paths at different strain rates, (b) relationship between normalized peak shear stress and axial strain, (c) relationship between ρ_0 and *OCR* and (d) relationship between ρ_q and *OCR*.

Fig.4.42 (a) presents the effective stress paths at different confining pressures (50 kPa, 100 kPa, 200 kPa and 400 kPa) and at different strain rates (0.26 %/h, 2.57 %/h and 25.89 %/h). We obtained three parallel failure lines for the three different strain rates (Fig.4.36 (a)). Thus, the peak friction angle, ϕ', appears independent of the strain rate. Its mean value is 24°.

The strain rate of 0.26 %/h is chosen as the reference strain rate $\dot{\varepsilon}_{a0}$ for each *OCR* test series. For *OCR*=7, 14, 28 and 56, the values of the coefficient, ρ_0, are 0.101, 0.128, 0.124 and 0.099, respectively. The average value of $\bar{\rho}_0$ is 0.113.

Fig. 4.42(*b*) shows the relationships between the normalized undrained shear strength (q_f/σ'_0) and the axial strain rate ($\dot{\varepsilon}_a$) summarized from Fig.4.38 (d), Fig.4.39 (d), Fig.4.40 (d), and Fig.4.41 (d). For each *OCR*, the set of test points is fitted with a straight line in a semi-log diagram, and the equations of these lines are shown in Fig.4.42 (b). The slope of each line reflects

the rate of the undrained strength increase with the strain rate. The relationship between the slope of q_f/σ'_0 and $\log(\dot{\varepsilon}_a)$ can be represented by Eq. (4.3).

Fig.4.42 (b) shows that higher *OCR* values correspond to larger values of the slope for *OCR*s equal to 7, 14, 28 and 56, the values of the slope are 0.172, 0.263, 0.418 and 0.717, respectively.

Fig.4.42 (c) shows the relationship between ρ_0 and *OCR*, in which the values of ρ_0 have the irregular distribution with an increase in *OCR*. Fig.4.42 (d) shows the relationship between ρ_q and *OCR*, in which ρ_q appears to increase with an increase in *OCR*. It can be concluded that for Merville clay the strain rate influence on the normalized undrained shear strength is greater for higher *OCR*s.

4.3.5 Undrained shear strength anisotropy

Based on the test results shown in Table 4.5 and in Fig.4.43 and Fig.4.44, it is noticeable that there are fissure effects in some of the natural specimens prepared in the vertical direction. The deviatoric stress for the specimen V200 increases continuously up to an axial strain of 15%. The axial strains corresponding to the peak stresses of the specimens V100 and V200 are 9.30% and 3.92%, respectively. Unlike the stress-strain curves of the vertical specimens, the peak stresses can be easily observed at axial strains less than 3.0% for the horizontal specimens in Fig.4.44 (a). The microstructure and maybe the fissure orientation seem to play a significant role in the anisotropic behavior of Merville clay.

At the same confining pressure, the value of the shear strength for a horizontal intact specimen (H200) is 1.7 times greater than that of the vertical intact specimen (V200). For the other two confining pressures (100 kPa and 50 kPa), there are 1.2 times and 2.5 times greater. After the peak stress, the deviatoric stress reached rapidly the residual stress for all the horizontal specimens, whereas the evolution of the deviatoric stress was more progressive after the peak stress for the vertical specimens.

Fig.4.43 (b) and Fig.4.44 (b) present the pore pressure evolution versus the axial strain. For each direction, the higher confining pressure caused a higher pore pressure. The pore pressure evolution was not significantly affected by the specimen orientation.

Fig.4.43 (c) and Fig.4.44(c) present the effective stress paths for the specimens prepared in the vertical and horizontal directions, respectively. The paths turned to the right for the horizontal specimens, but turned slightly to the left at the beginning of the loading, then to right for the vertical specimens.

In his paper, Burland (1990) presented the test results on London clay samples prepared in the vertical and horizontal directions (Fig.4.45 (a)). There is a unique intact failure line for the London clay, but the tests were performed at higher consolidation pressures. The six stress paths of Merville clay were summarized in Fig.4.45 (b). It can be noticed that there are two intact failure lines for these two directions. The horizontal specimens appear more resistant than the vertical ones. This could be the consequence of the in situ stress history. The important OCR led to stresses higher in the horizontal directions than in the vertical one, and consequently to an oriented microstructure. This aspect is less marked for London clay collected more deeply and tested at higher consolidation stresses during the triaxial tests.

Table 4.5 Test results on natural specimens prepared at different directions (vertical and horizontal).

Unit	Specimen name	Depth (m)	Long axe	Initial state of specimens				Effective confining pressure σ'_0 (kPa)	Features at the maximum deviatoric stress			
				γ_h (kN/m^3)	γ_d (kN/m^3)	w_0 (%)	σ'_{v0} (kPa)		ε_f (%)	Angle α (º)	$(\sigma'_a-\sigma'_r)_f/2$ (kPa)	$(\sigma'_a+\sigma'_r)_f/2$ (kPa)
SC2	V50	6.05	Vertical	19.7	14.9	32.1	84.2	50.5	11.82	75	72.1	119.1
	V100	6.36	Vertical	19.7	15.0	31.7	87.2	100.0	9.30	66	148.2	218.6
	V200	6.58	Vertical	19.5	14.8	31.5	89.3	200.0	3.92	64	179.3	282.0
	H50	6.28	Horizontal	19.6	14.9	31.5	86.4	49.8	2.27	69	177.1	196.9
	H100	6.47	Horizontal	19.4	14.8	31.3	88.2	98.8	2.54	52	192.6	244.7
	H200	6.67	Horizontal	19.4	14.8	31.1	90.1	200.0	2.75	67	304.9	414.5

Table 4.6 Test results on reconstituted specimens (CIUC and CIUE).

Unit	Depth (m)	Specimen name	Initial state of specimens			Consolidation pressure (kPa)		*OCR*	Features at the maximum (CIUC) or minimum (CIUE) deviatoric stress		
			σ'_v (kPa)	w (%)	m (g)	First stage	Second stage		ε_f (%)	$(\sigma'_a-\sigma'_r)_f/2$ (kPa)	$(\sigma'_a+\sigma'_r)_f/2$(kPa)
SC3	7 ~8	rCIUC1	300	38.8	123.0	400.0	99.4	4	14.89	96.1	186.3
		rCIUE1	300	38.9	122.9	399.5	99.6	4	-8.18	-85.0	108.5
		rCIUC2	300	38.1	123.5	399.9		1	8.22	154.2	362.7
		rCIUE2	300	37.8	125.2	289.9		1	-13.3	-114.1	193.6
SC2	10 ~11	rCIUC3	100	50.3	119.2	199.2		1	7.71	81.8	196.2
		rCIUC4	100	50.1	119.1	400.6		1	11.75	171.6	407.0
		rCIUC5	100	50.1	118.5	699.9		1	11.48	297.0	705.9

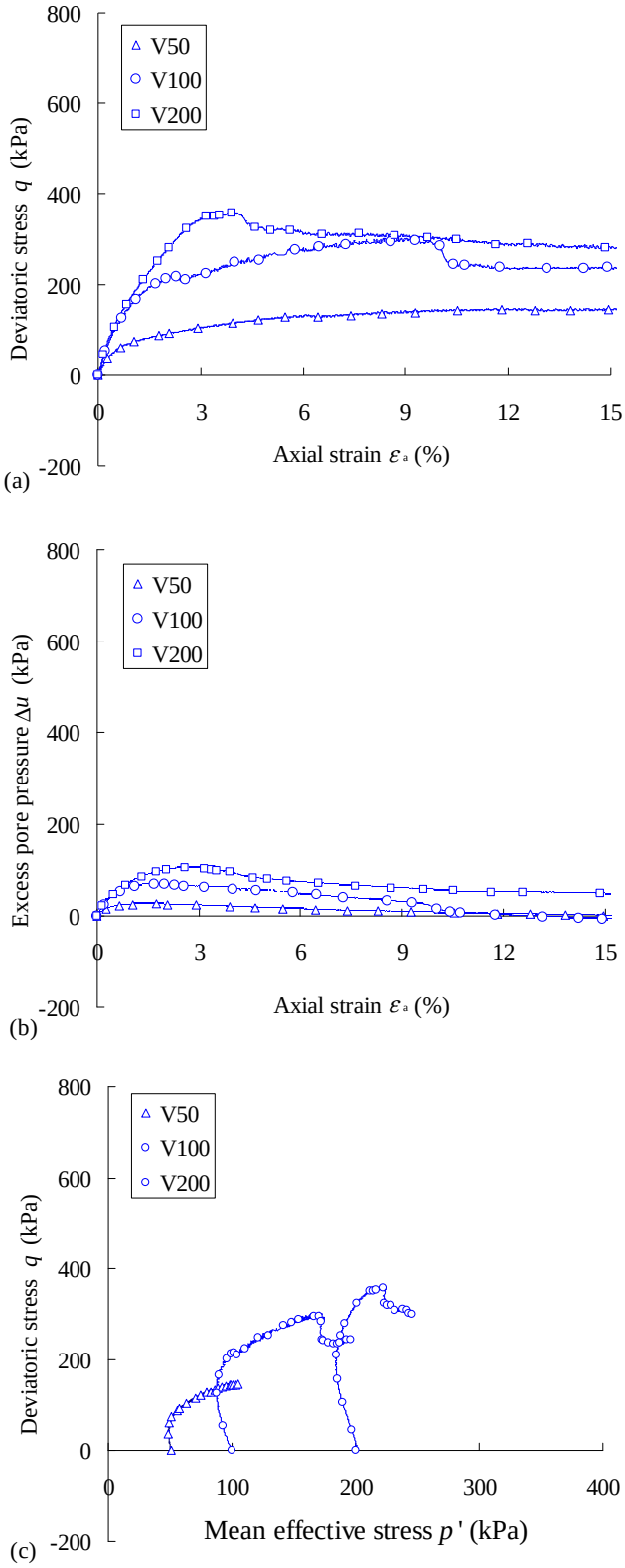

Fig. 4.43 CIUC test results on natural specimens prepared in the vertical direction: (a) deviatoric stress versus axial strain, (b) excess pore pressure versus axial strain and (c) effective stress paths.

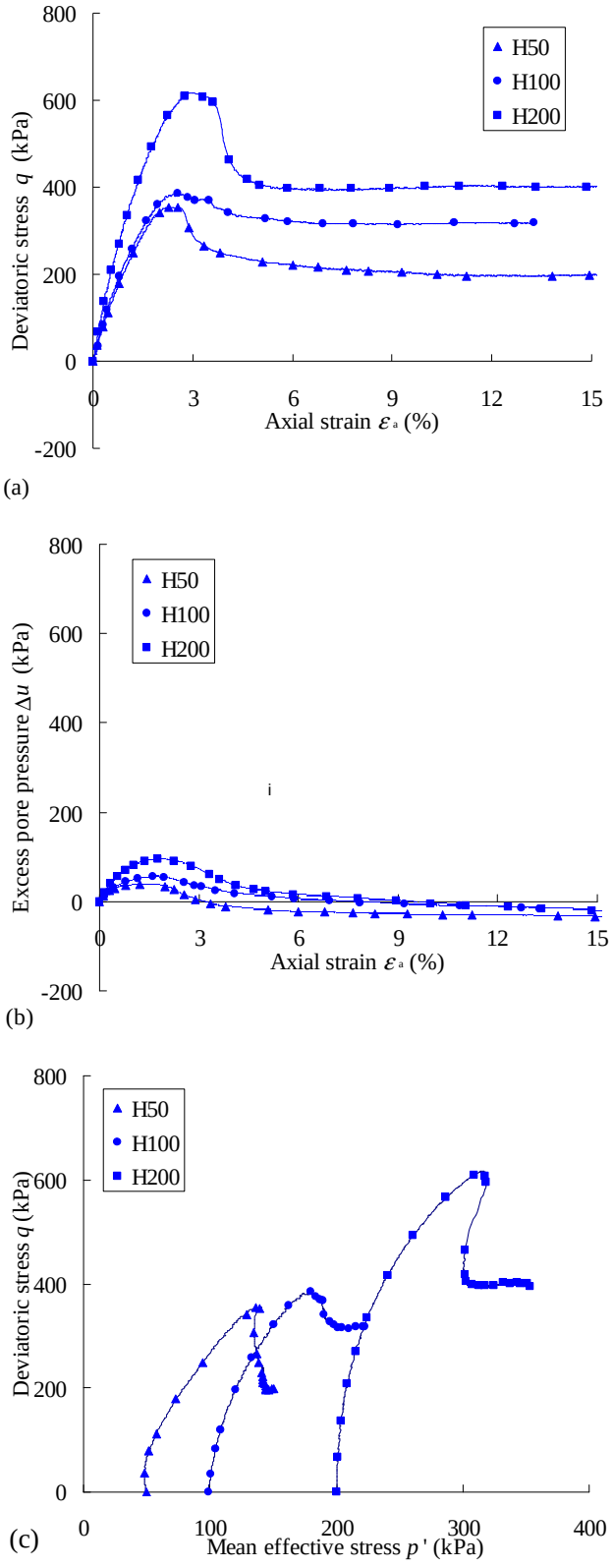

Fig. 4.44 CIUC test results on natural specimens prepared in the horizontal direction: (a) deviatoric stress versus axial strain, (b) excess pore pressure versus axial strain and (c) effective stress paths.

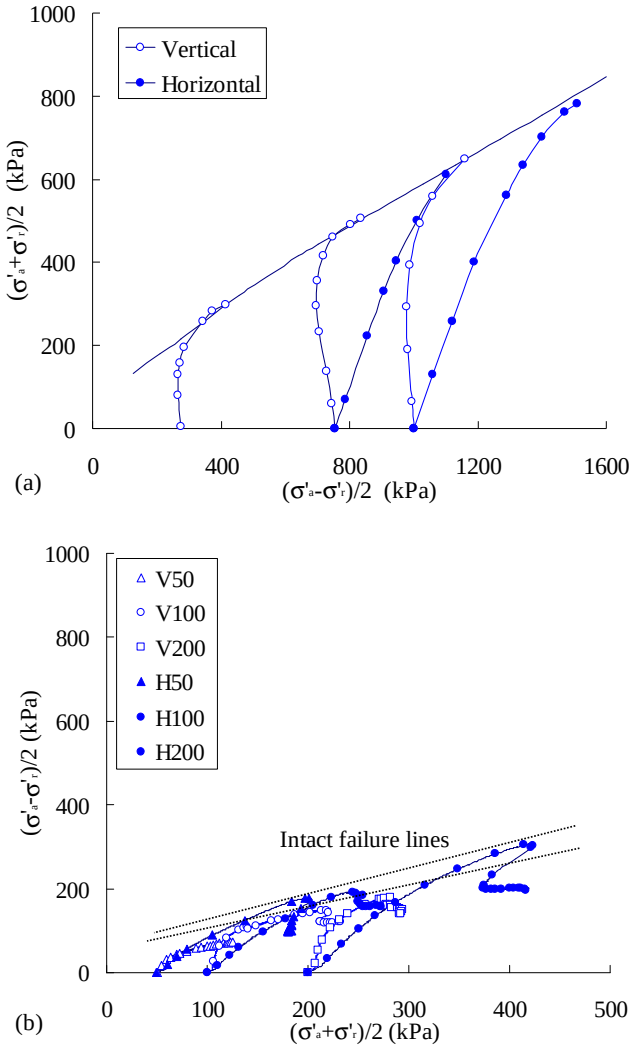

Fig. 4.45 (a) CIUC tests on vertical and horizontal natural specimens of London clay (Burland, 1990) and (b) tests on vertical and horizontal natural specimens of Merville clay.

4.3.6 Failure envelopes under triaxial condition

As presented in Table 4.1, Table 4.2, Table 4.3 and Table 4.5, the data on the undrained shear strength of natural samples are, overall, difficult to interpret. In fact, on one hand, the majority of these triaxial tests were done on the samples with fissures. On the other hand, these test specimens were broken during loading following different inclined sliding planes.

When the inclination α of the rupture plane is taken into account, the shear strength mobilized is not equal to: $t_f = (\sigma'_a-\sigma'_r)_f/2$, but equals to $\tau_f = [(\sigma'_a-\sigma'_r)_f/2]\sin(2\alpha)$.

Firstly, we traced the failure envelopes in the plane of $s' = [(\sigma'_a+\sigma'_r)/2$ and $t = (\sigma'_a-\sigma'_r)/2$ from the points of coordinates s'_f and t_f, which represented the state of the principal stresses applied to the specimens at the time of rupture (or the maximum deviatoric stress).

The observed inclination of the rupture plane is often very different from these values, it was also determined by plotting the rupture envelopes in the plane (σ', τ) from the points of coordinates σ'_f and τ_f that denote the normal and tangential components of the stresses. These stress components are applied to the fracture plane at the time of the failure (or the maximum deviatoric stress) which are calculated from the expressions:

$$\sigma'_f = s'_f + t_f \cos(2\alpha) \tag{4.4}$$

$$\tau_f = t_f \sin(2\alpha) \tag{4.5}$$

The results of all the UU, CIUC and CIUE tests of the natural specimens at the normal strain rate (2.57 %/h) were summarized in Fig. 4.46. These results include also the results on the vertical specimens in the anisotropic analysis and the results of the normal strain rate in the analysis of the strain-rate dependency.

Fig.4.46 (a) presents the test results obtained in the plane (s', t). Fig.4.46 (b) presented the test results taking into account the actual inclination α of the failure planes. Unfortunately, the inclinations of the rupture planes in the UU tests are not accounted. Thus, only CIUC and CIUE test results were presented.

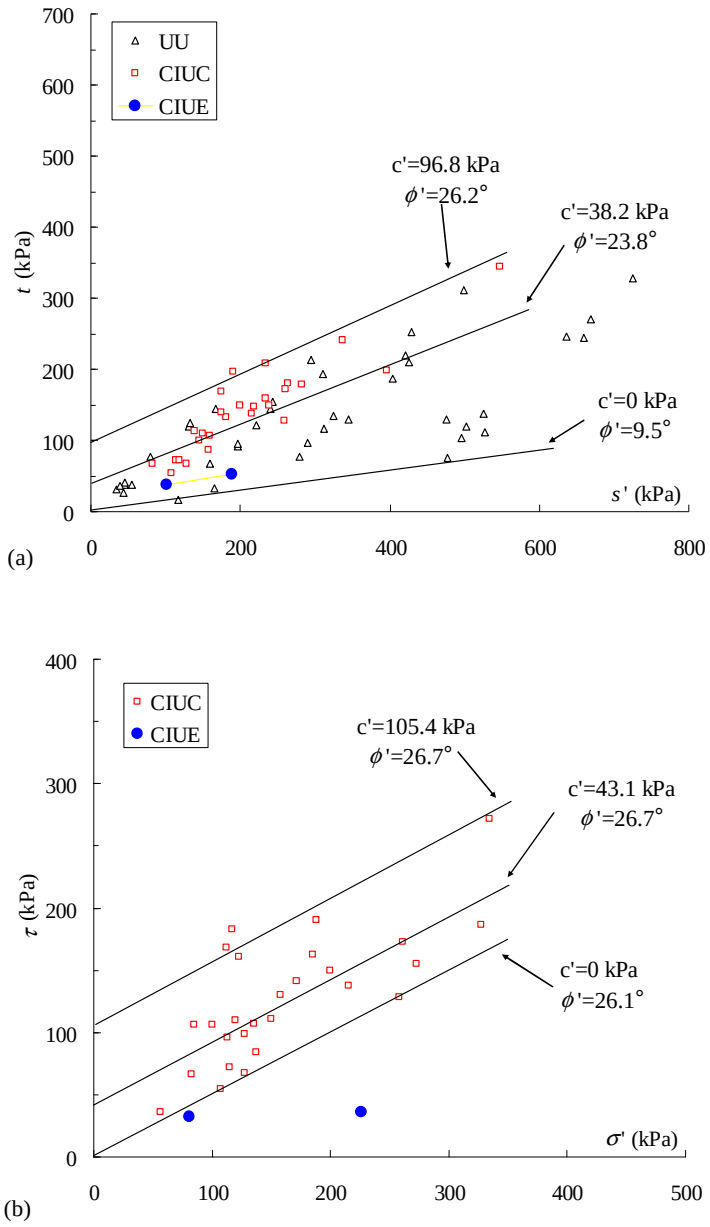

Fig. 4.46 (a) Failure envelopes obtained in the plane (*s*', *t*) and (b) failure envelopes taking into account the actual inclination α of the failure planes.

Based on Fig.4.46 (a), each point in compression test is limited by two straight lines defined by the following parameters: *c*' = 0 kPa, ϕ' = 9.5° and *c*' = 96.8 kPa, ϕ' = 26.2°. The average values of the strength parameters (obtained by the regression line) are *c*' = 38.2 kPa, ϕ' = 23.8° in compression with the determination coefficient R^2 equal 0.536.

Taking into account the resistance mobilized along the rupture planes led to substantially different results which are shown in Fig.4.46 (b). Most points in compression test are limited by two straight lines defined by the following parameters: *c*' = 0 kPa, ϕ' = 26.1° and *c*' = 105.4 kPa, ϕ'

= 26.7°. The average values of the strength parameters (obtained by the regression line) are c' = 43.1 kPa, ϕ' = 26.7° in compression with the determination coefficient R^2 equal 0.532.

4.3.7 Critical state line

The basic parameters and test results on the reconstituted specimens are shown in Table 4.6. In Fig.4.47 (a) and Fig.4.48 (a), the stress-strain curves showed that there was a tendency for the reconstituted specimens prepared at different depths to reach a stable state, although the specimen rCIUE1 did not seem to have reached the critical state. The stress paths of the reconstituted specimens were summarized in Fig.4.47 (c) and Fig.4.48 (c). In compression, the results show a unique critical state gradient M_c of 1.0, regardless of the nature of the clay at different depths. Based on the results of CIUE test results on reconstituted specimens, the critical state gradient in extension M_e equals 0.90.

In Fig.4.49, the stress paths of the compression tests on five reconstituted specimens are shown in e-log (p') plane. The initial void ratios of the reconstituted samples at the depth of 7 ~8 m and 10 ~11 m were 0.953 and 1.347, respectively. The points 1 and 2 represent the initial states of the reconstituted samples at the depths of 10 ~11 m and 7 ~8 m, respectively. The *ISO* line represents the isotropic consolidation line, and the *CSL* line represents the critical state line. As shown in Fig.4.49, the normally consolidated specimens have reached the critical state, but the over-consolidated specimen has not.

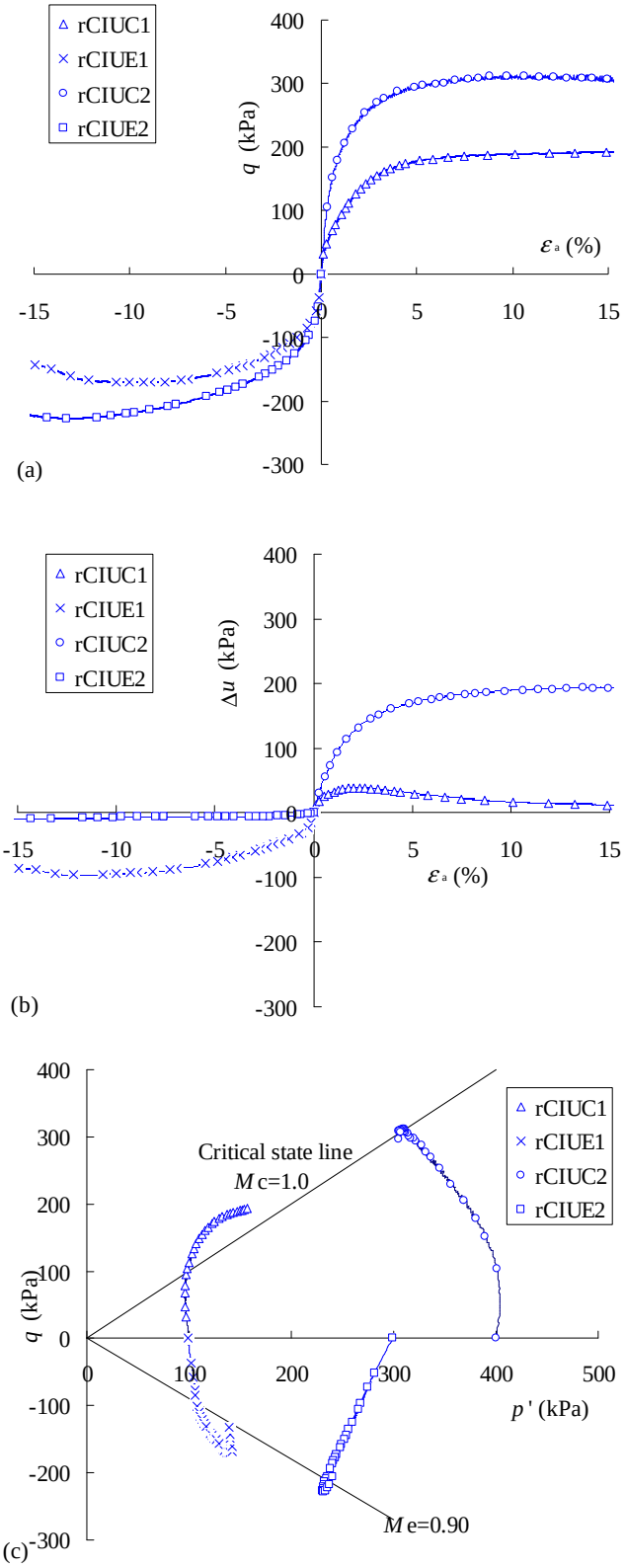

Fig. 4.47 Test results on reconstituted specimens from the borehole SC3 at the depth of 7 ~8 m: (a) deviatoric stress versus axial strain, (b) excess pore pressure versus axial strain and (c) effective stress paths.

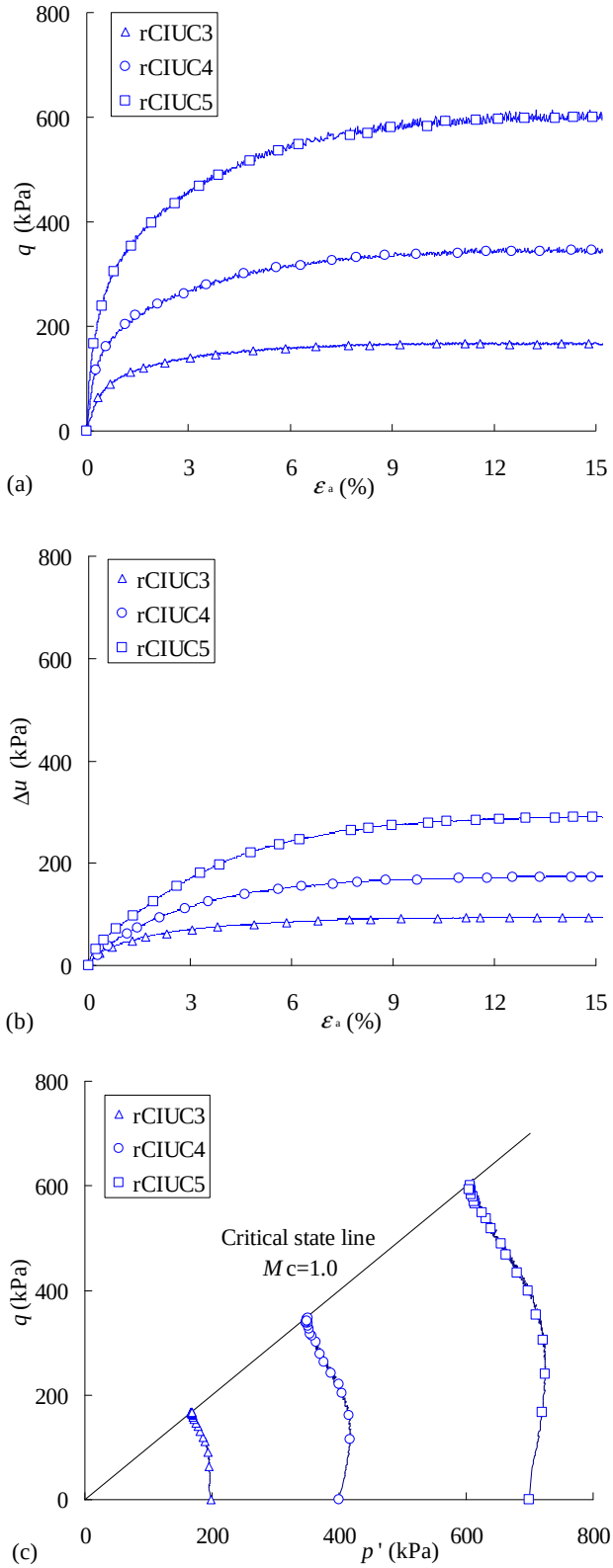

Fig. 4.48 Test results on reconstituted specimens from the borehole SC2 at the depth of 10 ~11 m: (a) deviatoric stress versus axial strain, (b) excess pore pressure versus axial strain and (c) effective stress paths.

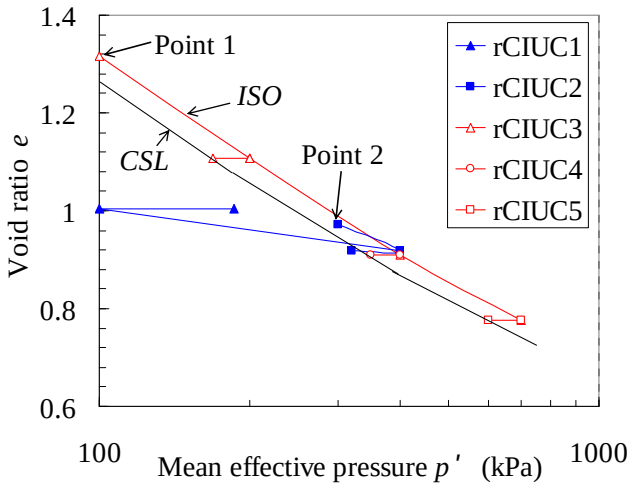

Fig. 4.49 Stress paths of compression tests of the reconstituted specimens in the *e*-log(*p'*) plane.

4.4 Conclusions

In this chapter, a series of UU, CIUC and CIUE tests were carried out on natural and reconstituted specimens of Merville clay. The purpose of this experimental program was to analyze the shear strength, the fissure influence, the strain rate effect and the anisotropic behavior of this natural clay. The critical state lines in compression and in extension were also obtained from the behavior of reconstituted specimens.

The following conclusions can be drawn from the present study:

(1) Due mainly to the influence of the fissures in the natural specimens, the results of UU and CIUC tests show significant scatter in the shear strength, as well as in the strain amplitude at failure.

(2) All the natural specimens of Merville clay can be divided into intact specimens and specimens with fissures. Based on the schemes in Fig.4.2 and Fig.4.35, the stress-strain curve of the intact specimen represents the predominance of the structural strength; whereas, when the specimen contains initial fissures, the frictional strength has the predominance.

(3) For both natural and reconstituted specimens, higher strain rates result in higher undrained shear strengths for different *OCR*s within the tested strain-rate range. For natural specimens with *OCR* values from 7 to 56, the average value of the strain rate influence parameter

$\bar{\rho}_0$ is 0.113. For reconstituted specimens with OCR values from 1 to 14, the average value of $\bar{\rho}_0$ is 0.090. These values indicate that the strain-rate effect on the undrained shear strength appears slightly greater for natural specimens than for reconstituted specimens.

(4) The correlation of the strain-rate parameter ρ_0 with *OCR* in not evident for natural specimens. However, ρ_q may be a better parameter to reflect both the strain-rate effect and the *OCR* influence.

(5) For Merville clay, at the same confining pressure, the value of the shear strength of the horizontal intact specimen is higher than that of the vertical intact specimen. There are two intact failure lines for these two directions, respectively.

(6) In the plane (*s*', *t*), the average values of the strength parameters (obtained by the regression line) are *c*' = 38.2 kPa, ϕ' = 23.8° in compression with R^2 =0.536. In the plane (σ', τ), the average values of the strength parameters (obtained by the regression line) are *c*' = 43.1 kPa, ϕ' = 26.7° in compression with R^2 =0.532.

(7) There is a unique critical state line with M_c =1.0 in the p'-q plane for the reconstituted samples of Merville clay from the different boreholes. The corresponding friction angle is equal to 25.4°, close to the friction angles determined by the regression lines obtained from the results on intact samples. The value of M_e is equal 0.90.

5 Behavior of Merville clay subjected to large number of cycles

5.1 Introduction

In Chapter 4, the main mechanical characteristics of Merville clay have been obtained from a series of monotonic tests.

In many cases, however, the soils of foundation are subjected not only to static stresses due to the weight of the structures, but also to cyclic stresses due to external forces, such as the actions of the wind and/or of the waves in the case of offshore or coastal structures. The effects of cyclic loading on clay behavior have been previously studied mainly with a low number of cycles (hundreds, thousands or ten thousands cycles). However, the behavior of clay subjected to large number of cyclic loading is an important foundation design consideration for the foundations of the structures described above. The wind and/or wave actions on the foundation cause the application of large numbers of cyclic forces and moments which have to be transmitted to and carried by the soil foundation. The need for the study on the test results with a great number of cycles (hundred thousand or even a million cycles) emerged.

In this chapter, we present the results of a series of stress-controlled undrained cyclic loading tests with more than a million cycles were performed on Merville clay.

5.2 Test program

The test program involved both repeated load tests and undrained triaxial tests, the latter being referred to as ‘single loading’ tests which were presented in Chapter 4. A computer-controlled GDS dynamic triaxial testing system (10 Hz / 1 kN) shown in Fig.4.1 (b) was used for performing the cyclic tests. The natural and reconstituted specimens were all 35 mm in diameter and 70 mm in height.

The magnitude of the deviatoric stress was determined from the output of a load cell, located above the triaxial cell. In the repeated load tests, the deviatoric stress was applied in the manner shown in Fig.5.1. It varied sinusoidally and the range of frequency from 0.1 Hz to 1 Hz was used.

5.2.1 Cyclic loading shape

In this thesis, we focus on stress-controlled tests which include symmetrical and non-symmetrical loading tests. As shown in Fig.5.1, when q_m equals 0, the cyclic tests are subjected by symmetrical loading, on the other hand, when q_m does not equal 0, the cyclic tests are subjected by non-symmetrical loading. Defined in Biarez & Hicher (1994), in case of one-way cyclic loading, the mean value q_m should be equal to q_{cy}. However, for q_m higher than q_{cy}, it is also called one-way cyclic loading. The cyclic stress is applied in compression or in extension and hence it varies between maximum and minimum values along the same direction. In case of two-way cyclic loading, on the other hand, the applied cyclic load alternates in either direction around a certain mean value, which means that q_m is less than q_{cy}. When the mean value is 0, it is termed as symmetrical two-way cyclic loading, otherwise unsymmetrical.

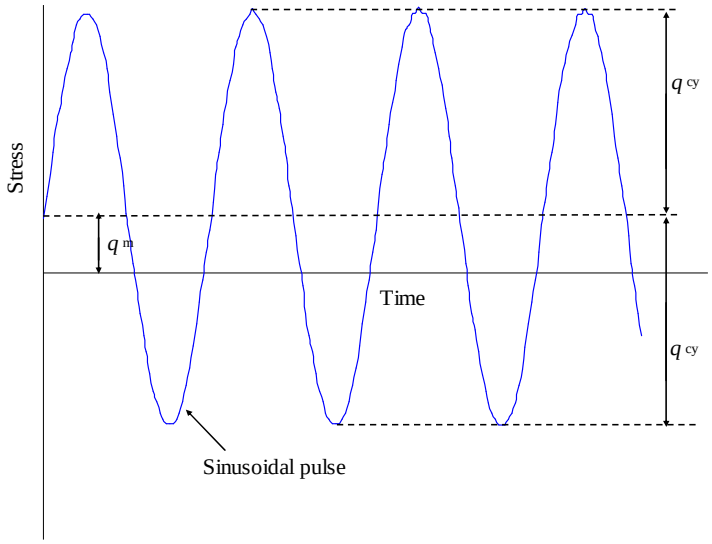

Fig. 5.1 Applied cyclic deviatoric stress.

In the following sections, we will present the results and interpretation of a series of symmetrical two-way cyclic loading tests on Merville clay.

5.2.2 Cyclic stress level

Hicher (1979) indicated that the strain development will reach a stabilized state, when the cyclic stress levels are below a certain magnitude which was called as the critical level of repeated loading (*CLRL*). At a certain effective confining pressure, the cyclic stress level is defined by:

$$R_c = \frac{q_{cy}}{q_{max}} \quad \text{or} \quad R_e = \frac{q_{cy}}{q_{min}} \tag{5.1}$$

where R_c and R_e are the cyclic stress levels, q_{cy} is the applied cyclic deviatoric stress at a certain effective confining pressure, q_{max} is the maximum deviatoric stress of the static compression tests at the same effective confining pressure, and q_{min} is the minimum deviatoric stress of the static extension tests at the same effective confining pressure.

The results of static triaxial tests on natural samples at the depth of 5 ~6m from the borehole SC1 were presented in Fig.4.13, Fig.4.14 and Fig.4.22 (a). The results of static triaxial tests for reconstituted samples at the depth of 7 ~8m from the borehole SC3 were presented in Fig.4.47. These static tests were already discussed in Chapter 4.

In this study, the effective confining pressure of the cyclic test on a natural sample was about 200 kPa. For the reconstituted samples, it was about 100 kPa for an OCR = 4. Thus, the values of q_{max} and q_{min} for the natural samples are 256.2 kPa and -104.0 kPa, respectively. The values of q_{max} and q_{min} for the reconstituted samples are 192.2 kPa and -170.0 kPa, respectively.

For the symmetrical two-way cyclic tests, as mentioned above, the mean value q_m is equal to 0. Thus the values of stress levels R_c were chosen from 0.1 to 1.0 to obtain the *CLRL* for both natural and reconstituted samples.

5.2.3 Shear strain based failure criteria

The semantic problem of defining failure in a cyclic loading test has not been specifically solved, and the proposed definitions have not been universally accepted.

If the specimen was broken during the cyclic loading, the failure of the specimen could be easily defined. However, many specimens do not exhibit a clear localized failure during cyclic loading. Some authors, such as Seed & Lee (1969), chose the condition of zero transient effective stress (liquefaction) as the stress failure criterion for sandy soils.

However, according to time-dependent creep and stress history, the clay behavior under cyclic loading is more complex and renders difficult to determine the stress failure criterion. Therefore, the failure criterion has often been defined in terms of strain amplitude for clays.

In this thesis, the failure criteria defined by Andersen et al. (1980, 1988) and Andersen (2004) were chosen. The failure is defined as either an average shear strain, γ_m, of 15% or a cyclic shear strain, γ_{cy}, of 15% (in triaxial tests the shear strain = 1.5 • the axial strain).

The experiments on repeated loading of Merville clay have used the axisymmetric triaxial test wherein the cell pressure is held constant and the deviatoric stress pulsed. Under these conditions, the measured vertical deformation consists of two components as illustrated in Fig. 5.2, the cyclic axial strain ε_{cy} and the permanent axial strain ε_m.

Besides the sudden collapse for the natural specimen, the sudden change of the strain amplitude within a few cycles is considered as a failure criterion for the clay samples, especially for the reconstituted samples in this thesis.

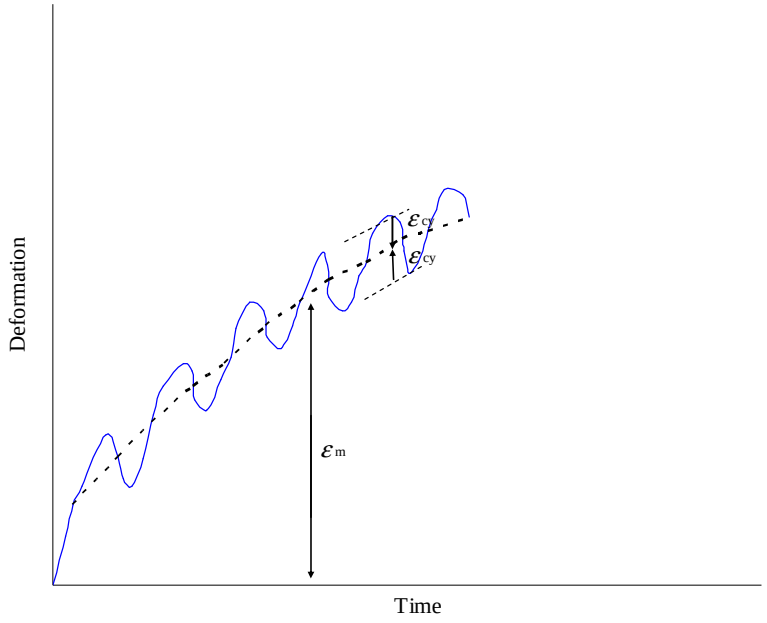

Fig. 5.2 Variation of deformation during a repeated load test (illustrative).

5.3 Cyclic test on natural sample

We prepared one natural specimen at the depth of 5 ~6m from the borehole SC1. We chose a small stress level R_c = 0.08 for this cyclic test. The basic parameters of this test are presented in Table 5.1. The results of the cyclic test are presented in Fig.5.5.

Table 5.1 Basic parameters for the natural specimen.

Water content (%)	33.5
Weight of specimen (g)	128.8
Degree of saturation (%)	100
Effective confining pressure (kPa)	194.0
OCR	14.2
Frequency (Hz)	0.1
Cyclic deviatoric stress q_{cy} (kPa)	20.0
Stress level R_c	0.08
Stress level R_e	0.19
Drainage type	Undrained

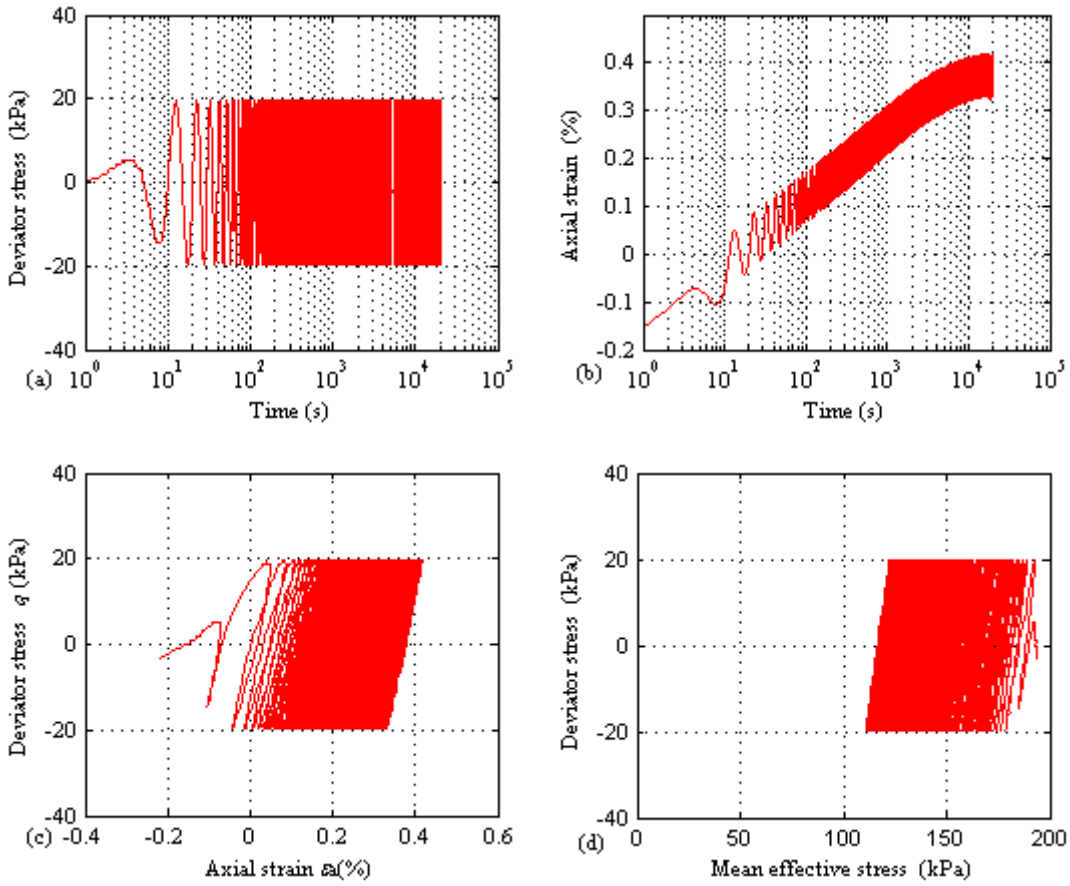

Fig. 5.3 Cyclic test result for the natural specimen of Merville clay: (a) cyclic deviatoric stress, (b) axial strain development during cyclic loading, (c) excess pore pressure development during cyclic loading and (d) effective stress path during cyclic loading.

When the cyclic loading reached about 20000 cycles, the specimen failed and the amplitude of the cyclic loading imposed by the loading program could not be maintained anymore. Then, taking out the specimen from the triaxial cell, we could observe that the specimen was already broken. In Fig.5.3 (b) and Fig.5.3 (c), the sudden changes in axial strain and excess pore pressure at about 18000 cycles were indeed the sign of the specimen failure.

As mentioned in Section 2.2.5 of Chapter 2, the Merville clay is a stiff, fissured clay. Before starting the triaxial testing, some micro-fissures already existed in the specimen. During the cyclic loading, these fissures were activated and developed within the specimen, leading to its failure before reaching 20000 cycles, even if the symmetrical two-way cyclic loading was applied at a low stress level (R_c = 0.08). We can conclude that the fissured clay is very sensitive to two-ways cyclic loading. We can also conclude that the uncertain distribution of fissures with the natural specimens could lead to very different responses under cyclic loading. We, therefore, decided to extend this study by performing cyclic tests on reconstituted samples. In order to remain as close as possible to the in situ condition, the reconstituted specimens were prepared in an overconsolidated state.

5.4 Cyclic test on reconstituted samples

In the laboratory, we prepared the reconstituted specimens from the Merville clay samples taken at the depth of 7 ~8 m from the borehole SC3. The preparation procedure of the reconstituted samples was introduced in Section 3.3.1.2. The preconsolidation pressure of the reconstituted specimens is 300 kPa. Then the specimens were firstly isotropically consolidated to 400 kPa, then isotropically unloaded to 100 kPa, thus the value of *OCR* equaled 4.

5.4.1 Test results

The loading frequency of the cyclic tests was taken equal to 1 Hz for practical reasons: we could therefore apply a large number of cycles (more than one million) in a reasonable time. Li et al. (2011) and Thammathiwat & Chim-oye (2004) indicated that, for a given number of cycles, larger shear strains are generated at lower frequency. However, the effect of the loading frequency will not be addressed in this study. For the loading frequency of 1 Hz, the test duration is about

11.6 days for one million cycles. The parameters for the reconstituted specimens and the cyclic tests are presented in Table 5.2. The test results are presented in Fig 5.4 to Fig.5.8.

Table 5.2 Parameters for reconstituted specimens and cyclic tests.

Test *N*º	1	2	3	4	5
Water content (%)	37.2	37.4	37.0	37.7	38.5
Weight of specimen (g)	125.4	124.3	125.4	127.5	124.4
Frequency (Hz)	1	1	1	1	1
Cyclic deviatoric stress (kPa)	21.4	41.7	84.7	92.8	101.0
Stress level	R_c = 0.11 R_e = 0.13	R_c = 0.22 R_e = 0.24	R_c = 0.44 R_e = 0.50	R_c = 0.48 R_e = 0.55	R_c = 0.52 R_e = 0.59
Consolidation type	Isotropic, effective confining pressure =100 kPa, *OCR* = 4.				
Number of cycles	1026575	1060200	1051480	1050520	6990
Drainage type	Undrained	Undrained	Undrained	Undrained	Undrained

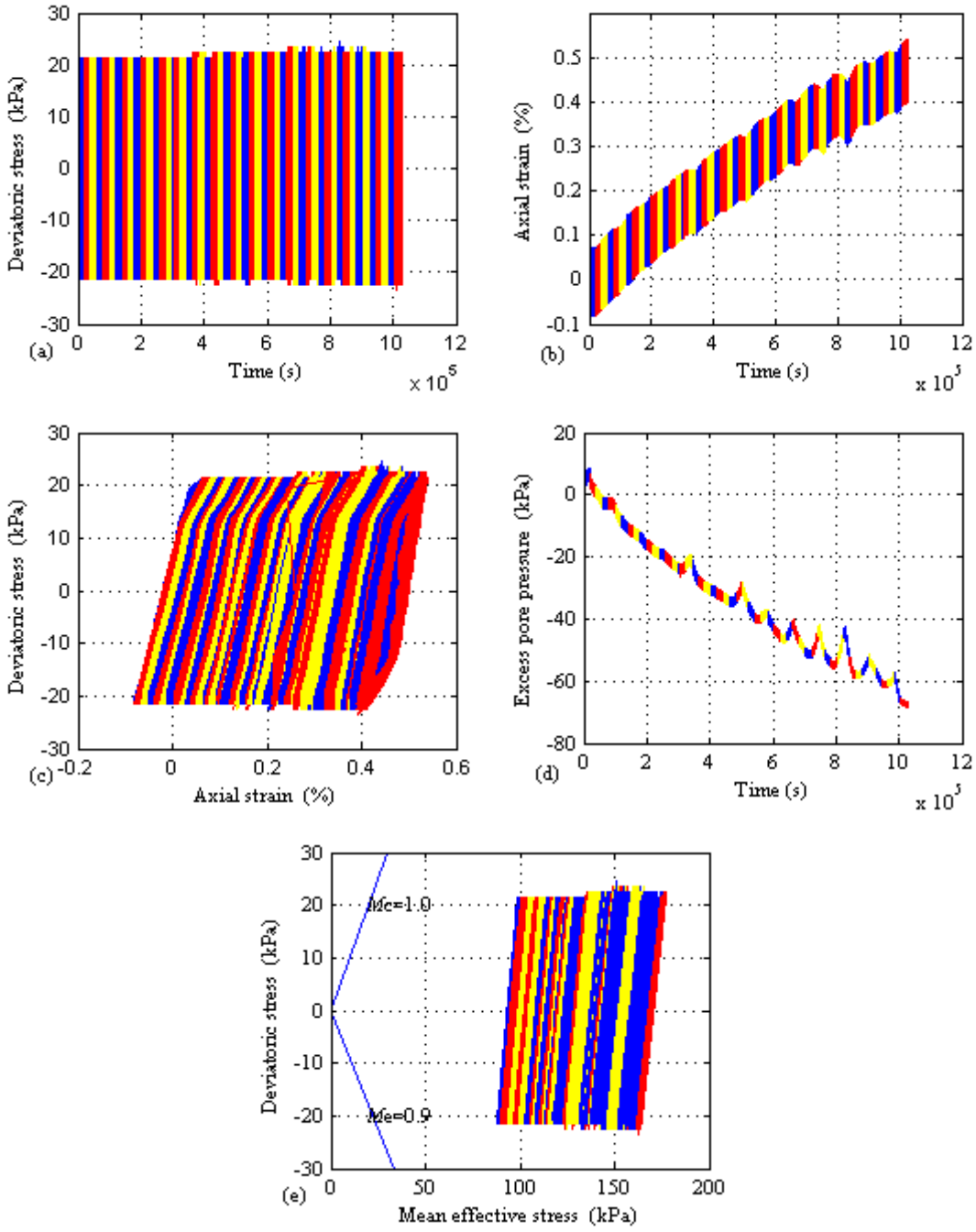

Fig. 5.4 Cyclic test results for the reconstituted specimens of Merville clay: (a) Applied cyclic deviatoric stress with stress level R_c =0.11, (b) axial strain development during cyclic loading, (c) hysteresis loops, (d) excess pore pressure development during cyclic loading and (d) effective stress path during cyclic loading.

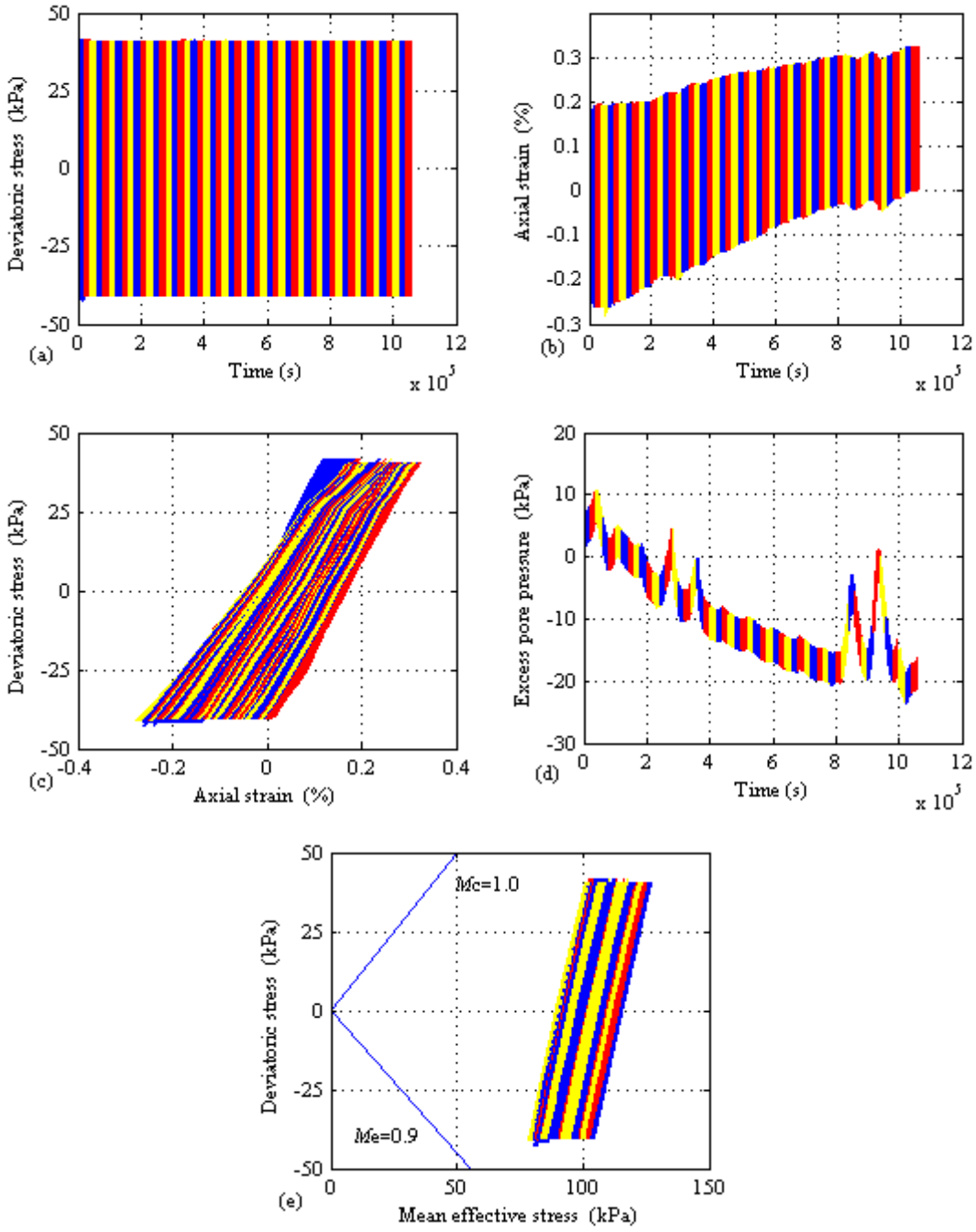

Fig. 5.5 Cyclic test results for the reconstituted specimens of Merville clay: (a) Applied cyclic deviatoric stress with stress level R_c =0.22, (b) axial strain development during cyclic loading, (c) hysteresis loops, (d) excess pore pressure development during cyclic loading and (d) effective stress path during cyclic loading.

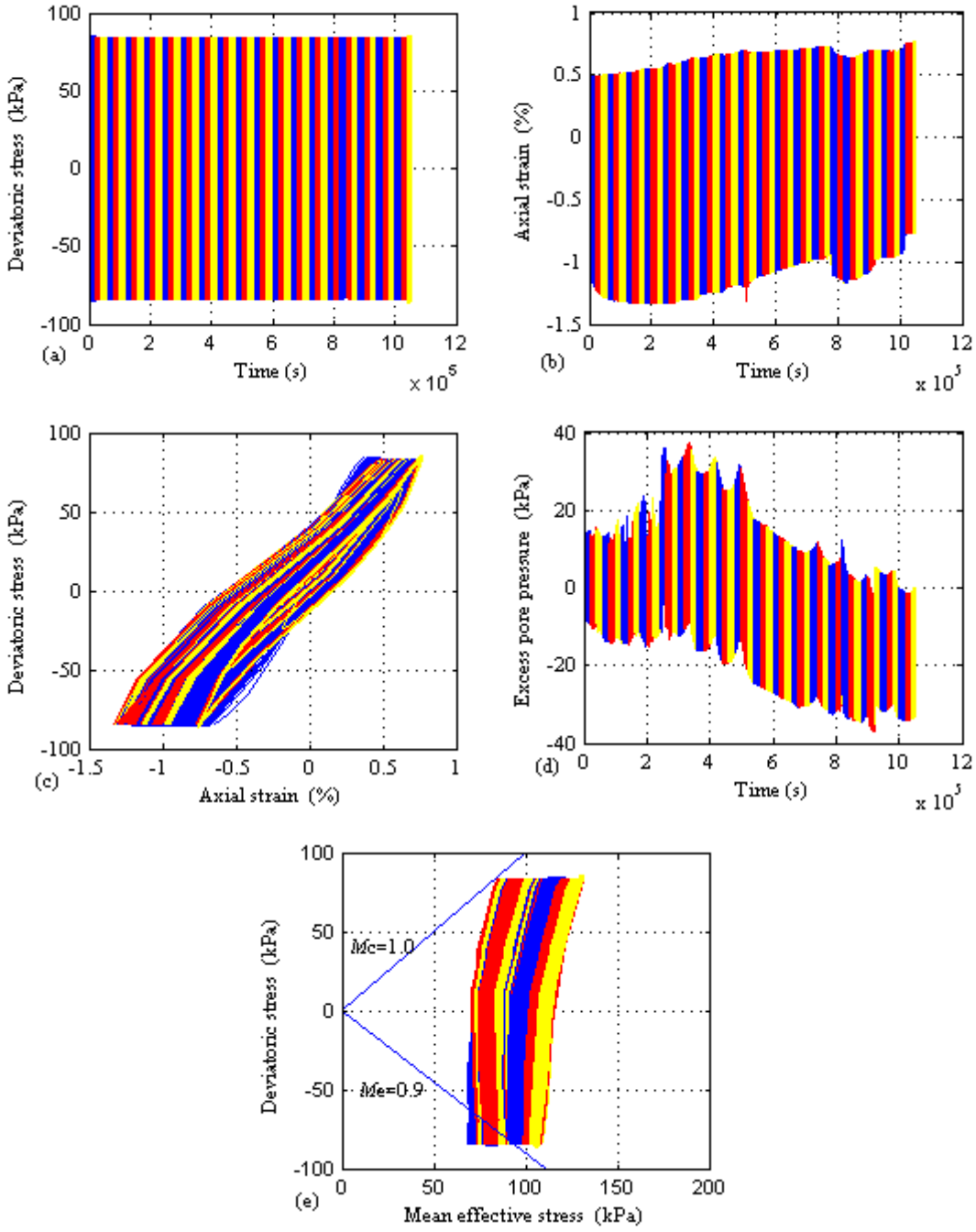

Fig. 5.6 Cyclic test results for the reconstituted specimens of Merville clay: (a) Applied cyclic deviatoric stress with stress level R_c =0.44, (b) axial strain development during cyclic loading, (c) hysteresis loops, (d) excess pore pressure development during cyclic loading and (d) effective stress path during cyclic loading.

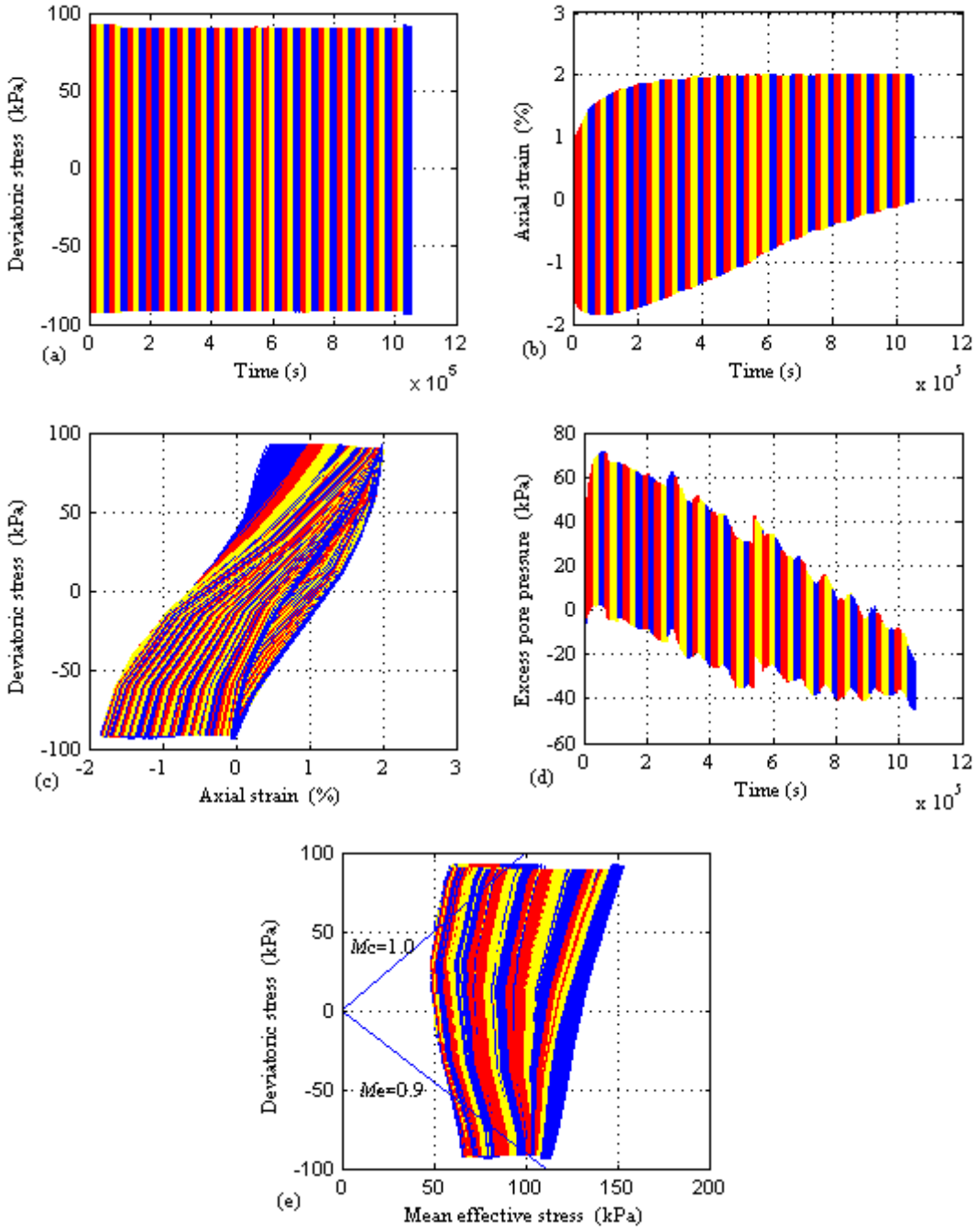

Fig. 5.7 Cyclic test results for the reconstituted specimens of Merville clay: (a) Applied cyclic deviatoric stress with stress level R_c =0.48, (b) axial strain development during cyclic loading, (c) hysteresis loops, (d) excess pore pressure development during cyclic loading and (d) effective stress path during cyclic loading.

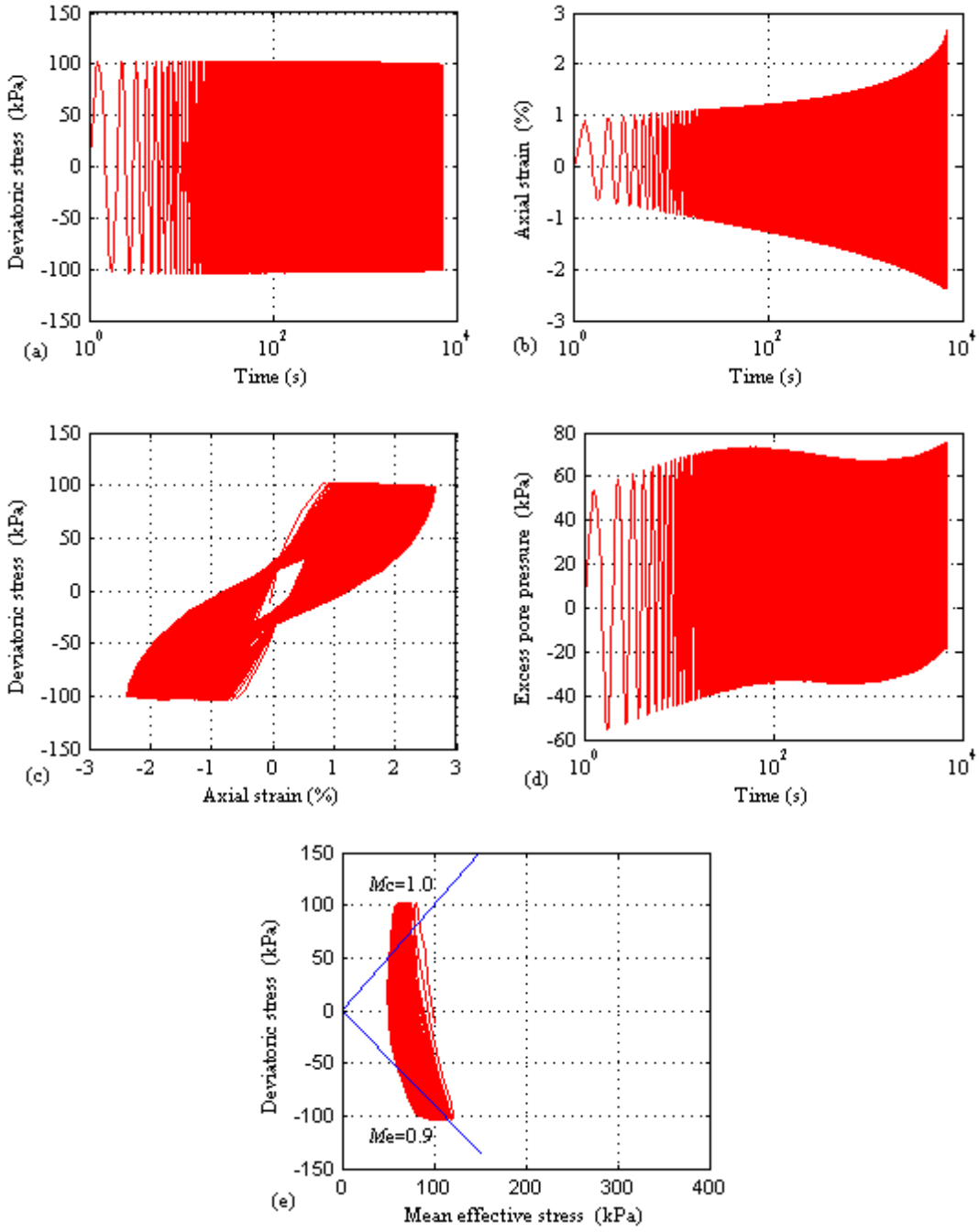

Fig. 5.8 Cyclic test results for the reconstituted specimens of Merville clay: (a) Applied cyclic deviatoric stress with stress level R_c =0.52, (b) axial strain development during cyclic loading, (c) hysteresis loops, (d) excess pore pressure development during cyclic loading and (d) effective stress path during cyclic loading.

5.4.2 Threshold value determination

Based on the results of these five cyclic tests, the excess pore pressures started to increase at the beginning of the cyclic loading, and then decreased until the end of the loading except in the

test with R_c =0.52. The probable reason for this phenomenon will be discussed later on in this chapter.

At low stress levels (R_c =0.11 and 0.22), the cyclic effective stress paths did not exceed the two critical state lines. For the test with R_c =0.44, the stress path only exceeded the critical state line in extension. However, the stress paths exceeded the two critical state lines for R_c =0.48 and 0.52. Thus, we examined carefully these two cyclic tests to check whether the specimens were broken or not before reaching one million cycles. We summarized the evolutions of the shear strains and excess pore pressures of these five tests in Fig.5.9 to Fig.5.10. The test at R_c = 0.52 was stopped after 6990 cycles due to the specimen failure.

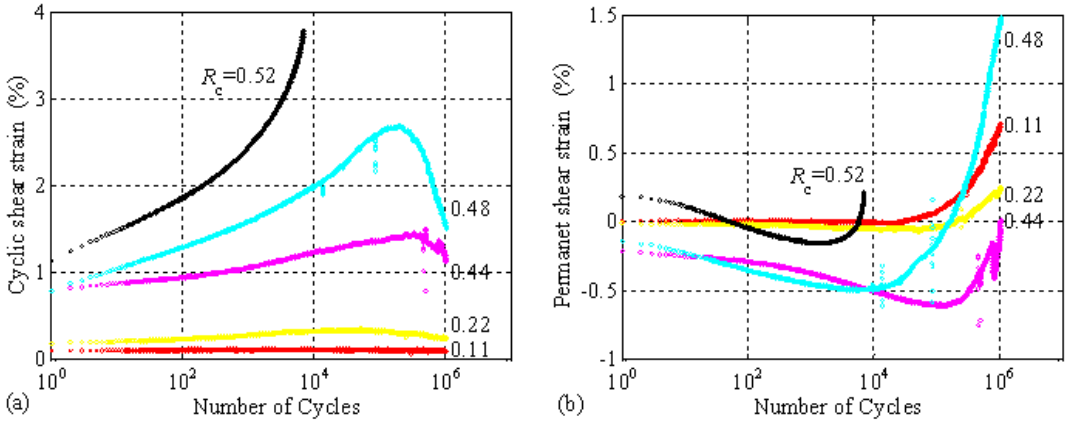

Fig. 5.9 Development of (a) cyclic shear strain and (b) permanent shear strain wtith the number of cycles of five cyclic tests with symmetrical cyclic loading on reconstituted samples of Merville clay.

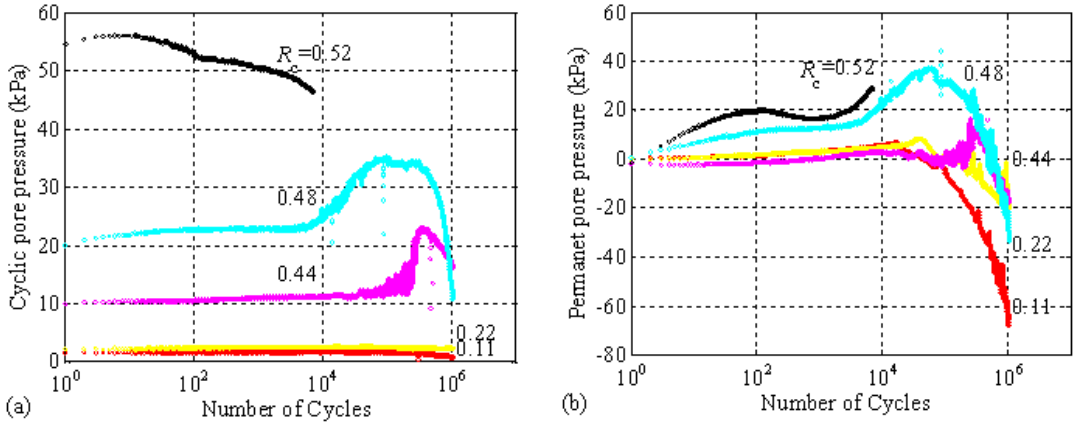

Fig. 5.10 Development of (a) cyclic pore pressure and (b) permanent pore pressure wtith the number of cycles of five cyclic tests with symmetrical cyclic loading on reconstituted samples of Merville clay.

Hicher (1979) stated that there is a state of stabilization in cyclic regime. It means that, for a significant number of cycles, there are no measurable changes of both the strain (cyclic and permanent) and the pore pressure (cyclic and permanent). Based on the results shown in Fig.5.9 and Fig.5.10, regular variations of the strain and pore pressure were observed at three stress levels R_c of 0.11, 0.22 and 0.44. However, a sudden change of the strain and pore pressure within a few cycles at the stress level R_c of 0.48 was observed. Thus, the specimen at R_c =0.48 was considered to have failed during the cyclic loading. We used the data up to 200000 cycles for this cyclic test at R_c =0.48.

Based on these results, we can conclude that there is a threshold value of the stress level R_c between 0.44 and 0.48. If Rc is higher than this value, the specimen would brake during cyclic loading, if R_c is smaller, the specimen will not fail.

5.4.3 Diagram of cyclic and permanent shear stresses

Based on the results shown in Fig.5.9 and Fig.5.10, the shear strains and excess pore pressures of these five cyclic tests were presented in Table 5.3.

Table 5.3 Results of cyclic tests on reconstituted samples at different stress levels.

R_c	Test results	Number of cycles						
		1E+0	1E+1	1E+2	1E+3	1E+4	2E+5	1E+6
0.52	$\gamma_m \pm \gamma_{cy}$ (%)	0.18 ±1.14	0.12 ±1.48	0 ±1.86	-0.15 ±2.44	0.21 ±3.78		
	$\Delta u_m \pm \Delta u_{cy}$ (kPa)	1.4 ±54.8	15.1 ±56	21.6 ±53	19.4 ±50.5	31.6 ±46.2		
0.48	$\gamma_m \pm \gamma_{cy}$ (%)	-0.14 ±0.79	-0.23 ±1.04	-0.35 ±1.29	-0.45 ±1.58	-0.49 ±1.99	0.1 ±2.68	
	$\Delta u_m \pm \Delta u_{cy}$ (kPa)	0.9 ±20	6.4 ±21.8	11.1 ±22.5	12.5 ±22.8	22 ±25	26 ±34	
0.44	$\gamma_m \pm \gamma_{cy}$ (%)	-0.21 ±0.78	-0.25 ±0.87	-0.28 ±0.94	-0.37 ±1.06	-0.51 ±1.22	-0.59 ±1.41	0.09 ±1.15
	$\Delta u_m \pm \Delta u_{cy}$ (kPa)	0.3 ±10	0.2 ±10.3	0.8 ±10.5	2.7 ±11	4.7 ±11.2	2.3 ±15	-15.7 ±16
0.22	$\gamma_m \pm \gamma_{cy}$ (%)	-0.01 ±0.18	-0.02 ±0.21	-0.02 ±0.24	-0.03 ±0.28	-0.05 ±0.32	-0.01 ±0.3	0.25 ±0.24
	$\Delta u_m \pm \Delta u_{cy}$ (kPa)	0.1 ±2.1	0.7 ±2.3	1.9 ±2.4	3 ±2.4	4.8 ±2.5	-2 ±2.5	-22 ±2.3
0.11	$\gamma_m \pm \gamma_{cy}$ (%)	0 ±0.10	0 ±0.11	0 ±0.11	0 ±0.11	0 ±0.12	0.17 ±0.1	0.72 ±0.14
	$\Delta u_m \pm \Delta u_{cy}$ (kPa)	0.8 ±1.7	0.9 ±1.6	1.8 ±1.7	3.3 ±1.7	5.6 ±1.7	-15.5 ±1.6	-67.5 ±0.75

The number of cycles to failure and the failure mode depends on the combination of permanent and cyclic stresses (Andersen, 1988). In this thesis, except for two cyclic tests (R_c =0.48 and 0.52), the three other specimens were not considered to be broken. Thus, according to the results of Drammen clay shown by Andersen (2004) in Fig.1.27 (a), the numbers of cycles at the end of the tests and at failure of the specimens of Merville clay were presented in a diagram including the permanent and cyclic stress levels shown in Fig.5.11 (a).

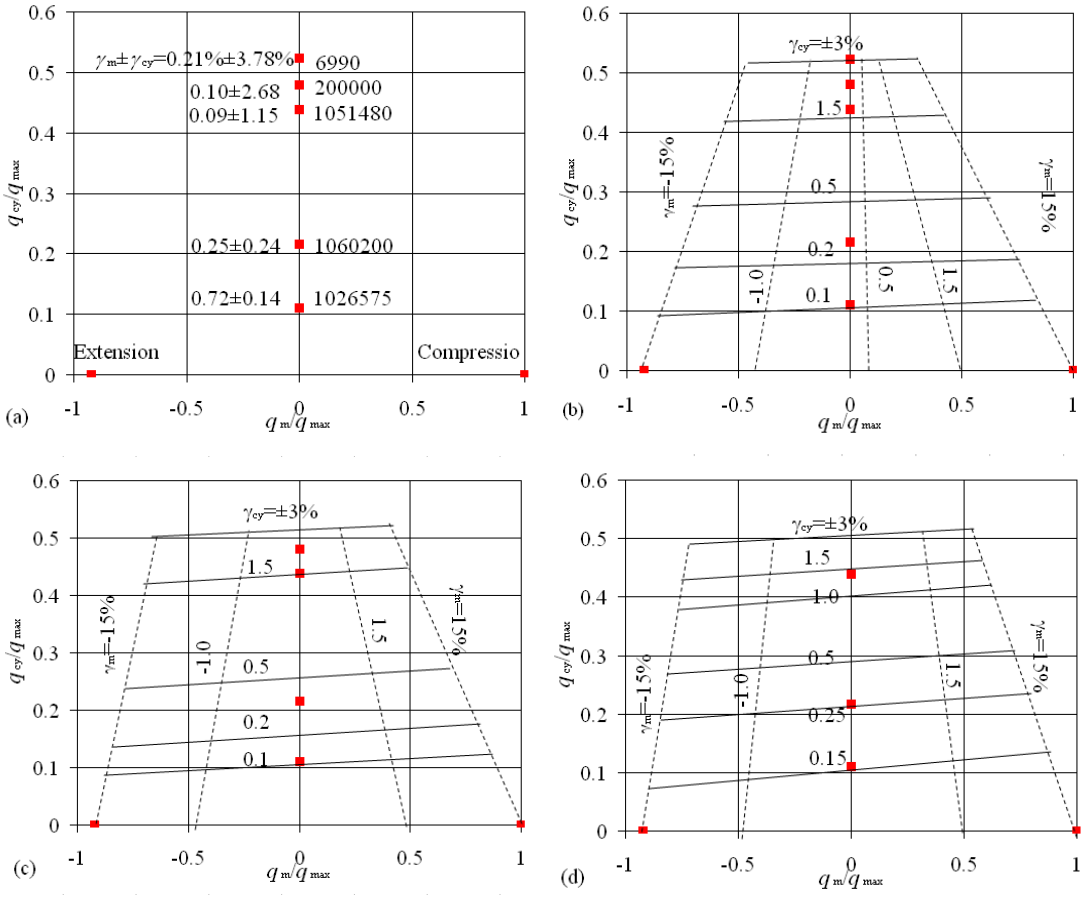

Fig. 5.11 (a) Number of cycles and shear strains to failure or termination on reconstituted samples of Merville clay with *OCR* =4, Permanent and cyclic shear strains at a give number of cycles: (b) 10000 cycles, (c) 200000 cycles and (d) 1000000 cycles.

From this diagram, the two points in the x axis represent the results of the monotonic triaxial tests (compression and extension). We can find that the cyclic axial strain increases as the stress level R_c increases, and the number of cycles at failure decreases as the stress level increases.

In his paper, Andersen (2004) presented the diagram of the relationship between permanent and cyclic stresses at a given number of cycles (such as 100 cycles) for Drammen clay (Fig.1.27 (b)). Based on this diagram, if the combination of the cyclic and permanent deviatoric stresses is given, we can predict the cyclic and permanent shear strains at this given number of cycles for this clay. According to this diagram, we presented our test results in Fig.5.11 (b) to Fig.5.11 (d) at three given number of cycles (10000, 200000 and 1000000 cycles). The specimen of the cyclic test at R_c =0.52 was broken at 6990 cycles, therefore the result of this test is presented only in Fig.5.11 (b). Similarly, the specimen of the cyclic test at R_c =0.48 being broken at about 200000 cycles, the results of four tests at 200000 cycles were presented in Fig.5.11 (c), and only the three

remaining tests at 1000000 cycles in Fig.5.11 (d). In these diagrams, because of the lack of results of non-symmertical cyclic loading tests, we just predicted some strain lines based on the results of monotonic tests and symmetrical cyclic loading tests of Merville clay.

According to Fig.1.27 (c), the cyclic shear strains as function of number of cycles with q_m =0 on Merville clay is presented in Fig.5.12.

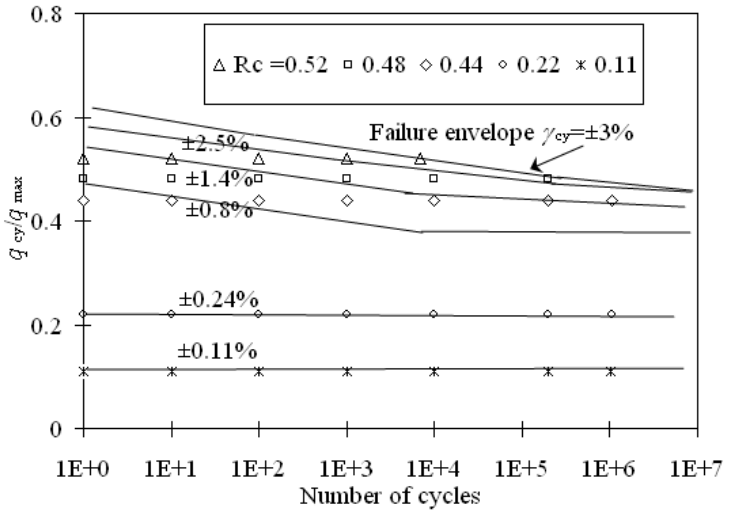

Fig. 5.12 Cyclic shear strain as function of number of cycles with q_m =0 in triaxial tests on Merville clay with OCR=4.

Based on Fig.5.12, when the cyclic shear strain reached 3%, the reconstituted sample of Merville clay could be considered as failed. At lower stress levels (R_c =0.11 and 0.22), the cyclic shear strain was almost constant during the cyclic loading.

The results on Black clay and Bentonite clay with *OCR*=4 shown by Hicher (1979) and the results of Drammen clay with *OCR*=4 shown by Andersen et al. (1980) were summarized for comparing with the results on Merville clay in Fig.5.13.

As shown in Fig.5.13, the variation of cyclic axial strain of Drammen clay is largest at the same stress level (for example: R_c =0.48 or 0.52), and smallest for Merville clay. The sensitivity of clays to cyclic loading is strongly dependant on the mineralogy as shown by Hicher (1979). Kaolinite type clays with rather small plasticity indexes are more sensitive to cyclic loading, as in the cases of Black clay and Drammen clay. Reconstituted Merville clay, with high plasticity index, has a stronger resistance to the structure evolution during cyclic loading.

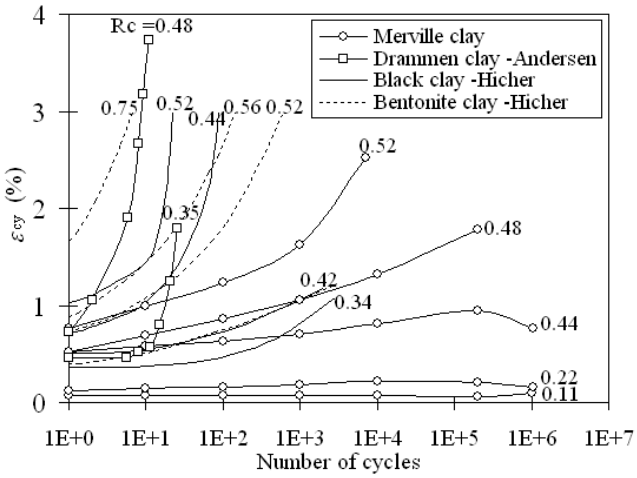

Fig. 5.13 The development of cyclic axial strain during symmetrical cyclic loading on four different clays with the same *OCR*.

5.4.4 Analysis on the development of pore pressure during cyclic loading

In this study, the development of pore pressure increased at the beginning of cyclic loading, then as the test time increased, the pore pressure started to decrease continuously to the end of the cyclic test. The decreasing amplitude of the pore pressure was larger than the increasing amplitude. This phenomenon could be observed in Fig.5.4 (d), Fig.5.5 (d), Fig.5.6 (d) and Fig.5.7 (d). It is hard to explain what happened to the samples during the cyclic tests. Firstly, we considered that the overconsolidated samples were not perfectly saturated with 7 days for consolidation. Then, another cyclic test had been done with 20 days for consolidation. The test had the same parameters as the Test 1 (R_c =0.11), except the consolidation time. The development of axial strain and pore pressure of these two tests were presented in Fig.5.14 (a) and Fig.5.14 (b).

At the same cyclic deviatoric stress of the symmetrical cyclic loading tests, the results in Fig.5.14 (a) shown that the cyclic and permanent axial strain of the test of comparison were both less than the results of Test 1 (R_c =0.11). The excess pore pressure of the test of comparison also decreased to the end of the test shown in Fig.5.14 (b). Thus, the short time of consolidation cannot be considered as the reason for producing the diminution of the excess pore pressure during cyclic loading.

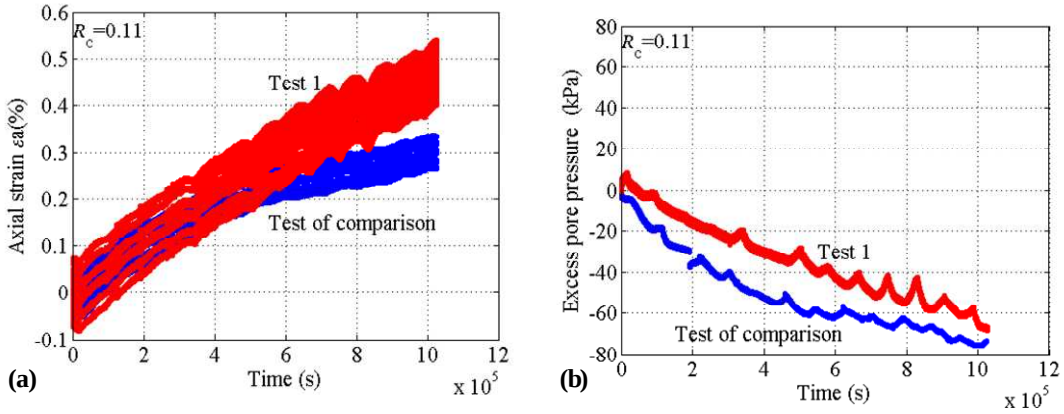

Fig. 5.14 (a) Development of axial strains and (b) development of excess pore pressures of Test 1 and the test of comparison with the stress level R_c equaling 0.11.

The time for performing the cyclic test with more than one million cycles is about 11.6 days for the cyclic loading phase only. During this time, creep could also happen during the cyclic loading. During the first few days, the effect of the cyclic loading is more pronounced than the effect of the creep.

A triaxial test was performed to study the creep effect. The reconstituted specimen had the same initial conditions than the reconstituted ones used for doing the study on the strain rate effect shown in Table 4.3. This specimen was firstly isotropically consolidated to 700 kPa, then isotropically unloaded to 50 kPa. Thus, the value of *OCR* was 14. A deviatoric stress of about 50 kPa was applied on the specimen in undrained condition. The time for applying the deviatoric stress was about 1 min. The developments of axial strain and excess pore pressure are shown in Fig.5.15 (a) and Fig.5.15 (b).

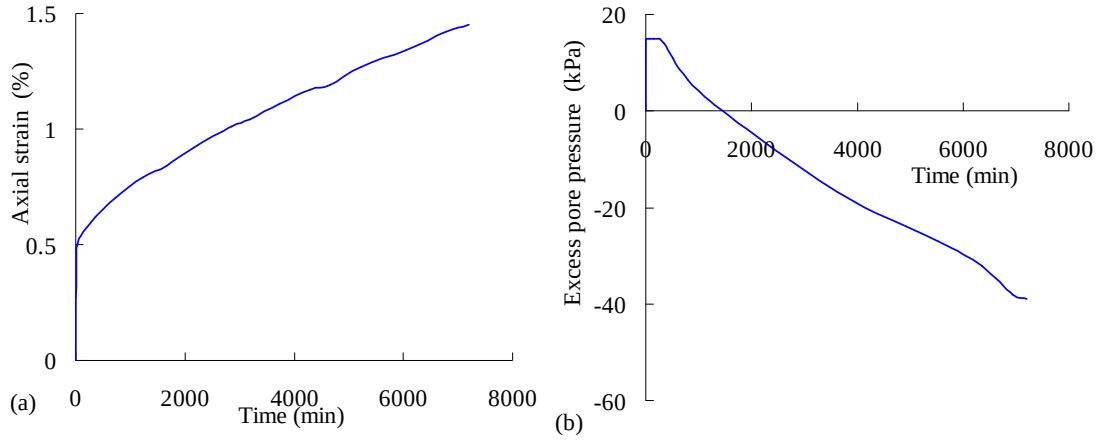

Fig. 5.15 (a) Development of axial strain and (b) development of excess pore pressures during the creep test.

We can see that the creep is not finished. Both the values of the axial strain and the excess pore pressure are still changing. We can notice, however, that there is a continuous decrease of the pore pressure. This phenomenon can help understanding that the diminution of the pore pressure can be affected by the creep during the undrained cyclic triaxial test.

5.4.5 Evolution of resilient modulus during cyclic loading

In his paper, Brown et al. (1975) proposed the definition of the resilient modulus as shown in Fig.5.16.

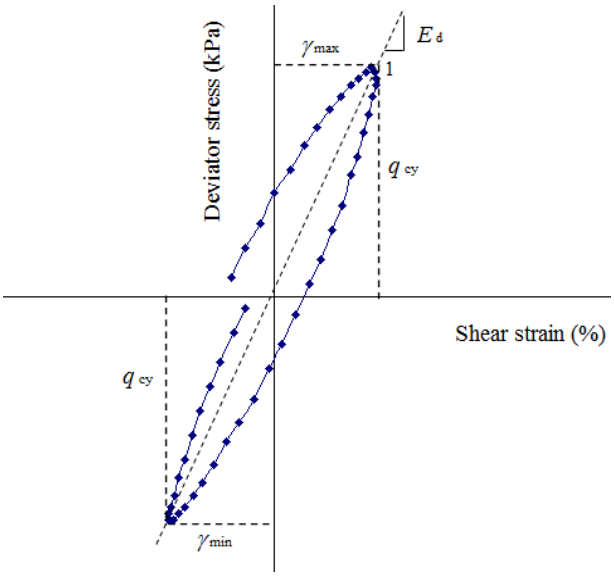

From Brown et al., (1975)

Fig. 5.16 Resilient modulus of one cycle in the cyclic test (illustrative).

Based on Fig.5.16, the resilient modulus E_d is defined as:

$$E_d = 2q_{cy} / (\gamma_{max} - \gamma_{min}) \tag{5.2}$$

Thus, the variations of the resilient modulus for the five cyclic tests on reconstituted samples of Merville clay are presented in Fig.5.17.

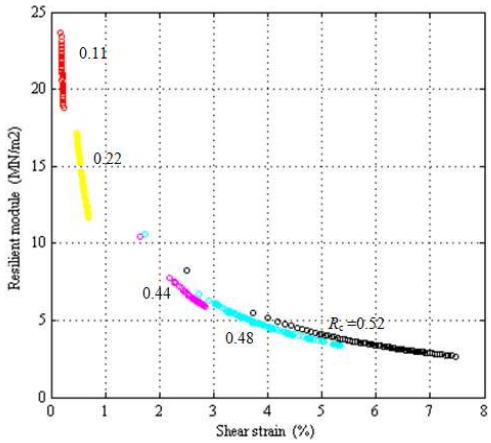

Fig. 5.17 Variations of resilient modulus during cyclic loading with different stress levels.

As the shear strain increases, the resilient modulus decreases for each stress level. In their results, Brown et al. (1975) showed that as the number of cycles increases, the resilient modulus decreases. In this study, the cyclic tests were stress-controlled tests. As shown in Fig.5.18 (a) and Fig.5.18 (b), the resilient modulus decreased as the number of cycles increased at stress levels of 0.52 and 0.48.

However, for the specimens not broken at the lower stress levels (R_c = 0.11, 0.22 and 0.44), as the number of cycles increased, the resilient modulus started to decrease at the beginning of the loading, then increased to the end of the cyclic test as shown in Fig.5.18 (c) to Fig.5.18 (e).

In Fig.5.18 (c), the values of the resilient modulus for the test at Rc = 0.44 are 10.81, 9.02, 6.91, 6.01, 6.02 and 7.54 MPa for cycles 1, 100, 10000, 200000, 400000 and 1051480, respectively. The process 1 represents the decrease of the resilient modulus as the number of cycles increases from 1 cycle to 200000 cycles. The process 2 represents the increase of the resilient modulus as the number of cycles increases from 200000 cycles to the end of the test.

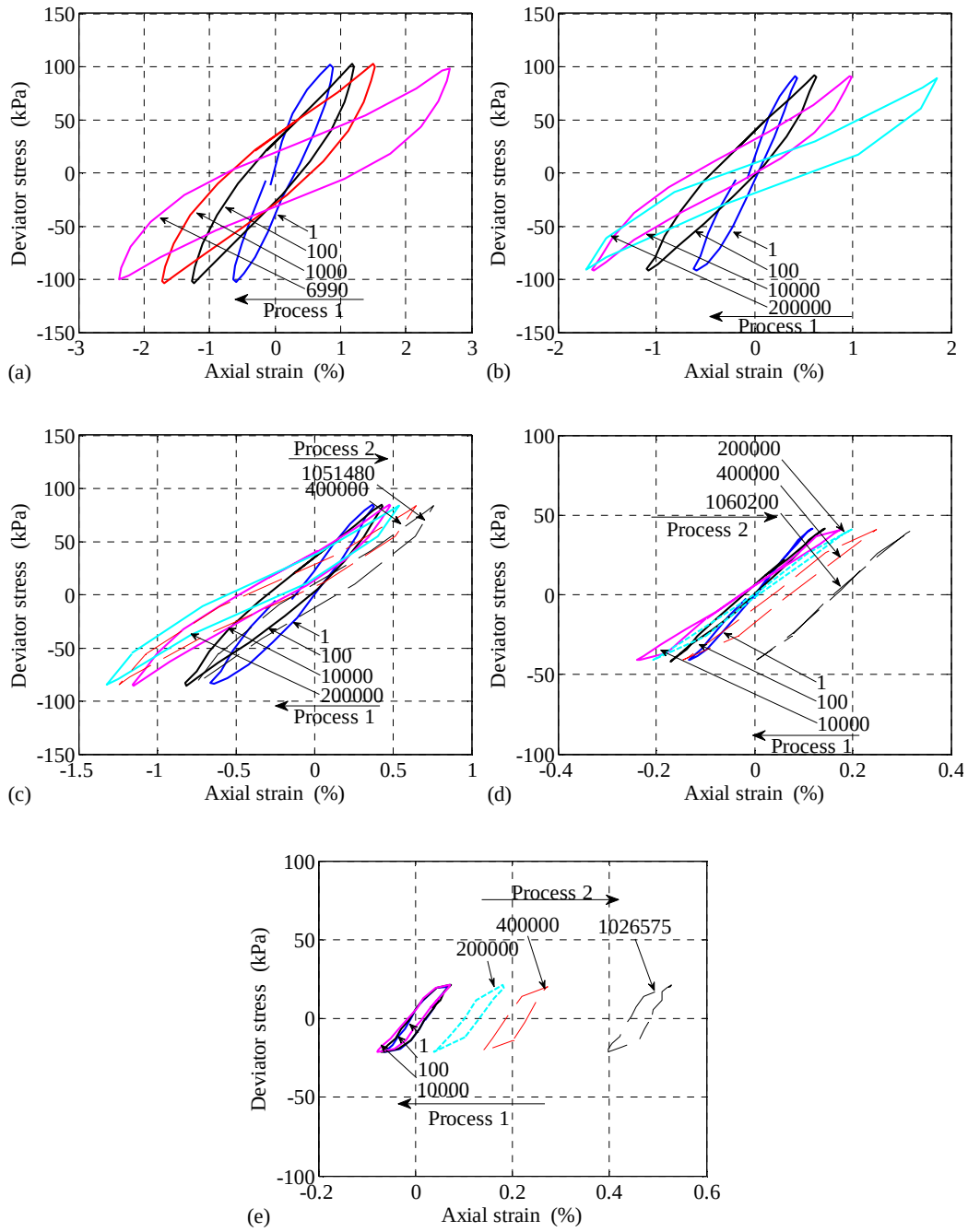

Fig. 5.18 Variations of resilient modulus according to the variable forms of cycles during cyclic loading with the stress level R_c equaling (a) 0.52, (b) 0.48, (c) 0.44, (d) 0.22 and (e) 0.11.

In Fig.5.18 (d), the values of the resilient modulus for the test at Rc = 0.22 are 21.78, 17.73, 13.12, 13.41, 13.80 and 17.03 MPa for cycles 1, 100, 10000, 200000, 400000 and 1060200, respectively. The process 1 represents the decrease of the resilient modulus as the number of cycles increases from 1 cycle to 10000 cycles. The process 2 represents the increase of the resilient modulus as the number of cycles increases from 10000 cycles to the end of the test.

In Fig.5.18 (e), the values of the resilient modulus for the test at Rc = 0.11 are 20.96, 19.91, 18.96, 19.90, 21.20 and 23.85 MPa for cycles 1, 100, 10000, 200000, 400000 and 1026575 respectively. The process 1 represents the decrease of the resilient modulus as the number of cycles increases from 1 cycle to 10000 cycles. The process 2 represents the increase of the resilient modulus as the number of cycles increases from 10000 cycles to the end of the test.

Thus, the test results showed that the cyclic strain increased and the resilient modulus decreased as the number of cycles increased for the stress-controlled tests. These phenomena can be observed in the results of the two tests with stress levels R_c of 0.48 and 0.52. The effect of the creep will be more effective on the clay behavior as the test time increases. However, at the beginning of the cyclic tests with the stress levels R_c of 0.11, 0.22 and 0.44, the resilient module decreased as the number of cycles increasing, and then they increased.

5.4.6 Post-cyclic recompression behavior

As mentioned above, five reconstituted specimens were used to perform the cyclic tests. Two of them with the stress levels of 0.48 and 0.52 failed, the other three specimens with stress levels of 0.11, 0.22 and 0.44 were not broken at the end of the cyclic tests. Then, monotonic compression triaxial tests were performed on these three specimens after the cyclic loading. The aim is to obtain the post-cyclic behavior. The results of undrained monotonic triaxial tests on reconstituted specimens of Merville clay with and without previous cyclic loading are presented in Fig.5.19.

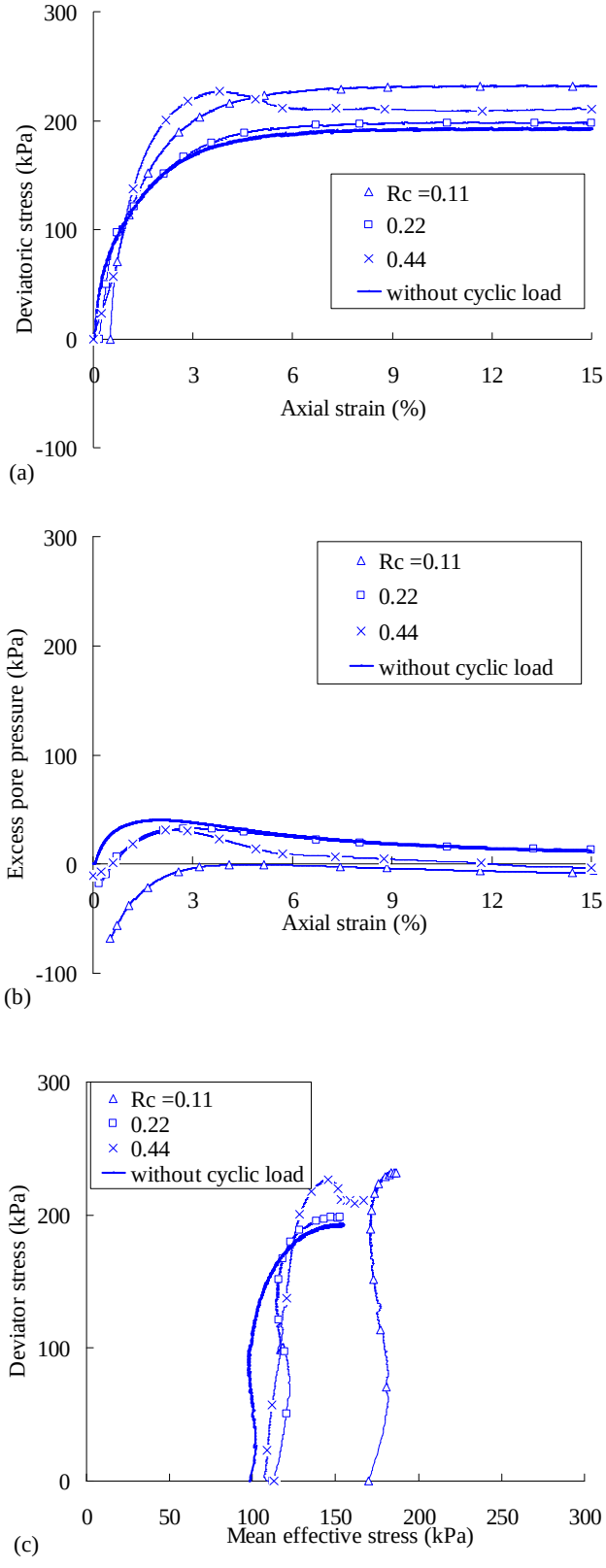

Fig. 5.19 Results of static triaxial tests on reconstituted samples with and without cyclic loading: (a) relationship between deviatoric stress and axial strain, (b) relationship between excess pore pressure and axial strain and (c) effective stress paths.

It appears from these figures that the undrained static strength has increased as a result of the cyclic loading. As mentioned above, the resilient modulus decreased at the beginning of the cyclic test, and then increased to the end of the cyclic test. That means that the specimen softened at the beginning, then hardened. Thus, that may be the reason why the static shear strength of the sample with previous cyclic loading is higher than the shear strength of the sample without previous cyclic loading.

5.5 Conclusions

In this chapter, a series of cyclic tests were carried out on the natural and reconstituted specimens. Based on the results of these tests, the following conclusions can be drawn:

(1) The Merville clay is a stiff, fissured clay. Due to the effect of the micro-fissures, we considered that the natural specimens were not suitable for performing the cyclic tests with a large number of cycles.

(2) There is a threshold value of the stress level R_c between 0.44 and 0.48. If the stress level is higher than that value, the specimen would fail during cyclic loading, otherwise, the specimen will not develop large cyclic strains.

(3) Based on the results of monotonic tests and symmetrical cyclic loading tests of Merville clay, we predicted the diagrams giving the strain contours as function of the permanent and cyclic stresses for a given number of cycles (10000, 200000 and 1000000 cycles. From these diagrams, if the combination of the permanent and the cyclic stresses is given, the permanent and the cyclic strains could be predicted for a given number of cycles.

(4) The resilient modulus decreased as the number of cycles increased at the stress levels of 0.52 and 0.48. For smaller stress levels, the resilient modulus started to decrease at the beginning of the tests, and then increased until the end of the tests. That means that the specimen softened at the beginning, then hardened.

(5) Summarizing the results on the samples with same OCR of Black clay, Bentonite clay, Drammen clay and Merville clay, we can observe that the variation of the cyclic axial strain of Drammen clay is the largest at the same stress level, and the smallest for Merville clay. The clay

microstructure, depending on the mineralogy of the constituents, plays a role in the clay sensitivity to cyclic loading.

(6) For tests at very long time, the effect of creep is a reason for explaining the diminution of the pore pressure during cyclic loading for overconsolidated reconstituted samples of Merville clay.

(7) The monotonic shear strength of the samples subjected to previous cyclic loading is higher than the shear strength of the sample without previous cyclic loading. This result shows that the sample hardened during cyclic loading.

6 Conclusions and Perspectives

6.1 Conclusions

This research aimed at finding a framework for the behavior of the Merville clay, a highly overconsolidated, stiff and structured soil, located beneath the depth of 3 m. Natural and reconstituted samples of this clay from different depths were tested.

The physical properties of Merville clay, which act as an indicator for the behavior of a soil, were identified in the laboratory of Ecole Centrale de Nantes. The water content range is 29.0% ~ 35.6%, the liquid limit range is 89.4% ~100.6%, the clay size content is about 26% and the specific gravity range is 2.51 ~2.77. Based on the soil profile and physical properties, it is possible to distinguish two layers in the Merville clay deposit: the upper layer from 3 m to 7m where microfissuration is clearly observable and the layer below from 7 m to 11 m which is less affected by the microfissuration. This is due to the higher decompression of the top layer.

The mechanical response of the natural samples is affected by the structure of the clay, because of the microcracking pattern but also because of the microstructural fabric. The microstructure of samples from the same depth before and after shearing was thus investigated by SEM. The imaging of the sample before shearing showed a typical detrital clay fabric with a rough shape of particles aggregated in domains, whereas the presence of non-oriented fabric and no rough shape for broken clay particles in the failure plane was observed in the sample after shearing. The chemical composition of the natural clay samples was examined by X-ray diffraction. The presence of illite, quartz and kaolinite was found, as well as the existence of the montmorillonite mineral as a secondary element.

Initially, natural samples were prepared for carrying out standard one-dimensional compression tests. The maximum vertical pressure (about 1 MPa) was not enough to estimate the preconsolidation effective stress. Thus, 1D compression tests at a higher pressure level were performed and the apparent preconsolidation pressure was obtained. This apparent preconsolidation pressure included two parts: the bonding effect and the real preconsolidation pressure.

Then, reconstituted samples were prepared by using the method presented by Burland (1990). 1D compression tests at both low and high pressures were performed again on reconstituted samples. Based on the test results of reconstituted samples, the intrinsic parameters were obtained. An empirical equation representing the intrinsic compression line of the Merville clay was proposed. The compression curves of the natural samples converged slowly towards the ICL. The test results of natural and reconstituted samples fitted well with the Biarez & Hicher's model. For tests at a high pressure level, the swelling curves of the natural samples became parallel to the SCL at high stresses, thus the values of swelling sensitivity became approximately equal to 1.0, confirming that the destructuration process was complete.

The existence of fissures affected the shear strength of natural samples obtained from UU tests at low confining pressures. Consolidated triaxial tests on natural samples exhibited different types of stress-strain curves, depending on the micro-fissures pattern within the samples. Thus, a peak in the deviatoric stress could not be observed for some natural specimens during CIUC and CIUE tests, whereas the axial strain at failure was in most cases smaller than 4% for the specimens when a peak deviatoric stress was observed. In some cases, the deviatoric stress stabilized at the residual strength after failure. However, in most cases, both the deviatoric stress and the excess pore pressure did not reach the residual state. The structural strength appears to be strongly affected by the existing microfissures. The fissured samples have a lower strength than the non-fissured samples and this aspect is more pronounced at small confining pressures. Taking into account the inclination of the failure plane, the values of the strength parameters have been obtained for CIUC and CIUE tests by plotting the test results in the plane (σ', τ). The average values of these parameters are c' = 43.1 kPa, ϕ' = 26.7° in triaxial compression.

This test discrepancy prevented us to define the Mohr-Coulomb's strength parameters for the natural samples. Based on the test results from reconstituted samples, two critical state lines in compression and extension were obtained, Mc =1.0 and Me =0.9, respectively.

Triaxial tests were also performed for analyzing the strain rate dependency of Merville clay at high *OCR*s. The values of *OCR*s for the tested natural samples were 7, 14, 28 and 56. The values of *OCR*s for the tested reconstituted samples were 1, 7 and 14. For both reconstituted and natural samples, higher strain rates resulted in higher undrained shear strengths at different *OCR*s.

The values of the strain rate parameters ρ_0 and ρ_q indicate that the strain-rate effect on the undrained shear strength is greater in natural samples than in reconstituted ones. The relationship between *OCR* and ρ_0 is not clear for the natural samples. Thus, ρ_q might be a better parameter to reflect both the strain rate effect and the *OCR* influence.

The effect of the anisotropy for the shear strength was analyzed by cutting samples in two different directions (horizontal and vertical). The shear strength of the sample prepared in a horizontal direction is greater than that of the sample prepared in a vertical direction. Two distinct failure envelopes were obtained for the two directions for intact Merville clay. This result differs from the results obtained on London clay for which the same failure envelope was found for vertical and horizontal samples.

The effects of cyclic loading on Merville clay were analyzed, based on the results obtained on five reconstituted samples prepared at the same *OCR* and subjected to symmetrical two-ways cyclic tests at different stress levels. A threshold value of the stress level was found. If the stress level is smaller than this threshold value, a state of equilibrium can be reached during cyclic loading. If the stress level is higher than this threshold value, the samples will fail for a given value of the number of cycles.

The numbers of cycles in relation with the permanent and cyclic shear strains were reported in stability diagrams based on these diagrams, if the combination of permanent and cyclic stresses is given, the shear strains could be predicted at a given number of cycles. For a given shear strain, the resilient modulus was found larger for a greater stress level. For samples reaching failure, the resilient modulus decreased during the cyclic loading. On the contrary, for the samples submitted to a stress level smaller than the threshold value, the resilient modulus decreased at the beginning of the tests, then increased until the end of the test.

Except for one sample which failed at a low number of cycles (less than 10^4 cycles), the development of the excess pore pressure increased at the beginning of the tests, and then continuously decreased until the end of tests for the other four samples. The development of the excess pore pressure and the evolution of the resilient modulus during cyclic loading with a large number of cycles can be due to the effect of creep. As the testing time increasing, the creep effect

would become greater and brought out the hardening of the specimens. As a consequence, the static shear strength of the specimens subjected to cyclic loading was higher than the shear strength of the sepcimens without previous cyclic loading.

6.2 Future work

This research work has highlighted the experimental static and cyclic behavior of reconstituted and natural samples of Merville clay. The clay structure and the microfissuration pattern affect the strength of the natural samples. This study could be prolonged by additional testing in order to enrich our knowledge of the behavior of a stiff overconsolidared clay.

Aiming to compare with the natural samples, an investigation of CT imaging for analyzing the microstructure of the reconstituted samples before and after shearing is advised to be done.

One-dimensional compression tests with unloading at medium pressures are suggested to be done for completing the swelling sensitivity in the range from low to high pressures.

The triaxial tests were performed on natural samples prepared in two directions (horizontal and vertical). More directions could be investigated to obtain a better view of the initial mechanical anisotropy of this clay.

In the diagrams of the relationship between permanent and cyclic stresses at some given number of cycles, only the results of symmetrical two-ways cyclic loading tests were presented. The results of non-symmetrical cyclic loading tests are required to complete these diagrams.

Further research testing of the creep effect on natural Merville clay as well as on overconsolidated reconstituted samples should also be undertaken in order to obtain a better understanding of the time-dependant behavior. The creep test results could then be compared with the cyclic test results.

This comprehensive series of experimental testing on an example of stiff overconsolidated clay constitutes a set of data which can now be used to construct and validate a constitutive model adapted to this particular type of materials. Our data could be complemented by other published data on Flanders clay and on London clay in order to enlarge the scope and in particular take into

account the influence of the geological history concerning samples coming from very different depths (from 3m in our study to more than 40 m in the case of London clay).

Reference

Alberro J., Santoyo E. (1973). "Long term behavior of Mexico City clay." Proceeding of the 8th International Conference on Soil Mechanics and Foundation Engineering, Moscow, 1: 1-9.

Ali H., Reiffsteck P., Baguelin F., Van de Graaf H., Bacconnet C., Gourves R. (2010). "Settlement of pile using cone loading test: load settlement curve approach." CPT 10: 2nd International Symposium on Cone Penetration Testing, France.

Andersen K.H. (1988). "Properties of soft clay under static and cyclic loading." Invited lecture. International Conference on Engineering Problems of Regional soils. Beijing, China. Proceeding: 7-26.

Andersen K.H. (2004), "Cyclic clay data for foundation design of structures subjected to wave loading." Proceedings of the International Conference on "Cyclic Behaviour of Soils and Liquefaction Phenomena", Bochum, Germany. : 371-387.

Andersen K.H., Kleven A., Heien D. (1988). "Cyclic soil data for design of gravity structures." ASCE, Journal of the Geotechnical Engineering, 114(GT5): 517-539.

Andersen K.H., Lauritzsen R. (1988). "Bearing capacity for foundation with cyclic loads." Journal of the Geotechnical Engineering, 114(GT5): 540-555.

Andersen K.H., Pool J.H., Brown S.F., Rosenbrand W.F. (1980). "Cyclic and static laboratory tests on Drammen clay." Journal of the Geotechnical Engineering, 106 (GT5): 499-529.

ASTM D 2850 – Standard Test Method for Unconsolidated-Undrained Triaxial Compression Test on Cohesive Soils.

ASTM D 4767 – Standard Test Method for Consolidated-Undrained Triaxial Compression Test on Cohesive Soils.

Atkinson J.H. (1975). "Anisotropic elastic deformations in laboratory tests on undisturbed London clay." Géotechnique, 25(2): 357-374.

Atkinson J.H., Richardson D., Stallebrass S.E. (1990). "Effect of stress history on the stiffness of overconsolidated soil." Géotechnique, 40(4): 531-540.

Azzouz A.S., Malek M.A., Baligh M.M. (1989). "Cyclic behavior of clays in undrained simple shear." Journal of the Geotechnical Engineering Division, 115(10): 637-657.

Ballester F., Sagaseta C. (1979). "Anisotropic elastoplastic undrained analysis of soft clays." Géotechnique, 29(3): 323-340.

Baudet B., Stallebrass S. (2004). "A constitutive model for structured clays." Géotechnique, 54(4): 269-278.

Biarez J., Hicher P.Y. (1994). "Elementary mechanics of soil behaviour: saturated remoulded soils." A.A.Balkema Publishers, Rotterdam.

Bishop A.W. (1966). "The strength of soils as engineering materials." The 6th Rankine Lecture, Géotechnique, 16(2): 91-130.

Bishop A.W., Webb D.L., Lewin P.I. (1965). "Undisturbed samples of London Clay from the Ashford Common shaft: strength-effective stress relationships." Géotechnique, 15(1): 1-31.

Bishop A.W., Wesley L.D. (1975). "A hydraulic triaxial apparatus for controlled stress path testing." Géotechnique, 25(4): 657-670.

Bjerrum L. (1967). "Engineering geology of Norwegian normally-consolidated marine clays as related to settlements of buildings." Géotechnique, 17(2): 81-118.

Bjerrum L. (1973). “Problems of soil mechanics and construction on soft clays and structurally unstable soils.” Proceedings of 8th International Conference on Soil Mechanics and Foundation Engineering, Moscow, Russia, 3: 111-159.

Bjerrum L., Kenney T.C. (1967). “Effect of structure on shear behavior of normally consolidated quick clays.” Proceedings of the Geotechnical Conference, Oslo, Norway, 2: 19-27.

Blyth F.G.H., de Freiteas M.H. (1984). “A Geology for Engineers.” London, Edward Arnold.

Bond A.J., Jardine R.J. (1991). “Effects of installing displacement piles in a high OCR clay.” Géotechnique, 41(3): 341-363.

Bond A.J., Jardine R.J. (1995). “Shaft capacity of displacement piles in a high OCR clay.” Géotechnique, 45(1): 3-23.

Borel S. (2000). “Thème 21 : Caractérisation de la déformabilité des sols au moyen d’essais en place. Caractéristiques géotechniques du site de Merville (Nord).” Rapport 1 21 04 9, mai 2000, LCPC Paris.

Borel S., Reiffsteck P. (2006). “ Caractérisation de la déformabilité des sols au moyen d’essais en place.” Rapport de LCPC, LCPC Paris.

Boudali M. (1995). “Comportement tridimensionnel et visqueux des argiles naturelles.” Thèse de doctorat, Université de Laval, Québec.

Boulanger R.W., Idress I.M. (2004). “Evaluating the potential for liquefaction or cyclic failure of silts and clays.” Report. No: UCD/CGM-04/01, Center for Geotechnical Modeling, University of California, Davis, California, America.

Boulanger R.W., Idress I.M. (2006). “Liquefaction susceptibility criteria for silts and clays.” Journal of Geotechnical and Geoenvironmental Engineering, 2006, 132(11): 1413-1426.

Brown S.F., Lashine A.D.F., Hyde A.F.L. (1975). “Repeated load testing of a silty clay.” Géotechnique, 25(1): 95-114.

Burland J.B. (1989). “Ninth Laurits Bjerrums memorial lecture: “Small is beautiful”- the stiffness of soils at small stains.” Canadian Geotechnical Journal, 26(4): 499-516.

Burland J.B. (1990). “On the compressibility and shear strength of natural soils.” Géotechnique, 40(3): 329-378.

Burland J.B., Rampello S., Georgiannou V.N., Calabresi G. (1996). “A laboratory study of the strength of four stiff clays.” Géotechnique, 46(3): 491-514.

Canépa Y., Borel S., Deconinck J. (2002). “Determination of the degradation curve of the shear modulus of a soil from field tests.” Paramètres de calcul géotechnique, Magnan, ENPC/LCPS press, Paris, 25-32.

Cafaro F., Cotecchia F. (2001). “Structural degradation and changes in the mechanical behaviour of a stiff clay due to weathering.” Géotechnique, 51(5): 441-453.

Casagrande A., Wilson S.D. (1951). “Effect of rate of loading on the strength of clays and clay shales at the constant water content.” Géotechnique, 2(3): 251-263.

Chandler R.J. (1966). “The measurement of residual strength in triaxial compression.” Géotechnique, 16(3): 181-186.

Chandler R.J. (1968). “A note on the measurement of strength in the triaxial compression tests.” Géotechnique, 18(2): 261-266.

Chandler R.J. (1972). “Lias clay: Weathering processes and their effect on shear strength.” Géotechnique, 22(4): 403-431.

Clayton C.R.I., Heymann G. (2001). “Stiffness of geometerials at very small strains.” Géotechnique, 51(3): 245-255.

Coop M.R., Cotecchia F. (1995). “The compression of sediments at the archeological site of Sibari.” Proceeding of 11th ECSMEF, Copenhagen 1: 19-26.

Costa Filho L.M. (1984). “Technical note: A note on the influence of fissures on the deformation characteristics of London Clay.” Géotechnique, 34(2): 268-272.

Cotecchia F. (1996). “The effects of structure on the properties of an Italian Pleistocene clay.” PhD thesis, University of London.

Cotecchia F., Chandler R.J. (1997). “The influence of structure on the prefailure behaviour of a natural clay.” Géotechnique, 47(3): 523-544.

Cotecchia F., Chandler R.J. (2000). “A general framework for the mechanical behaviour of clay.” Géotechnique, 50(4): 431-447.

Cuccovillo T., Coop M.R. (1997). “The measurements of local axial strains in triaxial tests using LVDTs.” Géotechnique, 47(1): 167-171.

Desrues J., Chambon R., Mokni M., Mazerolle F. (1996). “Void ratio evolution inside shear bands in triaxial sand specimens studied by computed tomography.” Géotechnique, 46(3): 529-546.

Díaz-Rodríguez J.A, Moreno P., Salinas G. (2000). “Undrained shear behavior of Mexico city sediments during and after cyclic loading.” Proceedings of the twelfth world conference on earthquake engineering, Auckland, New Zealand.

Dyvik R., Andersen K.H., Kalsnes B. (1989). “Model tests of gravity platforms, I. Description.” Journal of Geotechnical Engineering. 115(GT11): 1532-1549.

Ferber V., Abraham O. (2002). “Contribution of the seismic methods to the determination of initial moduli: application on the experimental site of Merville. Paramètres de calcul géotechnique.” Magnan, ENPC/LCPS press, Paris: 41-48.

Fookes P.G., Denness B. (1969). “Observational studies on fissure patterns in cretaceous sediments of South-East England.” Quarterly Journal of Engineering Geology, 1: 217-240.

Fookes P.G., Parrish D.G. (1969). “Observations on small-scale structural discontinuities in the London clay and their relationship to the regional geology.” Géotechnique, 19(4): 453-477.

Gasparre A. (2005). “Advanced laboratory characterisation of London clay.” PhD Thesis, Imperial College London.

Graham J., Crooks J.H.A., Bell A.L. (1983). “Time effects on the stress-strain behaviour of natural soft clays.” Géotechnique, 33(3): 327-340.

Graham J., Houlsby G.T. (1983). “Anisotropic elasticity of a natural clay.” Géotechnique, 33(2): 165-180.

Graham J., Crooks J.H.A., Bell A.L. (1983). “Time effects on the stress-strain behavior of natural soft clays.” Géotechnique, 33(3): 327-340.

Graham J., Crooks J.H., Lau S.L.K. (1988). “Yield envelops: identification and geometric properties.” Géotechnique, 38(1): 125-134.

Hattab M., Favre J-L. (2010). “Analysis of the experimental compressibility of deep water marine sediments from the Gulf of Guinea.” Marine and Petroleum Geology, 27(2): 486-499.

Hicher P.Y. (1979). “Contribution à l’étude de la fatigue des argiles.” Thèse de docteur-ingénieur, L’école Centrale des Arts et Manufactures.

Hicher P.Y. (1985). “Comportement mécanique des argiles saturées sur divers chemins de sollicitations monotones et cycliques application à une modélisation élastoplastique et viscoplastique.” PhD Thesis, University Paris VI.

Hicher P.Y., Shao J.F. (2002). “Elastoplasticité des sols et des roches: Modèles de comportement des sols et des roches 1.” Hermès Science Publications, Paris.

Hieng O.I. (1991). “Loi de comportement d’une argile raide (détermination des paramètres géotechniques de l’argile des Flandres). ” PhD Thesis, University Paris VI.

Hight D.W., Bennel J.D., Chana B., Davis P.D., Jardine R.J., Porovic E. (1997). “Wave velocity and stiffness measurements of the Crag and Lower London Tertiaries at Sizewell.” Géotechnique, 47(3): 451-474.

Hight D.W., Gasparre A., Nishimura S., Minh N.A., Jardine R.J., Coop M.R. (2007). “Characteristics of the London Clay from the Terminal 5 site at Heathrow Airport.” Géotechnique, 57(1): 3-18.

Hight D.W., Bond A.J., Legge J.D. (1992). “Characterization of the Bothkennar clay; an overview.” Géotechnique, 42(2): 303-347.

Hong Y., Yu G.M., Wu Y.X., Zheng X.Y. (2011). “Effect of cyclic loading on the residual strength of over-consolidated silty clay in a ring shear test.” Landslides, 8(2): 233-240.

Hyodo M., Yamamoto Y., Sugiyama M. (1994). “Undrained cyclic shear behaviour of normally consolidated clay subjected to initial static shear stress.” Soils and Foundations, 34(4): 1-11.

Jardine R.J., Symes M.J., Burland J.B. (1984). “The measurement of soil stiffness in the triaxial apparatus.” Géotechnique, 34(3): 323-340.

Josseaume H. (1998). “Engineering properties of the Flanders clay at Dunkirk and Calais.” Revue Française de Géotechnique, 84: 3-26.

Josseaume H., Hieng I.O., Stempfelet J.P. (1991). “Détermination des paramètres de compressibilité d’une argile raide à partir d’essais oedométriques à haute pression.” Bulletin de LCPC, 109-120.

Jovicic V., Coop M.R. (1997). “Stiffness of coarse-grained soils at small strains.” Géotechnique, 47(3): 545-561.

Jovicic V., Coop M.R., Simic, M. (1996). “Objective criteria for determining Gmax from bender element tests.” Géotechnique, 46(2): 357-362.

Kavvadas M., Amorosi, A. (2000). “A constitutive model for structured clays.” Géotechnique, 50(3): 263-273.

Lambe T.W., Whitman R.V. (1969). “Soil Mechanics.” John Wiley & Sons Inc., New York.

Lee K.L., Focht J.A. (1976). “Strength of clay subjected to cyclic loading.” Marine Geotechnology, 1(3): 165-185.

Lefebvre G., LeBoeuf D. (1987). “Rate effects and cyclic loading of sensitive clays.” Journal of Geotechnical Engineering, 113(35): 476-489.

Leroueil S., Kabbaj M., Tavenas F., Bouchard R. (1985). “Stress-strain-strain rate relation for the compressibility of sensitive natural clays.” Géotechnique, 35(2): 159-180.

Leroueil S., Tavenas F., Locat J. (1984). “Discussion on: Correlations between index tests and the properties of remoulded clays- Carrier W.D. and Beckman J.F.” Géotechnique, 35(2): 223-226.

Leroueil S., Vaughan P. R. (1990). “The General and Congruent Effects of Structure in Natural Soils and Weak Rocks.” Géotechnique, 40(3): 467- 488.

Li L.L., Dan H.B., Wang L.Z. (2011). “Undrained behavior of natural marine clay under cyclic loading.” Ocean Engineering, 38(16): 1792- 1805.

Lings M.L. (2001). “Drained and undrained anisotropic elastic stiffness parameters.” Géotechnique, 51(6): 555-565.

Lings M.L., Pennigton D.S., Nash D.F. (2000). “Anisotropic stiffness parameters and their measurement in a stiff natural clay.” Géotechnique, 50(2): 109-125.

Lo K.Y., Morin J.P. (1972). “Strength anisotropy and time effects of two sensitive clays.” Canadian Geotechnical Journal. 9(3): 261-277.

Locat J. (1982). “Contribution à l’étude de l’origine de la structuration des argiles sensibles de l’est du Canada.” PhD thesis, University of Sherbrooke.

Locat J., Lefebvre G. (1985). “The compressibility and sensitivity of an artificially sedimented clay soil : the Grande-Baleine marine clay, Quebec.” Marine Geotechnology, 6(1): 1-27.

Lupini J.F., Skinner A.E., Vaughan P.R. (1981). “The drained residual strength of cohesive soils.” Géotechnique, 31(2): 181-213.

Mayne P.W. (1985). “Stress anisotropy effects on clay strength.” Journal of the Geotechnical Engineering, 111(GT3): 356-366.

Mitachi T., Kitago S. (1976). “Change in undrained shear strength characteristics of saturated remoulded clays due to swelling.” Soils and Foundations, 16(1): 45-58.

Mitchell J.K., Soga K. (2005). “Fundamentals of Soil Behaviour(3rd edition).” Hoboken N.J., John Wiley& Sons Inc, America.

Molenkamp F. (1998). “Principle of axial shear apparatus.” Géotechnique, 48(3): 427-431.

Nakase A., Kamei T. (1986). “Influence of strain rate on undrained shear strength characteristics of K0-consolidated cohesive soils.” Soils and Foundations, 26(1): 85-95.

Nishimura S. (2005). “Laboratory study on anisotropy of natural London clay.” PhD Thesis, Imperial College London.

Pennington D.S., Nash D.F.T., Lings M.L. (1997). “Anisotropy of Go shear stiffness in Gault clay.” Géotechnique, 47(3): 391-398.

Pickering D.J. (1970). “Anisotropic elastic parameters for soils.” Géotechnique, 20(3): 271-276.

Prapaharan S., Chameau J.L., Holtz R.D. (1989). “Effect of strain rate on undrained strength derived from pressuremeter tests.” Géotechnique, 39(4): 615-624.

Puzrin A.M., Burland J.B. (1998). “Non-linear model of small-strain behaviour of soils.” Géotechnique, 20(4): 217-233.

Rangeard D. (2002). “Identification des caractéristiques hydro-mécaniques d’une argile par analyse inverse d’essais pressiométriques. ” PhD thesis, Ecole Centrale de Nantes, French.

Reiffsteck Ph. (2003). “ Le site de Merville – analyse des résultats des essais de laboratoire.” Rapport de recherche LCPC, LCPC Paris.

Richardson A.M., Whitman R.V. (1963). “Effect of strain rate upon undrained shear resistance of a saturated remoulded fat clay.” Géotechnique, 13(4): 310-324.

Samuels S.G. (1975). “Some properties of the Gault Clay from the Ely-Ouse Essex water tunnel.” Géotechnique, 25(2): 239-264.

Sangrey D.A. (1972). “Naturally cemented sensitive soils.” Géotechnique, 22(1): 139-152.

Sangrey D.A., Henkel D.J., Esrig M.I. (1969). “The effective stress response if a saturated clay soil to repeated loading.” Canadian Geotechnical Journal, 6(3): 241-252.

Sangrey D.A., France J.W. (1980). “Peak strength of clay soils after a repeated loading history.” International Symposium on Soils under Cyclic and Transient Loading, Swansea: 421-430.

Schmertmann, J.H. (1969). “Swell Sensitivity.” Géotechnique, 19(4): 530-533.

Seed H.B., Chan C.K. (1966). “Clay strength under earthquake loading conditions.” Journal of the Soil Mechanics and Foundations Division, American Society of Civil Engineers, 92(2): 53-78.

Seed H.B., Lee K.L. (1966). “Liquefaction of saturated sands during cyclic loading conditions.” Journal of the Soil Mechanics and Foundations Division, American Society of Civil Engineers, 92(6): 105-134.

Sheaham T.C, Ladd C.C., Germaine J.T. (1996). “Rate dependent undrained behavior of saturated clay.” ASCE, Journal of Geotechnical Engineering, 122(2): 99-108.

Sides G., Barden L. (1970). “The microstructure of dispersed and flocculated samples of kaolinite, illite and montmorillonite.” Canadian Geotechnical Journal, 8(3): 391-399.

Simpson B. (1992). “Retaining Structures: displacement and design.” Géotechnique, 42(4): 541-576.

Simpson B., O’Riordan N.J., Croft O.D. (1979). “A computer model for the analysis of ground movements in London Clay.” Géotechnique, 29(2): 149-175.

Skempton A.W. (1964) “Long term stability of clay slopes.” Géotechnique, 14(2): 77-101.

Skempton A.W. (1964). “Horizontal stresses in an overconsolidated Eocene clay.” Proceedings of the 5th International Conference on Soil Mechanics and Foundation Engineering, Paris, 1: 351- 357.

Skempton A.W. (1970). “The consolidation of clays by gravitational compaction.” Quarterly Journal of the Geological Society, 125: 373-411.

Skempton A.W., La Rochelle P. (1965). “The Bradwell slip: a short-term failure in London Clay.” Géotechnique, 15(3): 221-242.

Skempton A.W., Northey R.D. (1952). “The sensitivity of clays.” Géotechnique, 3(1): 30-53.

Skempton A.W., Schuster F.R.S., Petley D.J. (1969). “Joints and fissures in the London Clay at Wraysbury and Edgware.” Géotechnique, 19(2): 205- 217.

Smart P., Tovey N.K (1982). “Electron microscopy of soils and sediments: examples.” Oxford University Press.

Smith P., Jardine R.J., Hight D.W. (1992). “The yielding of Bothkennar clay.” Géotechnique, 42(2): 257-274

Soga K., Mitchell J.K. (1996). “Rate-dependent deformation of structured natural clays. In: T. G. Sheahan and V.N. Kaliakin (Eds), Measuring and Moldeling Time Dependent Soil Behavior.” Geotechnical Special Publication No. 61, ASCE, New York: 243-257.

Sorensen K.K., Baudet B.A., Simpson B. (2007). “Influence of structure on the time-dependent behaviour of a stiff sedimentary clay.” Géotechnique, 57(1): 113-124.

Stallebrass S.E., Taylor R.N. (1997). “The development and evaluation of a constitutive model for the prediction of ground movements in overconsolidated clay.” Géotechnique, 47(2): 235-353.

Tatsuoka F., Jardine R.J., Lo Presti D., Di Benodetto H., Kodaka T. (1997). “Theme lecture: Characterising the pre-failure deformation properties of geomaterials.” Proceedings, 15th International Conference on Soil Mechanics and Foundation Engineering, Hamburg, Germany, 4: 2129-2164.

Tavenas F., Leroueil S. (1977). “Effect of stresses and time on yielding of clays.” Proceedings of 9th International Conference on Soil Mechanics and Foundation Engineering, Tokyo, 1: 319-326.

Tavenas F., Leroueil S., La Rochelle P., Roy M. (1978). “Creep behaviour of an undisturbed lightly over-consolidated clay.” Canadian Geotechnical Journal, 15(3): 402-423.

Terzaghi K. (1936). “Stability of slopes of natural clay.” International Conference on Soil Mechanics and Foundation Engineering, Cambridge, 1: 161-165.

Thammathiwat A., Chim-oye W. (2004). “Behavior of strength and pore pressure of the soft Bangkok clay under cyclic loading.” Thammasat International Journal of Science and Technology, 9(4): 21-25.

Thiers G.F., Seed H.B. (1969). “Strength and stress-strain characteristics of clays subjected to seismic loading conditions.” Proceeding of ASTM STP, 450: 3-56.

Vaid Y.P., Campanella R.G. (1977). “Time-dependent behavior of undisturbed clays.” Journal of the Geotechnical Engineering Division, 103(7): 450: 3-56.

Vaughan P.R., Hight D.W., Sodha V.G., Walbanke H.J. (1978). “Factors controlling the stability of clays fills in Britain.” Clay Fills, Proceeding of the Conference held at the Institution of Civil Engineers, London: 205-217.

Veniale F. (1985). “The role of microfabric in clay soil stability.” Mineralogica et Petrographica Acta, 45-A: 101-119.

Viggiani G., Atkinson J.H. (1995). “Interpretation of bender element tests.” Géotechnique, 45(1): 149-154.

Vucetic M., Dobry R. (1988). “Degradation of marine clays under cyclic loading.” Journal of Geotechnical Engineering, 114(2): 133-149.

Wang J., Cai Y.Q. (2008). “Study on accumulative plastic strain model of soft clay under cyclic loading.” Chinese Journal of Rock Mechanics and Engineering, 27(2): 331-338.

Ward W.H., Marsland A., Samuels S.G. (1965). “Proprieties of the London Clay at the Ashford Common shaft: in-situ and undrained strength tests.” Géotechnique 15(4): 321-344.

Ward W.H., Samuels S.G., Butler, M.E. (1959). “Further studies of the proprieties of London Clay.” Géotechnique, 9(2): 33-58.

Wong R.C.K. (1999). “Mobilized strength components of Athabasca oil sand in triaxial compression.” Canadian Geotechnical Journal, 36(4): 718-735.

Yasuhara K., Hirao K., Hyde A.FL. (1992). “Effects of cyclic loading on undrained strength and compressibility of clay.” Soils and Foundations, 32(1): 100-116.

Yin Z.Y., Chang C.S. (2009). “Microstructural modeling of stress-dependent behaviour of clay.” International Journal of Solids and Structures, 46(6): 1373-1388.

Yudhbir, Rehman M.S. (1977). “Deformation and pore pressure response of a soft clay subjected to repeated loading.” Geotechnical Aspects of Soft Clays.

Zhu J.G., Yin J.H. (2000). “Strain-rate-dependent stress-strain behavior of overconsolidated Hong Kong marine clay.” Canadian Geotechnical Journal, 37(6): 1272-1282.